

**THE REACTIONS OF  
METALLOINTERCALATOR-PEPTIDE CONJUGATES AND DNA**

Thesis by  
Kimberly Davis Copeland

In Partial Fulfillment of the Requirements  
for the Degree of  
Doctor of Philosophy

California Institute of Technology  
Pasadena, California

2002

(Defended May 17, 2002)

## ACKNOWLEDGMENTS

I should start by thanking my research advisor, Professor Jackie Barton. Her enthusiasm is always contagious, and she has gathered a wonderful collection of people in her lab. I appreciate the independence that she gave to me during my six years in the Barton group. I had lots of room in which to grow. I am particularly thankful that she didn't let me go easily when I walked into her office to drop out of grad school.

As I've already mentioned, the members of the Barton group are wonderful—very generous in sharing their time and knowledge. Marilena Fitzsimons was a very patient guide when I first entered the group. I am thankful for the training she provided, but also for her laughter and wisdom. I owe many thanks to Ulrike Riese for her careful preparation and characterization of rhodium-peptide libraries. I enjoyed working with Bob Houser on the hydrolysis project, and I want to thank him for initiating the copper cleavage experiments. It was wonderful to briefly have Melanie Sanford as a labmate. She contributed a lot of humor to my first years of graduate school, and inspired us to study chrysi-peptide conjugates. I am also very thankful for my two SURF students, Alexis Lueras and Claire Mitchell. They were both ready to work hard and made valuable contributions to the Ru-peptide crosslinking project and the copper cleavage project. I want to thank Eric Stemp for providing me with a well-trained SURF student, and for helpful conversations about DNA-peptide crosslinking. Mo Renta has been a wonderful source of information, and I have appreciated all of her help during my time in the group. Brian Jackson and Sarah Delaney, because they sat so close to me and were just generally helpful, were regularly assaulted with questions. I particularly want to



thank Brian Jackson, Liz Carrico, Tashica Williams, and Sarah Delaney for fun conversation and friendship.

I am grateful to Dr. Suzanna Horvath and John Racs of the Beckman Institute Biopolymer Synthesis Center for their efficient and expert assistance with peptide synthesis. I also thank Dr. Mona Shahgholi for applying her skill with mass spectrometry to my DNA-peptide crosslinking adducts.

I want to thank Sarah Davis for long phone calls and unconditional love, Jim Davis for his example of discipline and hard work, and Cynthia Rais for being a witness to God's faithfulness. Finally, I'd like to thank Jeff Copeland. Jeff, thank you for giving me the opportunity to come to Caltech. Thanks for listening to me. Thanks for helping me to run a gel at home, and for taking my samples out of the speed vac. Thank you for six years of comfort, and hugs, and laughter. Praise God! We have *the* best mentor. He will be close as you persevere with your flies and worms.

"Take my yoke upon you and learn from me, for I am gentle and humble in heart, and you will find rest for your souls. For my yoke is easy and my burden is light."

– Matthew 11:29-30.

## ABSTRACT

A family of metallointercalator-peptide conjugates for reaction with DNA has been constructed. In these chimeras, the metallointercalator provides binding affinity for DNA and the peptide contributes reactivity. With the goal of creating an artificial nuclease, we have tethered metal-binding peptides to a sequence neutral intercalator,  $[\text{Rh}(\text{phi})_2\text{bpy}']^{3+}$  ( $\text{phi}$  = phenanthrenequinone diimine,  $\text{bpy}'$  = 4-butyric acid-4'-methyl-2,2'-bipyridine). This is a general strategy, and we have observed  $\text{Zn}^{2+}$ -promoted cleavage of plasmid DNA with widely different peptides: a designed helical peptide with histidine residues, and a hairpin peptide modeled after the active site of the *Bam*HI endonuclease. To optimize the peptide composition of our artificial nuclease we created a library of 16,000 conjugates, but no new active conjugates were identified with this combinatorial strategy. To achieve oxidative cleavage of the DNA backbone we have also used our intercalator-peptide conjugates to deliver copper to DNA. Tethered peptides containing histidine residues promote oxidative strand scission in DNA restriction fragments and oligonucleotides in the presence of  $\text{Cu}^{2+}$  and a reducing agent. Importantly, by comparing the photocleavage pattern of the rhodium intercalator with the copper cleavage pattern of the metal-binding peptide, the interactions of the conjugate with DNA could be dissected. Finally, short peptides were tethered to  $[\text{Ru}(\text{phen})(\text{bpy}')(\text{dppz})]^{2+}$  ( $\text{phen}$  = 1,10-phenanthroline,  $\text{dppz}$  = dipyridophenazine) to create fluorescent DNA crosslinking agents. Through a flash-quench reaction, the ruthenium intercalator generates guanine radicals in a DNA duplex. These guanine radicals can react with water or oxygen, but also with tethered peptides to produce

permanent DNA-peptide crosslinks. The DNA-peptide crosslinks were detected by gel electrophoresis and absorbance measurements, and characterized by mass spectrometry. Although they have low affinity for DNA, untethered peptides could also be crosslinked to DNA using the ruthenium chemistry. The peptide composition influences conjugate binding and the extent and pattern of crosslinking; indeed, positively charged residues were essential for effective crosslinking. Although the flexibility of our tethered peptides is an obstacle to the rational design of reactive conjugates, we have demonstrated that peptides can mediate a variety of reactions if delivered to DNA by metallointercalators.

## TABLE OF CONTENTS

	page	
ACKNOWLEDGMENTS	ii	
ABSTRACT	iv	
TABLE OF CONTENTS	vi	
LIST OF FIGURES	xiv	
LIST OF TABLES	xx	
<b>Chapter 1</b>	<b>Introduction: The Interactions of Metallointercalator-Peptide Conjugates with DNA</b>	<b>1</b>
1.1.	DNA	2
1.2.	DNA Metallointercalators for DNA Recognition and Electron Transfer Reactions	4
1.2.1.	Recognition of DNA by Octahedral Metallointercalators.	6
1.2.2.	Probing DNA Charge Transport with Metallointercalators.	8
1.3.	Attaching Peptides to Metallointercalators	9
1.3.1.	Synthesis of Metallointercalator-Peptide Conjugates.	11
1.3.2.	Novel DNA Recognition Properties with Tethered Peptides.	12
1.3.3.	Novel Reactions with Tethered Peptides.	18
1.4.	A Metallointercalator-Peptide Conjugate for DNA Hydrolysis	20
1.4.1.	DNA Hydrolysis.	20
1.4.2.	DNA Hydrolysis Promoted by Metal Ions and Complexes.	22

1.4.3.	A Rhodium-Metallopeptide Conjugate for DNA Hydrolysis.	36
1.4.4.	Variations on Rh-P1.	42
1.5.	New Tethered Peptides and New Reactions	47
1.6.	References	48
<b>Chapter 2</b>	<b>DNA Hydrolysis by a <i>Bam</i>HI Peptide Tethered to a Rhodium Intercalator</b>	<b>54</b>
2.1.	Introduction	55
2.2.	Materials and Methods	63
2.2.1.	Synthesis of the Metallointercalator Complex.	63
2.2.2.	Preparation of the Metallointercalator-Peptide Conjugate.	63
2.2.3.	Characterization of Intercalator-Peptide Conjugates by Mass Spectrometry and Amino Acid Analysis.	65
2.2.4.	Analysis of Intercalator-Peptide Conjugates by UV-Visible and Circular Dichroism Spectroscopy.	66
2.2.5.	Potentiometric Titration of the Rh-Bam Conjugate.	67
2.2.6.	Cleavage of Supercoiled Plasmid with Rh-Bam and Metal Ions.	67
2.2.7.	Photocleavage of a Plasmid Restriction Fragment by Rh-Bam.	69
2.2.8.	Oligonucleotide Cleavage Experiments with Rh-Bam.	70

2.3.	Results	71
2.3.1.	Synthesis of the Rh-Bam Conjugate.	71
2.3.2.	Characterization of the Rh-Bam Conjugate.	72
2.3.3.	Cleavage of Supercoiled Plasmid by Rh-Bam and Zinc.	80
2.3.4.	Testing Rh-Bam with a Variety of Metal Ions.	85
2.3.5.	DNA Photocleavage with Rh-Bam.	87
2.3.6.	Testing Rh-Bam for Oligonucleotide Hydrolysis Activity.	90
2.3.7.	Cleavage of Supercoiled Plasmid by Rh-Bam2 and Rh-Bam3.	93
2.4.	Discussion	95
2.4.1.	The Peptide.	96
2.4.2.	The Metal Cation.	100
2.4.3.	The DNA Metallointercalator.	104
2.4.4.	A Comparison of the Cleavage Activity of the Rh-P1 and Rh-Bam Conjugates.	106
2.5.	Conclusions	108
2.6.	References	109
<b>Chapter 3</b>	<b>The Development of a Metallointercalator-Peptide Library and Screening of the Library for DNA Hydrolysis Activity</b>	<b>113</b>
3.1.	Introduction	114
3.2.	Materials and Methods	118

3.2.1. Synthesis of Ligands and Metal Complex.	118
3.2.2. Synthesis of the Peptide Library.	122
3.2.3. Preparation of the Rhodium-Peptide Library.	125
3.2.4. Characterization of the Rhodium-Peptide Library.	126
3.2.5. Investigation of Library Release by UV-Visible Spectroscopy and HPLC.	126
3.2.6. Library Screening.	129
3.2.7. Identification of Selected Conjugates.	132
3.2.8. Resynthesis of Selected Conjugates.	132
3.2.9. Plasmid Cleavage Assays with Selected Conjugates.	134
3.3. Results	135
3.3.1. Preparation of the Rhodium-Peptide Library.	135
3.3.2. The Release of Rh-Peptide Conjugates from Solid Support by Irradiation.	144
3.3.3. The Development of a Screening Strategy to Select Artificial Nucleases.	150
3.3.4. Identification of the Conjugates Selected from Rh-LP2.	160
3.3.5. Testing Selected Conjugates Against Rh-P1 in Plasmid Cleavage Assays.	169
3.4. Discussion	169
3.4.1. The Rhodium-Peptide Library.	170
3.4.2. The Screening Strategy.	177
3.4.3. The Selection and Identification of Conjugates.	180

3.4.4.	The Promise and Problems of our Combinatorial Approach.	181
3.5.	Conclusions	183
3.6.	References	184
<b>Chapter 4</b>	<b>Oxidative DNA Cleavage by Copper-Binding Metallointercalator-Peptide Conjugates</b>	<b>187</b>
4.1.	Introduction	188
4.2.	Materials and Methods	197
4.2.1.	Synthesis of Ligands and Metal Complexes.	197
4.2.2.	Synthesis of Metallointercalator-Peptide Conjugates.	198
4.2.3.	Characterization of Metallointercalator-Peptide Conjugates by UV-Visible Spectroscopy and Mass Spectrometry.	200
4.2.4.	Photocleavage and Copper Cleavage of DNA Restriction Fragments.	202
4.2.5.	Photocleavage and Copper Cleavage of Oligonucleotides.	204
4.3.	Results	207
4.3.1.	Preparation of Metallointercalator-Peptide Conjugates.	207
4.3.2.	Photocleavage and Copper Cleavage of a Restriction Fragment by Rhodium-Peptide Conjugates.	210
4.3.3.	Photocleavage and Copper Cleavage of Oligonucleotide DNA by Rhodium-Peptide Conjugates.	218
4.3.4.	Photocleavage and Copper Cleavage of Oligonucleotides	224



	by Mismatch-Specific Rhodium-Peptide Conjugates.	
4.4.	Discussion	230
4.4.1.	The Copper-Binding Peptides.	231
4.4.2.	Oxidative Cleavage of DNA with Copper-Binding Peptides Tethered to Metallointercalators.	232
4.4.3.	Insights into the Interactions of Tethered Peptides and DNA.	234
4.4.4.	Development of a Mismatch-Specific Conjugate for DNA Cleavage.	238
4.5.	Conclusions	240
4.6.	References	241
<b>Chapter 5</b>	<b>DNA-Peptide Crosslinking with Metallointercalator-Peptide Conjugates</b>	<b>244</b>
5.1.	Introduction	245
5.2.	Materials and Methods	252
5.2.1.	Synthesis of Ligands and Metal Complexes.	252
5.2.2.	Preparation of Peptides and Metallointercalator-Peptide Conjugates.	253
5.2.3.	Characterization of Ruthenium-Peptide Conjugates by Mass Spectrometry and UV-Visible Spectroscopy.	254
5.2.4.	Characterization of Ruthenium-Peptide Conjugates by	256

	Circular Dichroism Spectroscopy.	
5.2.5.	Determination of DNA Binding Constants of Metallointercalator-Peptide Conjugates.	256
5.2.6.	Flash-Quench Crosslinking with Ruthenium-Peptide Conjugates and DNA.	257
5.2.7.	Characterization of Crosslinked Material by Spectroscopy and Mass Spectrometry.	259
5.3.	Results	260
5.3.1.	The Creation of Ruthenium-Peptide Conjugates.	260
5.3.2.	DNA Binding Constants of Ruthenium-Peptide Conjugates.	266
5.3.3.	Flash-Quench Crosslinking of Ruthenium-Peptide Conjugates and DNA.	269
5.3.4.	Impact of Peptide Composition on Crosslinking.	275
5.3.5.	Role of the Ruthenium Metallointercalator in Flash-Quench Crosslinking Reactions.	283
5.3.6.	Characterization of Crosslinked Material by Spectroscopy and Mass Spectrometry.	285
5.4.	Discussion	287
5.4.1.	Metallointercalator-Peptide Conjugates as a Model System for Studying DNA-Protein Crosslinking.	287
5.4.2.	The Tethered Peptide.	288
5.4.3.	The Ruthenium Metallointercalator.	292
5.4.4.	The Characterization of Crosslinking Adducts.	293

5.4.5. Insights and Applications for DNA-Protein Crosslinking.	294
5.5. Conclusions	295
5.6. References	296
<b>Chapter 6 Conclusions</b>	<b>301</b>
6.1. Conclusions	302
6.2. References	306

## LIST OF FIGURES

### **Chapter 1     Introduction: The Interactions of Metallointercalator-Peptide Conjugates with DNA**

1.1.	The Structure of DNA.	3
1.2.	DNA Metallointercalators.	5
1.3.	Synthesis of Metallointercalator-Peptide Conjugates.	11
1.4.	A Model for Recognition with a Metallointercalator-Peptide Conjugate.	17
1.5.	DNA Hydrolysis.	19
1.6.	Roles of Metal Ions in Promoting DNA Hydrolysis.	23
1.7.	A Rhodium-Peptide Conjugate for DNA Hydrolysis.	37
1.8.	A Model for DNA Binding and Cleavage by Rh-P1.	43

### **Chapter 2     DNA Hydrolysis by a *Bam*HI Peptide Tethered to a Rhodium Intercalator**

2.1.	The Structure of <i>Bam</i> HI bound to DNA.	57
2.2.	The Active Site Residues of the <i>Bam</i> HI Endonuclease.	58
2.3.	A Two-Metal Ion Mechanism for <i>Bam</i> HI.	59
2.4.	Schematic of the Rh-Bam Conjugate.	61
2.5.	Schematic of Conjugates with Designed Hairpin Peptides.	62

2.6.	Synthesis of the Rh-Bam Conjugate.	73
2.7.	UV-Visible Spectra of $[\text{Rh}(\text{phi})_2\text{bpy}']^{3+}$ , Rh-P1, Bam Peptide, and Rh-Bam.	75
2.8.	Circular Dichroism Spectra of Rh-Bam with Increasing $\text{Zn}^{2+}$ Concentration.	77
2.9.	Circular Dichroism Spectra of Rh-Bam with Increasing Trifluoroethanol.	78
2.10.	Cleavage of Plasmid DNA by Rh-Bam.	81
2.11.	Cleavage of pBR322 by Rh-Bam, $[\text{Rh}(\text{phi})_2\text{bpy}']^{3+}$ , and Bam Peptide.	82
2.12.	Cleavage of pBR322 by Rh-Bam Over a Wide Range of $\text{Zn}^{2+}$ Concentrations.	84
2.13.	Cleavage of pBR322 by Rh-Bam in a Metal Ion Buffer.	86
2.14.	Cleavage of pBR322 by Rh-Bam and a Variety of Metal Cations.	88
2.15.	Photocleavage of a Plasmid Restriction Fragment by $[\text{Rh}(\text{phi})_2\text{bpy}']^{3+}$ , Rh-P1 and Rh-Bam.	89
2.16.	Photocleavage of an Oligonucleotide by Rh-Bam.	91
2.17.	Incubation of Oligonucleotide with Rh-Bam and Divalent Cations.	92
2.18.	Cleavage of pBR322 by $[\text{Rh}(\text{phi})_2\text{bpy}']^{3+}$ , Rh-Bam, Rh-Bam2, and Rh-Bam3.	94
2.19.	A Comparison of the Sensitivity of Plasmid and Oligonucleotide Cleavage Assays.	107

## **Chapter 3     The Development of a Metallointercalator-Peptide Library and Screening of the Library for DNA Hydrolysis Activity**

3.1.	Combinatorial Chemistry.	115
3.2.	Schematic of Rhodium-Peptide Library 1 (Rh-PL1).	119
3.3.	Schematic of Rhodium-Peptide Library 2 (Rh-PL2).	120
3.4.	Synthesis of the Bpy" Ligand.	121
3.5.	Apparatus Used for Library Screening.	130
3.6.	Preparation of a Peptide Library by Split Pool Synthesis.	136
3.7.	Synthesis and Release of a Rhodium-Peptide Library.	137
3.8.	HPLC Analysis of Peptide Library 1 (PL1).	143
3.9.	The Release of Rh-Peptide from Solid Support with Irradiation.	145
3.10.	The Release of Rh-PL1 from Solid Support with Irradiation.	148
3.11.	HPLC Analysis of Rhodium-Peptide Library 1.	149
3.12.	The Impact of Rhodium Complex and Irradiation on the Spectra of a Fluorogenic DNA Substrate.	151
3.13.	A Plasmid Cleavage Assay for Library Screening.	153
3.14.	Two Rounds of Screening with Rh-Peptide Library 2.	155
3.15.	Single-Bead Screening with Rh-Peptide Library 2.	159
3.16.	The Edman Sequencing Reaction.	161
3.17.	Residue Incorporation at Variable Positions in Rh-LP2.	164
3.18.	Number of His, Lys, Glu, and Ala residues in Selected Peptides.	165
3.19.	Schematic of the Three Rhodium-Peptide Conjugates Selected by	167

## Library Screening.

- |       |   |     |
|-------|---|-----|
| 3.20. | Plasmid Cleavage Assays with Rh-P1, Rh-SP1, Rh-SP2, and Rh-SP3. | 168 |
| 3.21. | The Spectrum and Cleavage Mechanism of the Nitrobenzyl Linker   | 175 |

## **Chapter 4     Oxidative DNA Cleavage by Copper-Binding Metallointercalator-Peptide Conjugates**

- |       |   |     |
|-------|---|-----|
| 4.1.  | Metal Complexes for Oxidative Cleavage of DNA.  | 189 |
| 4.2.  | Intercalator-Peptide Conjugates for Oxidative Cleavage of DNA.  | 192 |
| 4.3.  | DNA Mismatches.   | 194 |
| 4.4.  | Rhodium Intercalators for DNA Mismatch Recognition.   | 195 |
| 4.5.  | Mismatch-Specific Intercalator-Peptide Conjugates for Oxidative Cleavage of DNA.                        | 196 |
| 4.6.  | UV-Visible Spectrum of $[\text{Rh}(\text{phen})(\text{bpy}'')(\text{chrysi})]^{3+}$ .                   | 201 |
| 4.7.  | The HPLC Chromatograms for the $[\text{Rh}(\text{phen})(\text{bpy}'')(\text{chrysi})]^{3+}$ Conjugates. | 209 |
| 4.8.  | Photocleavage and Copper Cleavage of a Restriction Fragment by Rh-P1.                                   | 212 |
| 4.9.  | A Bar Plot Comparing Photocleavage and Copper Cleavage with Rh-P1.                                      | 213 |
| 4.10. | Photocleavage and Copper Cleavage of a Restriction Fragment by $\text{Rh}''\text{-AHAHA-CONH}_2$ .      | 215 |

4.11.	Photocleavage and Copper Cleavage of a Restriction Fragment by Rh <sup>III</sup> -AHAAHA-COOH.	216
4.12.	A Bar Plot Comparing Photocleavage and Copper Cleavage with Rh <sup>III</sup> -AHAAHA-COOH.	217
4.13.	The Impact of Distamycin on the Photocleavage and Copper Cleavage of a Restriction Fragment by Rh-P1.	219
4.14.	The Impact of Distamycin on the Photocleavage and Copper Cleavage of a Restriction Fragment by Rh <sup>III</sup> -AHAAHA-COOH.	220
4.15.	Photocleavage and Copper Cleavage of an Oligonucleotide by Rh-P1.	221
4.16.	Photocleavage and Copper Cleavage of an Oligonucleotide by Rh-P1, Rh <sup>III</sup> -AHAAHA-COOH, and Rh-KGH.	223
4.17.	Photocleavage, Copper Cleavage, and Zinc Cleavage of a Duplex with a Mismatch Site by [Rh(phen)(bpy <sup>III</sup> -P1)(chrysi)] <sup>3+</sup> .	225
4.18.	Photocleavage and Copper Cleavage of a Hairpin with a Mismatch Site by [Rh(phen)(bpy <sup>III</sup> -AHAAHA-COOH)(chrysi)] <sup>3+</sup> .	226
4.19.	Photocleavage and Copper Cleavage of a Duplex with a Mismatch Site by [Rh(phen)(bpy <sup>III</sup> -AHAAHA-COOH)(chrysi)] <sup>3+</sup> .	228
4.20.	A Schematic Model for Photocleavage and Copper Cleavage with the [Rh(phen)(bpy <sup>III</sup> -AHAAHA-COOH)(chrysi)] <sup>3+</sup> Conjugate.	237



## Chapter 5     DNA-Peptide Crosslinking with Metallointercalator-Peptide Conjugates

5.1.	The Flash-Quench Cycle.	247
5.2.	A Ruthenium Metallointercalator-Peptide Conjugate for DNA Crosslinking, $[\text{Ru}(\text{phen})(\text{bpy}'\text{-AKYKG})(\text{dppz})]^{2+}$ .	251
5.3.	The Four Isomers of the Ruthenium Complex.	263
5.4.	HPLC Purification of Ruthenium-Peptide Conjugates.	264
5.5.	Circular Dichroism Spectra for the Ru-KYK Conjugate.	265
5.6.	The Determination of Binding Constants by Fluorescence Titration.	268
5.7.	Gel Analysis of Flash-Quench Crosslinking Reactions.	270
5.8.	Native Gel Analysis of Flash-Quench Crosslinking Reactions.	273
5.9.	Gel Analysis of Crosslinking with Ru-KYK and Ru-GYA.	276
5.10.	UV-Visible Spectra for Crosslinking Reactions.	282
5.11.	Gel Analysis of Crosslinking with Untethered and Tethered Peptides.	284
5.12.	Absorbance and Fluorescence Spectra for Crosslinked Material.	286

## LIST OF TABLES

<b>Chapter 1</b>	<b>Introduction: The Interactions of Metallointercalator-Peptide Conjugates with DNA</b>	
1.1.	DNA Recognition by Peptide Conjugates of $[\text{Rh}(\text{phi})_2\text{phen}']^{3+}$ .	13
1.2.	Transition Metal Complexes for DNA Hydrolysis.	24
1.3.	Lanthanide Metal Complexes for DNA Hydrolysis.	30
1.4.	Rate Enhancement with Artificial Nucleases.	34
1.5.	Plasmid Cleavage with Rh-P1.	40
1.6.	Rhodium-Peptide Conjugates Containing Variations on Peptide1 and Rate Constants for the Cleavage of pBR322.	45
<b>Chapter 2</b>	<b>DNA Hydrolysis by a <i>Bam</i>HI Peptide Tethered to a Rhodium Intercalator</b>	
2.1.	The Stability Constants of Divalent Metal Ions with Amino Acids.	102
<b>Chapter 3</b>	<b>The Development of a Metallointercalator-Peptide Library and Screening of the Library for DNA Hydrolysis Activity</b>	
3.1.	HPLC Conditions for Analysis of PL1 and Rh-PL1.	128
3.2.	Synthesis Conditions and Yield for Peptide Library 1.	139

3.3.	Synthesis Conditions and Yield for Peptide Library 2.	140
3.4.	Summary of Single-Bead Screening of Rh-PL2.	157
3.5.	Control Reactions for Single-Bead Plasmid Cleavage Screening.	160
3.6.	Summary of Sequencing Results for Selected Beads from Rh-PL2.	162
3.7.	A Ranking of the Selected Peptides.	166

#### **Chapter 4      Oxidative DNA Cleavage by Copper-Binding Metallointercalator-Peptide Conjugates**

4.1.	Conjugates of $[\text{Rh}(\text{phi})_2\text{bpy}]^{3+}$ .	207
4.2.	Conjugates of $[\text{Rh}(\text{phen})(\text{bpy}'')(\text{chrysi})]^{3+}$ .	208
4.3.	Conditions For Copper Cleavage Experiments with Mismatch-Specific Complexes and Conjugates.	229

#### **Chapter 5      DNA-Peptide Crosslinking with Metallointercalator-Peptide Conjugates**

5.1.	Ruthenium-Peptide Conjugates.	261
5.2.	DNA Binding Constants of Ruthenium-Peptide Conjugates.	267
5.3.	Percentage Crosslinked DNA with Ru-KYK and Ru-AYG Conjugates.	278
5.4.	Percentage of Crosslinking Product for Ruthenium-Peptide Conjugates.	279

## **Chapter 1**

### **Introduction: The Interactions of Metallointercalator-Peptide Conjugates and DNA**

## 1.1. DNA

DNA provides a set of instructions for the individual cells of an organism, and the chemical properties of the DNA polymer are carefully tuned to its remarkable role. The strength of its bonds, the array of functional groups displayed in its grooves, the conformational flexibility of the backbone—together all these features of DNA create a molecule for long-term information processing and storage.

DNA, deoxyribose nucleic acid, is a polymer of repeating nucleotide units (Figure 1.1). Each nucleotide unit consists of a negatively charged phosphate group, a deoxyribose sugar, and a heterocyclic aromatic base. The molecular instructions of DNA are encoded in the sequence of the four bases: adenine, cytosine, guanine, and thymine. Two polymers of DNA form a double helix, and in a perfectly matched helix, adenine is paired with thymine and guanine is paired with cytosine. The two strands of the helix are zippered together in antiparallel fashion by hydrogen bonds between the paired bases, and by stacking of the aromatic bases along the axis of DNA. Under physiological conditions the helix typically adopts a “B form” structure with a wide major groove and a narrow minor groove, yet DNA is not a uniform spiral. There are interesting variations in DNA structure that depend on the sequence of bases.<sup>1</sup>

The phosphodiester bonds that link nucleotide units provide just one example of careful tuning of both DNA and the proteins that manage DNA. The bond between phosphorus and oxygen is very stable, and the negatively charged phosphate is repulsive to nucleophiles.<sup>2</sup> The estimated half-life of the bond is 200 million years,<sup>3</sup> yet the cell is equipped with nucleases that can cleave the bond within seconds.<sup>4</sup> The stable

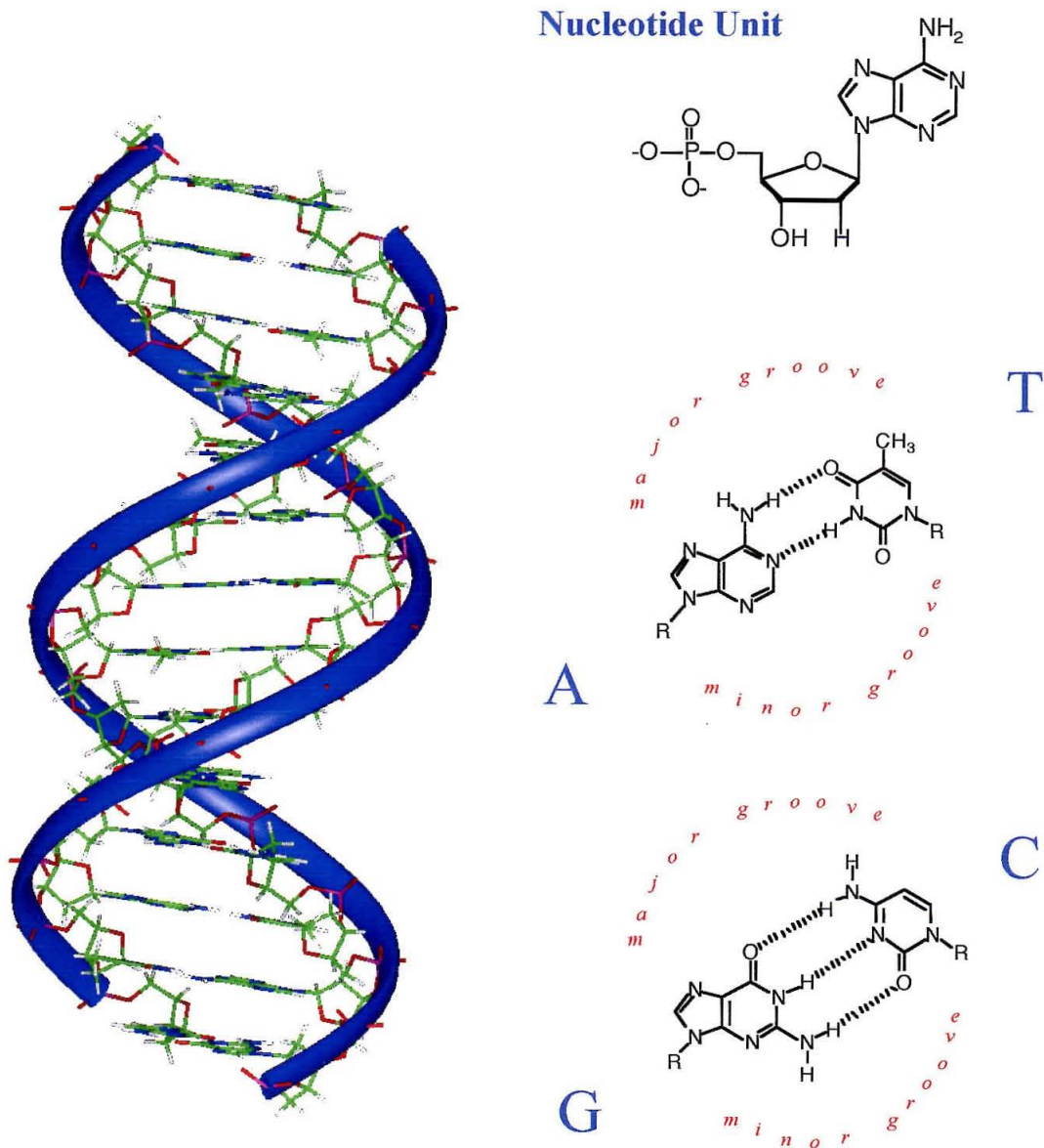


**Figure 1.1. The Structure of DNA.** DNA is a polymer of repeating nucleotide units.

Each nucleotide unit consists of a phosphate group, a deoxyribose sugar, and a heterocyclic aromatic base. Two polymers of DNA form a double helix, and in a perfectly matched helix, adenine pairs with thymine and guanine pairs with cytosine.

phosphodiester linkage protects the genetic material, but is susceptible to the enzymes that repair and remodel DNA.

In our research group, a family of metallointercalator complexes have played an important role in providing answers—and new questions—about the DNA molecule. What are the principles that govern site-selective recognition of nucleic acids by DNA binding proteins? Can we design small molecular tools for hydrolysis of the stable phosphodiester backbone? What factors control the flow of electrons through the stack of heterocyclic aromatic bases? Does the flow of electrons have an important biological role?

## **1.2. Metallointercalators for DNA Recognition and Electron Transfer Reactions**

We have developed a collection of metallointercalator complexes that bind to and interact with DNA (Figure 1.2). Our complexes are octahedral complexes of rhodium and ruthenium, and they boast aromatic heterocyclic ligands. The planar aromatic ligands insert deeply between the DNA base pairs, without causing significant disruptions in DNA conformation.<sup>5</sup> The affinity of these small molecules for DNA arises primarily from this intercalation;  $\pi$  orbital interactions between the ligand and the DNA bases provide 5 to 8 kcal of binding energy.<sup>6</sup> Favorable electrostatic attraction between the positively charged metal complex and the polyanionic DNA also contributes to binding.

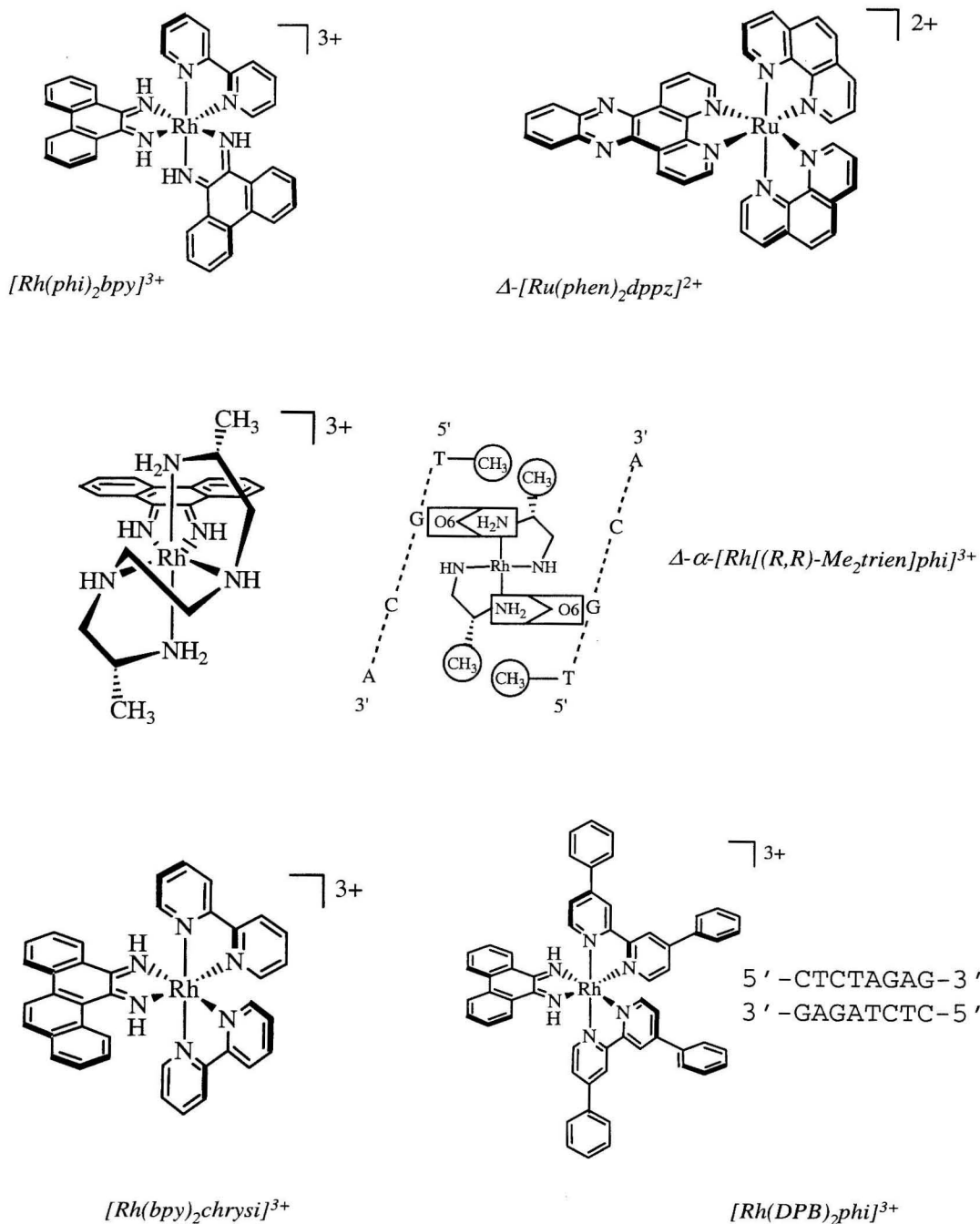


**Figure 1.2. DNA Metallointercalators.** The specific contacts of the  $[Rh[Me_2trien]phi]^{2+}$  complex and its TGCA recognition site are illustrated, and the 8 bp recognition site of the  $[Rh(DPB)_2phi]^{3+}$  complex is shown.



Our octahedral complexes of rhodium and ruthenium are inert and have a defined geometry and stereochemistry. The ancillary and intercalating ligands can be varied systematically to achieve the desired binding, electronic, or spectroscopic properties. Several of our complexes serve as photoreactive probes; for example, phenanthrene-quinone diimine (phi) complexes of rhodium(III) promote DNA strand cleavage upon irradiation. The sequence-neutral  $[\text{Rh}(\text{phi})_2\text{bpy}]^{3+}$  complex (bpy = 2,2'-bipyridine) has been employed for the photofootprinting of protein binding sites (Figure 1.2).<sup>7</sup> Our complexes also have rich spectroscopic properties, and display significant changes in absorbance and luminescence on DNA binding. For example, the  $[\text{Ru}(\text{phen})_2\text{dppz}]^{2+}$  complex (phen = 1,10-phenanthroline, dppz = dipyrrophenazine) is luminescent only when bound to DNA; it acts as a DNA light switch (Figure 1.2).<sup>8</sup> Additionally, the reduction potentials of our metallointercalators allow for redox reactions with DNA. All of these properties make our transition metal complexes very valuable as probes of DNA recognition<sup>6</sup> and DNA-mediated electron transfer.<sup>9</sup>

### 1.2.1. Recognition of DNA by Octahedral Metallointercalators.

The information in DNA is processed by a large number of noncovalent binding interactions between DNA and proteins. Using our small coordination complexes we have explored some of the principles that govern the site-specific recognition of nucleic acids. In our studies we have discovered that shape selection and direct readout are important in tuning DNA recognition.

A simple example of shape selection is provided by the chiral interactions of the  $[\text{Ru}(\text{phen})_2\text{dppz}]^{2+}$  metal complex with the right-handed B-DNA helix.<sup>6</sup> There is an

enantioselective preference for intercalation of the  $\Delta$ -isomer; the placement of the ancillary ligands of the  $\Delta$ -isomer fits the shape of the major groove and minimizes steric clashes with the DNA backbone. By changing only the shape, the bulk, and the symmetry of ligands, it is possible to create very selective metallointercalators; indeed, the  $[\text{Rh}(\text{DPB})_2\text{phi}]^{3+}$  complex (DPB = 4,4'-diphenyl-2,2'-bipyridyl) binds selectively to an eight base pair recognition sequence (Figure 1.2).<sup>10</sup>

The small metallointercalator  $\Delta\text{-}\alpha\text{-}[\text{Rh}[(\text{R,R})\text{-Me}_2\text{trien}]\text{phi}]^{3+}$  ((R,R)-Me<sub>2</sub>trien = 2R,9R-diamino-4,7-diazadecane) illustrates the direct readout strategy (Figure 1.2). This complex was designed to make specific hydrogen bonding contacts and van der Waal interactions with 5'-TGCA-3' sites. Photocleavage experiments demonstrated that the  $\Delta\text{-}\alpha$  isomer, and only the  $\Delta\text{-}\alpha$  isomer, targeted the 4 base pair site.<sup>11</sup> High resolution <sup>1</sup>H NMR and crystal structures confirmed that the complex made the intended interactions; the axial amines of the complex formed hydrogen bonds with the O6 of the guanine bases, and the pendant methyl groups were positioned for van der Waals contact with the methyl groups of the thymine bases.<sup>5,12</sup> Rigid octahedral intercalators, such as  $[\text{Rh}[\text{Me}_2\text{trien}]\text{phi}]^{3+}$ , provide an excellent scaffold for the delivery of functional groups to the major groove.

More recently we have used a steric-exclusion strategy to create a metal complex for DNA mismatch recognition. To specifically target mismatch sites, rhodium complexes were prepared with bulky intercalating ligands, 5,6-chrysenequinone diimine (chrysi) or benzophenazine-5,6-dione diimine (phzi) (Figure 1.2). Molecular modeling suggested that steric interactions would prevent binding of the chrysi or phzi ligands at standard intercalation sites; however, at mismatches, where the energetic cost of DNA

distortion had already been paid, the complexes were expected to bind.<sup>13</sup> This simple steric-exclusion strategy was successful, and the  $[\text{Rh}(\text{bpy})_2\text{chrysi}]^{3+}$  complex was demonstrated to selectively bind, and upon photoactivation, cleave in the vicinity of mismatch sites.<sup>14</sup> The binding constant at a CC mismatch was found to be 50 times larger than the nonspecific binding constant, and this selectivity allowed the discrimination of a single mismatch within a 2725 bp DNA plasmid heteroduplex.<sup>15</sup> The complex was tested against the eight possible base mismatches in sixteen sequence contexts, and cleavage was observed at 82% of the mismatch sites.<sup>16</sup>

### 1.2.2. Probing DNA Charge Transport with Metallointercalators.

Does the  $\pi$ -stacked array of base pairs in double-helical DNA serve as an effective medium for charge transport? Our metallointercalators are also uniquely suited to exploring this question.<sup>9</sup> Not only do our complexes possess rich spectroscopic and redox properties, they also directly access the DNA base stack. The crystal structure of the  $\Delta\text{-}\alpha\text{-}[\text{Rh}[(\text{R,R})\text{-Me}_2\text{trien}]\text{phi}]^{3+}$  complex shows deep intercalation of the phi ligand without disruption or kinking of the base pairs; in fact, the phi intercalator resembles another base pair simply inserted within the helix.<sup>5</sup> This access to the DNA base stack is typical of our metallointercalators and is critical to answering questions about DNA charge transport.

In an early experiment  $[\text{Rh}(\text{phi})_2\text{phen}]^{3+}$ , an electron acceptor, and  $[\text{Ru}(\text{phen})_2(\text{dppz})]^{2+}$ , an electron donor, were covalently attached to opposite ends of a DNA helix, and DNA was tested as a medium for electron transfer. For this pair of metallointercalators, separated by approximately 40 Å, the electron transfer rate was too

fast to be measured, and the  $\beta$  value was estimated at  $< 0.2 \text{ \AA}^{-1}$ .<sup>17</sup> DNA not only serves as a bridge for electron transfer, but also can serve as a reactant. With covalently attached metallointercalators we also have observed oxidative damage to DNA and the repair of a thymine dimer lesion from a distance.<sup>18,19</sup> When irradiated at low energy, tethered rhodium or ruthenium intercalators produce long-range oxidative damage at 5'-GG-3' sites, the sites with lowest oxidation potential. This long-range damage has been demonstrated over distances as great as 200  $\text{\AA}$ .<sup>20</sup> By constructing well-defined DNA assemblies with tethered metallointercalators, we have been able to systematically explore the impact of sequence and structure on DNA charge transport. These experiments are providing new insights into the mechanism of DNA charge transport.

### 1.3. Attaching Peptides to Metallointercalators

As we tuned and tampered with our metallointercalators to achieve novel properties, we began to consider the creation of metallointercalator-peptide chimeras. These chimeras would combine the high-affinity DNA binding, the spectroscopic properties, and the photocleavage chemistry of our metallointercalator with the attractive features of peptide chemistry. Metallointercalator-peptide chimeras are promising for a number of reasons. First, through solid-phase synthesis, peptides are conveniently prepared and purified. Since they are composed of readily available building blocks, it is facile to tune the peptide composition to achieve the desired properties and variations. In addition, strategies have been developed for promoting helical or hairpin

conformations, even in very short peptides.<sup>21</sup> The naturally occurring amino acids provide a diverse collection of functional groups that may augment and alter the DNA binding properties and the reactivity of our metallointercalators. Finally, by using the very functional groups that DNA binding proteins and nucleases employ, we create conjugates with biological relevance.

### 1.3.1. Synthesis of Metallointercalator-Peptide Conjugates.

We have developed general methods for coupling peptides to metallointercalators to achieve both interesting DNA recognition and reaction.<sup>22</sup> Two sequence neutral metallointercalators,  $[\text{Rh}(\text{phi})_2\text{bpy}]^{3+}$  and  $[\text{Rh}(\text{phi})_2\text{phen}]^{3+}$ , have been harnessed for the delivery of peptides to DNA. These phenanthrenequinone diimine complexes of rhodium bind DNA with high affinity ( $K_b > 10^6 \text{ M}^{-1}$ ) and with little sequence selectivity.<sup>23,24</sup> With photoactivation they cleave the DNA backbone. The ancillary bpy and phen ligands were modified with a carboxylate linker and coupled to peptides by formation of an amide bond.

Two different solid-phase strategies were used for the construction of metallointercalator-peptide chimeras (Figure 1.3). One approach involved the direct coupling of the coordinatively saturated rhodium complex bearing a carboxylate arm to the N-terminus of a resin-bound peptide. The second approach involved the coupling of the bidentate ligand with the carboxylate arm to the resin-bound peptide, and then in a second step, formation of the desired rhodium coordination complex. The coordination complex was stable during peptide deprotection and cleavage. Both strategies afforded the conjugate cleanly but with modest overall yield (5 to 20%).

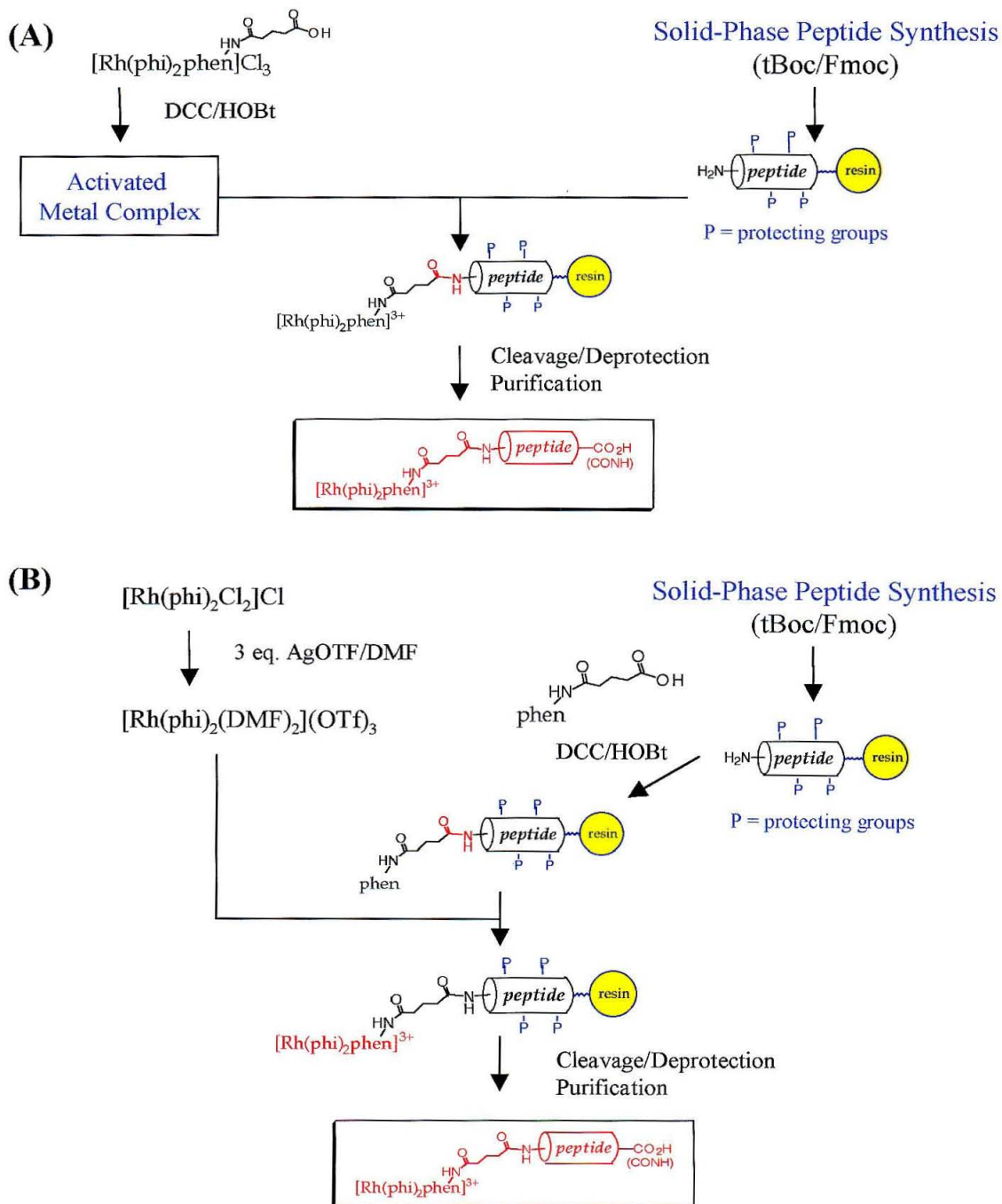


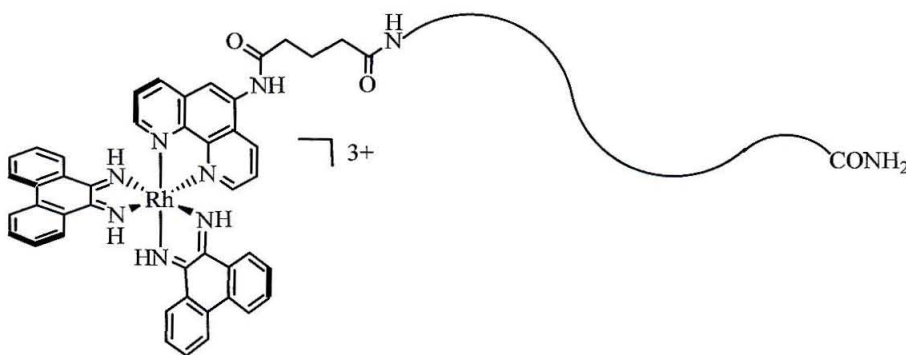
**Figure 1.3. Synthesis of Metallointercalator Peptide Conjugates.** We employed two different strategies for the synthesis of our conjugates: (A) direct coupling of complex and peptide, and (B) coupling of ligand and peptide, followed by complex formation.

### 1.3.2. Novel DNA Recognition Properties with Tethered Peptides.

Can we alter the DNA selectivity of metallointercalators with tethered peptides? Can we mimic and perhaps compete with natural DNA binding proteins by forming simple metallointercalator-peptide conjugates? To explore these questions we attached the recognition helices of two DNA binding proteins to sequence neutral DNA metallointercalators.<sup>25,26</sup>

The phage 434 repressor and the phage P<sub>22</sub> repressor provided a starting point for conjugate design. Both of these proteins use short helical peptides for specific DNA binding. When extracted from their protein architecture, these recognition helices display very low affinity for DNA ( $K_d \sim 10^3 \text{ M}^{-1}$ );<sup>25</sup> therefore, in our experiments, the intercalating rhodium complex plays an essential role. It provides DNA binding affinity and delivers the peptide to the major groove. The photocleavage chemistry of the complex also supplies a convenient strategy for identifying the DNA binding sites of the conjugates. By attaching simple helical peptides to metallointercalators, we created a family of conjugates that recognized specific DNA sites (Table 1.1). Although these conjugates did not capture all the features of natural DNA binding proteins, they did provide an interesting model system for exploring the principles of DNA binding and recognition.

First, we constructed metallointercalator-peptide complexes using peptides derived from the DNA recognition helix of the phage 434 repressor.<sup>25</sup> An 11-mer peptide ( $\alpha$ ) with the native sequence and a 14-mer peptide ( $\alpha_A$ ) with extra lysine residues and an alanine tail were attached to  $[\text{Rh}(\text{phi})_2\text{phen}']^{3+}$  ( $\text{phen}' = 5\text{-(amido glutaric acid)-1,10-phenanthroline}$ ) (Table 1.1). The helical content of the tethered peptides was found to be

**Table 1.1. DNA Recognition by Peptide Conjugates of [Rh(phi)<sub>2</sub>phen']<sup>3+</sup>.**

conjugate	peptide	DNA site <sup>a</sup>	K <sub>d</sub> <sup>b</sup> (x 10 <sup>8</sup> M)
<i>Derived from 434R Recognition Helix:</i>			
Rh-434R-α	T Q Q S I E Q L Q N G-CONH <sub>2</sub>	5'-NACAA-3'	
Rh-434R-α <sub>A</sub>	T Q Q S K K Q L Q N K A A A-CONH <sub>2</sub>	5'-NACAA-3'	
<i>Derived from P<sub>22</sub> Recognition Helix:</i>			
Rh-P <sub>22</sub> [E10]	A A N V A I A A W <b>R</b> E R A A-CONH <sub>2</sub>	5'-CCA-3'	5.7 ± 0.12
Rh-P <sub>22</sub> [D10]	A A N V A I A A W <b>D</b> R A A-CONH <sub>2</sub>		
Rh-P <sub>22</sub> [KKE10]	A A <b>K</b> V A I S Q <b>K</b> E R A A-CONH <sub>2</sub>	5'-CCA-3'	
Rh-P <sub>22</sub> [E6]	A A N V A <b>E</b> A A W A R A A-CONH <sub>2</sub>	5'-ACA-3'	9.9 ± 1.2
Rh-P <sub>22</sub> [E6E10]	A A N V A <b>E</b> A A W <b>E</b> R A A-CONH <sub>2</sub>	5'-CCA-3'	3.0 ± 0.5
Rh-P <sub>22</sub> [R6]	A A N V A <b>R</b> A A W A R A A-CONH <sub>2</sub>	5'-(G/T)CA-3'	

<sup>a</sup> The primary photocleavage site is indicated in bold.

<sup>b</sup> Dissociation constants were measured at 55 °C in the presence of 5 mM MnCl<sub>2</sub>, except Rh-P<sub>22</sub>[E6E10], which was measured in the absence of MnCl<sub>2</sub>. The dissociation constant of [Rh(phi)<sub>2</sub>phen']<sup>3+</sup> with random-sequence DNA is (7.0 ± 0.5) x 10<sup>-7</sup> M.



very low (12-15%) by circular dichroism;<sup>25</sup> nonetheless, the chimeras reproduced some features of operator recognition by the native 434R. The chimeras preferentially targeted the 5'-NACAA-3' site (N = any nucleotide, cleavage at italicized bases) and single-base variants of this site. The consensus operator half-site for 434R is actually 5'-ACAATAT-3', but only the 5'-ACAA-3' sequence is strictly conserved or directly contacted by the three Gln residues of the recognition helix.<sup>25</sup> The Rh-434R- $\alpha_A$  conjugate cleaved DNA at concentrations as low as 50 nM, and in chemical footprinting experiments, protected 7 to 10 base pairs of DNA around the target sites.

Though the conjugate mimicked the DNA recognition of the native protein, it did not match the selectivity of the 434R protein. The protein shows a 150-fold difference in selectivity for the 5'-ACAA-3' site relative to 5'-ACAN-3' or 5'-ACNA-3' sites. In contrast, the chimera only showed a four- to sixfold difference in photocleavage at the six operator site variants, and actually showed a slight preference for 5'-ACGA-3' over 5'-ACAA-3'.<sup>25</sup>

Tethering a peptide to the rhodium intercalator altered both the overall DNA binding affinity and the site selectivity. Specific photocleavage was observed at  $\leq 50$  nM rhodium-peptide concentrations, and no cleavage was detectable with  $[\text{Rh}(\text{phi})_2\text{phen}]^{3+}$  at these concentrations. The attachment of the peptide increased the binding affinity by more than an order of magnitude. At concentrations  $\geq 0.5$   $\mu\text{M}$ , the uncoupled rhodium complex cleaves DNA with a modest preference for 5'-ACA-3' and 5'-ATG-3'. Because the metal-peptide conjugate and the bare metal complex both preferentially cleave at these sites, it is not possible to neatly dissect the contribution of the complex and the peptide to selectivity. In addition, the  $\Delta$  isomer of the conjugate showed a two- to

threefold enhancement in photocleavage over the  $\Lambda$  isomer at the strongest sites. With the Rh-434R- $\alpha_A$  conjugate, recognition clearly depended on both the metallointercalator and the appended peptide.

We also constructed a family of metallointercalator-peptide conjugates containing peptides derived from the DNA recognition helix of the P<sub>22</sub> repressor (Table 1.1). Attachment of a 13-mer peptide (AANVAISQWERA-CONH<sub>2</sub>) based on this helix to [Rh(phi)<sub>2</sub>phen']<sup>3+</sup> produced a chimera that was specific for 5'-CCA-3' sites (photocleavage at italicized A).<sup>26</sup> In contrast to our results with the 434R conjugates, this conjugate does not target the natural binding site of the P<sub>22</sub> repressor protein. The tethered peptide also employs different residues than the natural protein to generate specific binding; indeed, the glutamate residue in position 10 of the tethered peptide, a residue that is actually buried in the native protein, was found to be absolutely essential to the selective recognition.<sup>26</sup> Though all other functional groups in the peptide could be mutated to alanine, even conservative changes of the glutamate abolished selectivity for 5'-CCA-3'. For example, incorporating glutamine, aspartate, or methylated glutamate at position 10 destroyed the selectivity of the complex.

How does a single carboxylate provide selectivity for a three base pair site? Circular dichroism studies suggested that glutamate was acting as a conformational switch in the peptide. There was a striking decrease in the helicity of the tethered peptide when the glutamate was mutated to aspartate.<sup>26</sup> There was also a correlation between the helical content of the peptide and the selectivity for the 5'-CCA-3' site. The specificity for this site was enhanced under conditions that favor helix formation: the addition of trifluoroethanol, the addition of divalent cations (Mn<sup>2+</sup>, Mg<sup>2+</sup>), and the elevation of

temperature (55 °C). In addition to serving as a conformational switch, it is possible that glutamate also participated in direct contacts with the preferred site; there is precedence for the specific interaction of glutamate side chains with the N4 of cytosine.<sup>26</sup> Additionally, shape selection may tune the complex for the 5'-CCA-3' site. There is evidence that 5'-Py-Py-Pu-3' sequences are somewhat open in the major groove, and this open groove may better accommodate the metallointercalator and the tethered peptide.<sup>26</sup> We modeled the interactions of the Rh-P<sub>22</sub>[E10] conjugate with a 5'-CCA-3' site, and the result is presented in Figure 1.4.<sup>26,27</sup>

Interestingly, single amino acid changes in the Rh-P<sub>22</sub>[E<sub>10</sub>] peptide produced multiple changes in the targeted base sequence. Switching the glutamate from position 10 to position 6 of the peptide generated a chimera that was specific for 5'-ACA-3' sites.<sup>27</sup> Removing the glutamate at position 10 and incorporating an arginine residue at position 6 resulted in more complex changes in the DNA recognition.<sup>27</sup> The Rh-P<sub>22</sub>[R6] complex preferred the 5'-(T/G)CA-3' site, but also targeted some sequences that differed from its consensus sequence by one base pair. These complex changes in selectivity may reflect a shift in the position of the  $\alpha$ -helix relative to the DNA,<sup>27</sup> and illustrate the difficulty of predictive tuning of sequence selectivity.

Through photocleavage titrations the dissociation constants of several metallointercalator-peptide conjugates were determined (Table 1.1).<sup>27</sup> As observed with DNA binding proteins, the Rh-P<sub>22</sub>[E10] complex derives most of its free energy of binding from a fairly sequence-neutral interaction (intercalation), and derives sequence discrimination from interactions between the peptide and the 5'-CCA-3' sequence. Comparison of the dissociation constant of Rh-P<sub>22</sub>[E10] for a 5'-CCA-3' site and the

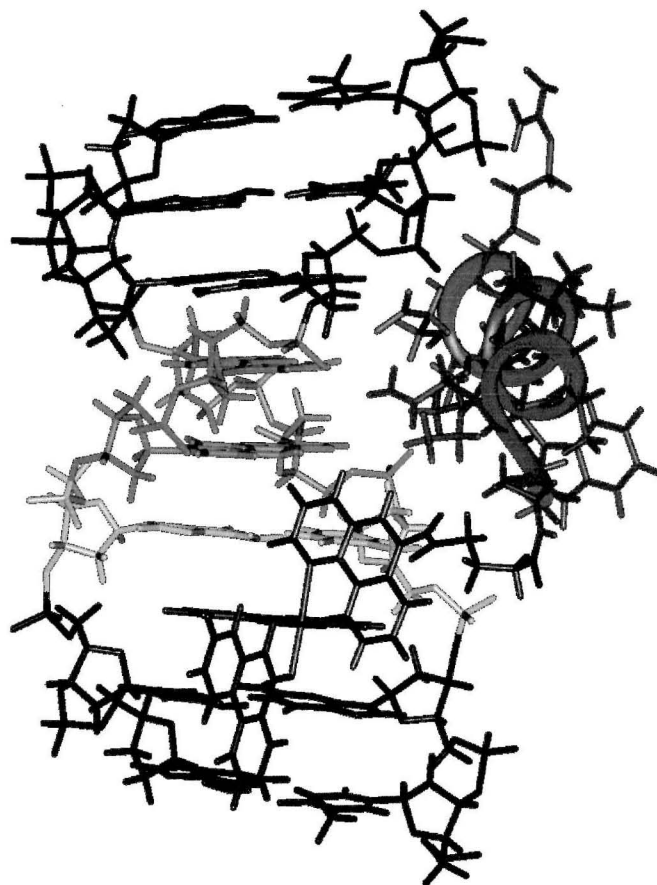


**Figure 1.4. A Model for Recognition with a Metallointercalator-Peptide Conjugate.**

According to our model, the Rh-[E10] complex assumes a helical conformation on DNA binding and Glu10 makes a base specific contact with the 5'-cytosine of a 5'-CCA-3' site. The base pairs recognized by the complex are shown in light gray. From photocleavage studies we know that the conjugate intercalates to the 3' side of adenine, and binds asymmetrically in the major groove. The refined model was constructed by energy minimization with restraints on the DNA structure, the relative position of Glu10 and the 5'-cytosine, and with the peptide starting in a canonical  $\alpha$ -helical conformation. The  $\Delta$  and  $\Lambda$  isomers of the conjugate targeted DNA with similar affinity, and for simplicity we modeled the  $\Delta$  isomer. Figure adapted from Hastings et al.<sup>27</sup>

dissociation constant of  $[\text{Rh}(\text{phi})_2\text{phen}']^{3+}$  for random-sequence DNA suggests a 1.7 kcal mol<sup>-1</sup> energetic advantage for binding of the conjugate at the 5'-CCA-3' site.<sup>27</sup>

Metallointercalators effectively deliver short peptides to DNA, and the functional groups in the peptide can augment and alter the binding affinity and selectivity of the construct. But metallointercalator-peptide conjugates are limited as mimics of naturally occurring DNA binding proteins. The metallointercalator binds to DNA with affinities that approach those of proteins ( $K_b = 10^6$  to  $10^{10} \text{ M}^{-1}$ ), but in contrast to proteins, they are not able to direct the secondary conformation of a peptide fragment or control the orientation of a fragment relative to DNA. The architecture of a DNA binding protein not only provides nonspecific binding affinity for the DNA but also predictably folds and positions the residues that will make specific contacts with DNA bases. The flexibility of our tethered peptide makes predictive design of site-specific chimeras unrealistic.

### 1.3.3. Novel Reactions with Tethered Peptides.

In addition to modifying the DNA binding properties of our metallointercalators by the attachment of peptides, we have also created metallointercalator-peptide conjugates that can mediate a variety of reactions with DNA. The functional groups in the tethered peptide are no longer exploited for DNA recognition, but rather for reaction. We included amino acid residues that coordinate metals or serve as nucleophiles.

Initially, we were interested in DNA hydrolysis (Figure 1.5). In the hydrolysis reaction, water attacks the phosphorus center to give a pentacoordinate intermediate. The intermediate collapses to give one of two sets of products, either a 3'-hydroxyl and 5'-phosphate or a 5'-hydroxyl and 3'-phosphate. The nuclease enzymes that catalyze this

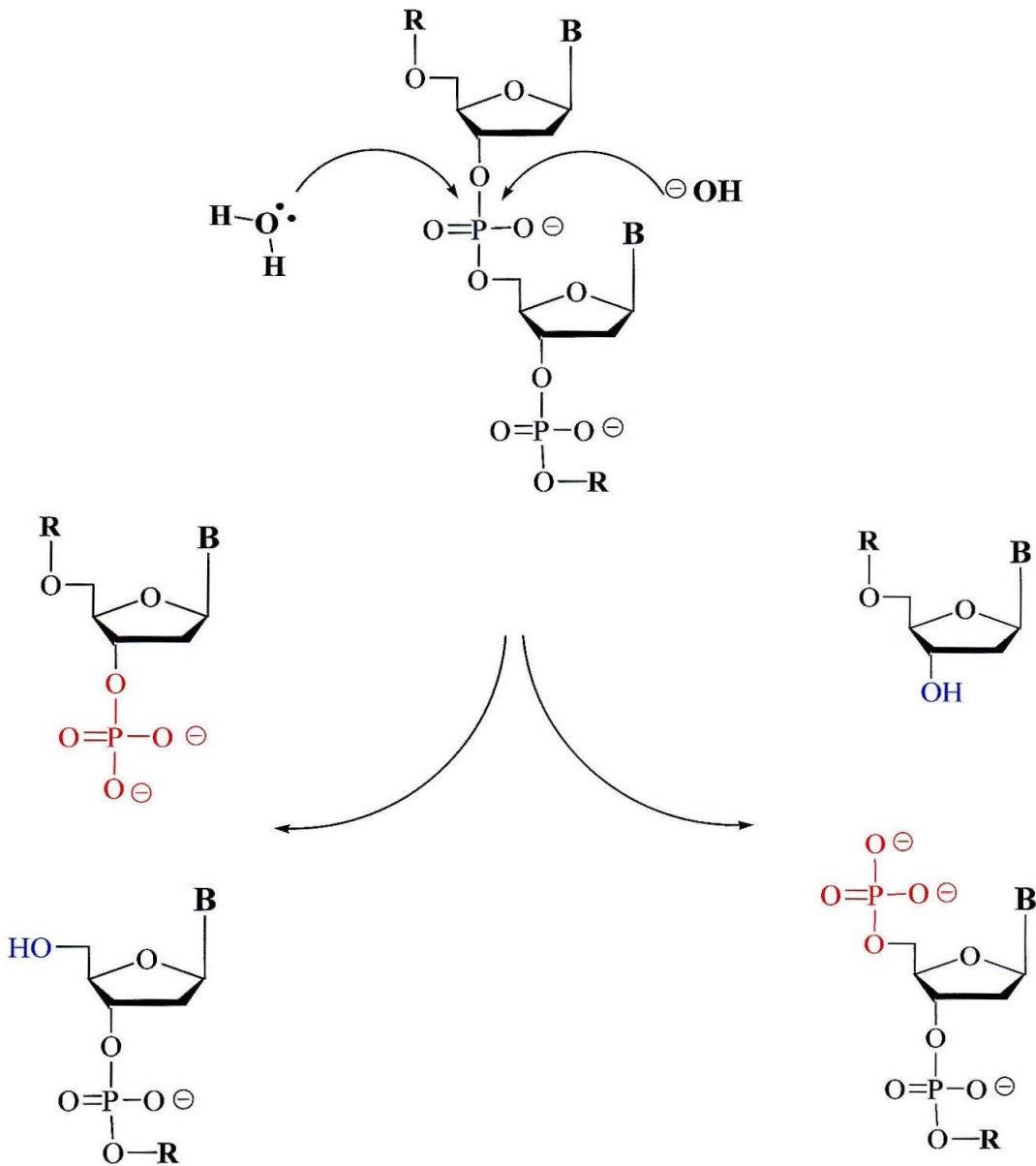


**Figure 1.5. DNA Hydrolysis.** Nucleophilic attack of water or hydroxide at phosphorus causes strand scission. The resulting products are either 3'-phosphates and 5'-hydroxyls, or as is observed with most naturally occurring enzymes, 5'-phosphates and 3'-hydroxyls.

reaction typically employ metal ions, and we have designed and tethered peptides that can coordinate metal ions. Can we mimic natural nucleases with these intercalator-peptide chimeras? Can we design a small molecular tool for hydrolysis of the stable phosphodiester backbone?

## **1.4. A Metallointercalator-Peptide Conjugate for DNA Hydrolysis**

### **1.4.1. DNA Hydrolysis.**

The phosphodiester bonds of DNA and RNA are remarkably resistant to hydrolysis under physiological conditions.<sup>2,3,28</sup> The half-life of DNA is 200 million years, and the half-life of RNA, shortened considerably by the presence of an intramolecular nucleophile, is 800 years.<sup>3</sup> By recruiting metal cofactors and forming extensive contacts with the nucleic acid substrate, nucleases are able to accelerate the phosphodiester hydrolysis reaction by factors as great as  $10^{16}$ , and thus make possible the manipulations of DNA and RNA that are essential for life.<sup>4</sup> Although many of these enzymes have been harnessed for use in the laboratory, there is a great deal of interest in the design of artificial nucleases, small molecular scissors that can bind at a specific sequence of interest and cleave DNA or RNA hydrolytically to produce phosphate and hydroxy termini (Figure 1.5). Such reagents would eliminate many of the potential problems (instability, stringent conditions, etc.) associated with the larger, natural DNA-binding enzymes, and would have wide applicability as tools in molecular biology, as probes of the structure and function of nucleic acids, or as therapeutic agents.

Customized artificial restriction enzymes with expanded recognition sites would be particularly useful for manipulation and sequencing of genomic DNA samples. In addition, well-characterized small molecules may provide insight into the roles metals play in natural hydrolases.<sup>29</sup>

To serve as a practical laboratory tool, to cleave RNA within minutes, an artificial ribonuclease must enhance the rate of hydrolysis by a factor of  $10^8$ . In contrast, rapid cleavage of DNA, requires  $10^{17}$ -fold rate enhancement.<sup>3</sup> The 2'-hydroxyl, by providing a built-in nucleophile, greatly facilitates the design of artificial ribonucleases. In addition, specific sites in single-stranded RNA can be conveniently targeted by the attachment of an artificial nuclease to complementary oligonucleotides. For these reasons, significant strides have been made towards small molecules for sequence specific RNA transesterification and hydrolysis.<sup>30,31</sup> Biomimetic hydrolysis of double-stranded DNA is a far more difficult goal, and there have been fewer successes.

A number of small molecules that cleave DNA by oxidative mechanisms have been developed.  $\text{Fe(EDTA)}^{2-}$  and  $[\text{Cu(phen)}_2]^+$  are two widely used and well-studied examples.<sup>32-34</sup> Although small molecules that promote oxidative strand scission are useful for many applications, they are not suited to all applications, and they do not contribute to our understanding of natural hydrolases. In contrast to hydrolytic agents, oxidative agents form products that are incompatible with enzymatic manipulation. In addition, some oxidative molecules create diffusible oxygen species and thus cause indiscriminate damage to DNA. Finally, oxidative agents require activation by light or the addition of an oxidant, and this limits their therapeutic potential.<sup>35</sup>



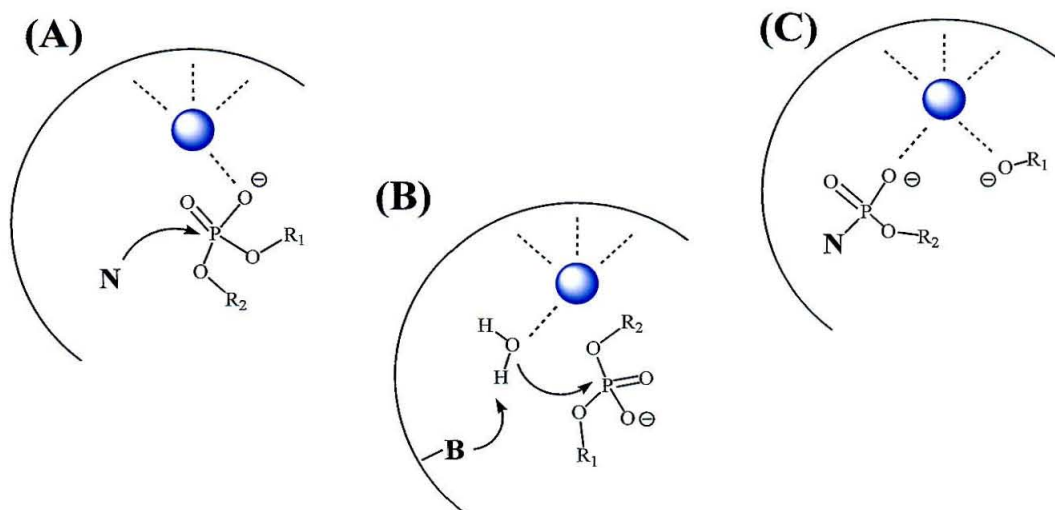
### 1.4.2. DNA Hydrolysis Promoted by Metal Ions and Complexes.

Though the imitation of deoxyribonucleases is a challenging goal, a small collection of molecules has been reported to cleave DNA hydrolytically. Natural nucleases employ metal ions, often more than one, for hydrolysis. The metal ions most frequently used are  $\text{Mg}^{2+}$ ,  $\text{Zn}^{2+}$ ,  $\text{Mn}^{2+}$ ,  $\text{Ca}^{2+}$ , and  $\text{Fe}^{2+}$ .<sup>29,36</sup> The metals play a critical role by activating water to serve as a nucleophile, activating the electrophile for the attack, or stabilizing the leaving group (Figure 1.6).<sup>3</sup> Taking their cue from nature, essentially all of the artificial nucleases also rely on transition metals or lanthanide metals for hydrolysis of the DNA backbone. Recent design efforts have combined metals with a variety of organic ligands, peptides, and antibiotics.<sup>37</sup>

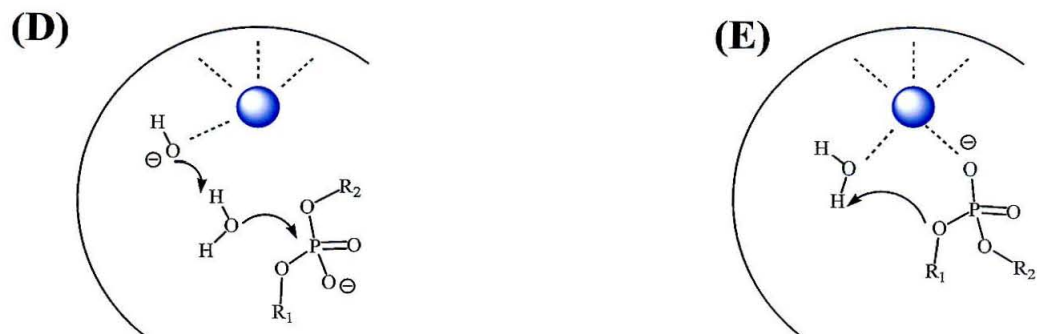
***Transition Metal Complexes for DNA Hydrolysis.*** The very first synthetic metal complex for DNA hydrolysis emerged from the Barton group.<sup>38,39</sup> The  $\text{Ru}(\text{DIP})_2\text{Macro}^{2+}$  (DIP = diphenylphenanthroline) complex binds to DNA by intercalation and bears two polyamine arms which coordinate and direct metal ions to the sugar phosphate backbone (Table 1.2). In the presence of copper (II), hydrogen peroxide, and a reducing agent this creature causes oxidative cleavage of DNA. In the presence of metals which are not redox active, such as zinc (II), cadmium (II), or lead (II), the  $\text{Ru}(\text{DIP})_2\text{Macro}^{2+}$  complex promotes hydrolysis of DNA. The complex gives products that are compatible with enzymatic manipulation; the nicks in a supercoiled plasmid can be religated with T4 DNA ligase.  $\text{Ru}(\text{DIP})_2\text{Macro}^{2+}$  serves two important roles; it supplies binding affinity for DNA and creates a scaffold to orient active metal centers.

Stable cobalt (III) complexes have been employed for years in the hydrolytic cleavage of amides, esters, and phosphates, and more recently they have been

## Direct Modes of Activation

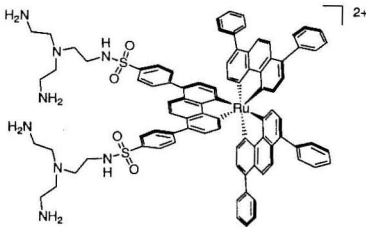
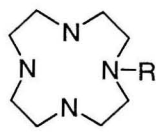
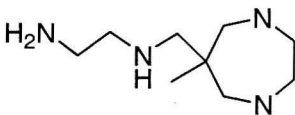
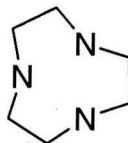
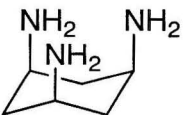



## Indirect Modes of Activation

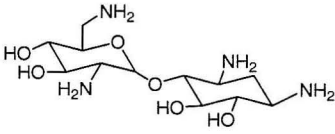
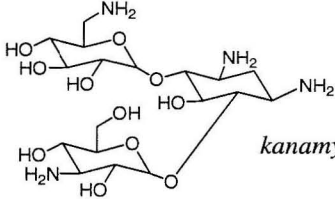
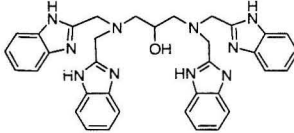
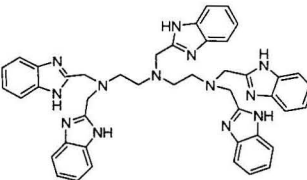
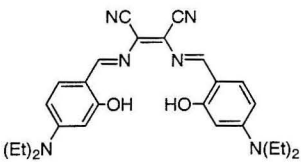
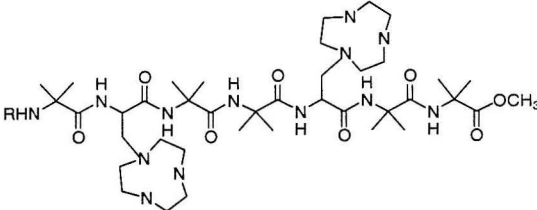
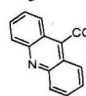


**Figure 1.6. Roles of Metal Ions in Promoting DNA Hydrolysis.** A metal ion can activate the phosphate ester bond for hydrolysis by several inner sphere mechanisms: **(A)** Lewis acid activation, **(B)** nucleophilic activation, or **(C)** leaving group activation. Additionally, a metal-coordinated hydroxide can act as a **(D)** general base catalyst or **(E)** general acid catalyst. Electrostatic interaction between the metal and uncoordinated phosphate ester may also accelerate hydrolysis.

**Table 1.2. Transition Metal Complexes for DNA Hydrolysis.**

Metal Ion	Ligand or Complex	Reference
$\text{Zn}^{2+}$ $\text{Cd}^{3+}$ $\text{Pb}^{2+}$		[38, 39]
$\text{Co}^{3+}$	<i>cyclen</i> 	[40]
	$\text{R} = \text{H}$ $\text{R} = [(\text{CH}_2)_6\text{N}^+(\text{CH}_3)_2]_2-(\text{CH}_2)_6\text{-cyclen}$	[41]
$\text{Co}^{3+}$	 <i>tamen</i>	[40]
$\text{Cu}^{2+}$	 <i>[9]-ane N<sub>3</sub></i>	[35]
$\text{Cu}^{2+}$	 <i>tach</i>	[44]
$\text{Cu}^{2+}$	 <i>His</i>	[45]

**Table 1.2. Transition Metal Complexes for DNA Hydrolysis. (Continued)**

Metal Ion	Ligand or Complex	Reference
$\text{Cu}^{2+}$	<i>neamine</i> 	[46]
$\text{Cu}^{2+}$	 <i>kanamycin A</i>	[42]
$2\text{Fe}^{3+}$	 <i>HPTB</i>	[47]
$2\text{Fe}^{3+}$	<i>DTPB</i> 	[48]
$2\text{Cr}^{3+}$		[49]
$\text{Zn}^{2+}$	 $\text{R} = \text{CH}_3\text{CO}$ $\text{R} = $ 	[51]

demonstrated to promote DNA hydrolysis. Tetraamine aqua hydroxo Co(III) complexes with the cyclen (1,4,7,10-tetraazacyclododecane) ligand or tamen (6-(4-amino-2-azabutyl)-6-methyl-1,4-diazacycloheptane)) ligand provide  $10^6$ -fold rate enhancements in plasmid hydrolysis (Table 1.2).<sup>40,41</sup> The mechanism of Co(III) promoted hydrolysis has been studied extensively with phosphate esters, and involves both Lewis acid activation of the phosphate and nucleophilic attack of a coordinated hydroxide.<sup>42</sup> The tetraamine ligands force a cis configuration of the labile coordination sites, and thus provide a template that positions the substrate and nucleophile for intramolecular attack. The  $pK_a$  of the coordinated water is estimated to be between 5 and 8. Cobalt complexes are substitutionally inert, and though they effectively promote hydrolysis, they do not show turnover behavior.<sup>42</sup> The affinity for DNA and thus the rate of hydrolysis can be increased by attaching peralkylammonium groups to the cobalt complexes or by linking two cyclen centers with a positively charged linker.<sup>41</sup>

A variety of copper (II) complexes have also been applied to DNA hydrolysis (Table 1.2); however, many of these complexes can also oxidize DNA in the presence of reducing agents, and this complicates both analysis and application. Macrocyclic copper complexes,  $Cu([9]aneN_3)^{2+}$  and  $Cu(i-Pr_3[9]aneN_3)^{2+}$ , cleave both single-stranded and double-stranded plasmid DNA near physiological pH and temperature.<sup>35,43</sup> With these complexes, DNA cleavage is reduced by 30% under anaerobic conditions, suggesting both an oxygen-dependent and an oxygen-independent mechanism. Though oxygen must be carefully excluded to favor the hydrolytic path, these copper complexes are well characterized and suitable for mechanistic studies.<sup>43</sup> Building on the promise of macrocyclic triamine complexes, a more active copper complex was created by the use of

the tach (cis,cis-1,3,5-triaminocyclohexane) ligand.<sup>44</sup> In addition, although the active species has not been characterized, recent studies show that a 3:1 mixture of copper chloride and L-histidine, when added to DNA substrates in large excess, effects hydrolysis of both dideoxynucleotides and plasmid.<sup>45</sup> Finally, the most efficient artificial nucleases reported to date are Cu(II) complexes of aminoglycosides.<sup>46</sup> Copper(II)-neamine and copper(II)-(kanamycin A) effectively cleave DNA in both the presence and absence of external reducing agents, and in contrast to most artificial nucleases, these complexes do show true catalytic behavior with turnover numbers of at least 100. The aminoglycosides display binding affinities of  $10^4$  to  $10^5 \text{ M}^{-1}$ , and this greatly enhances the reactivity of the copper center. Though direct product analysis has not been possible, several lines of evidence suggest a hydrolytic mechanism in the absence of reducing agents.

There have been a handful of reports of iron complexes that cleave DNA by hydrolytic mechanisms. Iron complexes are well known for their efficient oxidative DNA cleavage, or Fenton chemistry, and establishing a hydrolytic mechanism brings a heavy burden of proof. Several years ago, a dinuclear iron complex,  $\text{Fe}_2(\text{HPTB})(\text{OH})(\text{NO}_3)_4$  (HPTB = N, N, N', N'-tetrakis (2-benzimidazolylmethyl)-2-hydroxy-1,3-diaminopropane) was found to cleave plasmid DNA in the presence of  $\text{O}_2$  or  $\text{H}_2\text{O}_2$  and a reductant.<sup>47</sup> Interestingly, the termini produced in this reaction could be efficiently religated, and the authors suggested a "hydrolytic-like" mechanism in which a coordinated peroxide attacked the scissile phosphate to give exclusively 3'-hydroxyls and 5'-phosphates. Very recently, yet another dinuclear iron complex,  $\text{Fe}_2(\text{DTPB})(\mu\text{-O})(\mu\text{-Ac})\text{Cl}(\text{BF}_4)_2$  (DTPB = 1,1,4,7,7-penta(2'-benzimidazol-2-ylmethyl)-triazasheptane, Ac =

acetate) was applied to DNA hydrolysis.<sup>48</sup> This complex was found to cleave plasmid DNA and DNA restriction fragments under anaerobic conditions and without the addition of co-reactants. A  $10^{10}$ -fold enhancement was reported for plasmid cleavage, and the products of the cleavage reaction were compatible with enzymatic manipulation.

Though the evidence for a hydrolytic mechanism is rather sparse, there was also a recent report of plasmid hydrolysis with a chromium (III) complex.<sup>49</sup>  $\text{Cr}^{3+}$  was combined with a Schiff base ligand. This complex was found to bind weakly to DNA ( $K_b = 1.3 \times 10^3 \text{ M}^{-1}$ ), and to promote the conversion of supercoiled plasmid to the nicked and linear forms. Based on comparisons between different Schiff base ligands, it was proposed that pendant alkyl amines played a critical role in the cleavage reaction.

Salts and amino alcohol complexes of zirconium (IV) have been demonstrated to efficiently cleave both activated phosphodiester and a dinucleotide substrate.<sup>50</sup> Cleavage studies were carried out with a large excess of metal ion, 5 mM  $\text{Zr}^{4+}$ , and at pH 4 to prevent the precipitation of zirconium hydroxide. Though the efficiency of  $\text{Zr}^{4+}$  for DNA hydrolysis approaches that of the highly active  $\text{Ce}^{4+}$ , this metal ion is not compatible with physiological conditions.

Complexes with  $\text{Zn(II)}$  are particularly interesting because zinc does not access other redox states under physiological conditions; there is no possibility of oxidative cleavage. In addition,  $\text{Zn}^{2+}$  is commonly found in multi-nuclear transition metal centers in natural hydrolases. Using a strategy that is quite similar to the strategy employed in the Barton group, Sissi et al. created a heptapeptide with two artificial triazacyclononane residues for  $\text{Zn}^{2+}$  coordination (Table 1.2).<sup>51</sup> They used  $\text{C}^\alpha$ -tetrasubstituted  $\alpha$ -aminoisobutyric acid residues to induce a  $3_{10}$ -helix and thus position the  $\text{Zn}^{2+}$  centers on

one face of the peptide.<sup>52</sup> This dinuclear  $\text{Zn}^{2+}$  complex was active for plasmid hydrolysis, and showed evidence of cooperativity between the two metal centers; the dinuclear complex is 20 times more active than the mononuclear.<sup>51</sup> By attaching an acridine intercalator to the N-terminus of the peptide, the activity was improved for low complex concentrations.<sup>51</sup>

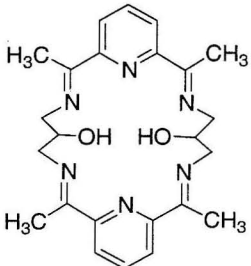
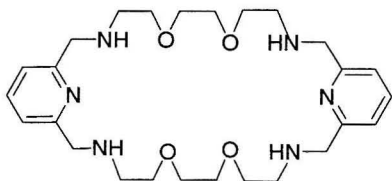
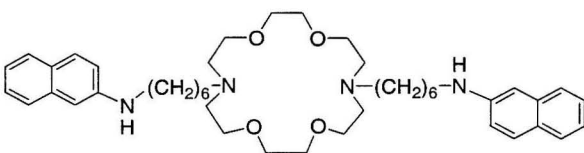
***Lanthanide Metals and Complexes for DNA Hydrolysis.*** The high charge densities, the high coordination numbers, and the fast ligand exchange rates of lanthanide ions make them very good candidates for artificial nuclease design efforts.<sup>36</sup> Many of the transition metal systems used for DNA cleavage must be tuned to avoid oxidative mechanisms, but apart from cerium, lanthanides have no accessible redox chemistry.<sup>36</sup> The free lanthanide (III) metals readily promote DNA hydrolysis,<sup>53</sup> but also precipitate as hydroxides near pH 9, and are toxic to biological systems.<sup>36</sup>

Effective ligand systems are required if researchers are to control and characterize lanthanide-mediated hydrolysis. Rapid ligand exchange is essential for effective catalysis, but it is also an obstacle to the design of a kinetically and thermodynamically stable ligand system.<sup>36</sup> It is difficult to package lanthanides without reducing their hydrolytic activity, and a wide variety of packaging materials have been considered.

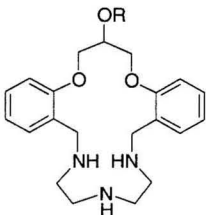
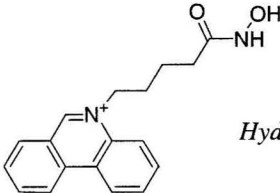
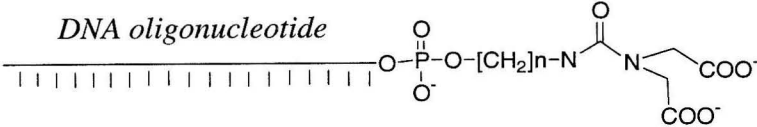
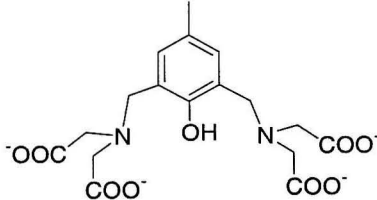
Lanthanide metals have been encapsulated with Schiff base macrocycles, crown ethers and azacrowns, polyaminocarboxylates, and peptide structures.<sup>36</sup> Morrow et al. originally demonstrated that Schiff base  $\text{Ln(III)}$  complexes could catalyze RNA hydrolysis,<sup>54</sup> and larger macrocycles that form binuclear complexes with  $\text{Ho}^{3+}$  or  $\text{Er}^{3+}$ , have since been applied to DNA plasmid hydrolysis (Table 1.3).<sup>55</sup> Complexes of  $\text{Eu(III)}$  or  $\text{Pr(III)}$  with nitrogen and oxygen-containing ionophores have been found to cleave



**Table 1.3. Lanthanide Complexes for DNA Hydrolysis.**

Metal Ion	Ligand or Complex	Reference
$\text{La}^{3+}$ $\text{Eu}^{3+}$ $\text{Pr}^{3+}$ $\text{Ce}^{3+}$	<i>Free metal</i> 0.05 to 10 mM	[53]
$\text{Ce}^{4+}$	<i>Free metal</i>	[66]
$2 \text{ Ho}^{3+}$ $2 \text{ Er}^{3+}$	 <i>Schiff-base Macrocycle</i>	[55]
$2 \text{ Pr}^{3+}$		[57]
$\text{Eu}^{3+}$		[56]

**Table 1.3. Lanthanide Complexes for DNA Hydrolysis. (Continued)**

Metal Ion	Ligand or Complex	Reference
Ln library	 <p data-bbox="747 407 897 468">M = Gd R = <math>\beta</math>-naphthyl</p> <p data-bbox="683 535 953 563"><i>Azacrown Ether Scaffold</i></p>	[58]
2 Eu <sup>3+</sup>	 <p data-bbox="683 854 873 883"><i>Hydroxamic Acid</i></p>	[61]
Ce <sup>4+</sup>	<p data-bbox="355 1201 631 1229"><i>DNA oligonucleotide</i></p> 	[67]
2 Ce <sup>4+</sup>	 <p data-bbox="908 1606 978 1635"><i>HXTA</i></p>	[73]

supercoiled plasmid with increased activity relative to the free metal ion, and pseudo-first-order rate constants on the order of  $10^{-4} \text{ s}^{-1}$  (Table 1.3).<sup>56,57</sup> With a parallel screening and synthesis strategy, an azacrown ether scaffold and the Gd(III) ion were selected for their ability to catalyze the hydrolysis of bis(*p*-nitrophenyl)phosphate (BNPP) and *p*-nitrophenylethyl phosphate (Table 1.3).<sup>58</sup> Though activity towards activated substrates is often a poor indicator of activity towards DNA substrates, the same metal complex was found to be effective for the cleavage of DNA plasmid. Recently, a chimeric peptide that combines helices from the engrailed homeodomain with the calcium binding loop of the EF-hand from calmodulin has been used to package and deliver lanthanide ions to DNA.<sup>59</sup> This chimera was demonstrated to bind Eu(III) and promote low levels of plasmid cleavage.<sup>60</sup> Though not exactly a small molecule, this artificial nuclease does address the need for both DNA binding and a metal active site.

Lanthanides have also been combined with polyhydroxyl ligands,<sup>56</sup> hydroxamic acids,<sup>61</sup> amino acids,<sup>62</sup> polymeric sugars,<sup>63</sup> or micelles<sup>64,65</sup> to solubilize the metal, albeit in a poorly characterized or heterogenous system.<sup>36</sup> For example, in one study an intercalator-linked hydroxamic acid was tested in plasmid relaxation studies with Ln(III) metal ions (Table 1.3). The affinity of a single hydroxamic group for  $\text{Ln}^{3+}$  is low, but presumably the intercalating ligand helps to create a binding pocket and facilitates binding of  $\text{Ln}^{3+}$  to both the DNA phosphates and hydroxamic acid group simultaneously.<sup>36,61</sup> In other studies, the addition of weakly coordinating polyalcohol ligands, such as glycerol and gluconate, or the addition of amino acid cofactors increased the rates of lanthanide-catalyzed plasmid hydrolysis by factors of 2 to 5.<sup>56,62</sup>

Cerium, because it can be oxidized to  $\text{Ce}^{4+}$ , is one of the most effective lanthanide metals for DNA hydrolysis, and has been demonstrated to hydrolyze dinucleotide and oligonucleotide substrates.<sup>66,67</sup> The high charge density of this metal ion, the formation of bimetallic hydroxoclusters, and the participation of the 4f orbitals in a weak covalent bond to phosphate oxygen combine to produce  $10^{11}$ -fold enhancements in hydrolysis.<sup>68</sup> Above pH 4,  $\text{Ce}^{4+}$  actually forms a hydroxide gel. Although efficient, this turbid system is not practical for many applications. Efforts are currently focused on the development of ligands that solubilize  $\text{Ce}^{4+}$  without reducing activity.<sup>69,70</sup> By attaching an iminodiacetate ligand to a DNA oligomer,  $\text{Ce}^{4+}$  was delivered to a complementary single-stranded DNA to promote site-specific cleavage (Table 1.3).<sup>71,72</sup> Most recently, a novel dicerium complex that cleaves both plasmid and linear DNA was reported (Table 1.3).<sup>73</sup> Notably, plasmid cleavage experiments suggest that the complex cleaves DNA by double-strand cutting.

***Progress and Problems in the Design of Artificial Nucleases.*** The artificial nucleases reported to date typically provide rate enhancements on the order of  $10^6$  to  $10^7$  (Table 1.4). It is difficult to rigorously compare the efficiency of these small molecules because they typically are tested with an excess of metal ion or metal complex relative to DNA substrate.<sup>37</sup> The reported data reflect only single turnovers, and must be corrected for the concentration of artificial nuclease. Recently, under true Michaelis-Menten conditions, the  $\text{Cu}^{2+}$  complexes of kanamycin and neamine were reported to hydrolyze DNA with greater than a millionfold rate enhancement.<sup>46</sup> This represents the most significant acceleration observed to date, and the experiments provide meaningful numbers that can be compared to other artificial or natural nucleases. The specificity

**Table 1.4. Kinetics of DNA Hydrolysis for Artificial Nucleases.<sup>a</sup>**

Complex	$K_m$ (M)	$k_{obs}$ <sup>b</sup> (s <sup>-1</sup> )	Enhancement <sup>c</sup>	$k_{obs}/K_m$ <sup>d</sup> (s <sup>-1</sup> M <sup>-1</sup> )	ref
Co <sup>3+</sup> -cyclen	9.8 x 10 <sup>-4</sup>	2.2 x 10 <sup>-4</sup>	2.0 x 10 <sup>7</sup>	0.22	[41]
Co <sup>3+</sup> -tamen	ND	5.0 x 10 <sup>-5</sup>	5.0 x 10 <sup>6</sup>	ND	[40]
Cu(9aneN <sub>3</sub> )	ND	~ 1 x 10 <sup>-5</sup>	~ 1 x 10 <sup>6</sup>	ND	[35]
Cu-neamine	3.9 x 10 <sup>-6</sup>	5.2 x 10 <sup>-4</sup>	5.2 x 10 <sup>7</sup>	130	[46]
Cu-neamine*	4.2 x 10 <sup>-5</sup>	9.9 x 10 <sup>-4</sup>	9.99 x 10 <sup>7</sup>	24	[46]
Eu <sup>3+</sup>	3.9 x 10 <sup>-5</sup>	6.9 x 10 <sup>-5</sup>	7.0 x 10 <sup>6</sup>	1.8	[56]
Eu <sup>3+</sup> -ionophore	5.7 x 10 <sup>-4</sup>	5.8 x 10 <sup>-4</sup>	5.8 x 10 <sup>7</sup>	1.0	[56]
(Pr <sup>3+</sup> ) <sub>2</sub> -ionophore	3.0 x 10 <sup>-4</sup>	2.5 x 10 <sup>-4</sup>	2.5 x 10 <sup>7</sup>	0.83	[57]
Rh-P1	ND	2.5 x 10 <sup>-5</sup>	2.5 x 10 <sup>6</sup>	ND	[75]
Mg-MutT dGTPase	2.84 x 10 <sup>-4</sup>	4.0	4.0 x 10 <sup>11</sup>	1.4 x 10 <sup>4</sup>	[37]
Mg-EcoRV	2.2 x 10 <sup>-11</sup>	1.2 x 10 <sup>-2</sup>	1.2 x 10 <sup>9</sup>	5.5 x 10 <sup>8</sup>	
Mn-EcoRV	5.0 x 10 <sup>-10</sup>	1.5 x 10 <sup>-2</sup>	1.5 x 10 <sup>9</sup>	3.0 x 10 <sup>7</sup>	

<sup>a</sup> Table adapted from Sreedhara and Cowan, 2001.<sup>37</sup> ND = no data available.

<sup>b</sup> The data listed for Cu-neamine\* was determined with excess DNA substrate and reflects a true  $k_{cat}$  value. For all other complexes a  $k_{obs}$  value, generally determined at saturation levels, is reported.

<sup>c</sup> Enhancement was determined by assuming  $k = 1 \times 10^{-11} \text{ s}^{-1}$  for unpromoted ds DNA hydrolysis.

<sup>d</sup> The specificity constants of individual complexes provide a measure of the efficiency of DNA hydrolysis.

constant for one of the most efficient artificial nucleases, Cu-neamine, is still 3 to 8 orders of magnitude shy of the specificity constants for typical enzymes (Table 1.4).

Model studies with crystallographically characterized dinuclear metal complexes have provided very valuable insights into the roles that metals play in activating a phosphodiester bond for cleavage.<sup>3</sup> There are significant advantages in placing two metal centers together for the cooperative activation of a substrate. A number of laboratories have created ligands that incorporate two metals, and this represents a promising strategy for future design.<sup>47-49,55,57,73</sup>

Most of the small molecules designed for DNA hydrolysis have very modest affinity for DNA and no selectivity for a DNA sequence. DNA binding and recognition has been largely neglected, though it is an important aspect of biomimetic hydrolysis of DNA. Occasionally researchers tack positively charged groups or acridine moieties onto their design, but very little effort has been invested in creating artificial nucleases that bind to DNA. Even complexes with modest affinity for DNA, such as the copper aminoglycosides, are a step in the right direction. To truly mimic natural nucleases, future design efforts must strive for ligands that bind to DNA with high affinity and selectivity.<sup>37</sup>

Though plasmid cleavage assays are a very convenient method for screening metals and complexes for activity, they provide a very low hurdle, and they provide very little chemical information.<sup>70,74</sup> Plasmid substrates are large and uncharacterized, and they are not compatible with direct product analysis. The inherent strain of a plasmid substrate, or the presence of a few damaged sites may contribute to reactivity. Many metal complexes that cleave plasmid substrates are inactive towards linear DNA

substrates.<sup>70</sup> Studies with dinucleotide and oligonucleotide substrates are much more challenging but also more informative.

Although progress has clearly been made towards the design of artificial nucleases for DNA hydrolysis, we are still far from creating practical laboratory tools.

#### **1.4.3. A Rhodium-Metallopeptide Conjugate for DNA Hydrolysis.**

The delivery of metal ions to DNA is a common strategy for the hydrolysis of the phosphodiester bond. Indeed, this strategy is observed both in natural nucleases and in essentially all of the reported artificial nucleases. Our approach to targeting the DNA backbone also takes advantage of metal ions, and in a chemically well-defined manner. Rather than employing ligands that only weakly associate with DNA, perhaps through electrostatic interactions, we have linked a peptide to a DNA-intercalating metal complex. The peptide coordinates the divalent cation, and the metallointercalator efficiently delivers both peptide and metal ion to the DNA backbone. Our conjugate has three important components: (i) a designed peptide with residues for metal coordination, (ii) the coordinated divalent cation, and (iii) a DNA-binding metallointercalator. We have demonstrated hydrolysis of plasmid DNA and oligonucleotide substrates with a zinc-binding peptide (P1 = Asp-Pro-Asp-Glu-Leu-Glu-His-Ala-Ala-Lys-His-Glu-Ala-Ala-Ala-Lys-CONH<sub>2</sub>) tethered to a DNA-intercalating rhodium complex (Figure 1.7).<sup>75,76</sup>

***Components of the Rh-P1 Conjugate.*** The reactive peptide of Rh-P1 was designed de novo to be  $\alpha$ -helical and to contain histidine residues for metal coordination. To encourage helicity we incorporated alanine residues, glutamate and lysine to form salt

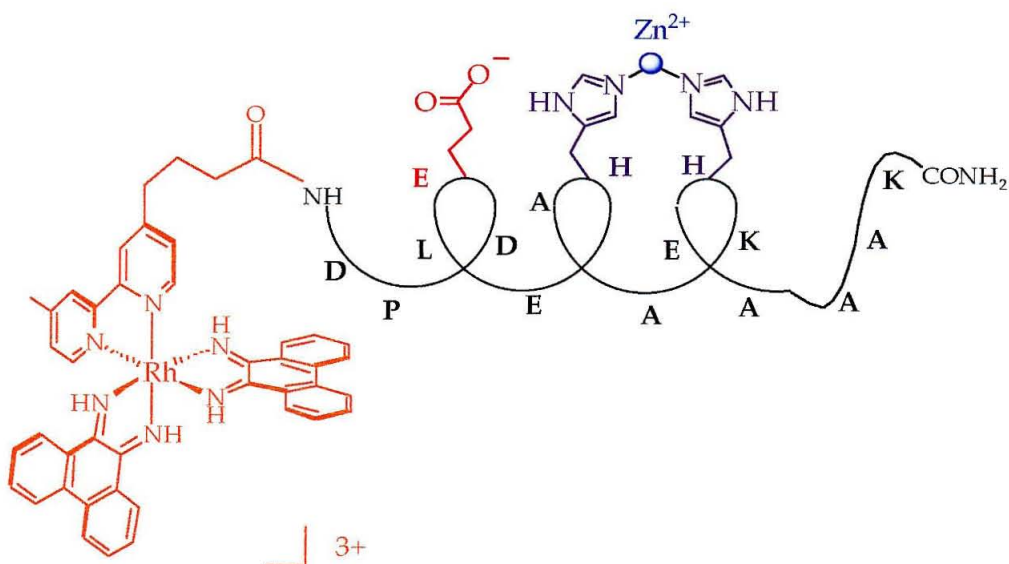


**Figure 1.7. A Rhodium-Peptide Conjugate for DNA Hydrolysis.** The Rh-P1 conjugate combines DNA binding and reactive moieties. The rhodium intercalator binds in the major groove with high affinity and the tethered peptide binds divalent cations to promote reaction at the DNA backbone.



bridges, positively charged lysine at the C-terminus of the peptide, and negatively charged aspartate at the N-terminus of the peptide. Charged residues have previously been demonstrated to interact favorably with the helix dipole. After considering the active sites of several hydrolytic metalloenzymes, the P1 peptide was designed with a coordination site for  $\text{Zn}^{2+}$  consisting of two histidine residues at  $i$  and  $i+4$  positions in the peptide. In a helical peptide, these two histidine residues would be positioned on one face of the helix. The His- $\text{Zn}^{2+}$ -His motif has been observed in naturally occurring and designed helices.<sup>77,78</sup>

Zinc is a very promising candidate metal for an artificial nuclease. There is now considerable appreciation for the catalytic and structural roles that  $\text{Zn}^{2+}$  plays in proteins and enzymes;<sup>79</sup> indeed, hundreds of proteins with  $\text{Zn}^{2+}$  centers have been identified and characterized. Under physiological conditions, zinc exists as a divalent cation. The d shell of  $\text{Zn}^{2+}$  is completely filled, and this has several important consequences.  $\text{Zn}^{2+}$  tolerates a variety of coordination environments, is relatively labile, is not redox-active, and is spectroscopically silent. Catalytic zinc centers usually have distorted tetrahedral geometry and commonly involve histidine and solvent coordination.<sup>80</sup>  $\text{Zn}^{2+}$  very effectively promotes the nucleophilicity of bound water, in some instances lowering the pKa of water from about 16 to 7.<sup>81</sup> All of these characteristics make  $\text{Zn}^{2+}$  an ideal metal cation for incorporation into our metallointercalator-peptide conjugate. In particular, the flexible coordination geometry and the low coordination number of  $\text{Zn}^{2+}$  are well suited for coordination by a short peptide.

The DNA-binding portion of the Rh-P1 conjugate,  $[\text{Rh}(\text{phi})_2\text{bpy}]^{3+}$ , is known to intercalate with high affinity from the major groove ( $K_b > 10^7 \text{ M}^{-1}$ ), and upon

photoactivation to cleave DNA at the binding site.<sup>23,24</sup> The photocleavage reaction occurs upon irradiation of the metal complex at 313 nm, and proceeds through abstraction of a hydrogen atom from the deoxyribose ring and subsequent strand scission.<sup>24</sup> This oxidative cleavage of the DNA reveals the binding sites of the intercalator, and is a very convenient property as we seek to design metallointercalator conjugates for DNA hydrolysis. The photocleavage pattern observed for  $[\text{Rh}(\text{phi})_2\text{bpy}]^{3+}$  suggests sequence neutral binding, with only a slight preference for 5'-Pu-Py-Pu-Py-3' sites.<sup>82</sup>

**Plasmid Cleavage with Rh-P1.** In the presence of  $\text{Zn}^{2+}$ , micromolar concentrations of the Rh-P1 conjugate converted supercoiled (I) pBR322 DNA to nicked (II) and linear (III) forms.<sup>75</sup> The results of plasmid cleavage experiments with Rh-P1 are summarized in Table 1.5. The metallointercalator, the tethered peptide, and the divalent cation were all essential for efficient cleavage of pBR322. Under typical plasmid cleavage conditions (5  $\mu\text{M}$  Rh-P1, 40  $\mu\text{M}$  DNA base pairs, pH 6, 37 °C), a pseudo-first-order rate constant of  $(2.5 \pm 0.2) \times 10^{-5} \text{ s}^{-1}$  was determined for the disappearance of supercoiled plasmid. This represents a  $10^6$  enhancement in rate, and is comparable to the rates achieved with other artificial nucleases (Table 1.4).<sup>75</sup> The levels of DNA cleavage achieved by Rh-P1 decreased as the pH was increased above pH 6. The sensitivity of the reaction to pH is likely, at least in part, the result of decreased solubility of  $\text{Zn}^{2+}$  at higher pH. It appears that the coordination environment created by the Rh-P1 conjugate is insufficient to prevent precipitation of zinc hydroxide.<sup>83</sup>

The helicity and activity of the Rh-P1 conjugate are both very sensitive to  $\text{Zn}^{2+}$  concentration, and each reaches a maximum at stoichiometric amounts of  $\text{Zn}^{2+}$ .<sup>76</sup> These results are consistent with the coordination model in which His7 and His11 bind zinc ion

**Table 1.5. Cleavage of Supercoiled Plasmid pBR322 DNA by Rh-P1.**

Conditions <sup>a</sup>	% I <sub>M</sub>	% II <sub>M</sub>	% III <sub>M</sub>
Control	82	18	
[Rh(phi) <sub>2</sub> bpy'] <sup>3+</sup>	65	35	
P1 + Zn <sup>2+</sup>	72	28	
Rh-P1 + EDTA	69	31	
Rh-P1	56	40	4
Rh-P1+ 0.5 eq Zn <sup>2+</sup>	17	53	30
Rh-P1 + 1.0 eq Zn <sup>2+</sup>	18	44	38
Rh-P1 + 2.0 eq Zn <sup>2+</sup>	44	39	17
Rh-P1 + 4.0 eq Zn <sup>2+</sup>	45	41	14
Zn <sup>2+</sup>	65	31	4
Rh-P1 + 1.0 eq Cd <sup>2+</sup>	50	50	
Cd <sup>2+</sup>	81	19	
Rh-P1 + 1.0 Cu <sup>2+</sup>	55	45	
Cu <sup>2+</sup>	50	50	
Rh-P1 + 1.0 eq Fe <sup>2+</sup>	20	80	
Fe <sup>2+</sup>	70	30	

<sup>a</sup> All experiments were conducted using pBR322 DNA (32 or 40  $\mu$ M bp) in sodium borate buffer (20 mM, pH 7). Tabulated are the additional reagents used at 5  $\mu$ M concentration unless otherwise noted. The samples were incubated for 24 h at 37 °C. The amounts of supercoiled (I<sub>M</sub>), nicked (II<sub>M</sub>), and linear (III<sub>M</sub>) monomer were quantitated and the results of several trials were averaged. Variations of 5 to 10% were observed between experiments. Table adapted from Fitzsimons, 1998.<sup>76</sup>

on one face of the  $\alpha$  helix. Presumably as  $\text{Zn}^{2+}$  is increased above stoichiometric concentration, the His residues begin to separately coordinate zinc, and no longer nucleate helix formation. The interesting correlation between helical content and activity suggests that the conformation of the peptide is important in the activation of DNA for hydrolysis.

Although the results presented in Table 1.5 are typical, the Rh-P1 conjugate did not promote plasmid cleavage in every experiment. When plasmid cleavage was observed the level of cleavage was quite consistent (hence the reasonable errors for the data in Table 1.5). Yet even under the conditions best suited for Rh-P1 hydrolysis (pH 6 and stoichiometric  $\text{Zn}^{2+}$ ), cleavage of the plasmid was not always achieved. This irreproducibility seems to be largely due to the solubility of  $\text{Zn}^{2+}$  and to the sensitivity of the Rh-P1 conjugate to  $\text{Zn}^{2+}$  concentration.<sup>83</sup>

***Linear DNA Cleavage with Rh-P1.*** Importantly, the Rh-P1 conjugate cleaves not only supercoiled substrates but also linear oligonucleotides. With oligonucleotide substrates, it is possible to characterize the products and the specificity of hydrolysis activity through high-resolution gel electrophoresis. The Rh-P1 cleavage products for a 17-mer and 42-mer duplex were found to contain exclusively 3'-hydroxyl and 5'-phosphate termini.<sup>75,76</sup> This provides direct evidence for a hydrolytic mechanism; oxidative cleavage generally produces phosphate termini and never hydroxyl termini. Also, the fact that 3'-phosphate and 5'-hydroxyl termini were not observed suggests regioselective delivery of the reactive moiety to DNA.

In addition, the photocleavage reaction mediated by  $[\text{Rh}(\text{phi})_2\text{bpy}']^{3+}$  provides a convenient method for determining the intercalation sites of the Rh-P1 conjugate. By

comparing photocleavage patterns and hydrolysis patterns, we gained structural insights into the interactions of the Rh-P1 conjugate with DNA.<sup>76</sup> Attachment of the P1 peptide to  $[\text{Rh}(\text{phi})_2\text{bpy}]^{3+}$  did not dramatically change the photocleavage properties of the rhodium complex. The peptide appears to reduce the damage intensity slightly, but does not change its distribution. Qualitative comparisons of the sites of most intense photocleavage and most intense hydrolysis damage reveal a consistent pattern of photoactivated oxidative damage at a given base and hydrolysis of the phosphodiester linkage of the adjacent 3' base. From previous studies we know that  $[\text{Rh}(\text{phi})_2\text{bpy}]^{3+}$  cleaves with 5' asymmetry, so we can assign the intercalation site on the basis of our photocleavage pattern. A model consistent with the cleavage pattern is presented in Figure 1.8.

Again, as with plasmid cleavage studies, the Rh-P1 conjugate does not always cleave when it is incubated with oligonucleotides under the ideal conditions; in fact, achieving cleavage of short duplexes is more difficult than achieving cleavage of plasmid substrates.

#### 1.4.4. Variations on Rh-P1.

We have explored each component of the Rh-P1 conjugate: the composition of P1 has been mutated, the system has been tested with a variety of redox active and inactive metals, and the P1 peptide has been tethered to other intercalators.<sup>83</sup>

***Varying the Peptide.*** One strength of the peptide strategy is the ability to vary residues systematically to assess the features of the Rh-P1 conjugate that contribute to DNA hydrolysis activity. Several key residues in the P1 peptide were individually



**Figure 1.8. A Model for Rh-P1 Photocleavage and Hydrolysis.**  $[\text{Rh}(\text{phi})_2\text{bpy}']^{3+}$  intercalates at the center of a 5'-Pu-Py-Pu-Py-3' site and promotes photoactivated oxidative cleavage at the pyrimidine on the 5' side of the intercalation site. The peptide reaches to the 3' phosphodiester linkage and gives  $\text{Zn}^{2+}$ -promoted hydrolysis. Figure adapted from Fitzsimons, 1998.<sup>76</sup>

mutated and the effects of these mutations were examined by circular dichroism and in plasmid cleavage assays (Table 1.6).<sup>83</sup> Not surprisingly, these mutation studies suggest that the essential feature of the Rh-P1 conjugate is the coordination site formed by His7 and His11. From study of the Rh-P4 conjugate, in which His7 and His11 were mutated to glutamates, it is clear that the histidine pair plays a critical role in  $\text{Zn}^{2+}$  coordination and cleavage activity. Circular dichroism studies indicate that the Rh-P4 conjugate does not coordinate  $\text{Zn}^{2+}$  in the same manner as the Rh-P1, Rh-P2, Rh-P3, and Rh-P5 conjugates. Rh-P4 was the only conjugate that did not show a small but consistent maximum in helicity at stoichiometric  $\text{Zn}^{2+}$ . The Rh-P4 conjugate also gave the lowest pseudo-first-order rate constant for plasmid cleavage (Table 1.6).

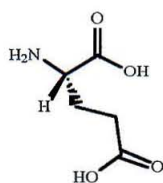
The mutation strategy also allowed us to assess the importance of the glutamic acid residue in position 4. This residue was originally designed to participate in the hydrolysis reaction by acting as a coordinating ligand, a hydrogen bond acceptor with His, or as a general base catalyst. We examined the function of this Glu residue by replacing it with Ala (Rh-P5 conjugate), by shifting it to the C-terminal side of the peptide (Rh-P2 and Rh-P3 conjugates), and by replacing it with glutamic acid analogues with longer carbon chains and extended reach (Rh-P6 and Rh-P7 conjugates). While the histidine residues were found to be critical for efficient DNA cleavage, this nearby glutamate was found not to be a source of enhancement. All of the conjugates with changes in glutamic acid position within the peptide display rate constants that closely match the rate constant of the Rh-P1 conjugate (Table 1.6). Glutamic acid analogues that extend the reach of the acid functional group also do not show increased activity relative to the Rh-P1 conjugate.

**Table 1.6. Metal-Peptide Conjugates Containing Variations on Peptide 1 and Rate Constants for the Cleavage of pBR322.**

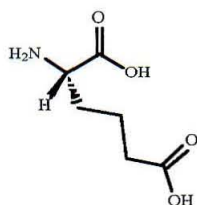
	Rhodium-Peptide Conjugate	$k_{\text{obs}}^a$ ( $10^{-6} \text{ s}^{-1}$ )
RP1	Rh- DPD <b>E</b> LEHAAK <b>H</b> EAAAK-CONH <sub>2</sub>	25
RP2	Rh- DPDALEHAAK <b>H</b> EA <b>E</b> AK-CONH <sub>2</sub>	15
RP3	Rh- DPD <b>E</b> LEHAAK <b>H</b> EA <b>E</b> AK-CONH <sub>2</sub>	17
RP4	Rh- DPD <b>E</b> LE <b>E</b> AAK <b>E</b> EA <b>E</b> AK-CONH <sub>2</sub>	6
RP5	Rh- DPDALEHAAK <b>H</b> EAAAK-CONH <sub>2</sub>	20
RP6	Rh- DPD <b>E</b> <sup>*</sup> LEHAAK <b>H</b> EAAAK-CONH <sub>2</sub>	
RP7	Rh- DPD <b>E</b> <sup>**</sup> LEHAAK <b>H</b> EAAAK-CONH <sub>2</sub>	

<sup>a</sup> Rate constants were determined with pBR322 (40  $\mu\text{M}$  bp), rhodium-peptide conjugate (5  $\mu\text{M}$ ), and  $\text{ZnCl}_2$  (5  $\mu\text{M}$ ) in sodium borate (20 mM at pH 6.0) at 37 °C. The uncertainty in the rate constant values was < 8%.

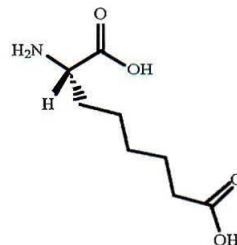
$\text{E}^*$  =  $\alpha$ -aminoadipic acid,  $\text{E}^{**}$  =  $\alpha$ -aminosuberic acid.



**Glutamic Acid**



**$\alpha$ -Aminoadipic Acid**



**$\alpha$ -Aminosuberic Acid**



**Varying the Divalent Metal Cation.** Zinc (II) is not the only metal ion that can be effectively delivered to the DNA by the Rh-P1 conjugate (Table 1.5). Cadmium can be substituted for zinc ion with some loss of activity in plasmid cleavage assays. Like  $\text{Zn}^{2+}$ ,  $\text{Cd}^{2+}$  also has a filled d shell, but it is a much softer metal with a larger radius and greater polarizability.<sup>80</sup> Two redox-active metals were also tested with Rh-P1. Combining the Rh-P1 conjugate with  $\text{Fe}^{2+}$  resulted in 80% nicked plasmid. This activity is considerable, but it still does not match the results achieved with  $\text{Zn}^{2+}$ , and the efficient Fenton chemistry associated with  $\text{Fe}^{2+}$  makes a hydrolytic mechanism unlikely. In plasmid cleavage assays,  $\text{Cu}^{2+}$ , without the rhodium complex, promoted considerable formation of nicked plasmid even at 5  $\mu\text{M}$  concentrations. Interestingly, the addition of the Rh-P1 conjugate actually caused a decrease in the percentage of nicked plasmid generated by  $\text{Cu}^{2+}$ . Apparently the conjugate provided modest protection for the plasmid, perhaps by sequestering some of the copper or by blocking access to the DNA backbone.

**Varying the Intercalator.** In our initial design, the sequence-neutral intercalator  $[\text{Rh}(\text{phi})_2\text{bpy}]^{3+}$  was selected for conjugation with our peptide, but in the Barton group we have a host of intercalators to harness for peptide delivery. We have attached P1 to ethidium, an organic intercalator.<sup>84</sup>

In contrast to  $[\text{Rh}(\text{phi})_2\text{bpy}]^{3+}$ , ethidium intercalates via the minor groove of DNA, and perhaps would reverse the regioselectivity of P1 mediated cleavage. However, attachment of the peptide to N-8-glycylethidium did not produce an active nuclease; in fact, the ethidium-peptide conjugate appears to form a tridentate chelate of  $\text{Zn}^{2+}$  that can no longer intercalate into DNA. Visible and CD spectra suggested that the two histidine residues of P1 and one of the exocyclic nitrogen amines of ethidium coordinated  $\text{Zn}^{2+}$ .<sup>84</sup>

Our detailed biochemical and structural studies of sequence-specific metallointercalators provide us with a valuable foothold as we seek to design a restriction enzyme mimic. A true artificial nuclease would selectively hydrolyze a specific sequence in a DNA duplex. Although several laboratories have attached artificial nucleases to oligonucleotides and thus have achieved selective hydrolysis of a complementary RNA or DNA strand,<sup>31,71,72</sup> effective strategies for targeting duplex DNA have not yet been devised. Harnessing a sequence-specific metallointercalator to deliver a reactive moiety to duplex DNA would be a very effective way of generating sequence-specific hydrolysis.

## 1.5. New Tethered Peptides and New Reactions

Our experiments with Rh-P1 suggest that stereospecific hydrolysis of DNA can be accomplished under mild conditions with low concentrations of intercalator-peptide complex. The general strategy of appending metal-coordinating peptides to DNA metallointercalators provides a new approach to the hydrolysis of the phosphodiester backbone of DNA. Building on our success with Rh-P1, we introduced some dramatic changes in the peptide composition of our artificial nuclease. We looked to nature for inspiration, and decided to append a short peptide from the active site of *Bam*HI to a rhodium intercalator (Chapter 2). We also turned to combinatorial chemistry for optimization the P1 peptide (Chapter 3). In addition to pursuing hydrolysis chemistry, we have exploited Cu<sup>2+</sup>-binding peptides for oxidative cleavage of DNA (Chapter 4).

Finally, by tethering short peptides to a ruthenium intercalator we have studied DNA-peptide crosslinking reaction (Chapter 5). Our metallointercalators have allowed us to deliver a wide range of short peptides to DNA for reaction.

## 1.6. References

1. Bloomfield, V. A.; Crothers, D. M.; Tinoco, Jr., I. *Nucleic Acids: Structure, Properties, and Functions*; University Science Books: Sausalito, California, 2000.
2. Williams, N. H.; Takasaki, B.; Wall, M.; Chin, J. *Acc. Chem. Res.* **1999**, 32, 485-493.
3. Westheimer, F. H. *Science* **1987**, 235, 1173-1178.
4. Linn, S. M.; Llyod, R. S.; Roberts, R. J. *Nucleases*; 2<sup>nd</sup> ed.; Cold Spring Harbor Laboratory Press: Plainview, New York, 1993.
5. Kielkopf, C. L.; Erkkila, K. E.; Hudson, B. P.; Barton, J. K.; Rees, D. C. *Nat. Struct. Biol.* **2000**, 7, 117-121.
6. Johann, T. W.; Barton, J. K. *Phil. Trans. R. Soc. Lond. A* **1996**, 354, 299-324.
7. Uchida, K.; Pyle, A. M.; Morii, T.; Barton, J. K. *Nucl. Acids Res.* **1989**, 17, 10259-10279.
8. Friedman, A. E.; Chambron, J.-C.; Sauvage, J.-P.; Turro, N. J.; Barton, J. K. *J. Am. Chem. Soc.* **1990**, 112, 4960-4962.
9. Núñez, M. E.; Barton, J. K. *Curr. Op. Chem. Bio.* **2000**, 4, 199-206.
10. Sitlani, A.; Dupureur, C. M.; and Barton, J. K. *J. Am. Chem. Soc.* **1993**, 115, 12589.

11. Krotz, A. H.; Hudson, B. P.; Barton, J. K. *J. Am. Chem. Soc.* **1993**, *115*, 3877-3882.
12. Hudson, B. P.; Barton, J. K. *J. Am. Chem. Soc.* **1998**, *120*, 6877-6888.
13. Rajsiki, S. R.; Jackson, B. A.; Barton, J. K. *Mutation Research* **2000**, *447*, 49-72.
14. Jackson, B. A.; Barton, J. K. *J. Am. Chem. Soc.* **1997**, *119*, 12986-12987.
15. Jackson, B. A.; Alekseyev, V. Y.; Barton, J. K. *Biochemistry* **1999**, *38*, 4655-4662.
16. Jackson, B. A.; Barton, J. K. *Biochemistry* **2000**, *39*, 6176-6182.
17. Murphy, C. J.; Arkin, M. R.; Jenkins, Y.; Ghatlia, N. D.; Turro, N. J.; Barton, J. K. *Science* **1993**, *262*, 1025-1029.
18. Hall, D. B.; Holmlin, R. E.; Barton, J. K. *Nature* **1996**, *382*, 731-735.
19. Dandliker, P. J.; Holmlin, R. E.; Barton, J. K. *Science* **1997**, *275*, 1465-1468.
20. Núñez, M. E.; Hall, D. B.; Barton, J. K. *Chem. Biol.* **1999**, *6*, 85-97.
21. DeGrado, W. *Ann. Rev. Biochem.* **1999**, *68*, 779-819.
22. Sardesai, N. Y.; Lin, S. C.; Zimmermann, K.; Barton, J. K. *Bioconj. Chem.* **1995**, *6*, 302-312.
23. Pyle, A.; Long, E.; Barton, J. K. *J. Am. Chem. Soc.* **1989**, *111*, 4520-4522.
24. Sitlani, A.; Long, E. C.; Pyle, A. M.; Barton, J. K. *J. Am. Chem. Soc.* **1992**, *114*, 2303-2312.
25. Sardesai, N. Y.; Barton, J. K. *J. Biol. Inorg. Chem.* **1997**, *2*, 762-771.
26. Sardesai, N. Y.; Zimmermann, K.; Barton, J. K. *J. Am. Chem. Soc.* **1994**, *116*, 7502-7508.
27. Hastings, C. A.; Barton, J. K. *Biochemistry* **1999**, *38*, 10042-10051.
28. Eigner, J.; Boedtker, H.; Michaels, G. *Biochim. Biophys. Acta* **1961**, *51*, 165-168.
29. Hegg, E. L.; Burstyn, J. N. *Coord. Chem. Rev.* **1998**, *173*, 133-165.

30. Morrow, J. R.; Kolasa, K. A.; Amin, S.; Chin, K. O. A. *Adv. Chem.* **1995**, 246, 431-447.
31. Trawick, B. N.; Daniher, A. T.; Bashkin, J. K. *Chem. Rev.* **1998**, 98, 939-960.
32. Dervan, P. B. *Science* **1986**, 232, 464-471.
33. Meunier, B. *Chem. Rev.* **1992**, 92, 1411-1456.
34. Sigman, D. S.; Mazumder, A.; Perrin, D. M. *Chem. Rev.* **1993**, 93, 2295-2316.
35. Hegg, E.; Burstyn, J. *Inorg. Chem.* **1996**, 34, 7474-7481.
36. Franklin, S. J. *Curr. Op. Chem. Biol.* **2001**, 5, 201-208.
37. Sreedhara, A.; Cowan, J. A. *J. Biol. Inorg. Chem.* **2001**, 6, 337-347.
38. Basile, L. A.; Barton, J. K. *J. Am. Chem. Soc.* **1987**, 109, 7458-7550.
39. Basile, L. A.; Raphael, A. L.; Barton, J. K. *J. Am. Chem. Soc.* **1987**, 109, 7550-7551.
40. Dixon, N.; Geue, R.; Lambert, J.; Moghaddas, S.; Pearce, D.; Sargeson, A. *Chem. Commun.* **1996**, 1287-1288.
41. Hettich, R.; Schneider, H. *J. Am. Chem. Soc.* **1997**, 119, 5638-5647.
42. Chin, J. *Acc. Chem. Res.* **1991**, 24, 145.
43. Deck, K. M.; Tseng, T. A.; Burstyn, J. N. *Inorg. Chem.* **2002**, 41, 669-677.
44. Itoh, T.; Hisada, H.; Sumiya, T.; Hosono, M.; Usui, Y.; Fujii, Y. *J. Chem. Soc. Chem. Commun.* **1997**, 677-678.
45. Ren, R.; Yang, P.; Zheng, W.; Hua, Z. *Inorg. Chem.* **2000**, 39, 5454-5463.
46. Sreedhara, A.; Freed, J. D.; Cowan, J. A. *J. Am. Chem. Soc.* **2000**, 122, 8814-8824.
47. Schnaith, L. M. T.; Hanson, R. S.; Que, Jr., L. *Proc. Natl. Acad. Sci. USA* **1994**, 91, 569-573.

48. Liu, C.; Yu, S.; Dongfeng, L.; Liao, Z.; Sun, X.; Xu, H. *Inorg. Chem.* **2002**, *41*, 913-922.
49. Vijayalakshmi, R.; Kanthimathi, M.; Subramanian, V.; Nair, B. U. *Biochem. Biophys. Res. Commun.* **2000**, *271*, 731-734.
50. Ott, R.; Kramer, R. *Angew. Chem. Int. Ed.* **1998**, *37*, 1957-1960.
51. Sissi, C.; Rossi, P.; Felluga, F.; Formaggio, F.; Palumbo, M.; Tecilla, P.; Toniolo, C.; Scrimin, P. *J. Am. Chem. Soc.* **2001**, *123*, 3169-3170.
52. Rossi, P.; Felluga, F.; Tecilla, P.; Formaggio, F.; Crisma, M.; Toniolo, C.; Scrimin, P. *J. Am. Chem. Soc.* **1999**, *121*, 6948-6949.
53. Roigk, A.; Hettich, R.; Schneider, H. *Inorg. Chem.* **1998**, *37*, 751-756.
54. Morrow, J. R.; Buttrey, L. A.; Shelton, V.; Berback, K. A. *J. Am. Chem. Soc.* **1992**, *114*, 1903-1905.
55. Zhu, B.; Zhao, D.; Ni, J.; Zeng, Q.; Huang, B.; Wang, Z. *Inorg. Chem. Commun.* **1999**, 351-353.
56. Rammo, J.; Hettich, R.; Roigk, A.; Schneider, H. *Chem. Commun.* **1996**, 105-106.
57. Ragunathan, K. G.; Schneider, H. *Angew. Chem. Int. Ed. Engl.* **1996**, *35*, 1219-1221.
58. Berg, T.; Simeonov, A.; Janda, K. D. *J. Comb. Chem.* **1999**, *1*, 96-100.
59. Kim, Y.; Welch, J. T.; Lindstrom, K. M.; Franklin, S. J. *J. Biol. Inorg. Chem.* **2001**, *6*, 173-181.
60. Welch, J. T.; Sirish, M.; Lindstrom, K. M.; Franklin, S. J. *Inorg. Chem.* **2001**, *40*, 1982-1984.
61. Hashimoto, S.; Nakamura, Y. *J. Chem. Soc. Perkin Trans. 1*, **1996**, 2623-2627.
62. Roigk, A.; Schneider, H.-J. *Eur. J. Org. Chem.* **2001**, 205-209.

63. Sumaoka, J.; Kajimura, A.; Imai, T.; Ohno, M.; Komiyama, M. *Nucleosides Nucleotides* **1998**, *17*, 613-623.
64. Bracken, K.; Moss, R. A.; Ragunathan, K. G. *J. Am. Chem. Soc.* **1997**, *119*, 9323-9324.
65. Kimizuka, N.; Watanabe, E.; Kunitake, T. *Chem. Lett.*, **1999**, 29-30.
66. Takasaki, B.; Chin, J. *J. Am. Chem. Soc.* **1994**, *116*, 1121-1122.
67. Komiyama, A.; Takeda, N.; Takahashi, Y.; Uchida, H.; Shiiba, T.; Lokdama, T.; Yashiro, M. *J. Chem. Soc. Perkin Trans.* **1995**, *2*, 269-274.
68. Komiyama, M.; Takeda, N.; Shigekawa, H. *Chem. Commun.* **1999**, 1443-1451.
69. Komiyama, M.; Sumaoka, J. *Curr. Op. Chem. Biol.* **1998**, *2*, 751-757.
70. Ott, R.; Kramer, R. *Appl. Microbiol. Biotechnol.* **1999**, *52*, 761-767.
71. Komiyama, M. *J. Biochem.* **1995**, *118*, 665-670.
72. Matsumura, K.; Endo, M.; Komiyama, M. *J. Chem. Soc., Chem. Commun.* **1994**, 2019-2020.
73. Branum, M. E.; Tipton, A. K.; Zhu, S.; Que, Jr., L. *J. Am. Chem. Soc.* **2001**, *123*, 1898-1904.
74. Bashkin, J. K. *Curr. Op. Chem. Biol.* **1999**, *3*, 752-758.
75. Fitzsimons, M. P.; Barton, J. K. *J. Am. Chem. Soc.* **1997**, *119*, 3379-3380.
76. Fitzsimons, M. P. *Ph.D. Thesis* **1998**, California Institute of Technology.
77. Ghadiri, M. R.; Choi, C. *J. Am. Chem. Soc.* **1990**, *112*, 1630-1632.
78. Matthews, B. W. *Acc. Chem. Res.* **1988**, *21*, 333-340.
79. Berg, J. M.; Shi, Y. *Science* **1996**, *271*, 1081-1085.
80. Christianson, D. W. *Adv. Prot. Chem.* **1991**, *42*, 281-355.

81. Groves, J. T.; Olson, J. P. *Inorg. Chem.* **1985**, *24*, 2717-2720.
82. Sitlani, A.; Barton, J. K. *Biochemistry* **1994**, *33*, 12100-12108.
83. Copeland, K. D.; Fitzsimons, M. P.; Houser, R. P.; Barton, J. K. *Biochemistry* **2002**, *41*, 343-356.
84. Houser, R. P.; Fitzsimons, M. P.; Barton, J. K. *Inorg. Chem.* **1999**, *38*, 1368-1370.



## Chapter 2

### DNA Hydrolysis by a *Bam*HI Peptide Tethered to a Rhodium Intercalator

## 2.1. Introduction

By attaching a metal-binding peptide to a rhodium intercalator, we have developed a new strategy for DNA hydrolysis. As described in the previous chapter, our intercalator-peptide conjugates have three essential components: (i) a peptide with residues for metal coordination, (ii) a coordinated divalent cation, and (iii) a DNA-binding metallointercalator. The metallointercalator contributes binding affinity for DNA, and the metal-binding peptide contributes reactivity.<sup>1</sup> The very first conjugate we created, Rh-P1, consists of a designed 13-mer peptide with histidine residues, zinc(II) ion, and the sequence-neutral  $[\text{Rh}(\text{phi})_2\text{bpy}']^{3+}$  intercalator. This conjugate was demonstrated to cleave plasmid and oligonucleotide DNA substrates through  $\text{Zn}^{2+}$ -promoted hydrolysis.<sup>1,2</sup>

Though Rh-P1 provides a  $10^6$ -fold enhancement in DNA hydrolysis, and matches the activity of most of the other artificial nucleases described in the literature, it is still a very poor mimic of a natural hydrolase. In addition, the metal coordination site created by the P1 peptide is not able to prevent precipitation of zinc, and as a result, we have observed inconsistent cleavage results with this conjugate.<sup>2</sup> Efforts to improve the activity of the P1 peptide, for example by the introduction of additional or unnatural acid residues, were not successful,<sup>2</sup> and we began to consider more dramatic changes in the tethered peptide.

Specifically, we looked to naturally occurring restriction enzymes as a basis for new design. *Bam*HI, a type II restriction endonuclease, partners with methylase enzymes to protect *Bacillus amyloliquefaciens* H from invading DNA.<sup>3</sup> Like other type II

restriction enzymes, *Bam*HI requires divalent cations (typically  $\text{Mg}^{2+}$ ), recognizes a short palindromic site, and cleaves both DNA strands to give 5'-phosphate and 3'-hydroxyl termini.<sup>4</sup> Conveniently, most of the critical, metal-binding residues in *Bam*HI are clustered on a single  $\beta$  hairpin.<sup>3,5</sup> To create a second generation of intercalator-peptide conjugates, the  $\beta$  hairpin from *Bam*HI was synthesized and tethered to a rhodium intercalator.

The structure of *Bam*HI bound to a 12 base pair duplex containing its recognition site (5'-GGATCC-3') has been determined (Figure 2.1).<sup>3</sup> The protein consists of a central  $\beta$ -sheet and flanking  $\alpha$ -helices, and binds to DNA as a dimer. Three important catalytic residues, Asp94, Glu111, and Glu113, have been identified through mutagenesis and analysis of the crystal structure.<sup>3,6,7</sup> These residues are found clustered on the  $\beta$ 4 and  $\beta$ 5 strands of a  $\beta$  meander (Figure 2.2).<sup>3</sup>

Although restriction endonucleases have been the workhorses of molecular biology for many years, their mechanisms are still debated.<sup>4,5</sup> Certainly the DNA cleavage reaction involves nucleophilic attack by an activated water, and the in-line displacement of a 3'-hydroxyl leaving group. The proposed models differ in the number of cations involved in hydrolysis, and in the method of nucleophilic activation.<sup>4</sup> Based on structures determined in the presence of  $\text{Mn}^{2+}$  and  $\text{Ca}^{2+}$ , a two-metal mechanism has been suggested for *Bam*HI (Figure 2.3).<sup>4</sup> According to this model, two metal ions are positioned in the active site, with 4 Å separation, by Glu77, Asp94, and Glu111. Metal A activates the attacking water molecule, and metal B stabilizes the leaving group. Both metals help to stabilize the pentavalent transition state. Meanwhile, Glu113 may act as a

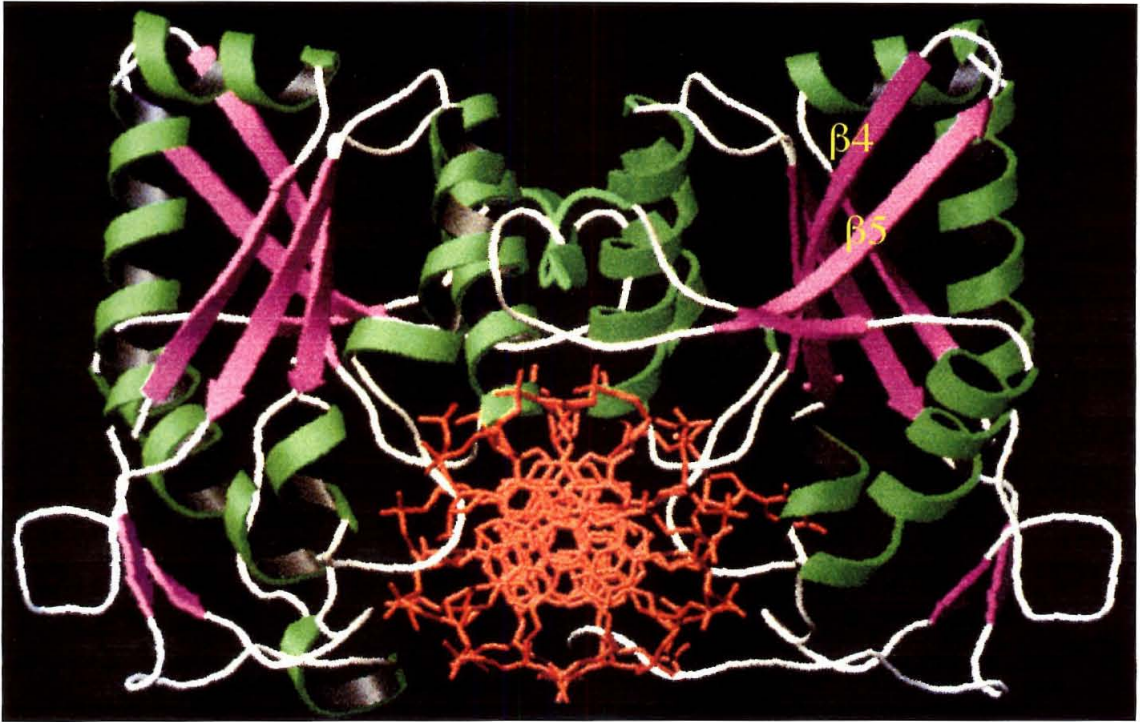


**Figure 2.1. The Structure of *Bam*HI Bound to DNA.** The *Bam*HI endonuclease binds as a dimer and cleaves DNA at palindromic GGATCC sites. Three important acidic residues are located at the base of the  $\beta 4$ - $\beta 5$  hairpin. Figure adapted from Newman et al., 1995.<sup>3</sup>

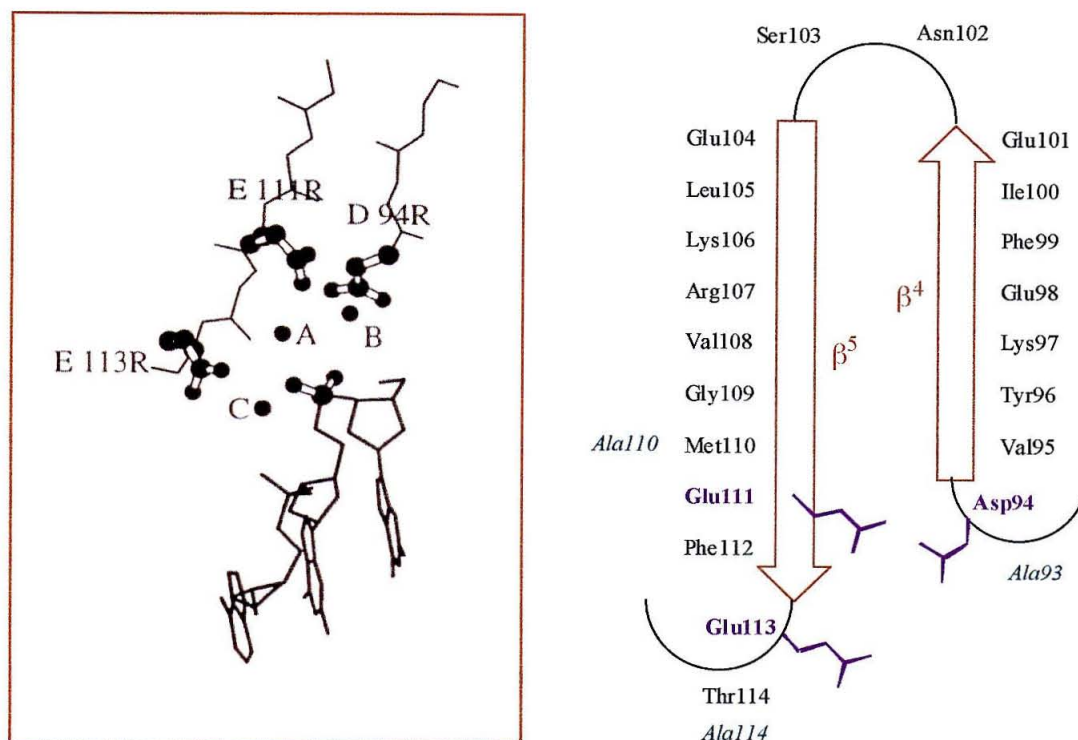


**Figure 2.2. The Active Site of the *Bam*HI Endonuclease.** Three acidic residues position metal ions and activate water for catalysis in the active site of *Bam*HI (left, adapted from Newman, et al).<sup>3</sup> This view of the active site comes from the crystal structure of the *Bam*HI-DNA complex. It is proposed that positions A and B are occupied by  $\text{Mg}^{2+}$ , and position C by the attacking water molecule. The three acidic residues are all found at the base of a  $\beta$  hairpin (right). With only a few changes in sequence, we have synthesized and tethered this peptide to a rhodium intercalator.

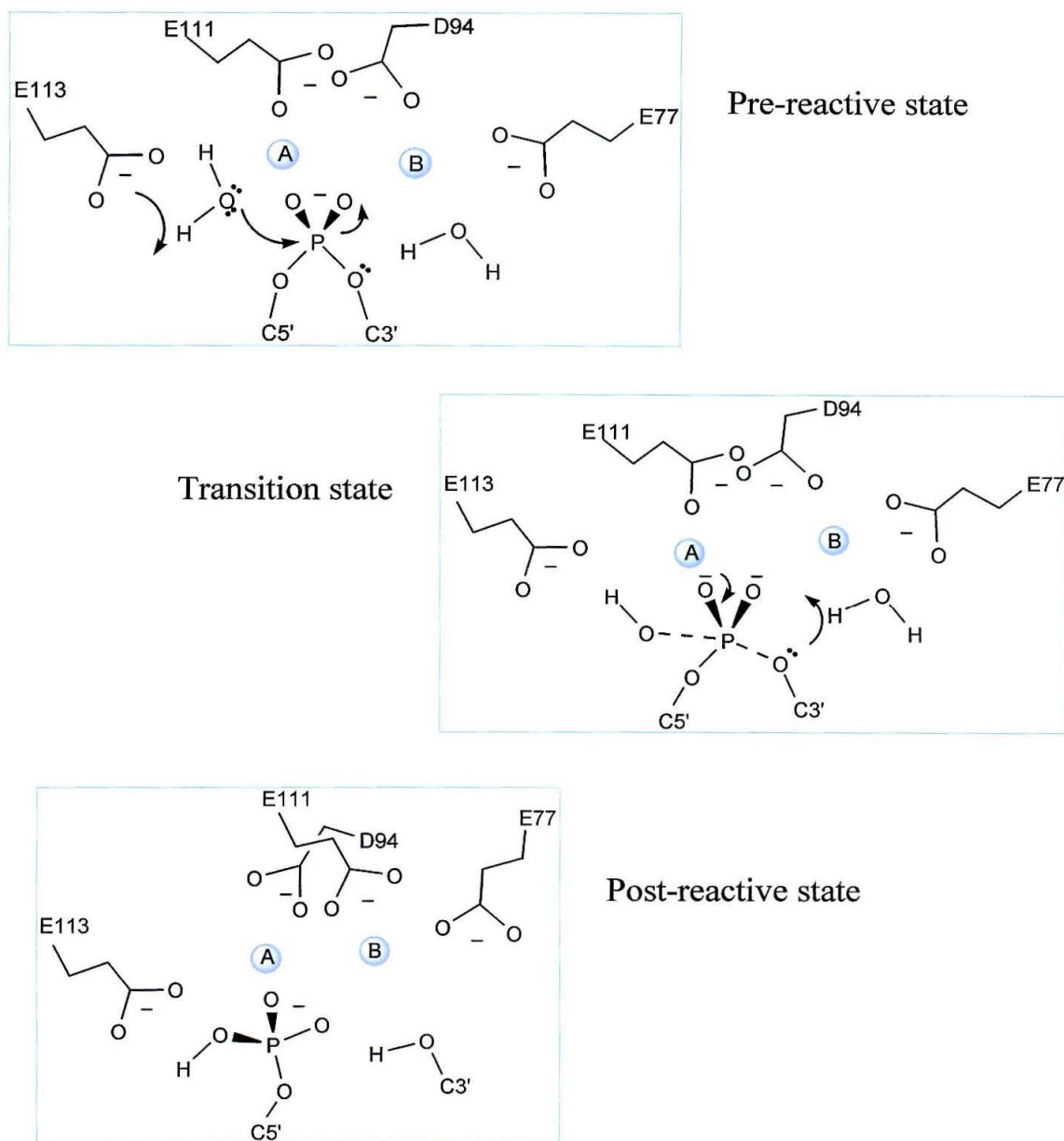


**Figure 2.3. A Two-Metal Ion Mechanism for *Bam*HI.** A two-metal ion mechanism was proposed after examination of *Bam*HI-DNA structures determined in the presence of  $\text{Mn}^{2+}$  and  $\text{Ca}^{2+}$ . Metal A and Glu113 activate the attacking water molecule, and metal B stabilizes the negative charge that develops on the leaving group. Both metals help to stabilize the pentacovalent transition state. Figure adapted from Viadiu *et al.*, 1998.<sup>5</sup>

base to accept a proton from the attacking water molecule.

The Rh-Bam conjugate was prepared by tethering a 22-mer peptide from *Bam*HI (*Ala-Asp-Val-Tyr-Lys-Glu-Phe-Ile-Glu-Asn-Ser-Glu-Leu-Lys-Arg-Val-Gly-Ala-Glu-Phe-Glu-Ala-CONH<sub>2</sub>*) to  $[\text{Rh}(\text{phi})_2\text{bpy}']^{3+}$  (Figure 2.4). Remarkably, this novel conjugate does indeed cleave plasmid DNA in the presence of zinc ion. It was not immediately obvious that the peptide would retain structure or its ability to coordinate divalent cations outside of its protein context, but based on our plasmid cleavage results, the conjugate is competent for delivering a variety of metal cations to the DNA backbone. With Rh-Bam we have demonstrated that our strategy for DNA hydrolysis is a general one.

With the goal of improving the solubility and conformational stability of our tethered Bam peptide, we also designed two shorter hairpin peptides. The designed hairpins still include three acidic residues for metal coordination, but forcing turns and residues with a high propensity for hairpin formation were introduced. These peptides were tethered to  $[\text{Rh}(\text{phi})_2\text{bpy}']^{3+}$  to create the Rh-Bam2 and Rh-Bam3 conjugates (Figure 2.5).



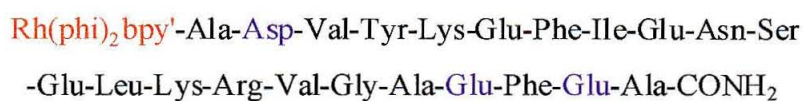
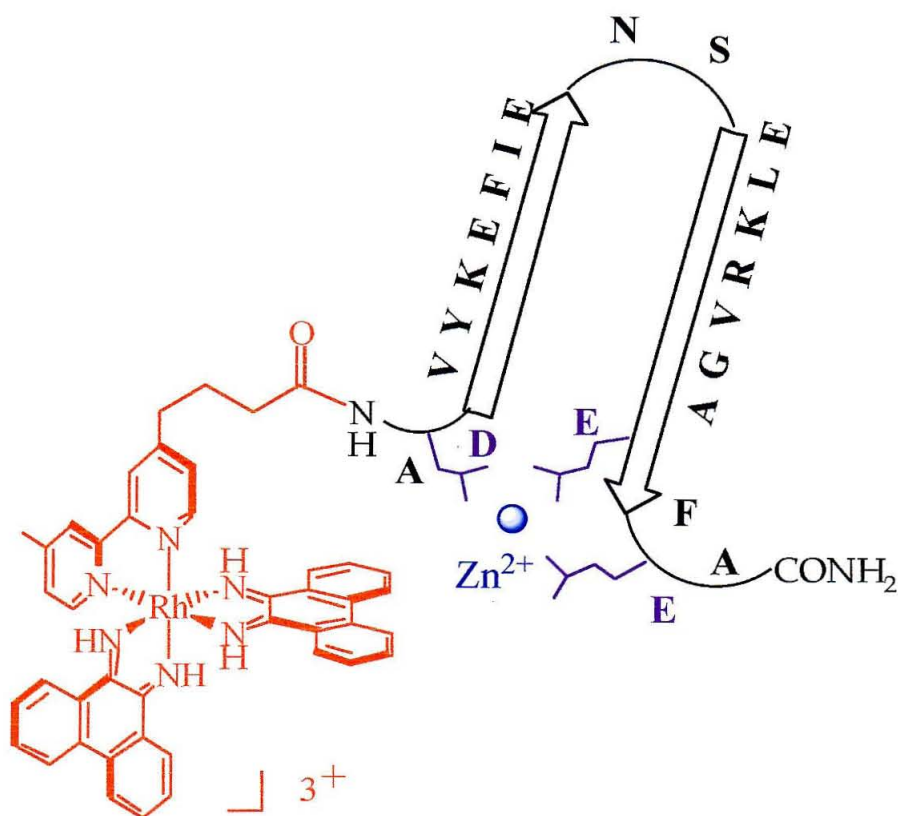


**Figure 2.4. Schematic of the Rh-Bam Conjugate.** A 22 amino acid peptide from *Bam*HI is tethered to the sequence neutral  $[\text{Rh}(\text{phi})_2\text{bpy}']^{3+}$  complex. The rhodium intercalator provides binding affinity, and the peptide contributes  $\text{Zn}^{2+}$ -promoted reactivity.



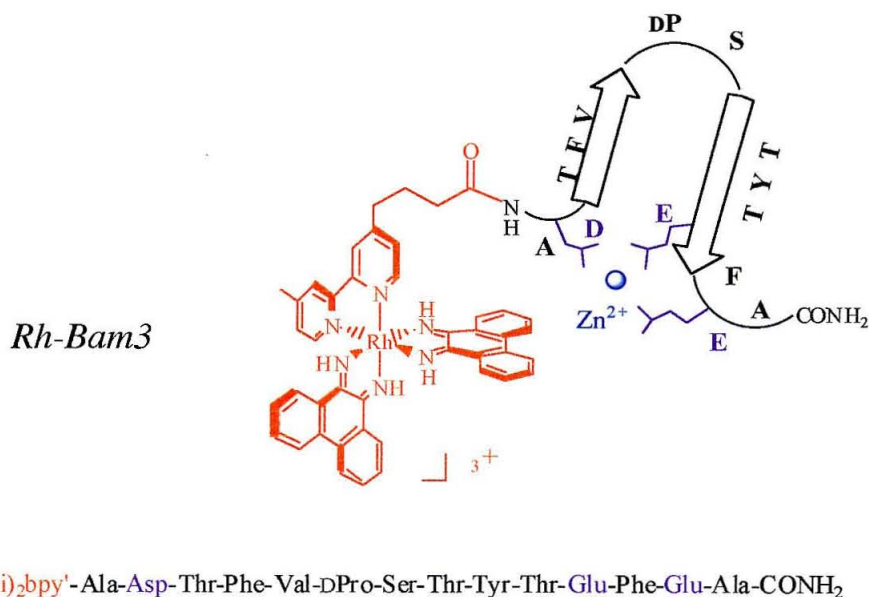
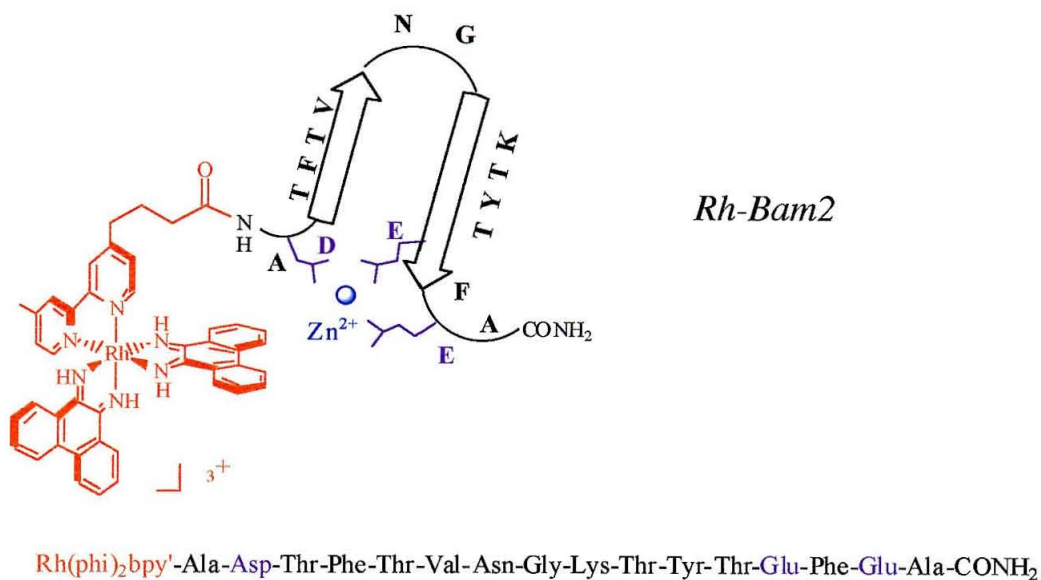


**Figure 2.5. Schematic of Conjugates with Designed Hairpin Peptides.** 16 and 13 amino acid peptides were tethered to  $[\text{Rh}(\text{phi})_2\text{bpy}']^{3+}$  to create the Rh-Bam2 and Rh-Bam3 conjugates. The peptides were designed with forcing turns (Asn-Gly and DPro-Ser) and included residues that have a high propensity for  $\beta$  hairpin formation.

## 2.2. Materials and Methods

### 2.2.1. Synthesis of the Metallointercalator Complex.

**4-Butyric acid-4'-methyl-2,2'-bipyridine (bpy')**. The bpy' ligand was synthesized according to literature methods.<sup>8,9</sup>

**Bis (phenanthrenediimine quinone) (4-Butyric acid-4'-methyl-2,2'-bipyridine) Rhodium(III) Trichloride,  $[Rh(\phi)_2bpy']Cl_3$  (Rh)**. The rhodium complex was also prepared according to published methods.<sup>10</sup> Importantly, the diaminophenanthrene (DAP) ligand must be freshly prepared from phenanthrenequinone via the hydroxime, and immediately used for coordination to the rhodium complex. DAP obtained from Aldrich gave very inconsistent and extremely low yields.

### 2.2.2. Preparation of Metallointercalator-Peptide Conjugates.

**Automated Synthesis of Peptides.** Peptides were prepared by the Beckman Institute Biopolymer Synthesis Center at Caltech using an ABI433 peptide synthesizer and N-Fmoc-L- $\alpha$ -amino acids. The peptides were assembled on an Fmoc amide resin to create peptides with an amide cap at the C-terminus. The amino acids were pentafluorophenyl esters and the amino acid protecting groups employed were as follows: Arg(Pmc), Asn(Trt), Asp(OtBu), Glu(OtBu), Lys(tBoc), Ser(tBu), and Tyr(tBu). At each step the terminal Fmoc protecting group was removed with 2% (v/v) 1,8-diazabicyclo[5.4.0]undec-7-ene (DBU) in N,N-dimethylformamide (DMF). The amino acid esters were activated with HOBt (4 eq. per coupling), and capping was carried out using 0.3 M acetic anhydride/HOBt in 9:1 DMF/CH<sub>2</sub>Cl<sub>2</sub>. Couplings were monitored by

the ninhydrin assay and the cycle was repeated until > 99% efficiency was achieved. The peptide-resins were received and stored dry at 4 °C.

***Removal of the N-terminal Fmoc Protecting Group.*** The peptide-resin (100 mg, 12  $\mu$ mol) was placed on a medium sintered glass funnel and soaked with DMF for 5 minutes. A 2% (v/v) solution of DBU in DMF was drained slowly through the funnel over a 30 minute period. The peptide-resin was rinsed with DMF,  $\text{CH}_2\text{Cl}_2$ , and 1:1  $\text{CH}_2\text{Cl}_2$ :methanol. After thorough rinsing the peptide-resin was dried on a lyophilizer.

***Coupling of the Metallointercalator and Peptide.*** The resin bound peptides were combined with racemic  $[\text{Rh}(\text{phi})_2\text{bpy}']\text{Cl}_3$  (1-2 eq.), Benzotriazole-1-yl-oxy-tris-pyrrolidino-phosphonium hexafluorophosphate (PyBOP) (3 eq.), and diisopropylethylamine (DIPEA) (6 eq.) in DMF and stirred at ambient temperature overnight. The conjugates were cleaved from the resin and deprotected with a cocktail of trifluoroacetic acid (TFA), water, and ethanedithiol. The cleaved conjugates were precipitated in ice-cold t-butyl methyl ether, collected by centrifugation, dissolved in 5% acetic acid, and lyophilized.

***HPLC Purification.*** The intercalator-peptide conjugates were HPLC purified on a semipreparative Vyadac C18 reversed phase column using a water (0.1% TFA)/acetonitrile (0.1% TFA) gradient and a flow rate of 4 mL/minute. The percentage of acetonitrile was increased from 15 to 40% over 20 minutes. Chromatograms were monitored at 220 and 360 nm, and the desired product eluted at 28 to 30 minutes. After lyophilization, the intercalator peptide conjugates were obtained as fluffy orange solids in 2 to 10% yield.

### 2.2.3. Characterization of Intercalator-Peptide Conjugates by Mass Spectrometry and Amino Acid Analysis.

Electrospray ionization mass spectrometry (ESI MS) was carried out with two instruments: (i) a Finnigan LCQ Ion Trap Mass Spectrometer, and (ii) a Perkin Elmer/Sciex API 365 Triple Quadrupole Electrospray Tandem Mass Spectrometer in the Protein/Peptide Micro Analytical Laboratory (PPMAL) at Caltech. Matrix-assisted laser desorption ionization time-of-flight mass spectrometry (MALDI MS) was carried out by the PPMAL using a Voyager-Rp Mass Spectrometer containing a PerSeptive Biosystem/Vestec Lasertech II reflector. Amino acid analysis was completed at the City of Hope Division of Immunology using a Beckman System 6200 Instrument with a 12 cm sodium column for the analysis of hydrolyzed amino acids.

***Rh-Bam:*** [*Rh(phi)bpy'-ADVKEFIENSELKRVGAEFEA-CONH<sub>2</sub>*]. ESI MS (i) m/z observed (calculated): (Rh-Bam + 2H)<sup>5+</sup> 660.1 (660.1); (Rh-Bam + H)<sup>4+</sup> 824.7 (824.8); (Rh-Bam)<sup>3+</sup> 1099.3 (1099.5); (Rh-Bam - H)<sup>2+</sup> 1648.5 (1648.7). MALDI MS m/z: (Rh-Bam - 2H)<sup>+</sup> 3295.8 (3296.5); (Rh-Bam - phi - 2H)<sup>+</sup> 3090.87 (3090.3); (Rh-Bam - 2phi - 2H)<sup>+</sup> 2883.7 (2886.08); and smaller species from peptide fragmentation. Amino acid analysis observed (calculated): Asx 2.067 (2), Ser 1.051 (1), Glu 5.409 (5), Gly 1.638 (1), Ala 2.623 (3), Val 2.073 (2), Ile 0.892 (1), Leu 1.041 (1), Tyr 0.671 (1), Phe 1.955 (2), Lys 1.955 (2), Arg 0.959 (1).

***Rh-Bam2:*** [*Rh(phi)bpy'-ADTFTVNGKTYTEFEA-CONH<sub>2</sub>*]. ESI MS (ii) m/z observed (calculated): (Rh-Bam2)<sup>3+</sup> 848.7 (848.8); (Rh-Bam2 - H)<sup>2+</sup> 1272.6 (1272.6). Amino acid analysis observed (calculated): Asx 1.732 (2), Thr 3.405 (4), Glu 2.370 (2), Gly 1.378 (1), Ala 1.848 (2), Val 0.792 (1), Tyr 0.976 (1), Phe 1.976 (2), Lys 1.028 (1).

***Rh-Bam3:*** [*Rh(phi)bpy'*-ADTFVDPSTYTEFEA-CONH<sub>2</sub>]. ESI MS (ii) m/z observed (calculated): (Rh-Bam3)<sup>3+</sup> 776.7 (776.8); (Rh-Bam3 - H)<sup>2+</sup> 1164.6 (1164.6). Amino acid analysis observed (calculated): Asp 1.246 (1), Thr 3.075 (3), Ser 1.049 (1), Glu 2.225 (2), Pro 1.001 (1), Ala 2.111 (2), Val 0.364 (1), Tyr 0.904 (1), Phe 2.002 (2).

#### 2.2.4. Analysis of Intercalator-Peptide Conjugates by UV-Visible and Circular Dichroism Spectroscopy.

Electronic spectra were recorded using a Beckman DU 7400 Spectrophotometer. The concentration of free peptide was determined using the protein extinction coefficient  $\epsilon_{205} = 31$  (1 mg/mL solution),<sup>11</sup> and the concentration of intercalator-peptide was determined using the molar absorptivity coefficient  $\epsilon_{349}(\text{isosbestic}) = 23,600 \text{ M}^{-1} \text{ cm}^{-1}$ .<sup>10</sup>

Circular Dichroism spectra were recorded using a Jasco-600 Spectropolarimeter or an Aviv 62A DS Circular Dichroism Spectrometer. CD samples of the intercalator-peptide conjugates (3 to 5  $\mu\text{M}$ ) were prepared in sodium borate buffer (20 mM, pH 6 to 7). Helical content was estimated from the mean residue ellipticity at 222 nm.<sup>12</sup>

### 2.2.5. Potentiometric Titration of the Rh-Bam Conjugate.

An aqueous solution of the Rh-Bam conjugate (600  $\mu\text{L}$ , 200  $\mu\text{M}$ ) and an aqueous solution of 1:1 Rh-Bam: $\text{Zn}^{2+}$  (850  $\mu\text{L}$ , 100  $\mu\text{M}$ ) were titrated with 2  $\mu\text{L}$  aliquots of 10 mM NaOH. The solutions were continuously stirred with a magnetic stir bar. The pH was monitored using a Beckman  $\phi 45$  pH meter.

### 2.2.6. Cleavage of Supercoiled Plasmid with Rh-Peptide and Metal Ions.

**Plasmid DNA.** Plasmid DNA (pBR322 or pUC19) was obtained from NEBiolabs and dialyzed on centricon filters to remove EDTA. Alternatively, pUC19 was amplified using DH5 $\alpha$  cells, isolated using a QIAGEN kit, treated with a metal-chelating resin (Chelex 100, Biorad), and dialyzed on centricon filters.

**Metal Solutions.** Aqueous solutions of  $\text{ZnCl}_2$  were prepared by two methods. In the first method,  $\text{ZnCl}_2$ , a very hygroscopic salt, was weighed and dissolved in water. Alternatively, zinc metal was weighed and dissolved in concentrated hydrochloric acid, and then diluted with water. Though more accurate, this second method resulted in more acidic solutions. Aqueous solutions of magnesium, manganese, iron, copper, cadmium, lead, nickel, cobalt, cerium, and lanthanum were prepared by dissolving the chloride salts in water.

**Buffers.** Sodium borate (20 mM), HEPES (15 mM), and a pH-independent metal ion buffer were used in plasmid cleavage experiments. The metal ion buffer was prepared by combining EDTA (11 mM),  $\text{MnCl}_2$  (21 mM), and  $\text{ZnCl}_2$ . Sodium borate (25 mM) was also added to the metal ion buffer to maintain the pH. As described by Perrin

et al.,<sup>13</sup> the concentration of free  $\text{Zn}^{2+}$ ,  $[\text{M}^I]$ , can be determined with the following equation:

$$[\text{M}^I] = [\text{M}^I]_T \beta^{\text{II}} ([\text{M}^{\text{II}}]_T - [\text{L}]_T) / \beta^I ([\text{L}]_T - [\text{M}^I]_T),$$

where  $\text{M}^I$  is  $\text{Zn}^{2+}$ ,  $\text{M}^{\text{II}}$  is  $\text{Mn}^{2+}$ , L is EDTA, and T indicates the total concentration.  $\beta^I$  and  $\beta^{\text{II}}$  are the stability constants for zinc (II) and manganese (II) with EDTA ( $\log \beta^I = 16.7$ ,  $\log \beta^{\text{II}} = 14.1$ ).<sup>13</sup>

Care was taken to avoid metal contamination in cleavage reactions. Purified water from a Millipore Milli-Q Plus water system was used for the cleaning of glassware and the preparation of solutions. The sodium borate and HEPES buffers were passed through a metal-chelating column (Chelex 100, BioRad) prior to use. All solutions were stored in plastic containers.

**Plasmid Cleavage Experiments.** In a typical plasmid cleavage experiment intercalator-peptide (5  $\mu\text{M}$ ), divalent metal cation (5 to 500  $\mu\text{M}$ ), and plasmid (40  $\mu\text{M}$  base pairs) were combined in buffer and incubated at 37 °C for 24 to 48 hours. The reactions were quenched by the addition of a mixture of EDTA, sodium dodecyl sulfate, glycerol, bromophenol blue, and xylene cyanol. The cleavage products were analyzed by electrophoresis on 1% agarose gels. The gels were stained with ethidium bromide, and visualized with UV light. Gels were quantitated using an LKB Bromma Ultrascan XL Enhanced Densitometer and Pharmacia Gelscan XL software.

### 2.2.7. Photocleavage of a Plasmid Restriction Fragment by Rh-Bam.

**Preparation of a Radiolabeled Restriction Fragment.** A 175-mer restriction fragment of pUC19 was prepared by digestion with *Bam*HI and *Bgl*II. A 5' radiolabel was incorporated after the *Bam*HI digestion and before the *Bgl*II digestion. To add the labeled phosphate, the plasmid was first treated with shrimp alkaline phosphatase and then incubated with polynucleotide kinase and [ $\gamma$ - $^{32}$ P]-ATP. The labeled fragment was purified on a 10% native gel, and recovered from the excised gel band by the crush and soak method.<sup>14</sup> The fragment was desalted, dried under vacuum, and quantitated using a Beckman LS 5000TD scintillation counter. The labeled 175-mer was combined with calf thymus DNA and buffer to create DNA stock solutions.

**Oligonucleotide Sequencing Reactions.** To create migration standards, standard A+G and C+T Maxam-Gilbert sequencing reactions were completed with the labeled fragment.<sup>14</sup>

**Photocleavage Experiment.** The labeled fragment (100  $\mu$ M bp) was combined with [Rh(phi)<sub>2</sub>bpy']<sup>3+</sup>, Rh-P1, or Rh-Bam (2.5, 5, 7.5, and 10  $\mu$ M) in buffer (20 mM Tris-HCl, pH 7.85). The samples (40  $\mu$ L total volume) were irradiated for 5 minutes at 313 nm with an Oriel Model 6140 1000 W Hg/Xe lamp equipped with a monochromator and a 300 nm cutoff filter. A light control sample (L) was irradiated in the absence of rhodium complex, and a dark control sample (D) contained rhodium complex but was not irradiated. Following irradiation the samples were dried under vacuum, resuspended in a formamide running buffer, and analyzed by polyacrylamide gel electrophoresis. The samples were denatured by heating at 90 °C for approximately 10 minutes and then were loaded on a 7% polyacrylamide gel. The gel was electrophoresed for approximately 2



hours at 2000 V (90 W maximum), and dried at 80 °C under vacuum. The gel was visualized using a phosphor screen, a Molecular Dynamics PhosphorImager, and ImageQuant software.

### 2.2.8. Oligonucleotide Cleavage Experiments with Rh-Bam.

**Preparation of Radiolabeled Duplex.** A 27-mer duplex substrate was prepared for Rh-Bam studies. The oligonucleotides (A: 5'-CCG CGC ATC ACG GCA CTA CGG CTC GTC-3' and B: 5'-GAC GAG CCG TAG TGC CGT GAT GCG CGG-3') were synthesized on an ABI 391 DNA synthesizer, and HPLC purified on a Dynamax C<sub>18</sub> reverse phase column. One strand of the duplex was 5'-labeled by incubation with T4 polynucleotide kinase and [ $\gamma$ -<sup>32</sup>P]-ATP. The labeled strand was isolated on a 10% polyacrylamide gel, excised, recovered by the crush and soak method,<sup>14</sup> and desalted on Nensorb columns. The radioactive samples were quantitated using a Beckman LS 5000TD scintillation counter. The labeled strand was annealed with unlabeled strand and complement strand by heating to 90 °C and cooling slowly to room temperature.

**Oligonucleotide Sequencing Reactions.** To create migration standards, standard A+G and C+T Maxam-Gilbert sequencing reactions were completed with the labeled strand.<sup>14</sup> To remove the terminal phosphate and create migration standards with terminal hydroxy groups, the standard Maxam-Gilbert products were treated with T4 polynucleotide kinase for 1 hour at 37 °C.

**Photocleavage Experiments.** The labeled duplex (10  $\mu$ M) was combined with intercalator-peptide conjugate (2.5, 5, 10  $\mu$ M) in buffer (50 mM Tris-HCl, 20 mM sodium acetate, 18 mM NaCl pH 7). The samples (20 to 40  $\mu$ L total volume) were

irradiated for 15 minutes at 313 nm with the Hg/Xe lamp. A light control sample (L) was irradiated in the absence of intercalator-peptide conjugate, and a dark control sample (D) contained intercalator-peptide conjugate but was not irradiated. Following irradiation the samples were dried under vacuum, resuspended in a formamide running buffer, denatured at 90 °C, and analyzed by polyacrylamide gel electrophoresis. A 20% polyacrylamide gel was run for approximately 2 hours at 2000 V (90 W maximum). The gel was visualized using a phosphor screen, a Molecular Dynamics PhosphorImager, and ImageQuant software.

**Hydrolysis Experiments.** For hydrolysis experiments, samples containing labeled duplex, Rh-Bam, divalent cation, and sodium borate buffer (20 mM, pH 6.6) were incubated at 37 °C for 24 to 48 hours. After incubation, the samples were dried under vacuum, resuspended in a formamide running buffer, and analyzed by polyacrylamide gel electrophoresis as described above.

## 2.3. Results

### 2.3.1. Synthesis of the Rh-Bam Conjugate.

We have synthesized and tethered a  $\beta$  hairpin peptide from the *Bam*HI enzyme to a DNA metallointercalator to create a novel reagent for DNA hydrolysis. The 22-mer peptide was prepared by solid-phase synthesis with Fmoc protection, and the metallointercalator,  $[\text{Rh}(\text{phi})_2\text{bpy}]^{3+}$ , was prepared by literature methods.<sup>8-10</sup> These two pieces were joined by the direct coupling strategy (Figure 2.6).<sup>15</sup> To produce the desired

amide linkage, the Bam peptide, still on the synthesis resin, was combined with activated rhodium complex. The bpy' linker of racemic  $[\text{Rh}(\text{phi})_2\text{bpy}']^{3+}$  was activated with N,N'-dicyclohexylcarbodiimide (DCC) and 1-hydroxybenzotriazole (HOBt), or with PyBOP and diisopropylethylamine (DIPEA). It was found that the PyBOP/DIPEA combination provided cleaner reaction and slight improvement in the conjugate yield. After the coupling reaction, the conjugate was cleaved from the resin and deprotected by treatment with TFA. The rhodium intercalator is compatible with standard peptide coupling strategies, and the addition of  $[\text{Rh}(\text{phi})_2\text{bpy}']^{3+}$  to the N-terminus of a peptide is as simple as the addition of an amino acid to a growing peptide chain. The Rh-Bam conjugate was purified by reverse phase HPLC. Only one major peak was observed in the chromatogram (220 and 360 nm) of the crude material. This peak was isolated and lyophilized to give a fluffy orange solid in 2 to 10% yield.

### 2.3.2. Characterization of the Rh-Bam Conjugate.

**Mass Spectrometry and Amino Acid Analysis.** The isolated chimera was characterized by mass spectrometry and amino acid analysis. Both ESI and MALDI mass spectrometry confirmed the covalent attachment of the Bam peptide and the rhodium intercalator. Electrospray mass spectrometry is a particularly effective method for studying intercalator-peptide conjugates,<sup>16</sup> and for Rh-Bam,  $m/z$  peaks corresponding to the  $5^+$ ,  $4^+$ ,  $3^+$  and  $2^+$  ions were observed. All closely matched the calculated masses. The results obtained by MALDI were more complicated. The rhodium complex absorbs

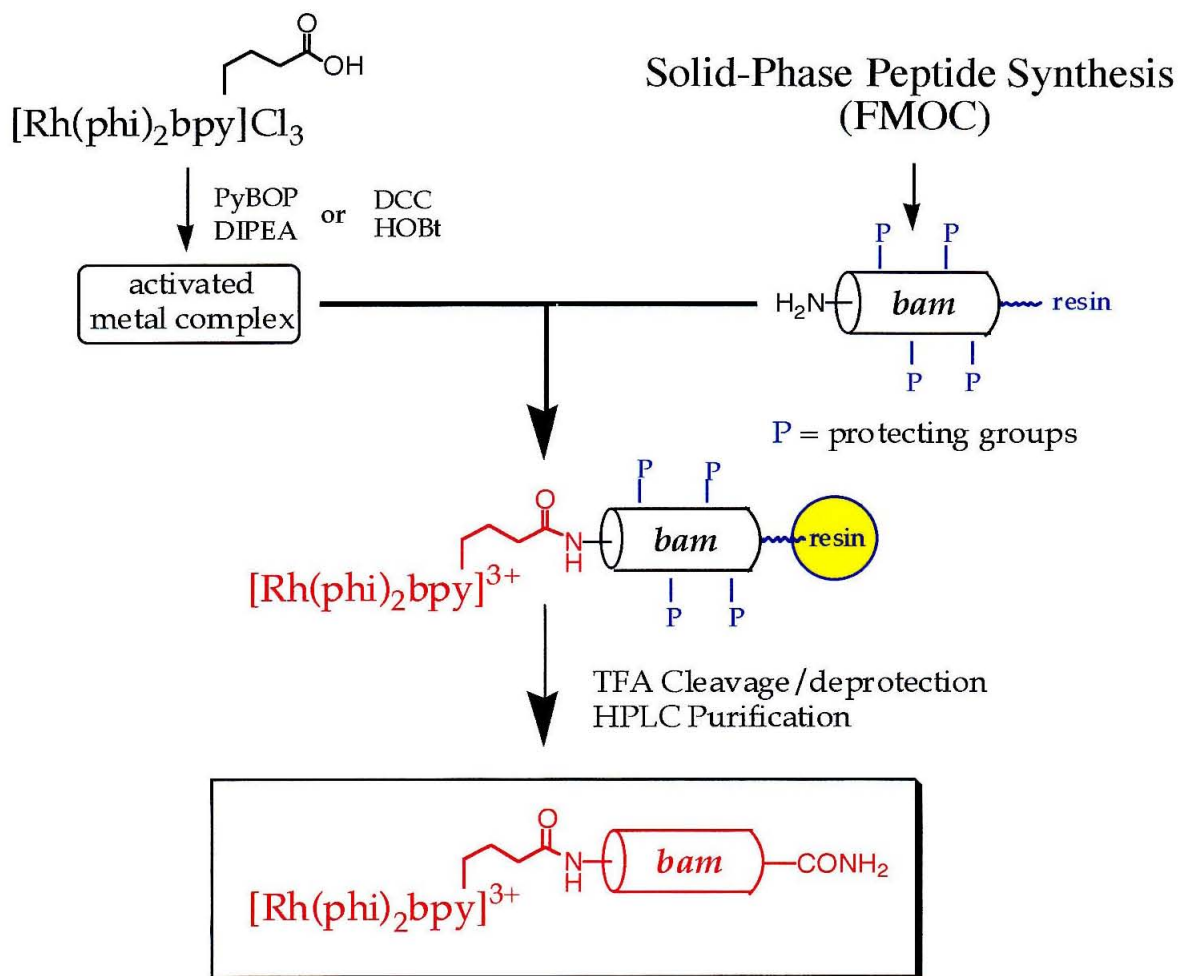


**Figure 2.6. Synthesis of the Rh-Bam Conjugate.** The Bam peptide was prepared by solid-phase peptide synthesis. The activated rhodium complex was combined with the peptide resin to form an amide linkage. The conjugate was cleaved from the resin and deprotected by treatment with TFA, and was finally purified by HPLC.

strongly around 330 nm, and the laser used for sample desorption in MALDI has been found to promote ligand loss.<sup>17-18</sup> The mass spectra for Rh-Bam contained three peaks corresponding to the molecular ion ( $m/z$  3295.8, calc. 3296.5), the molecular ion less one phi ligand ( $m/z$  3090.9, calc. 3090.3) and the molecular ion less two phi ligands ( $m/z$  2883.7, calc. 2886.1). Loss of the bpy' ligand ( $m/z$  2782.76, calc. 2783.2) was also observed. In addition, a number of peaks of lower mass were observed ( $m/z$  2317.4, 1735.2), and these peaks may correspond to peptide fragmentation. Amino acid analysis also confirmed the successful preparation of our conjugate, and a 1:1 ratio of peptide to metal complex.

**Electronic Spectroscopy.** The UV-visible spectrum of the Rh-Bam conjugate is simply the sum of the individual spectra of  $[\text{Rh}(\text{phi})_2\text{bpy}']^{3+}$  and the Bam peptide, and is essentially identical to the spectra of Rh-P1 (Figure 2.7). The absorption of the rhodium complex in the visible region, a region where the peptide does not absorb, provides a convenient handle for quantitation. The molar absorptivity constant for  $[\text{Rh}(\text{phi})_2\text{bpy}']^{3+}$  is  $23,600 \text{ M}^{-1}\text{cm}^{-1}$  at 349 nm.<sup>10</sup> The spectrum of Rh-Bam shows pH dependent changes that arise from protonation of the phi ligands, but 349 nm is an isosbestic point.<sup>10</sup> In addition, the fact that attachment of the Bam peptide to the rhodium complex does not significantly perturb the spectra suggests that there is little interaction between residues in the peptide and the phi ligands.

**Circular Dichroism Spectroscopy.** Circular dichroism spectroscopy is a convenient tool for the study of protein and peptide conformation, and we applied this tool to probe the structure of the Rh-Bam conjugate. Spectra were collected for samples containing Rh-Bam (5  $\mu\text{M}$ ) and varying amounts of  $\text{Zn}^{2+}$ . The addition of  $\text{Zn}^{2+}$  produced

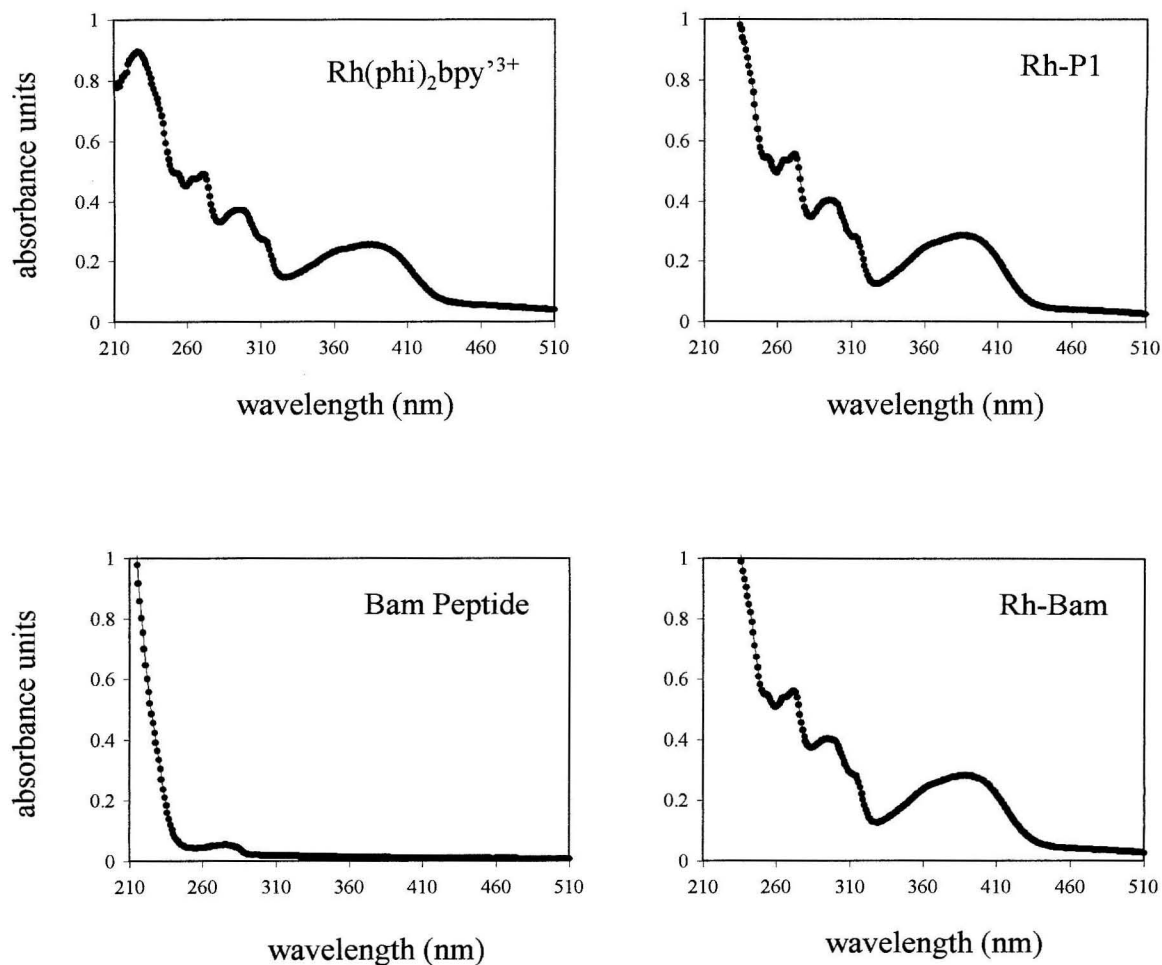


**Figure 2.7.** UV-Visible Spectra of  $[\text{Rh}(\text{phi})_2\text{bpy}']^{3+}$ , Rh-P1, Bam Peptide, and Rh-Bam. The spectra were recorded for 8.5  $\mu\text{M}$  rhodium complex in water at pH 5.

changes in the Rh-Bam spectrum; a weak negative band emerged between 220 and 230 nm, and the negative band between 200 and 210 nm increased in intensity (Figure 2.8). In contrast to Rh-P1, which showed maximum helical content at stoichiometric  $\text{Zn}^{2+}$ , there was little change in the spectrum as  $\text{Zn}^{2+}$  was increased from 1 to 5 equivalents.

The bands that emerge as Rh-Bam is titrated with  $\text{Zn}^{2+}$  are actually typical of a random coil or irregular peptide.<sup>19,20</sup> Peptides lacking order often have an intense negative band near 200 nm that arises from  $\pi\pi^*$  transitions, and a feature at 220 nm, either positive or negative, that arises from  $n\pi^*$  transitions.<sup>19</sup> Although the addition of  $\text{Zn}^{2+}$  triggers some change in peptide structure, the Rh-Bam conjugate appears to be fairly disordered.

Rh-Bam spectra were also collected for samples containing increasing amounts of trifluoroethanol (TFE). Halogenated alcohols, particularly TFE, have been found to induce structure in short peptides by favoring the formation of hydrogen bonds, and with Rh-Bam we did observe significant changes as TFE was increased from 0 to 50% (Figure 2.9). The changes that occurred for Rh-Bam were actually very similar to the changes that occurred with Rh-P1; negative bands emerged between 200 and 210 nm and at 220 nm. Negative bands at 208 nm and 222 nm are characteristic of  $\alpha$ -helical conformation, but are also sometimes observed for Type I and II'  $\beta$  turns.<sup>19,20</sup> Helix-like spectra are rather common for samples containing halogenated alcohols, and may indicate a mixture of  $\alpha$ -helix and aperiodic conformers.<sup>19</sup> The helical content was estimated from the ellipticity at 222 nm.<sup>12</sup> With 0% TFE the Rh-P1 and Rh-Bam conjugate showed 7.5 and 3.5% helicity. With 25% TFE the helicity increased to 46% and 65%. As expected, the

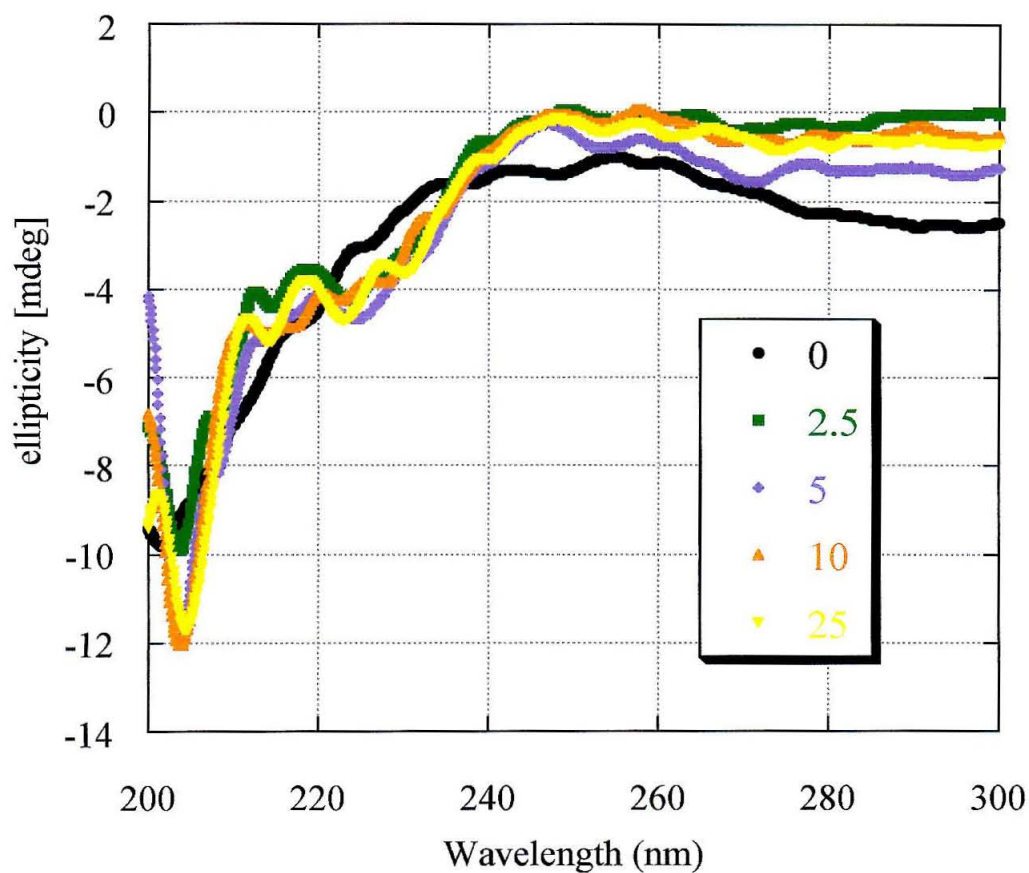


**Figure 2.8. Circular Dichroism Spectra of Rh-Bam with increasing  $\text{Zn}^{2+}$**

**Concentration.** Spectra were collected for samples of Rh-Bam (4  $\mu\text{M}$ ) and  $\text{ZnCl}_2$  (0, 2.5, 5, 10, 25  $\mu\text{M}$ ) in Na borate buffer (pH 7.1).



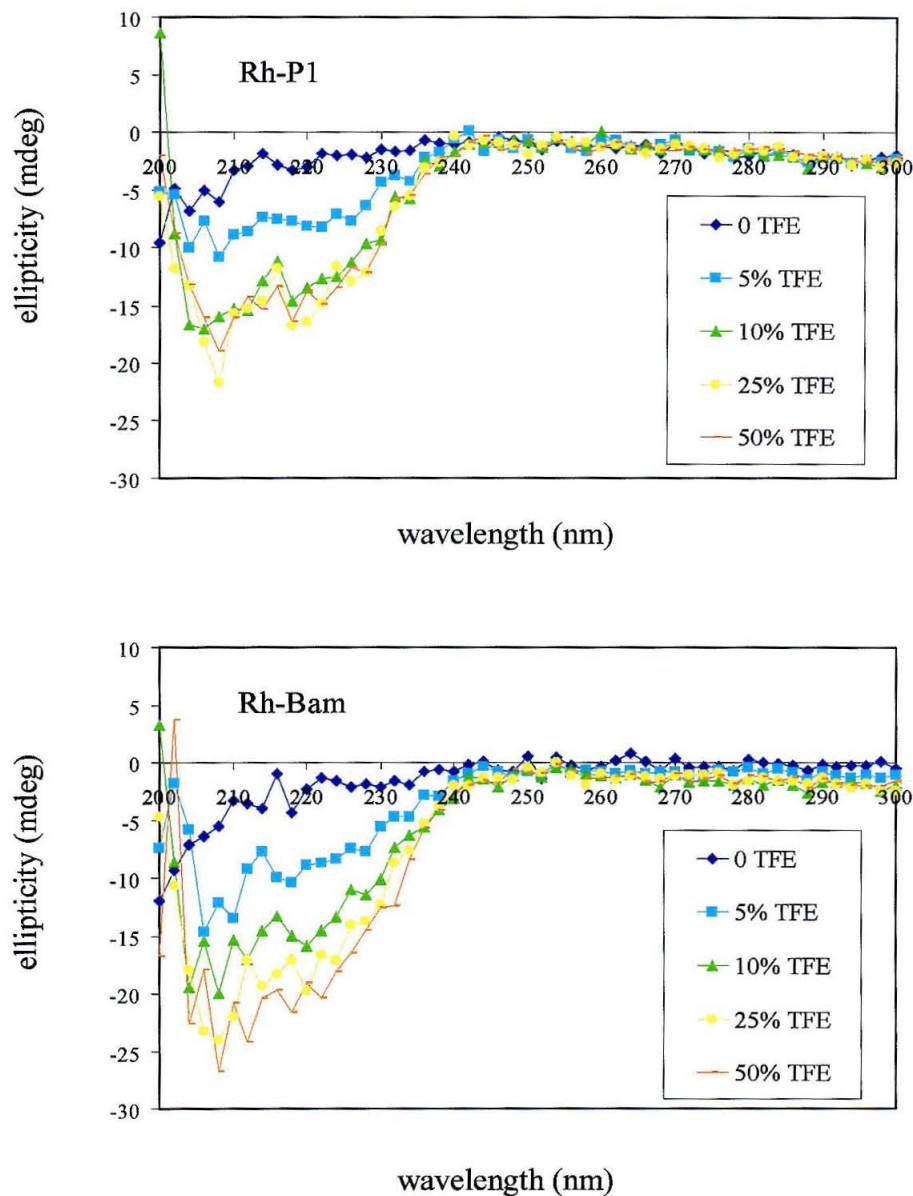


**Figure 2.9. Circular Dichroism Spectra of Rh-P1 and Rh-Bam with Increasing Trifluoroethanol.** Spectra were collected for samples of Rh-P1 (top) and Rh-Bam (bottom) in 0, 5, 10, 25, and 50% TFE.

Rh-P1conjugate seems to have a greater propensity for hairpin formation. In the presence of TFE, Rh-Bam is somewhat structured, but there is no clear evidence for a hairpin structure. Unfortunately, the intense absorbance of the rhodium complex prevents CD investigations in the presence of DNA.

***Potentiometric Titration of Rh-Bam.*** To explore the solubility properties of the Rh-Bam conjugate and to probe the  $pK_a$  of individual Bam residues, a potentiometric titration was completed for Rh-Bam. An aqueous solution of Rh-Bam (200  $\mu\text{M}$ ) was titrated with dilute sodium hydroxide. As the pH was increased from 3.5 to 4, orange precipitate began to form, and this precipitate continued to collect as the pH was adjusted to 5. The precipitate began to redissolve as the pH of the solution was raised above 5.5. Titration of a sample containing Rh-Bam (100  $\mu\text{M}$ ) and stoichiometric  $\text{Zn}^{2+}$ , also produced orange precipitate between pH 3.5 and 5.5. In addition, a black precipitate was observed above pH 8. It appears that the conjugate is fairly insoluble between pH 3.5 and 6.5, and that zinc hydroxide precipitates above pH 8.

The Rh-Bam conjugate has a large number of acidic residues (5 Glu and 1 Asp) that are expected to have  $pK_a$  values between 3 and 5, phi imine protons with a  $pK_a$  value of approximately 7, and a few basic residues (2 Lys and 1 Arg) that are expected to have  $pK_a$  values between 8.5 and 9.5. The titration curve had very broad inflections, and did not provide specific information about  $pK_a$  values.

### 2.3.3. Cleavage of Supercoiled Plasmid by Rh-Bam and Zinc.

The Rh-Bam conjugate was tested in plasmid cleavage assays to determine if the short Bam peptide could still promote DNA hydrolysis outside of its protein architecture. Upon cleavage, a supercoiled plasmid (I) is converted into a nicked product (II) that migrates more slowly on an agarose gel. Double-stranded cleavage or multiple cleavage events within a 12 to 16 base pair stretch produces a linear product (III) with intermediate mobility.

As can be seen in Figure 2.10, like Rh-P1 and its derivatives, the Rh-Bam conjugate converted supercoiled plasmid to a nicked product in the presence of  $\text{Zn}^{2+}$ . Rh-Bam appears to promote DNA hydrolysis under mild conditions (pH 6, 37 °C), and at low conjugate concentrations. With only 5  $\mu\text{M}$  Rh-Bam and 5  $\mu\text{M}$   $\text{Zn}^{2+}$ , a large fraction of the plasmid (73%) was converted to a nicked product. Linear product was not observed in this experiment, and was rarely observed with Rh-Bam in plasmid cleavage assays.

Tethering the Bam peptide to a metallointercalator and including divalent cation in the reaction mixture were both essential for effective cleavage. The untethered Bam peptide is expected to have very low affinity for DNA, and thus to have little impact on plasmid cleavage levels. An experiment with untethered Bam peptide showed little cleavage with 5  $\mu\text{M}$   $\text{Zn}^{2+}$ , and very modest cleavage at 500  $\mu\text{M}$   $\text{Zn}^{2+}$  (Figure 2.11). As intended, the rhodium intercalator serves to deliver the reactive  $\text{Zn}^{2+}$ -binding peptide to the DNA backbone, making efficient cleavage possible at micromolar concentrations.

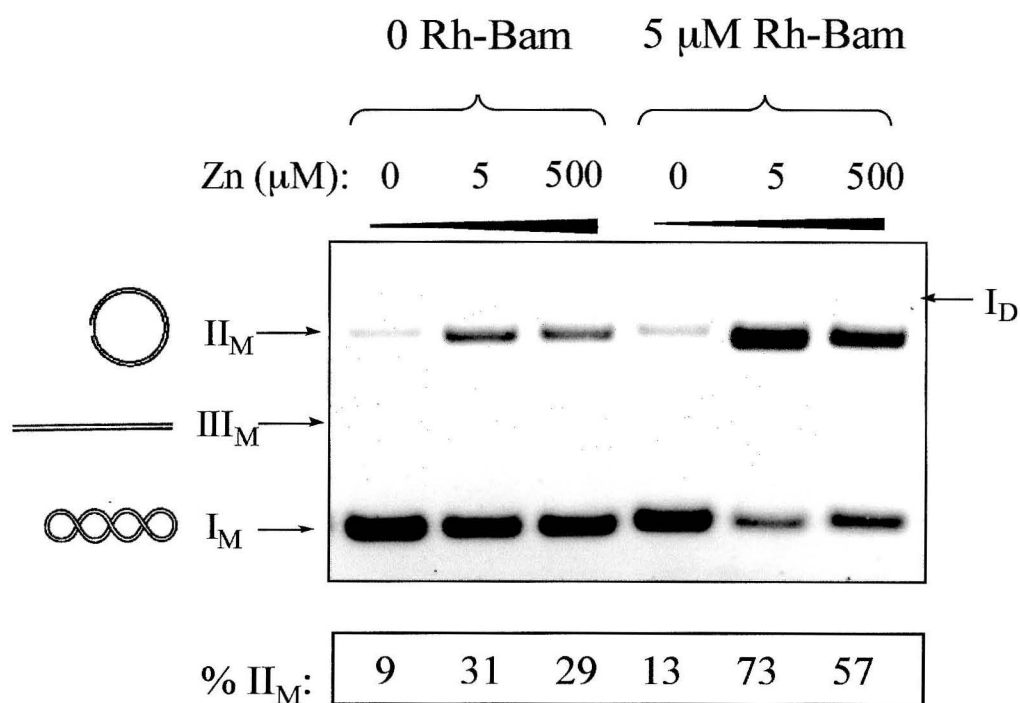


**Figure 2.10. Cleavage of Plasmid DNA by Rh-Bam.** In the presence of  $\text{Zn}^{2+}$ , 5 or 500  $\mu\text{M}$ , the Rh-Bam conjugate converts supercoiled pUC19 ( $\text{I}_\text{M}$ ) to the open circular form ( $\text{II}_\text{M}$ ). The percentage of open circular product is indicated below each lane. No linear plasmid ( $\text{III}_\text{M}$ ) was observed. For this experiment, Rh-Bam (5  $\mu\text{M}$ ),  $\text{Zn}^{2+}$ , and plasmid (40  $\mu\text{M}$  bp) were incubated in buffer (20 mM HEPES, 2 mM Na Borate, pH 6) for 24 h at 37  $^\circ\text{C}$ . The products were analyzed by agarose gel electrophoresis.

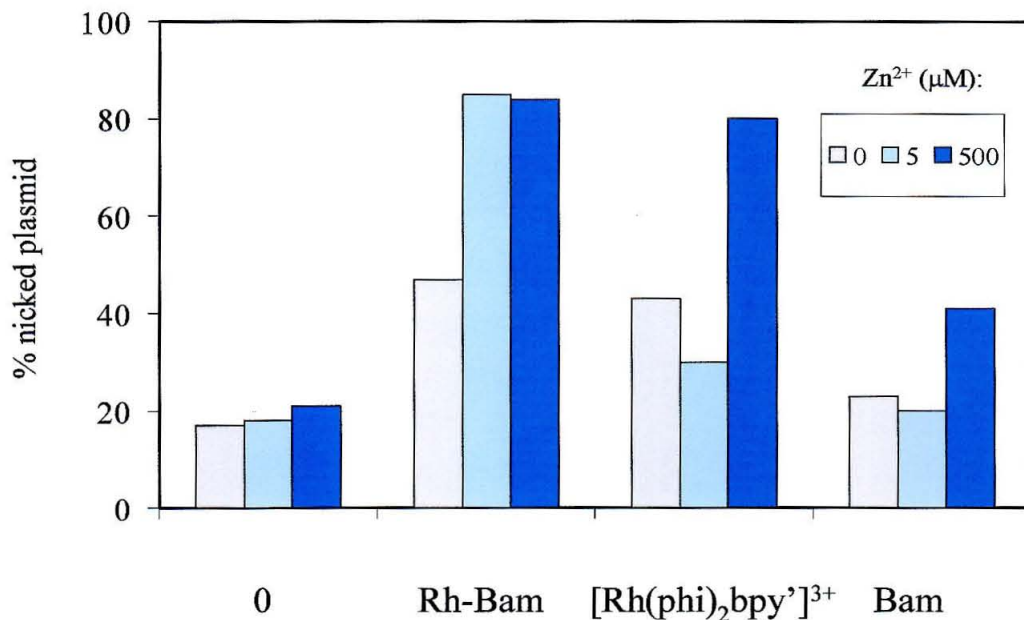


**Figure 2.11. Cleavage of pBR322 by Rh-Bam , [Rh(phi)<sub>2</sub>bpy']<sup>3+</sup>, and Bam Peptide.**

Plasmid (20 μM), metal complex or peptide (5 μM), and Zn<sup>2+</sup> (0, 5, or 500 μM) were combined in a sodium borate buffer (25 mM, pH 6.6). The reactions were incubated for 48 h at 37 °C, and were analyzed by agarose gel electrophoresis. A bar plot showing the percentage of nicked plasmid is presented.

In some experiments, the  $[\text{Rh}(\text{phi})_2\text{bpy}']^{3+}$  complex alone gave  $\text{Zn}^{2+}$ -promoted cleavage of the plasmid substrate (Figure 2.11). This formation of nicked plasmid cannot be attributed to photocleavage. The cleavage is  $\text{Zn}^{2+}$ -dependent, and the reaction samples were kept in the dark throughout the incubation. Though the Rh-Bam conjugate is more effective, particularly at lower  $\text{Zn}^{2+}$  concentrations, the rhodium intercalator, perhaps employing the pendant carboxylate, appears to mediate DNA-cation interactions.

As was observed for the entire family of Rh-P1 conjugates, Rh-Bam cleaved plasmid most effectively at pH 6. Plasmid cleavage levels dropped dramatically as the pH was increased from 6 to 7 (data not shown), and cleavage was never observed above pH 7. Below pH 5.5 or 6, depurination of the DNA substrate can occur and large amounts of nicked plasmid are produced even in control reactions without conjugate. The pronounced pH dependence of Rh-Bam cleavage may be related to the decreased solubility of  $\text{Zn}^{2+}$  at higher pH.

In contrast to Rh-P1, which showed maximum hydrolysis activity with stoichiometric  $\text{Zn}^{2+}$ , the Rh-Bam conjugate tolerated a range of  $\text{Zn}^{2+}$  concentrations. In one set of reactions with Rh-Bam,  $\text{Zn}^{2+}$  was varied between 2.5  $\mu\text{M}$  (0.5 equivalents) and 10 mM (2000 equivalents) (Figure 2.12). The percentage of nicked plasmid steadily increased with zinc ion concentration to 100  $\mu\text{M}$  and then decreased slightly at higher concentrations.

The impact of  $\text{Zn}^{2+}$  concentration on Rh-Bam cleavage levels was more carefully examined through the preparation of metal ion buffers. A metal ion buffer contains a metal-chelating ligand, an excess of weakly binding metal ion, and the desired metal ion.

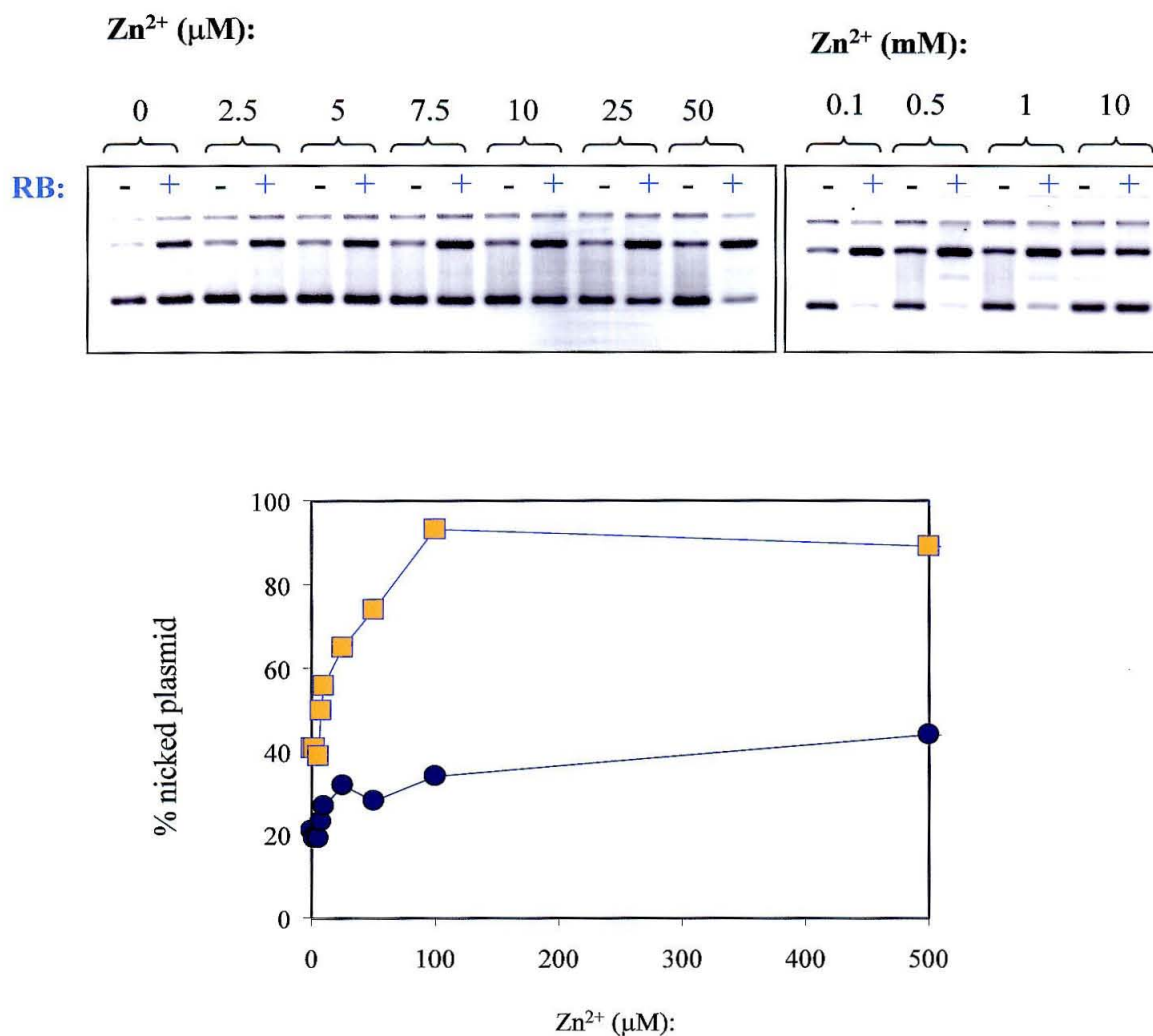


**Figure 2.12. Cleavage of pBR322 by Rh-Bam Over a Wide Range of Zn<sup>2+</sup>**

**Concentrations.** Plasmid (40 μM) was combined with Rh-Bam (5 μM) and Zn<sup>2+</sup> in a Na borate buffer (25 mM, pH 6.25). The reactions were incubated for 40 h at 37 °C, and were analyzed by agarose gel electrophoresis (top). A plot of the percentage of nicked plasmid vs. Zn<sup>2+</sup> concentration is shown for the Rh-Bam (orange squares) and control (blue circles) reactions.

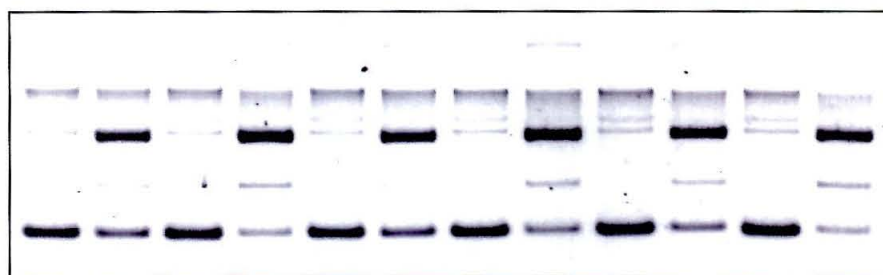
In this buffer system, the effective concentration of the desired metal ion is pH-independent and can be calculated from the stability constants of the two metals.<sup>13</sup> We used EDTA,  $\text{Mn}^{2+}$ , and  $\text{Zn}^{2+}$  in our metal ion buffers. In the experiment presented in Figure 2.13, the effective  $\text{Zn}^{2+}$  concentration was varied from 0 to 9  $\mu\text{M}$ . Rh-Bam gave similar amounts of nicked and linear product for each  $\text{Zn}^{2+}$  concentration; indeed, even the reaction without  $\text{Zn}^{2+}$  showed 61% nicked and 4% linear product. This result raised the possibility of using divalent cations other than  $\text{Zn}^{2+}$  in combination with Rh-Bam. Although the reaction was free of  $\text{Zn}^{2+}$ , it did contain millimolar quantities of  $\text{Mn}^{2+}$ .

Like Rh-P1, Rh-Bam sometimes failed to cleave plasmid substrates even under optimized conditions; in fact, the problem seems to be aggravated by the poor solubility of the Rh-Bam conjugate. Between pH 6 and 7, the Rh-Bam complex is much less soluble than Rh-P1, and it is not possible to prepare solutions with concentrations greater than 200  $\mu\text{M}$  Rh-Bam. With the Rh-Bam conjugate a delicate balance must be achieved; below pH 7 the Rh-Bam conjugate is not particularly soluble, and above pH 7 the solubility of  $\text{Zn}^{2+}$  limits reaction. Inconsistent cleavage results with Rh-Bam prevented kinetic analysis, and frustrated rigorous comparisons between Rh-P1 and Rh-Bam. In general the Rh-Bam conjugate appears to be less effective than Rh-P1 for the cleavage of plasmid DNA.

#### **2.3.4. Testing Rh-Bam with a Variety of Metal Ions.**

The Rh-Bam conjugate was tested with a variety of cations, both redox active and inactive, in plasmid cleavage experiments. Typical results for 24 h and 48 h incubations





<b>Rh-Bam:</b>	-	+	-	+	-	+	-	+	-	+	-	+
<b>Zn<sub>eff</sub> (μM):</b>	0		2.5		4.2		5.0		6.3		9.0	
<b>pH:</b>	6.4		6.5		6.6		6.3		6.3		6.5	
<b>% nicked:</b>	8	61	8	74	8	61	8	72	8	68	8	71
<b>% linear:</b>	0	4	0	9	0	4	0	8	0	8	0	12

**Figure 2.13. Cleavage of pBR322 by Rh-Bam in a Metal Ion Buffer.** Plasmid (40 μM) and Rh-Bam (5 μM) were combined in a Zn<sup>2+</sup> buffer (11 mM EDTA, 21 mM Mn, variable Zn, 25 mM Na borate). The effective Zn<sup>2+</sup> concentration ranged from 0 to 9, and the pH ranged from 6.3 to 6.5. The samples were incubated for 24 h at 37 °C, and then analyzed by agarose gel electrophoresis.

are presented in Figure 2.14.  $\text{Mg}^{2+}$ , the cofactor employed in the active site of the *Bam*HI restriction enzyme, showed slightly lower cleavage levels than  $\text{Zn}^{2+}$ , and  $\text{Mn}^{2+}$  was still lower.  $\text{Fe}^{2+}$  and  $\text{Cu}^{2+}$ , both redox active metals, gave significant plasmid cleavage even in control reactions that did not contain Rh-Bam; in fact, the addition of Rh-Bam actually reduced the  $\text{Cu}^{2+}$ -mediated damage to the DNA substrate.  $\text{Cd}^{2+}$ , just below  $\text{Zn}^{2+}$  in the periodic table, is also effective for cleavage; it gave higher levels of nicked plasmid after 24 h in the presence of Rh-Bam, but also gave higher levels of background cleavage in the absence of Rh-Bam.  $\text{Ni}^{2+}$  and  $\text{Co}^{2+}$  were very comparable with  $\text{Zn}^{2+}$ . With  $\text{Pb}^{2+}$  and the lanthanide metal ions,  $\text{Ce}^{3+}$  and  $\text{La}^{3+}$ , very high levels of plasmid cleavage were observed for 500  $\mu\text{M}$  metal ion even without the addition of Rh-Bam. For 5  $\mu\text{M}$   $\text{Pb}^{2+}$ ,  $\text{Ce}^{3+}$ , or  $\text{La}^{3+}$  the addition of Rh-Bam greatly increased reaction, and produced significant levels of nicked plasmid.

### 2.3.5. DNA Photocleavage with Rh-Bam.

The  $[\text{Rh}(\text{phi})_2\text{bpy}']^{3+}$  complex binds to DNA in a predominantly sequence neutral manner, and upon photoactivation, abstracts a hydrogen atom from the ribose ring to produce DNA strand scission. A slight preference for 5'-Pu-Py-Pu-Py-3' sites is observed in DNA photocleavage reactions (cleavage at italicized Py).<sup>16,21,22</sup> To explore the impact of the tethered Bam peptide on the DNA binding and photocleavage properties of the rhodium intercalator, experiments were completed with a 175 base pair restriction fragment (Figure 2.15).

Samples containing plasmid restriction fragment and  $[\text{Rh}(\text{phi})_2\text{bpy}']^{3+}$ , Rh-P1, or Rh-Bam were irradiated at 313 nm. For all three metal complexes, photocleavage

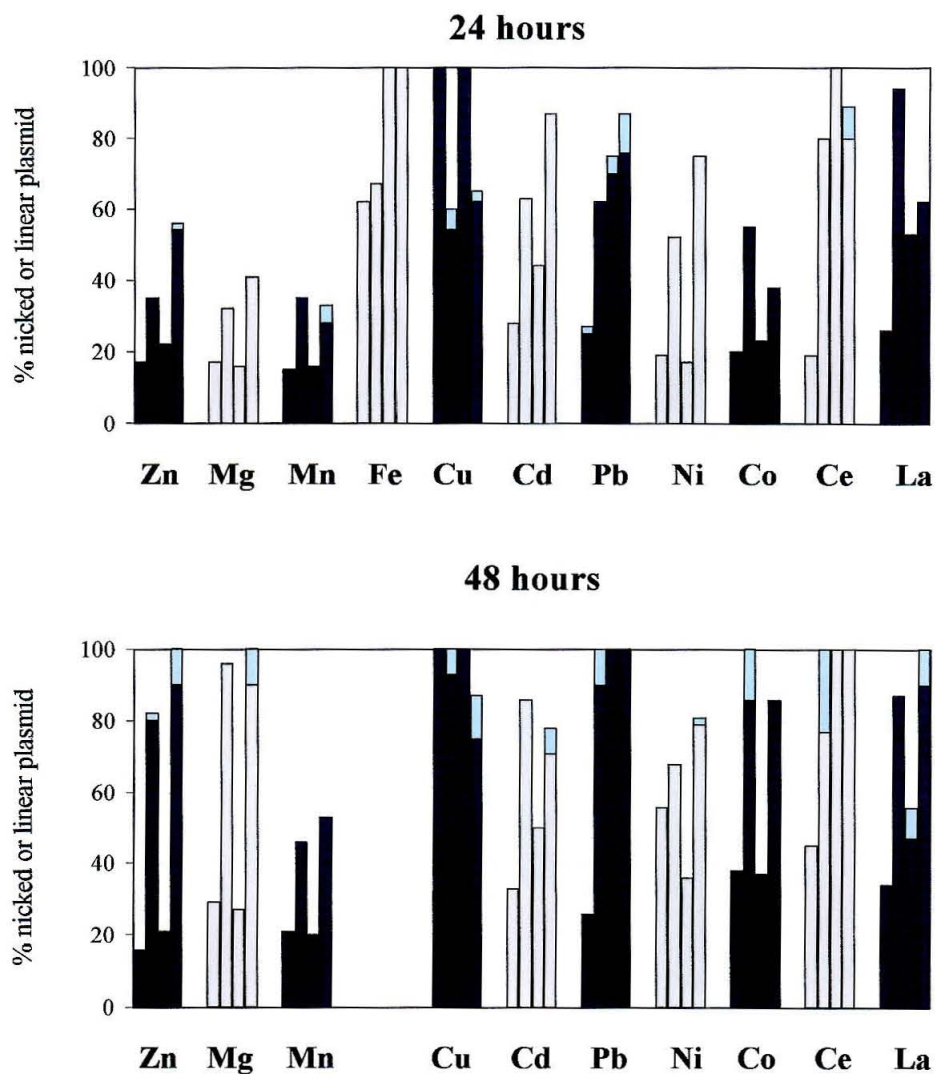


**Figure 2.14. Cleavage of pBR322 by Rh-Bam and a Variety of Metal Cations.**

Plasmid (20  $\mu\text{M}$  bp), Rh-Bam (0 or 5  $\mu\text{M}$ ), and a variety of metal cations (5 or 500  $\mu\text{M}$ ) were combined in sodium borate buffer (20 mM, pH 6-6.5). The percentage of nicked (gray or black bars) and linear (blue bar) product is shown for 24 h (top) and 48 h (bottom) incubation at 37 °C. From left to right, the four bars are: 0 Rh-Bam, 5  $\mu\text{M}$   $\text{M}^{2+}$ ; 5  $\mu\text{M}$  Rh-Bam, 5  $\mu\text{M}$   $\text{M}^{2+}$ ; 0 Rh-Bam, 500  $\mu\text{M}$   $\text{M}^{2+}$ ; and 5  $\mu\text{M}$  Rh-Bam, 500  $\mu\text{M}$   $\text{M}^{2+}$ .

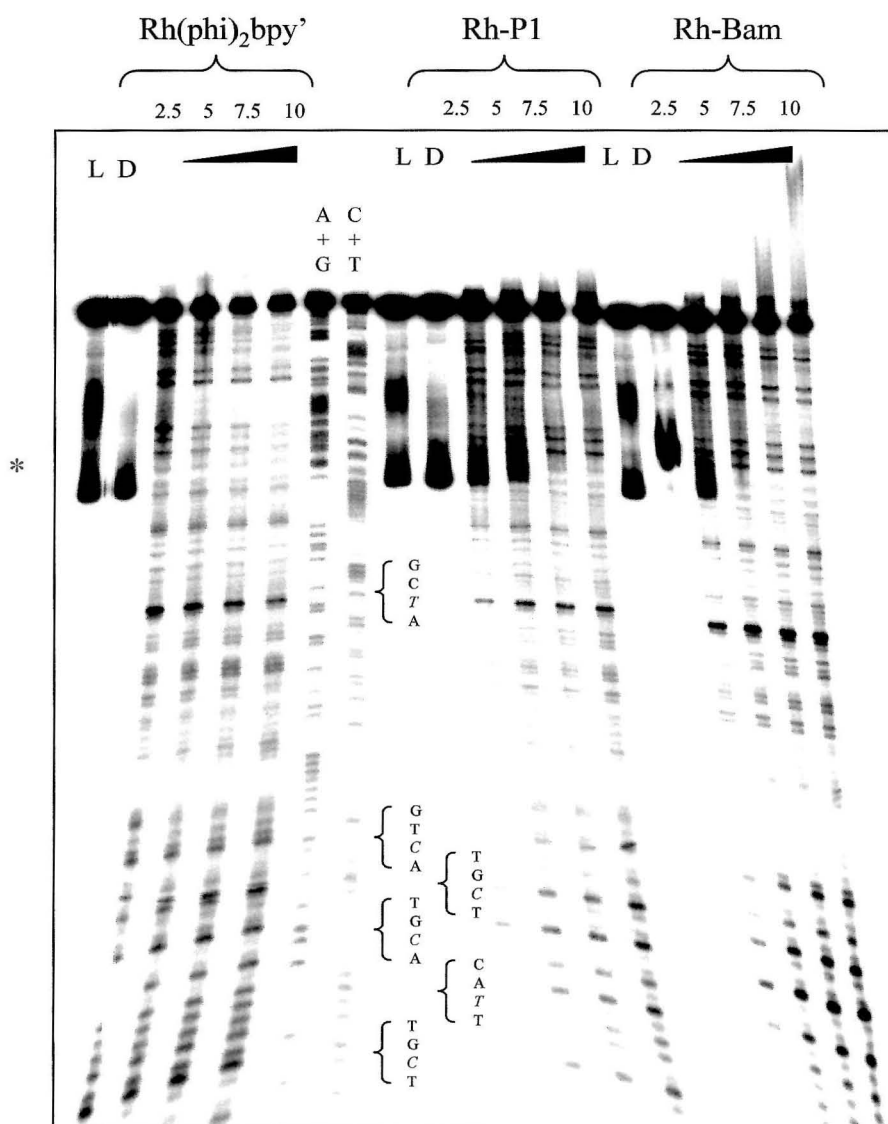


**Figure 2.15. Photocleavage of a Plasmid Restriction Fragment by  $\text{Rh}(\phi)_2\text{bpy}'\text{]}^{3+}$ ,  $\text{Rh-P1}$ , and  $\text{Rh-Bam}$ .** A restriction fragment (100  $\mu\text{M}$  bp, 5'-labeled), Rh complex (2.5, 7.5, 5, 10  $\mu\text{M}$ ), and  $\text{Zn}^{2+}$  were combined in buffer (25 mM Tris-HCl, pH 7.85). The samples were irradiated at 313 nm for 5 min, and analyzed by 7% PAGE. Lanes are labeled as follows: A+G, C+T, Maxam-Gilbert reactions; L, light control, 5 min irradiation; D, dark control, 10  $\mu\text{M}$  Rh. The sites with most intense photocleavage are labeled with the 4 base sequence. The asterisk indicates a band due to renaturation.

occurred across the plasmid restriction fragment with only modest sequence selectivity. As expected, the damage at 5'-Pu-Py-Pu-Py-3' sites was a bit more intense. Though the efficiency of photocleavage was reduced slightly by the attachment of either the P1 or Bam peptides, the pattern of damage was not perturbed. These particular peptides do not contribute DNA recognition characteristics to the conjugate. These photocleavage results also confirm that there is no significant interaction between the Bam peptide and the metallointercalator; they are separate components. The peptide does not block DNA intercalation or prevent DNA photocleavage.

#### **2.3.6. Testing Rh-Bam for Oligonucleotide Hydrolysis Activity.**

The plasmid cleavage assay is very sensitive and very convenient, but oligonucleotide cleavage experiments provide valuable information about the mechanism and molecular details of cleavage. Importantly, and in contrast to Rh-P1, the Rh-Bam conjugate has not been demonstrated to cleave linear oligonucleotide DNA. Rh-Bam has been tested with a variety of oligonucleotide substrates, but despite parallel experiments that gave as much as 90% conversion of plasmid to a nicked form, no damage to an oligonucleotide substrate was observed. It is also noteworthy that very little linear plasmid was produced in Rh-Bam reactions with supercoiled plasmid DNA; in fact, in some reactions that produced 60 to 70% nicked plasmid, no linear plasmid was observed (Figure 2.10).

A typical oligonucleotide cleavage experiment is presented in Figures 2.16 and 2.17. A 27 base pair duplex was combined with Rh-Bam and irradiated. Again, fairly

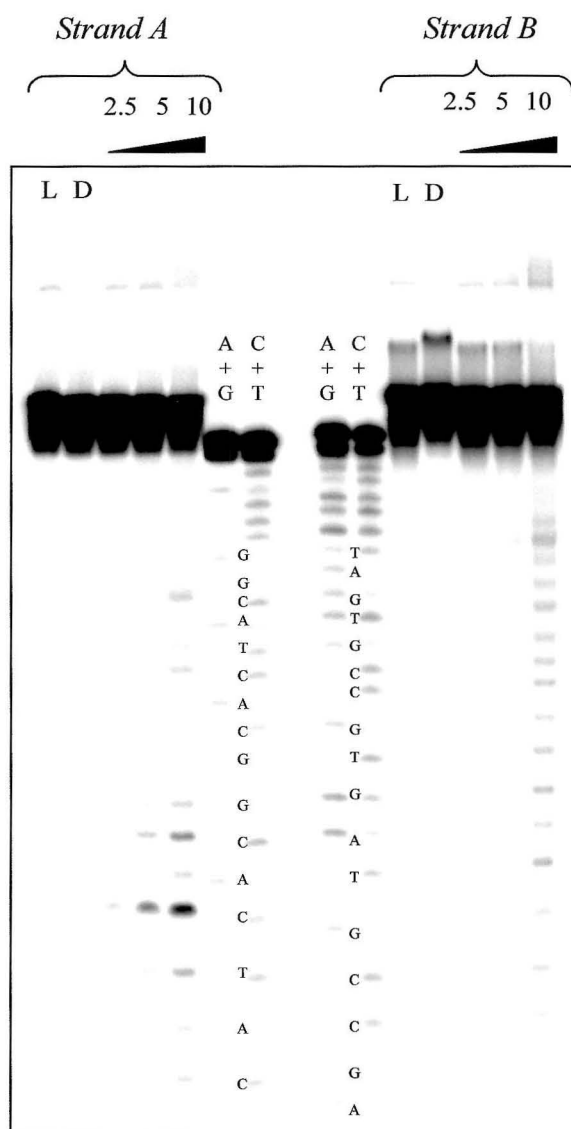


**Figure 2.16. Photocleavage of an Oligonucleotide by Rh-Bam.** A 27-mer duplex (10  $\mu$ M, 5'-labeled, strand A and strand B) and Rh-Bam (2.5, 5, 10  $\mu$ M) were combined in buffer (25 mM Tris-HCl, 20 mM Na acetate, pH 7). The samples were irradiated at 313 nm for 15 min, and analyzed on a 20% polyacrylamide gel. Lanes are labeled as follows: A+G, C+T, Maxam-Gilbert sequencing reactions; L, light control, 15 min irradiation of duplex; D, dark control, no irradiation of duplex and 10  $\mu$ M Rh-Bam.

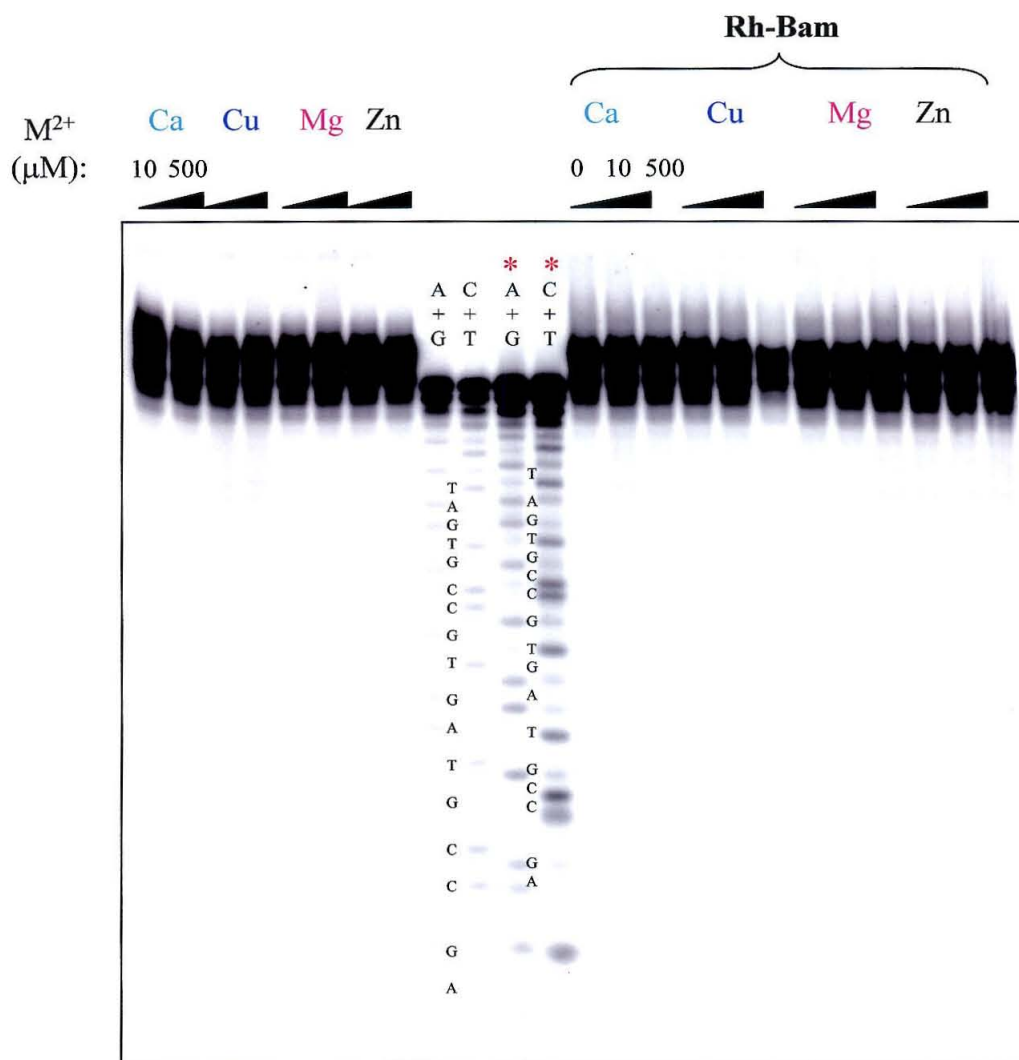


**Figure 2.17. Incubation of Oligonucleotide with Rh-Bam and Divalent Cations.**

A 27-mer duplex (40  $\mu M$  bp, 5'-labeled strand B), Rh-Bam (10  $\mu M$ ), and a variety of metal cations (Ca, Cu, Zn, Mg) were combined in Na borate buffer (20 mM, pH 6.6). The samples were incubated for 40 h at 37  $^{\circ}C$ , and analyzed on a 20% polyacrylamide gel. A+G, C+T: standard Maxam-Gilbert sequencing reactions; \*A+G, \*C+T: dephosphorylated Maxam-Gilberts.

sequence-neutral cleavage was observed on both oligonucleotide strands. The most intense damage was observed at the 5'-TCAC-3' and 5'-ACGG-3' sites in strand A. The 27 base pair duplex was also incubated with Rh-Bam and four different metal ions (Ca, Cu, Mg, and Zn) for 40 h. Even with this extended reaction time, no significant cleavage of the oligonucleotide substrate was observed. Even with 500  $\mu\text{M}$   $\text{Cu}^{2+}$ , under conditions that caused extensive degradation of plasmid DNA, the oligonucleotide was not damaged.

### **2.3.7. Cleavage of Supercoiled Plasmid by Rh-Bam2 and Rh-Bam3.**

Two metallointercalator-peptide conjugates with designed hairpin peptides were prepared and tested alongside the Rh-Bam conjugate. The Rh-Bam2 and Rh-Bam3 conjugates contain acidic residues for metal coordination, forcing turns, and residues with high propensity for hairpin formation. It was hoped that the designed hairpins would have improved solubility and greater conformational stability than the tethered Bam peptide.

The Rh-Bam2 and Rh-Bam3 conjugates were characterized by mass spectrometry, amino acid analysis, and electronic spectroscopy. The circular dichroism spectra obtained for these two conjugates had no striking features; the designed peptides may actually be disordered.

In plasmid cleavage experiments Rh-Bam2 and Rh-Bam3 showed little cleavage activity (Figure 2.18). The levels of nicked plasmid obtained with Rh-Bam2 and Rh-Bam3 matched the levels obtained with the  $[\text{Rh}(\text{phi})_2\text{bpy}]^{3+}$  complex, but were



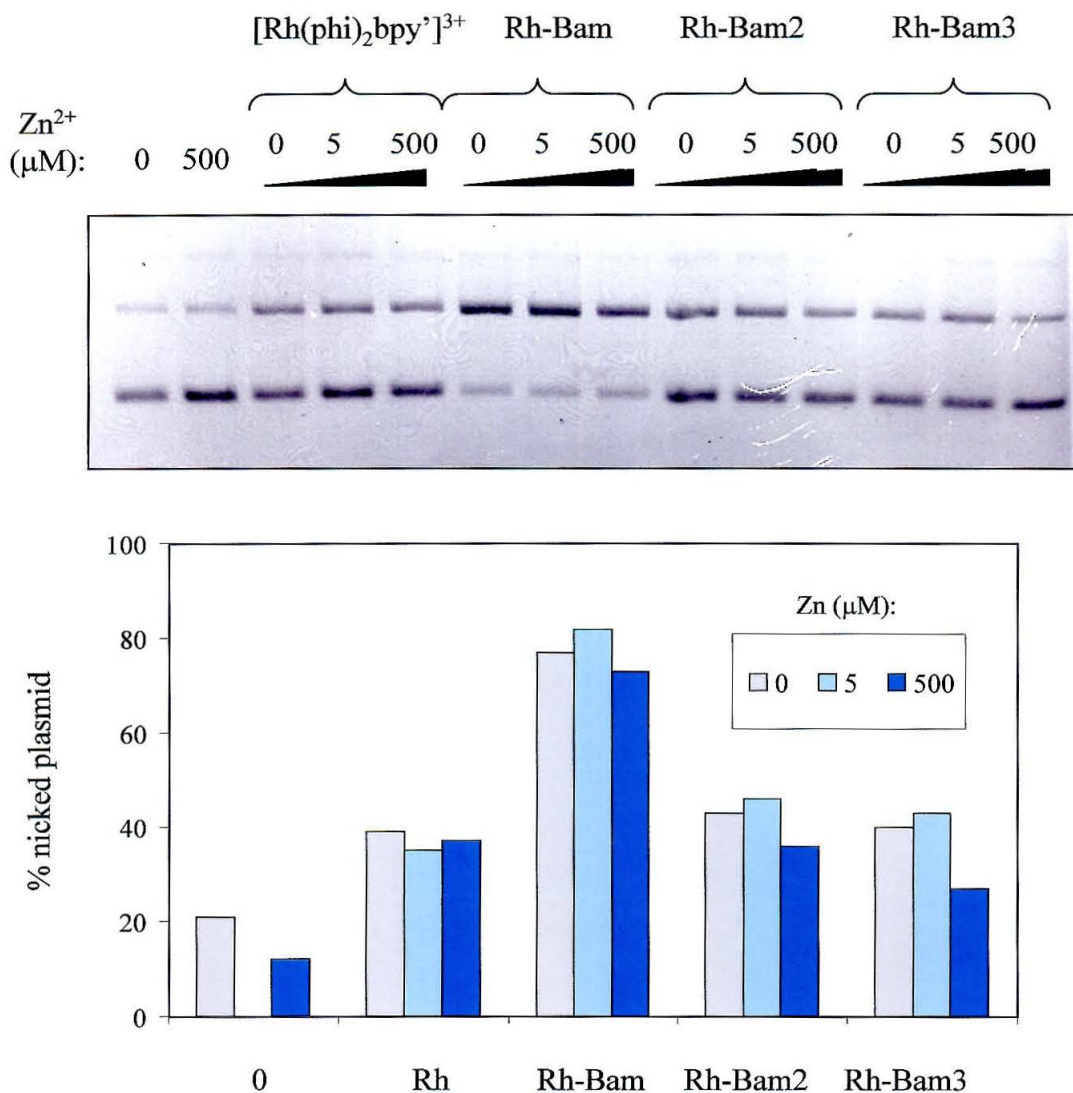


**Figure 2.18. Cleavage of pBR322 by  $[\text{Rh}(\text{phi})_2\text{bpy}']^{3+}$ , Rh-Bam, Rh-Bam2, and Rh-Bam3.** Plasmid (20  $\mu\text{M}$ ), metal complex (10  $\mu\text{M}$ ), and  $\text{Zn}^{2+}$  (0, 5, or 500  $\mu\text{M}$ ) were combined in a Na borate buffer (25 mM, pH 6.3 - 6.5). The reactions were incubated for 24 h at 37  $^{\circ}\text{C}$ , and analyzed by agarose gel electrophoresis. A bar plot showing the percentage of nicked plasmid for each metal complex is presented.

significantly lower than the levels with Rh-Bam. By redesigning the Bam peptide, we have eliminated features that contribute to cleavage activity.

In Figure 2.18, it is also interesting to note that there is no  $\text{Zn}^{2+}$  dependence observed for Rh-Bam cleavage. Although plasmid preparations were extensively dialyzed or were treated with metal-chelating resin prior to cleavage experiments, it is possible that this particular plasmid stock was contaminated with metal ion, perhaps  $\text{Fe}^{2+}$ .

## 2.4. Discussion

By coupling DNA intercalators and metal-binding peptides, we have created chimeras that bind to DNA with high affinity and cleave the DNA backbone by  $\text{Zn}^{2+}$ -promoted hydrolysis. Our very first chimera, Rh-P1, consisted of a designed helical peptide containing histidine residues for  $\text{Zn}^{2+}$  coordination, and a  $[\text{Rh}(\text{phi})_2\text{bpy}']^{3+}$  metallointercalator.<sup>1</sup> While small systematic changes in the P1 peptide allowed a clarification of mechanism, much larger changes in peptide composition provided a test of the overall strategy.

We have now demonstrated that our approach to DNA hydrolysis is a general one; significant changes in the tethered peptide do not abolish the cleavage activity of the chimera.<sup>2</sup> In the case of Rh-Bam, a hairpin peptide inspired by the active site of the *Bam*HI endonuclease was appended to  $[\text{Rh}(\text{phi})_2\text{bpy}']^{3+}$  (Figure 2.4) and successfully applied to the conversion of supercoiled plasmid to nicked product.

### 2.4.1. The Peptide.

There are both advantages and disadvantages to employing peptides to create the coordination environment for divalent cations. Through solid-phase synthesis, peptides are readily prepared and purified. Since they are composed of readily available building blocks, it is facile to tune the peptide composition to achieve the desired properties and variations. A great deal of effort has been invested in the creation of short peptide systems with defined secondary structure,<sup>23</sup> and the elucidated principles can be incorporated into the design of tethered peptides. Also, because we are using the ligands that enzymes use for orienting and presenting metal ions in an active site, our conjugates likely have biological relevance.

On the other hand, short peptides do not provide a rigid or well-defined coordination environment. In contrast to many of the small synthetic ligands employed in other laboratories for metal-promoted DNA hydrolysis,<sup>24-28</sup> our peptides are very flexible. Indeed, our designed  $\alpha$ -helix is only modestly helical,<sup>1,16</sup> and it is not clear whether the 22-mer derived from *Bam*HI retains any of its native conformation outside of the *Bam*HI environment.

Additionally, these short peptides offer little control over the stoichiometry of metal binding, the intramolecularity of metal coordination, and the associated solubility properties. Zinc hydroxide precipitates above neutral pH, and our flexible peptides, with only naturally occurring amino acids, are not effective at solubilizing the  $\text{Zn}^{2+}$  ion. Additionally, depending on the composition of the peptide, solubility of the conjugate becomes an important issue. Despite these difficulties, DNA cleavage chemistry was

achieved with two widely different peptides: the de novo designed P1 peptide, and now, the Bam peptide.

**The Bam Peptide.** The Bam peptide (NH<sub>2</sub>-Ala-**Asp**-Val-Tyr-Lys-Glu-Phe-Ile-Glu-Asn-Ser-Glu-Leu-Lys-Arg-Val-Gly-Ala-**Glu**-Phe-**Glu**-Ala-CONH<sub>2</sub>) is twenty-two amino acids long and contains the three acidic residues (shown in bold) that are essential to *Bam*HI cleavage activity. Only very slight changes in the hairpin sequence were made prior to appending the peptide; an alanine residue was added to the N-terminus of the peptide to give flexibility to the peptide-DNA interaction, and methionine and threonine residues were replaced with alanine residues to simplify the synthesis and reactivity of the peptide (Figure 2.2).

Although glutamate and aspartate are employed for metal coordination in the active site of *Bam*HI and all type II restriction endonucleases, they are not the best candidates for the creation of short, metal-binding peptides. Histidine actually has a higher stability constant for Zn<sup>2+</sup> (See Table 2.1).<sup>29-31</sup> In a protein environment the metal-binding properties of acidic residues can be carefully tuned, but in a floppy peptide there is little opportunity for tuning. Residues that tightly bind metals are the best choice. It is very interesting that we can cleave plasmid DNA with a tethered peptide that only bears acidic residues.

With all of its acidic residues, the Bam peptide is negatively charged. This may decrease the interactions between the peptide and the polyanionic backbone of DNA. We have observed that the inclusion of Lys residues in tethered peptides can increase binding affinity of the conjugate,<sup>32,33</sup> and can greatly increase DNA-peptide interaction.<sup>34</sup>

The structure of the appended Bam peptide was investigated by circular dichroism spectroscopy. Although some interesting changes occurred in the CD spectrum of Rh-Bam with the addition of  $\text{Zn}^{2+}$  (Figure 2.8), the intensity and position of the bands are consistent with a random coil or disordered peptide conformation. The addition of TFE to Rh-Bam samples actually produced a helix-like spectrum (Figure 2.9), but this is not uncommon with halogenated solvents.<sup>19</sup> The CD spectra observed for  $\beta$  turns and hairpins are weak and highly variable compared to the spectra for  $\alpha$ -helices,<sup>20</sup> so the absence of striking features in the CD of Rh-Bam does not rule out a population of  $\beta$ -hairpin. Interactions between Rh-Bam and DNA might induce some structure in the Bam peptide, but the strong absorbance of the rhodium complex prevents CD study of Rh-Bam structure in the presence of DNA. Notably, the peptide contains a total of six acid residues, and it is possible that any of these residues might be involved in zinc coordination and delivery, particularly if the peptide is not folding into a hairpin conformation.

The Bam peptide is only modestly soluble, and potentiometric titrations resulted in precipitation of the Rh-Bam conjugate around pH 4 as the acidic groups were deprotonated. Rh-Bam redissolved as the pH increased to 7, but at this pH, free  $\text{Zn}^{2+}$  began to precipitate. In reactions with Rh-Bam, therefore, the pH must be carefully balanced to prevent precipitation of conjugate or zinc ion.

We have observed plasmid cleavage with the Rh-Bam conjugate between pH 6 to 7, and with a variety of metal cations. Rh-Bam is an artificial nuclease, albeit a picky one. The conformational flexibility of the appended Bam peptide, the low solubility of the Rh-Bam conjugate, and the failure of the acidic residues to solubilize  $\text{Zn}^{2+}$  at higher

pH are all obstacles to effective DNA cleavage. The cleavage activity observed with Rh-Bam has been very promising, but also inconsistent. With the goal of improving the conformational stability and solubility of our appended hairpin, we designed two additional peptides.

***De Novo Designed Hairpin Peptides.*** Although the design of  $\beta$  hairpins is quite challenging, there have been several reports in the literature of short peptides which fold into stable  $\beta$  hairpin conformations, and useful principles for design are emerging.<sup>35-38</sup> It is very clear that turn residues are critical to successful hairpin design; they constrain the peptide and allow for a network of hydrogen bonds between the strands. Aromatic and  $\beta$  branched residues have a high intrinsic preference for forming  $\beta$  sheet. Statistical surveys of  $\beta$  sheet proteins and host-guest studies suggest that Trp, Phe, Tyr, Thr, Ile, and Val are good candidate residues.<sup>39-43</sup>

To further explore the possibility of delivering metal cations to DNA with hairpins and acidic residues, we have designed two shorter hairpin peptides (Bam2 and Bam3). The designed hairpins still include three acidic residues for metal coordination, but also contain forcing turns and residues with a high propensity for hairpin formation.

Bam2, a 16-mer peptide, includes residues with high  $\beta$  sheet propensity (Thr, Tyr, Phe, and Val) and near the center of the peptide, contains asparagine and glycine. This pair of residues is expected to promote a type I'  $\beta$  turn.<sup>44</sup> The Bam2 peptide is very similar to a  $\beta$  hairpin peptide studied by Serrano et al.<sup>36</sup> Bam3 peptide consists of 14 amino acids, and contains D-proline and serine. It has been observed that a heterochiral pair of amino acids, DX-LX, favors the type II'  $\beta$  turn, a turn which creates a very tight

hairpin.<sup>44</sup> The DPro-Ser pair has been successfully applied in previous hairpin design efforts.<sup>45</sup>

The designed hairpin peptides were attached to  $[\text{Rh}(\text{phi})_2\text{bpy}']^{3+}$  (Figure 2.5), and were tested in plasmid cleavage experiments alongside Rh-Bam. Neither Rh-Bam2 nor Rh-Bam3 was as effective as Rh-Bam for plasmid cleavage. Although our design efforts were not fruitful, this is an interesting result. By shortening and altering the composition of our hairpin peptide, we have dramatically reduced cleavage activity. Appending a peptide with three acidic residues to a DNA intercalator is not sufficient to create an artificial nuclease; the Rh-Bam conjugate has some important features that provide DNA cleavage activity.

#### 2.4.2. The Metal Cation.

As was described in Chapter 1,  $\text{Zn}^{2+}$  plays an important structural or catalytic role in hundreds of proteins and enzymes.<sup>46</sup>  $\text{Zn}^{2+}$  has a filled d shell, and thus it tolerates a variety of coordination geometries, forms labile coordination complexes, and does not access other redox states.<sup>47</sup> In addition,  $\text{Zn}^{2+}$  very effectively promotes the nucleophilicity of bound water.<sup>48</sup> All of these characteristics make  $\text{Zn}^{2+}$  a very promising candidate metal ion for an artificial nuclease. The Bam peptide does not contain any histidine residues, the most common  $\text{Zn}^{2+}$  ligand in catalytic sites,<sup>47</sup> but because  $\text{Zn}^{2+}$  is a borderline hard-soft Lewis acid, glutamate and aspartate can also serve as coordinating ligands.

The Rh-Bam complex does cleave supercoiled plasmid in the presence of  $\text{Zn}^{2+}$  (Figure 2.10). In natural and artificial nucleases, metals have been found to play a

number of different roles, including activation of the nucleophile, activation of the electrophile, and stabilization of the leaving group.<sup>49</sup> We have not defined the role of the metal cation in our intercalator-peptide conjugate system, but we have determined that it plays an essential role. Occasionally the cleavage activity of our intercalator-peptide conjugates did not show any dependence on  $\text{Zn}^{2+}$  (Figure 2.18), but this is most likely due to metal contamination in the plasmid stock solution.

In contrast to Rh-P1, which shows maximum helicity and activity at stoichiometric amounts of  $\text{Zn}^{2+}$ , the Rh-Bam conjugate maintains cleavage activity as  $\text{Zn}^{2+}$  concentration is raised significantly above stoichiometric levels (Figure 2.12). This observation suggests that  $\text{Zn}^{2+}$  is not playing a critical role in nucleating the formation of an active peptide conformation.

For both the Rh-P1 family of conjugates and Rh-Bam, DNA cleavage decreased as the pH increased above pH 6. The reason for the sensitivity of the reaction to pH is likely, at least in part, the result of decreased solubility of zinc at higher pH. It appears that the coordination environment created by Rh-P1 or Rh-Bam is insufficient to prevent precipitation. This issue of solubility has made it very difficult to control the hydrolysis of DNA by our metal-peptide.

$\text{Zn}^{2+}$  is not the only metal that can be effectively delivered to DNA by the Rh-Bam conjugate. We have tested Rh-Bam with  $\text{Mg}^{2+}$ ,  $\text{Mn}^{2+}$ ,  $\text{Fe}^{2+}$ ,  $\text{Co}^{2+}$ ,  $\text{Ni}^{2+}$ ,  $\text{Cu}^{2+}$ ,  $\text{Cd}^{2+}$ ,  $\text{Pb}^{2+}$ ,  $\text{La}^{3+}$ , and  $\text{Ce}^{3+}$ , and have observed promising plasmid cleavage with several of these cations. These metal cations range from hard ( $\text{Mg}^{2+}$ ) to soft ( $\text{Cd}^{2+}$ ), and the ionic radii vary from 0.65 ( $\text{Mg}^{2+}$ ) to 1.2 Å ( $\text{Pb}^{2+}$ ).<sup>47</sup> In contrast to  $\text{Zn}^{2+}$ , which prefers tetrahedral coordination, most of these metals require octahedral coordination environments.<sup>47</sup> The



stability constants for a variety of metal ions with His, Asp, and Glu are presented in Table 2.1.

**Table 2.1. Stability Constants of Divalent Metal Ions with Amino Acids.<sup>a</sup>**

Metal Ion	$\log K_1^b$	$\log K_1$	$\log K_1$
	His	Asp	Glu
<b>Zn<sup>2+</sup></b>	6.7	5.6	4.6
<b>Mg<sup>2+</sup></b>	--	2.4	1.9
<b>Mn<sup>2+</sup></b>	3.5	3.8	3.3
<b>Fe<sup>2+</sup></b>	5.9	4.3	4.6
<b>Cu<sup>2+</sup></b>	10.3	8.5	7.9
<b>Cd<sup>2+</sup></b>	5.6	4.4	4.3
<b>Pb<sup>2+</sup></b>	6.4	6.0	--
<b>Ni<sup>2+</sup></b>	8.7	6.9	5.6
<b>Co<sup>2+</sup></b>	7.0	5.9	4.7
<b>Ce<sup>3+</sup></b>	4.5	5.1	--
<b>La<sup>3+</sup></b>	3.8	4.8	--

<sup>a</sup> Stability constants are averages of literature values.<sup>29-31</sup>

<sup>b</sup>  $K_1 = [ML]/[M][L]$  where M is the metal ion and L is the free amino acid ligand. The values for  $K_2$  (not shown) follow the same general trend.

Rh-Bam, which includes acidic residues that should be particularly effective for coordinating hard ions, can also promote plasmid cleavage with  $\text{Mg}^{2+}$ . Magnesium is the ion used by most restriction enzymes, including *Bam*HI, in DNA hydrolysis.  $\text{Mg}^{2+}$  is redox inert, has a high charge density, possesses a coordination number of 6, and prefers hard oxoanion ligands.  $\text{Mg}^{2+}$  is extensively hydrated, preferring water over bulkier ligands, but it does not activate water for nucleophilic attack to the same extent as  $\text{Zn}^{2+}$ .<sup>50</sup>  $\text{Zn}^{2+}$  gives higher percentages of nicked plasmid than  $\text{Mg}^{2+}$  when incubated with Rh-Bam and supercoiled plasmid, and this is not surprising given the properties of these two important biological metal ions. Rh-P1 is not able to hydrolyze plasmid in the presence of  $\text{Mg}^{2+}$ , presumably because histidine is not an effective ligand for hard cations like  $\text{Mg}^{2+}$ .

Modest plasmid cleavage is also observed with  $\text{Mn}^{2+}$ , another hard metal ion. Although the levels of background cleavage increase, cobalt, nickel, and cadmium can be substituted for zinc ion.  $\text{Cd}^{2+}$  also has a filled d shell, but it is a softer metal than  $\text{Zn}^{2+}$ , with a larger radius and greater polarizability.<sup>47</sup> At 500  $\mu\text{M}$  concentrations, lead and the lanthanide metal ions,  $\text{Ce}^{3+}$  and  $\text{La}^{3+}$ , promote extensive plasmid degradation even without Rh-Bam. At lower concentrations Rh-Bam is required for efficient DNA cleavage. Rh-Bam is a useful tool for delivering low concentrations of lead or lanthanide ion to DNA.

Two redox-active metals,  $\text{Fe}^{2+}$  and  $\text{Cu}^{2+}$  have also been tested with the Rh-Bam conjugate. Iron mediates efficient Fenton chemistry, and with or without Rh-Bam,  $\text{Fe}^{2+}$  gave extensive plasmid degradation. In plasmid cleavage assays,  $\text{Cu}^{2+}$ , without rhodium complex, promoted considerable formation of nicked plasmid even at 5  $\mu\text{M}$

concentrations. As was observed previously with Rh-P1, the addition of the Rh-Bam conjugate actually caused a decrease in the percentage of nicked plasmid generated by  $\text{Cu}^{2+}$ . Apparently the conjugates provided modest protection for the plasmid, perhaps by sequestering some of the copper or by blocking access to the DNA backbone. Notably, very little damage was observed when an oligonucleotide duplex was incubated with 500  $\mu\text{M}$   $\text{Cu}^{2+}$  (Figure 2.17). This result emphasizes the differences between supercoiled plasmid and linear DNA cleavage assays. The plasmid cleavage observed with both iron and copper likely occurred by an oxidative mechanism.

#### 2.4.3. The DNA Metallointercalator.

In contrast to many of the artificial nucleases described in the literature, our intercalator-peptide conjugates bind to DNA with high affinity. The  $[\text{Rh}(\text{phi})_2\text{bpy}]^{3+}$  complex intercalates from the major groove with  $K_b > 10^7 \text{ M}^{-1}$ .<sup>21</sup> This allows us to target DNA using low conjugate concentrations. The intercalator is an essential component of our design, and very little plasmid cleavage is observed with untethered peptide (Figure 2.11). Though it is not as effective as Rh-P1 or Rh-Bam, we have observed some plasmid cleavage with the  $[\text{Rh}(\text{phi})_2\text{bpy}]^{3+}$  alone (Figure 2.11). Particularly at high metal concentrations, it appears that the carboxylate arm of the complex may facilitate delivery of cations to DNA. Of course, it is possible that the rhodium intercalator is more than a passive delivery system. The strain and unwinding that results from DNA intercalation may be a factor in the DNA hydrolysis observed with our conjugates (See below).

In addition to delivering the peptide and metal ion to DNA, the  $[\text{Rh}(\text{phi})_2\text{bpy}']^{3+}$  complex serves as a photoactive probe; it cleaves DNA when irradiated at 313 nm.<sup>21,22</sup> The photocleavage reaction proceeds through abstraction of a hydrogen atom from the ribose ring and subsequent strand scission.<sup>51</sup> This oxidative reaction reveals the binding sites of the intercalator, and provides valuable information about the interactions of our intercalator-peptide conjugate with DNA.

As was observed with the Rh-P1 conjugate,<sup>16</sup> the intercalator and Bam peptide are separate components. Both electronic spectroscopy and DNA photocleavage studies suggest that there is little interaction between the peptide and the rhodium complex (Figures 2.7 and 2.15). The peptide does not wrap around the complex to prevent intercalation; indeed, the intensity of photocleavage damage is reduced only slightly by the addition of the bulky peptide to the photoactive rhodium complex (Figure 2.15). The peptide also does not change the DNA recognition properties of the rhodium intercalator. The pattern of damage across a plasmid restriction fragment is nearly identical for  $[\text{Rh}(\text{phi})_2\text{bpy}']^{3+}$  and Rh-Bam (Figure 2.15).

A true artificial restriction enzyme would selectively hydrolyze a specific sequence in a DNA duplex. Although we selected a sequence-neutral intercalator for our initial studies, metallointercalators can be tuned to recognize a sequence or a mismatch site in DNA. The attachment of peptides to a mismatch-specific rhodium intercalator is described in Chapter 4.

#### 2.4.4. A Comparison of the Cleavage Activity of the Rh-P1 and Rh-Bam

##### Conjugates.

Two metallointercalator-peptide conjugates, Rh-P1 and Rh-Bam, have been demonstrated to cleave supercoiled plasmid. Both conjugates are most effective at pH 6, but as was observed with Rh-P1, Rh-Bam sometimes failed to cleave plasmid substrates even under optimized conditions.

There were some notable differences in the cleavage properties of Rh-P1 and Rh-Bam. The activity of Rh-P1 drops sharply above stoichiometric concentrations of  $\text{Zn}^{2+}$ , whereas Rh-Bam effectively cleaves plasmid with stoichiometric or with excess  $\text{Zn}^{2+}$ . Though Rh-Bam generally gives lower levels of plasmid cleavage than Rh-P1, it is certainly more tolerant of variations in the metal ion and metal ion concentration employed for cleavage.

Rh-Bam effectively cleaves supercoiled plasmid, but unlike Rh-P1, it does not often produce linear plasmid and has not yet been demonstrated to cleave DNA oligonucleotides. It is noteworthy that many of the artificial nucleases in the literature have only been reported to cleave supercoiled DNA, and have not been demonstrated to cleave linear substrates. The plasmid cleavage assay is at least an order of magnitude more sensitive than the cleavage assay with an oligonucleotide (Figure 2.19),<sup>16</sup> and in some cases, the weak activity of the reagent may be the source of the difficulty. However, this difference in assay sensitivity does not appear to account for the lack of reaction of Rh-Bam on oligonucleotides.

The strain inherent in a supercoiled plasmid or a few damaged sites in a 3 kilobase plasmid may be an important factor in activating DNA for hydrolysis.<sup>52</sup> The failure of

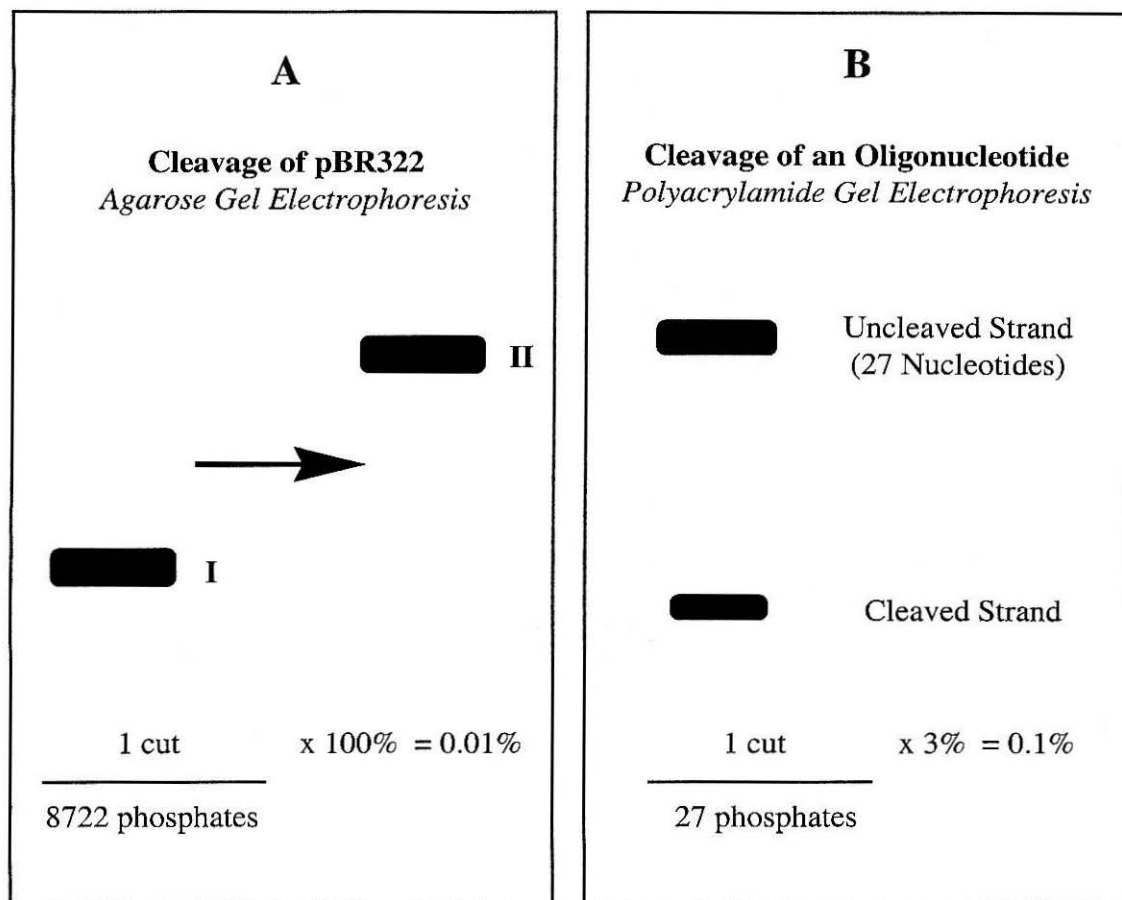


**Figure 2.19. A Comparison of Plasmid and Oligonucleotide Cleavage Assays.**

To obtain complete conversion of a supercoiled plasmid into a nicked substrate, one nick per plasmid is required, i.e., 1 cleaved phosphodiester bond out of 8722 phosphodiester bonds (pBR322 has 4361 base pairs). This represents cleavage at 0.01% of the possible sites. To obtain a detectable cleavage band (3%) from a 27-mer labeled oligonucleotide requires cleavage at 1 phosphodiester bond out of 27 phosphodiester bonds, or cleavage at 0.1% of the possible sites. The plasmid assay is at least one order of magnitude more sensitive than the oligo assay. Figure adapted from Fitzsimons, 1998.<sup>16</sup>

Rh-Bam to produce linear DNA in the plasmid cleavage assay or to cleave duplex substrates is notable in this context. Intercalation could be considered a source of strain energy, and it is possible that the conjugate containing the shorter P1 peptide exploits this strain energy more effectively than Rh-Bam.

Because Rh-Bam has not been demonstrated to cleave oligonucleotides, it has not been possible to analyze the cleavage products and thus directly establish the hydrolytic chemistry. Nonetheless, the requirement for redox-inactive  $\text{Zn}^{2+}$  in Rh-Bam cleavage assays and the similarity in other reaction characteristics to Rh-P1 points to hydrolysis as the probable mechanism.

## 2.5. Conclusions

With the goal of developing artificial nucleases for DNA hydrolysis, metal-coordinating peptides have been tethered to a DNA-intercalating rhodium complex to deliver metal ions to the sugar phosphate backbone. The intercalator,  $[\text{Rh}(\text{phi})_2\text{bpy}']^{3+}$ , provides DNA binding affinity, and a metal-binding peptide contributes reactivity. Zinc(II)-promoted cleavage has now been demonstrated for two widely different tethered metallopeptides. The Rh-P1 conjugate boasts a designed helical peptide with histidine residues for  $\text{Zn}^{2+}$  coordination, and cleaves both supercoiled plasmid and linear DNA substrates. More recently a peptide modeled after the active site of the *Bam*HI endonuclease was attached to  $[\text{Rh}(\text{phi})_2\text{bpy}']^{3+}$ , and was found to cleave supercoiled plasmid with a variety of metal cations. Although we did not improve the activity of our

intercalator-peptide conjugate by turning to the *Bam*HI enzyme for inspiration, we did establish that our strategy for DNA hydrolysis is a general one.

## 2.6. References

1. Fitzsimons, M. P.; Barton, J. K. *J. Am. Chem. Soc.* **1997**, *119*, 3379-3380.
2. Copeland, K. D.; Fitzsimons, M. P.; Houser, R. P.; Barton, J. K. *Biochemistry* **2002**, *41*, 343-356.
3. Newman, M.; Straelecka, T.; Dorner, L. F.; Schildkraut, I.; Aggarwal, A. K. *Science* **1995**, *269*, 656-663.
4. Pingoud, A.; Jeltsch, A. *Nucl. Acids Res.* **2001**, *29*, 3705-3727.
5. Viadiu, H.; Aggarwal, A. K. *Nat. Struct. Biol.* **1998**, *5*, 910-916.
6. Xu, S.-Y.; Schildkraut, I. *J. Biol. Chem.* **1991**, *266*, 4425-4429.
7. Dorner, L. F.; Schildkraut, I. *Nucl. Acids Res.* **1994**, *22*, 1068-1074.
8. Ciana, L. D.; Hamachi, I.; Meyer, T. J. *J. Org. Chem.* **1989**, *54*, 1731-1735.
9. Gillard, R. D.; Osborn, J. A.; Wilkinson, G. J. *J. Chem. Soc.* **1965**, 1951-1965.
10. Pyle, A. M.; Chiang, M. Y.; Barton, J. K. *Inorg. Chem.* **1990**, *29*, 4487-4495.
11. Scopes, R. K. *Protein Purification: Principles and Practice*; 3<sup>rd</sup> ed.; Springer-Verlag: New York, 1994.
12. Lehrman, S. R.; Tuls, J. L.; Lund, M. *Biochemistry* **1990**, *29*, 5590-5596.
13. Perrin, D. D.; Dempsey, B. *Buffers for pH and Metal Ion Control*; Chapman and Hall: London, 1974.



14. Maniatis, T.; Fritsch, E. F. *Molecular Cloning*; Cold Spring Harbor Laboratory: Plainview, New York, 1982.
15. Sardesai, N. Y.; Lin, S. C.; Zimmermann, K.; Barton, J. K. *Bioconj. Chem.* **1995**, *6*, 302-312.
16. Fitzsimons, M. P. *Ph.D. Thesis* **1998**, California Institute of Technology.
17. Sitlani, A.; Long, E. C.; Pyle, A. M.; Barton, J. K. *J. Am. Chem. Soc.* **1992**, *114*, 2303-2312.
18. Lin, S. C. *Ph.D Thesis* **1997**, California Institute of Technology.
19. Woody, R. W. in *The Peptides*; Academic Press: 1985, pp 15-104.
20. Perczel, A., Hollosi, M. in *Circular Dichroism and the Conformational Analysis of Biomolecules* (Fasman, G. D., Ed.); Plenum Press: New York, 1996, pp 285-380.
21. Pyle, A. M.; Long, E. C.; Barton, J. K. *J. Am. Chem. Soc.* **1989**, *111*, 4520-4522.
22. Uchida, K.; Pyle, A. M.; Morii, T.; Barton, J. K. *Nucl. Acids Res.* **1989**, *17*, 10259-10279.
23. DeGrado, W. *Ann. Rev. Biochem.* **1999**, *68*, 779-819.
24. Hettich, R., Schneider, H. *J. Am. Chem. Soc.* **1997**, *119*, 5638-5647.
25. Hegg, E., Burstyn, J. *Inorg. Chem.* **1996**, *34*, 7474-7481.
26. Ren, R., Yang, P., Zheng, W., Hua, Z. *Inorg. Chem.* **2000**, *39*, 5454-5463.
27. Itoh, T., Hisada, H., Sumiya, T., Hosono, M., Usui, Y., Fujii, Y. *J. Chem. Soc. Chem. Commun.* **1997**, 677-678.
28. Branum, M. E., Tipton, A. K., Zhu, S., Que, Jr., L. *J. Am. Chem. Soc.* **2001**, *123*, 1898-1904.

29. Sillen, L. G.; Martell, A. E. in *Stability Constants of Metal-Ion Complexes* ed.; The Chemical Society, Burlington House, 1964, pp 504-507.
30. Martell, A. E.; Smith, R. M. in *Critical Stability Constants* ed.; Plenum Press: New York, 1974; Vol. 1, pp 61-62.
31. Perrin, D. D. in *Organic Ligands* ed.; Pergamon Press: Oxford, 1979, pp 412-416.
32. Sardesai, N. Y.; Zimmermann, K.; Barton, J. K. *J. Am. Chem. Soc.* **1994**, *116*, 7502-7508.
33. Hastings, C. A.; Barton, J. K. *Biochemistry* **1999**, *38*, 10042-10051.
34. Copeland, K. D.; Lueras, A. M. K.; Barton, J. K., manuscript in preparation.
35. Blanco, F. J.; Jimenez, M. A.; Herranz, J.; Rico, M.; Nieto, J. L. *J. Am. Chem. Soc.* **1993**, *115*, 5887-5888.
36. Ramirez-Alvarado, M.; Blanco, F. J.; Serrano, L. *Nat. Struct. Biol.* **1996**, *3*, 604-611.
37. Sieber, V.; Moe, G. R. *Biochemistry* **1996**, *35*, 181-188.
38. Kortemme, T.; Ramirez-Alvarado, M.; Serrano, L. *Science* **1998**, *281*, 253.
39. Williams, R. W.; Chang, A.; Juretic, D.; Loughran, S. *Biochim. Biophys. Acta* **1987**, *916*, 200-204.
40. Kim, C. A.; Berg, J. M. *Nature* **1993**, *362*, 267-270.
41. Smith, C. K.; Regan, L. *Science* **1995**, *270*, 980-982.
42. Minor, Jr., D. L.; Kim, P. S. *Nature* **1994**, *367*, 660-663.
43. Minor, Jr., D. L.; Kim, P. S. *Nature* **1994**, *371*, 264-267.
44. Wilmot, C. M.; Thornton, J. M. *J. Mol. Biol.* **1988**, *203*, 221-232.
45. Struthers, M. D.; Cheng, R. P.; Imperiali, B. J. *J. Am. Chem. Soc.* **1996**, *118*, 3073-3081.

46. Berg, J. M. Shi, Y. *Science* **1996**, 271, 1081-1085.
47. Christianson, D. W. *Adv. Prot. Chem.* **1991**, 42, 281-355.
48. Groves, J. T., Baron, L. A. *J. Am. Chem. Soc.* **1989**, 111, 5442-5448.
49. Williams, N.H.; Takasaki, B.; Wall, M.; Chin, J. *Acc. Chem. Res.* **1999**, 32, 485-493.
50. Cowan, J. A. *Chem. Rev.* **1998**, 98, 1067-1087.
51. Sitlani, A.; Barton, J. K. *Biochemistry* **1994**, 33, 12100-12108.
52. Bashkin, J. K. *Curr. Op. Chem. Biol.* **1999**, 3, 752-758.

## **Chapter 3**

### **The Development of an Intercalator-Peptide Library and Screening of the Library for DNA Hydrolysis Activity**

### 3.1. Introduction

Combinatorial chemistry is a powerful tool for the generation of novel compounds with a desired activity. A combinatorial experiment typically involves three steps: (i) creation of a library of compounds, (ii) screening of the library for a compound with activity, and (iii) identification of the selected compound (Figure 3.1).<sup>1</sup> Often the library is generated by a highly parallel synthesis strategy. Molecular building blocks are combined to intentionally generate a mixture of compounds; the rational design and synthesis of pure compounds gives way to molecular diversity. Depending on the nature of the library, the selected compounds can be identified by deconvolution,<sup>2</sup> tagging strategies,<sup>3</sup> or various characterization methods, for example, mass spectrometry or sequencing.

Though many researchers have wrestled with the design of small metal complexes for DNA hydrolysis, only a few have applied combinatorial methods to improve or optimize their artificial nucleases. Of course, *in vitro* evolution has produced a large number of nucleic acid molecules that can cleave RNA and DNA.<sup>4-6</sup> Can highly parallel strategies be adapted to transition metal and lanthanide metal nucleases? The examples from the literature are limited, involve small libraries or noncovalent cofactors, and rely on model phosphate substrates.

Janda et al. used parallel synthesis to generate a library of macrocyclic lanthanide-ligand complexes.<sup>7</sup> Four different azacrown ether scaffolds were prepared, and combined with 15 different lanthanide nitrates to generate a library of 60 complexes. These complexes were tested in a parallel screening assay for their ability to hydrolyze a variety

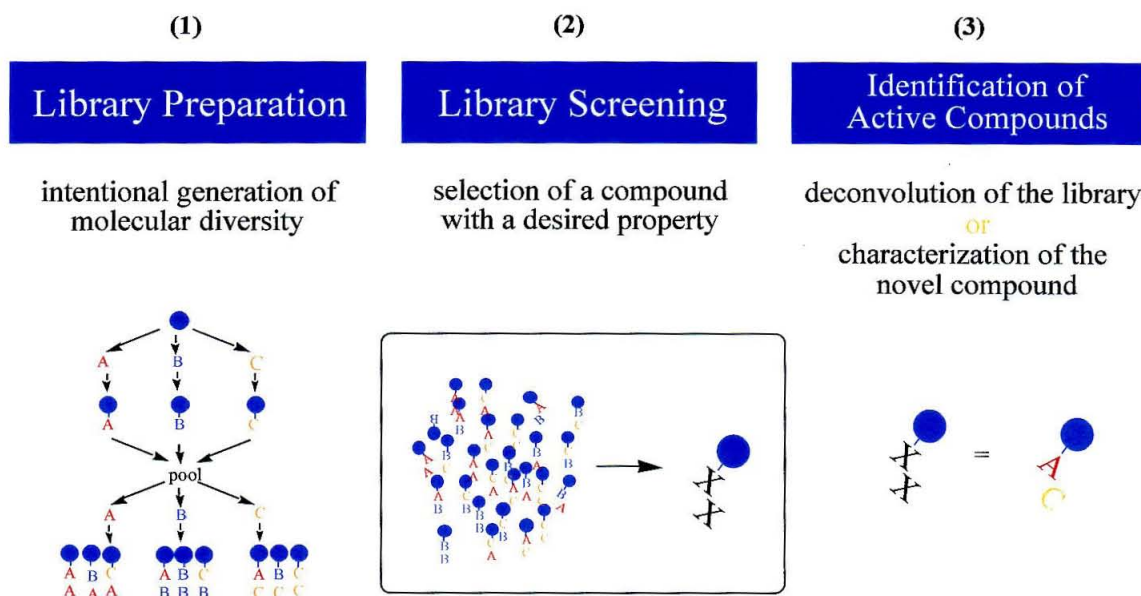


**Figure 3.1. Combinatorial Chemistry.** Combinatorial chemistry involves three steps: (1) preparation of a library of compounds, (2) screening of a library to select an active compound, and (3) identification of the selected compound.

of nitrophenyl phosphate substrates. These substrates are very compatible with library screening because the hydrolysis reaction can be followed through monitoring the absorbance at 405 nm. To test the library against DNA, 24 complexes were tested in a plasmid cleavage assay. This assay is less convenient than a colorimetric assay, but it did reveal a promising candidate for DNA hydrolysis. The azacrown ether-Gd complex exhibited a  $k_{\text{cat}}$  value of  $7.5 \times 10^{-5} \text{ min}^{-1}$  and a  $K_m$  of  $7.4 \mu\text{M}$ .

Berkessel et al. generated a library of undecapeptides, and combined this library with a variety of metals (Cu, Fe, Zn, Eu, Zr, Ce, and Co).<sup>8</sup> The 625 different peptides were prepared by a split-pool strategy to give one compound on each synthesis bead. The peptides were tested while still on the resin for the hydrolysis of 5-bromo-4-chloroindolyl phosphate. Several  $\text{Zr}^{4+}$ -peptide combinations were found to be effective for hydrolysis of the indolyl substrate or bis(*p*-nitrophenyl) phosphate (BNPP), but they were not tested against DNA. As might be expected, compounds that efficiently cleave model substrates do not always show activity against the relevant biological molecule. Although colorimetric screens with model substrates are very convenient, they do not necessarily bring us any closer to small molecules for DNA hydrolysis.

Finally, Schneider et al. tested a variety of noncovalently bound cofactors for  $\text{Eu}^{\text{III}}$ -catalyzed hydrolysis of BNPP and DNA.<sup>9</sup> The activities of combinations of amino acid, azacrown, acid, and imidazole cofactors were tested by a plasmid cleavage assay. Combinations of serine, histidine, and aspartic acid, as well as an azacrown with pendant imidazole rings, were found to increase the rate of hydrolysis relative to  $\text{Eu}^{\text{III}}$  alone.

Although the design of an effective library method is quite challenging, we believed that the Rh-P1 conjugate would provide a good starting point for a

combinatorial experiment. Rh-P1 binds to DNA with high affinity, and provides  $\text{Zn}^{2+}$ -promoted hydrolysis of both plasmid and oligonucleotides.<sup>10,11</sup> The rate of plasmid hydrolysis is enhanced by a factor of  $10^6$  in the presence of DNA. To improve the activity of our artificial nuclease, we decided to use a combinatorial approach to optimize the peptide composition of Rh-P1. Peptides are composed of readily available amino acid building blocks, and have been synthesized on solid support for decades. In addition, unknown peptides can be identified through Edman sequencing<sup>12</sup> or mass spectrometry.<sup>13</sup> For these reasons, peptides are particularly suited for library preparation.

We prepared peptide libraries on solid support using a split-pool technique.<sup>1</sup> The split-pool method allows large libraries to be generated very quickly, and it also ensures that only one type of compound will be attached to each bead. To allow for off-bead screening, the peptide library was prepared with a photocleavable linker. The peptide libraries were coupled to a rhodium intercalator to create intercalator-peptide conjugates. Two different libraries were prepared. A very small library, rhodium-peptide library 1 (Rh-PL1), contained only 27 members; three positions in a 13-mer peptide were randomized with Glu, His, and Lys (Figure 3.2). This very modest library was primarily used for optimization studies. The second library, rhodium-peptide library 2 (Rh-PL2), contained over 16,000 members (Figure 3.3). Using the 16-mer peptide of Rh-P1 as a starting point, seven positions were randomized with Ala, Glu, His, and Lys. This library of conjugates was screened for DNA hydrolysis activity using a plasmid cleavage assay, and the most promising compounds were identified through Edman sequencing.

This combinatorial experiment was a collaborative project with Dr. Ulrike Riese. We both contributed ideas for the design of the library, but Ulrike completed the



synthesis of the library single-handedly. Ulrike also tested the properties of the photocleavable linker through release studies with a model substrate and Rh-PL1. I tested the different screening approaches, and carried out bead-by-bead screening of Rh-LP2.

## 3.2. Materials and Methods

### 3.2.1. Synthesis of Ligands and Metal Complex.

**4-Valeric acid-4'-methyl-2,2'-bipyridine (bpy'').** The bpy'' ligand, which contains one more methylene unit than bpy', was prepared by Dr. Ulrike Riese (Figure 3.4). This ligand was obtained by coupling the deprotonated 4,4'-dimethyl-2,2'-bipyridine with an orthoester. The orthoester (1-(3-bromopropyl)-4-methyl-2,6,7-trioxabicyclo[2.2.2]octane) was prepared as described in the literature.<sup>14</sup> The coupling product was converted to the ester by hydrolysis with NaHSO<sub>4</sub>, and the desired acid was obtained by saponification with KOH. The synthesis of bpy'' gave average single step yields of 85%. m. p. 143-145 °C; <sup>1</sup>H-NMR (400 MHz, CD<sub>2</sub>Cl<sub>2</sub>): δ/ppm = 1.74 (m, 4H), 2.15 (br s, OH), 2.39 (t, 2 H, J<sub>H,H</sub> = 6.9 Hz), 2.73 (t, 2 H, J<sub>H,H</sub> = 7.0 Hz), 7.16 (t, 2 H, J<sub>H,H</sub> = 4.6 Hz), 8.23 (d, 2 H, J<sub>H,H</sub> = 10.8 Hz), 8.52 (t, 2 H, J<sub>H,H</sub> = 4.8 Hz); <sup>13</sup>C-NMR (400 MHz, 1:9 d<sub>6</sub>-DMSO/CDCl<sub>3</sub>): δ/ppm = 20.7, 24.1, 29.3, 33.4, 34.7, 120.7, 121.5, 123.4, 124.2, 147.6, 148.4, 148.5, 151.7, 155.5, 155.6, 175.0; MS (ESI): *m/z* (rel. int.) = 271.2 (100) [M+H]<sup>+</sup>, 253.2 (19) [M-OH]<sup>+</sup>, 184.2 (13); Comp. Anal.: found (calc. for C<sub>16</sub>H<sub>18</sub>N<sub>2</sub>O<sub>2</sub>) = C 70.10 (71.09), H 6.98 (6.71), N 10.09 (10.36).

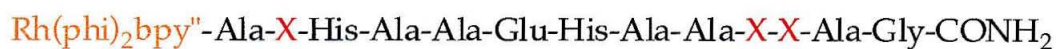
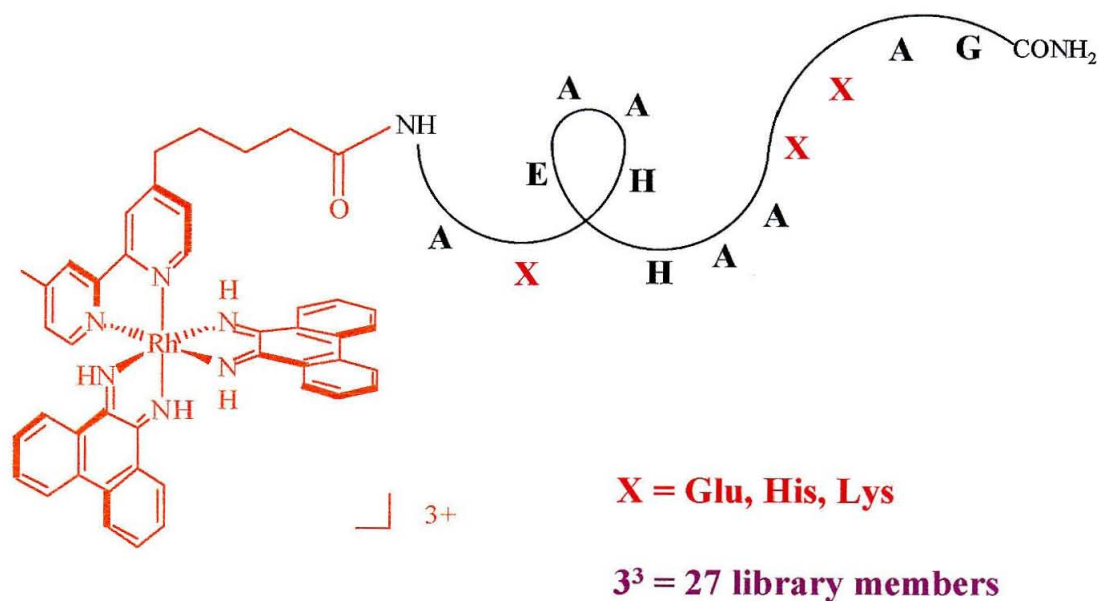


**Figure 3.2. Schematic of Rh-Peptide Library 1.** A 13 amino acid peptide with three variable positions (X) was prepared. The three variable positions were substituted with Glu, His, or Lys to create a small peptide library with 27 members. The peptide library was tethered to the  $[\text{Rh}(\text{phi})_2\text{bpy}^{3+}]^{3+}$  complex.

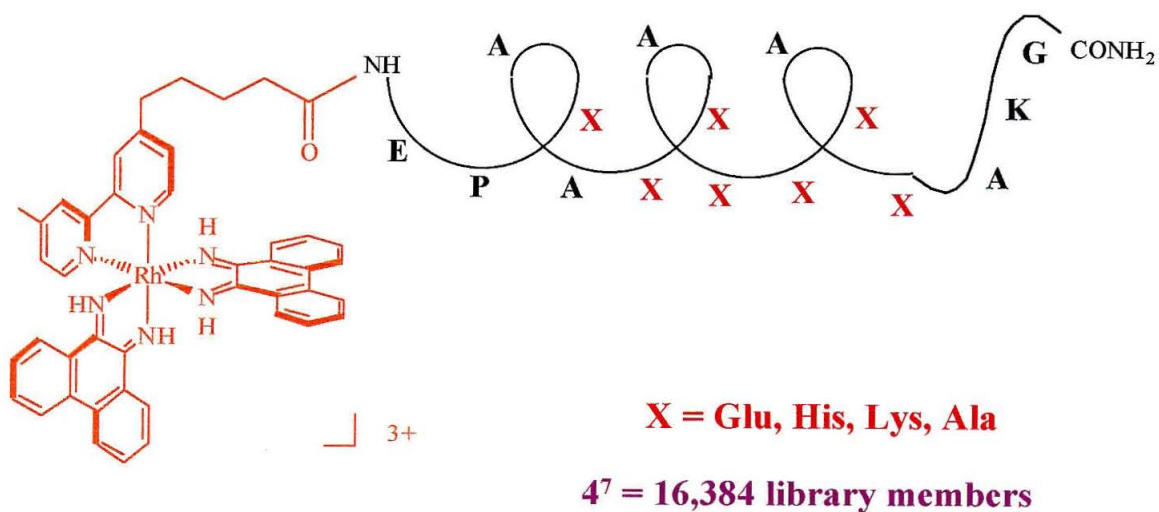


**Figure 3.3. Schematic of Rh-Peptide Library 2.** A 16 amino acid peptide with seven variable positions (X) was prepared. The variable positions were substituted with Ala, Glu, His, or Lys to create a peptide library with 16,000 members. The peptide library was tethered to the  $[\text{Rh}(\text{phi})_2\text{bpy}^{3+}]^{3+}$  complex.

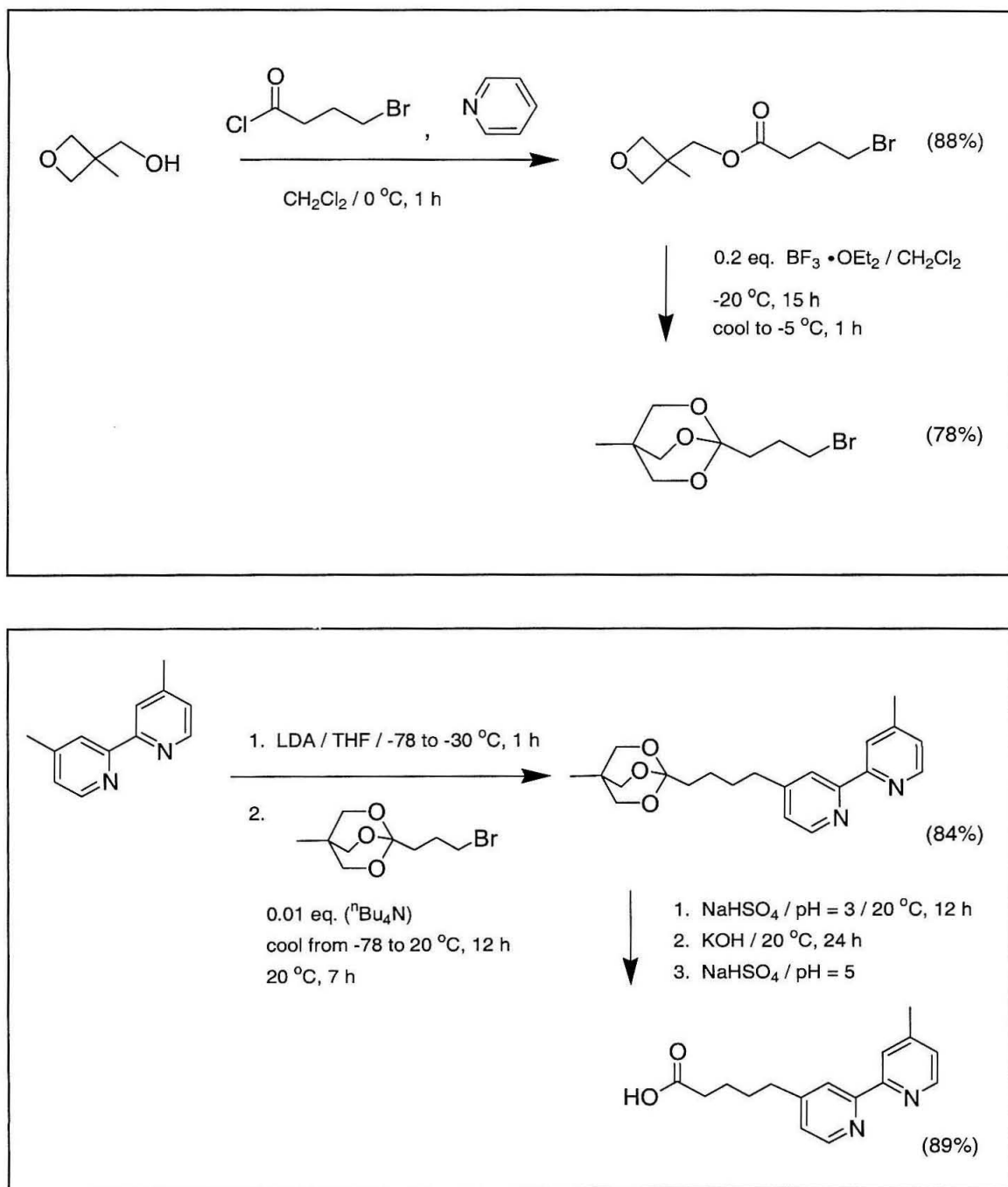


**Figure 3.4. Synthesis of the Bpy'' Ligand.** An ortho-ester was prepared (top) and coupled to deprotonated 4,4'-dimethyl-2,2'-bipyridine (bottom).

**Diaminophenanthrene.** Fresh diaminophenanthrene was prepared from phenanthrenequinone via the hydroxime by Dr. Ulrike Riese.<sup>15</sup> The oxime was reduced with tin chloride in concentrated hydrochloric acid, and the resulting hydrochloride was treated with sodium carbonate to give the free amine.<sup>16</sup> Since diaminophenanthrene is sensitive to oxygen and moisture, it was immediately coordinated to the rhodium center.

**Bis(phenanthrenequinone diimine) (4-Valeric acid-4'-methyl-2,2'-bipyridine) Rhodium(III) Trichloride,  $[Rh(phi)_2bpy'']Cl_3$ .** The rhodium complex was prepared according to literature methods by Dr. Ulrike Riese.<sup>17</sup>

### 3.2.2. Synthesis of the Peptide Library.

The peptide libraries were prepared on Tentagel resin with a nitrobenzyl linker. They were generated by manual solid-phase synthesis with Fmoc protection.<sup>18</sup> Coupling reactions were carried out in dimethylformamide (DMF), and a minimum amount of solvent was used to ensure a high concentration of the activated species. (Benzotriazole-1-yl-oxy)tris (pyrrolidino) phosphonium hexafluorophosphate (PyBOP), 7-aza-1-hydroxy-benzotriazole (HOAt) or 1-hydroxy-benzotriazole (HOBt), and diisopropylethylamine were employed for activation of the carboxy terminus. Four equivalents of the activated amino acid were used for each coupling, and all couplings were carried out at least twice. The coupling reactions were monitored by the ninhydrin assay.<sup>19</sup> A solution of 50% piperidine in DMF was used for the deprotection of the N-terminus.

**Chemicals.** The synthesis resin (Fmoc-aminoethyl-photolinker Nova Syn TG), PyBOP, HOBt, and amino acids (Fmoc-Ala-OH, Fmoc-Glu(OtBu)-OH, Fmoc-Gly-OH,

Fmoc-His(Trt)-OH, Fmoc-Lys(Boc)-OH) were obtained from Nova Biochem. Peptide synthesis grade diisopropylethylamine (DIPEA), piperidine, and trifluoroacetic acid were obtained from Perkin Elmer. Technical grade DMF (99.8%) and HPLC grade DMF, dichloromethane (DCM), and methanol were obtained from VWR. Peptide synthesis grade DCM and DMF were obtained from Fluka. 1,2-Ethanedithiol was obtained from Fluka, and HOAt from Aldrich.

**Apparatus.** The resin was pooled in a glass randomization vessel (chromatography column, 3 cm x 10 cm for 0.6-1.2 g of resin, 5 cm x 10 cm for 3.5 g of resin). The vessel was fit with a medium glass sintered frit and two-way valve, and was connected to vacuum and argon. Amino acid coupling reactions were carried out in polypropylene reaction tubes. A motorized rocking platform was used for agitation of the individual coupling reactions. Resin was transferred with disposable polyethylene pipets.

**Synthesis of Peptide Library 1 (PL1).** The Tentagel resin with photocleavable linker (600 mg, 130  $\mu$ m beads) was swollen for 2 h in technical grade DMF (5 mL) with gentle shaking in a polypropylene tube. The beads were washed with technical grade DMF (5 x 8 mL, 2 min per wash). (1) Deprotection of N-terminus. The swollen resin was combined with 8 mL of 50% piperidine in technical grade DMF in the randomization vessel to remove the Fmoc protecting group. After 10 minutes the piperidine solution was removed and fresh 50% piperidine was added. After another 10 minutes the beads were washed with technical grade DMF (8 x 8 mL, 2 min per wash), and then with peptide synthesis grade DMF (3 x 8 mL). (2) Amino Acid Coupling Reactions. For the non-randomized positions all the beads were next placed in a single polypropylene reaction tube. For the randomized positions the beads were distributed equally into

polypropylene vessels using a polyethylene pipette. Once in the polypropylene reaction tube, the beads were allowed to settle and most of the supernatant DMF was removed. The appropriate Fmoc protected amino acid (4 eq.) and HOAt or HOBt (4 eq.) were added to the reaction vessel. PyBOP (4 eq.) and DIPEA were added to the tube to initiate the coupling reaction. The reaction vessel was sealed and rocked gently. Each coupling was repeated at least twice. After the first coupling (coupling A) the supernatant was removed from the reaction tube and fresh amino acid, HOAt or HOBt, PyBOP, and DIPEA were added. To assess the progress of a coupling reaction, approximately 5 mg of resin were removed from the reaction vessel and washed with peptide synthesis grade solvents. The resin was dried under vacuum and analyzed by the ninhydrin assay. (3)

*Pooling and Washing the Resin.* Once the coupling reaction was complete (coupling yield  $\geq 97\%$ ) in an individual reaction vessel, the supernatant was removed and discarded, and the beads were transferred to the randomization vessel. The collected resin in the randomization vessel was rinsed with technical grade DMF (8 x 8 mL, 2 min per wash). The deprotection, splitting, coupling, pooling, and washing steps were repeated until the full-length peptide was assembled. After thorough washing with HPLC grade DMF, the protected library was stored in peptide synthesis grade DMF at 8 °C in the dark.

***Synthesis of Peptide Library 2 (PL2).*** The synthesis of PL2 was analogous to the synthesis of Rh-PL1, but the amount of resin, solvent, and reagent was increased by a factor of 6. The Tentagel resin beads used for this library had a larger diameter (140 to 170  $\mu\text{m}$ ) and greater mechanical stability than the beads used for PL1.

### 3.2.3. Preparation of the Rh-Peptide Libraries.

***Deprotection of the N-terminus.*** The resin bearing the peptide library (150 mg for PL1 and 600 mg for PL2) was transferred to the randomization vessel. The Fmoc protecting group was removed with 50% piperidine in DMF as described above. The resin was rinsed with technical grade DMF, peptide synthesis grade DMF, and 1:1 HPLC grade methanol/peptide synthesis grade DCM. The resin was then dried under vacuum.

***Coupling the Rhodium Complex.*** Dry resin was massed into a polypropylene reaction tube. For PL2, 103 mg of resin was used for the coupling reaction. This corresponds to 15.2  $\mu\text{mol}$  of peptide. For PL1, 530 mg of resin or 93  $\mu\text{mol}$  of peptide was coupled. The dry resin was resuspended and gently rocked in peptide synthesis grade DMF for 1 h. The supernatant DMF was removed and  $[\text{Rh}(\text{phi})_2\text{bpy}''']\text{Cl}_3$  (1.25 eq.), HOBt (4 eq.), PyBOP (4 eq.), and DIPEA were added to the reaction tube. The tubes were capped and rocked gently for 18 h. The beads were then rinsed with HPLC grade DMF (10x) and 1:1 methanol:DCM (10x). The beads were transferred by a polyethylene pipet to a Buchner funnel and dried under vacuum. The libraries were stored dry in polypropylene vessels at - 20 °C in the dark.

***Deprotection of Peptide Sidechains.*** Rh-peptide library resin was transferred to a polypropylene tube. A cocktail of TFA, ethanedithiol, and water (95:5:5) was bubbled briefly with argon and then added to the tube. The tube was rocked gently for 4 h. The resin was then transferred to a 2 mL Buchner funnel with medium glass frit and rinsed with DCM (3 x 2 mL), 10% DIPEA in DCM (3x), DMF (5x), DCM (3x), and 1:1 DCM:methanol (3x). The resin was placed on the lyophilizer overnight.



### 3.2.4. Characterization of the Rhodium-Peptide Library.

**Amino Acid Analysis.** Approximately 200 beads of PL1 (counted under the microscope) in water were transferred to a cuvette and irradiated for 4 h at 375 nm. Approximately 300 beads of PL2 in water were transferred to a cuvette and irradiated for 1.5 h at 370 nm. The solutions were filtered to remove resin, transferred to a glass microtube, and submitted to the Division of Immunology at the City of Hope for amino acid analysis. The analysis was completed with a Beckman System 6200 Instrument with a 12 cm sodium column for the analysis of hydrolyzed amino acids. Peptide Library 1, observed (expected): Asp 0.56 (0), Thr 0.053 (0), Ser 0.072 (0), Glu 2.535 (2), Gly 1.132 (1), Ala 6.171 (6), His 2.427 (3), Lys 0.919 (1). Peptide Library 2, observed (expected): Glu 2.080 (2.75), Pro 1.136 (1), Gly 1.168 (1), Ala 7.988 (6.75), His 1.2171 (1.75), Lys 3.207 (2.75). Approximately 13  $\mu$ g of PL1 (Average MW = 1298.4) was detected by amino acid analysis. This corresponds to a release of 50 pmole per bead. Approximately 7.4  $\mu$ g of PL2 (Average MW = 1597.6) was detected. This corresponds to a release of 15 pmol per bead.

**Edman Sequencing.** To assess the quality of the library and to estimate the yield for rhodium coupling, 113 beads from Rh-PL1 were submitted for Edman sequencing at the Peptide/Protein Mass Analysis Laboratory (PPMAL) at Caltech. An ABI 492 Procise Protein Microsequencer was used for the analysis.

### 3.4.5. Investigation of Library Release by UV-Visible Spectroscopy and HPLC.

**Conjugate Release Monitored by Absorbance Measurement.** The release of intercalator-peptide conjugate from solid support was studied with Rh-PL1, but also with

a model peptide-conjugate system. A 7-mer peptide (Glu-His-Ala-Ala-Lys-His-Ser) was assembled by automated peptide synthesis on Tentagel resin with the nitrobenzyl linker. The synthesis was carried out with Fmoc chemistry as described in Chapter 2.

The resin, bearing either Rh-PL1 or Rh-EHAAKHS, was suspended in an aqueous solution of sodium borate, and was transferred to a UV-vis quartz cuvette (1 cm x 1 cm) containing a micro stirbar. The cuvette was placed in the beam of an Oriel Model 6140 1000 W Hg/Xe lamp equipped with a monochromator and a 300 nm cutoff filter, and was irradiated with constant stirring. The irradiation wavelength, the slit width of the lamp, the pH of the buffer, and the time of irradiation were varied.

To estimate the extent of release, an absorbance spectrum was obtained with a DU 7400 Spectrophotometer, and the absorbance at 349 nm was recorded. The concentration of rhodium-peptide conjugate in the solution was calculated using the extinction coefficient of  $[\text{Rh}(\text{phi})_2\text{bpy}]^{3+}$ ,  $\epsilon_{349}$  (isosbestic) =  $23,600 \text{ M}^{-1} \text{ cm}^{-1}$ . To estimate the percentage of conjugate released from the resin, the concentration of rhodium complex in the sample was divided by an estimated concentration for total release of rhodium-conjugate. This estimated concentration was based on the average loading of the resin beads, and the yield of the rhodium coupling reaction.

Typically, to obtain an absorbance spectrum, the resin was allowed to settle and the cuvette was simply moved from the beam of the lamp to the spectrophotometer. In one experiment with Rh-LP1, an aliquot of buffer and beads was actually removed from the cuvette at several time points. The aliquot was filtered to collect the buffer. The resin beads were then rinsed with a 0.1% solution of TFA in acetonitrile. Two rinses

were collected and combined with the buffer. An absorbance measurement was obtained for this sample and adjusted for sample dilution.

**HPLC Analysis of Peptide Library 1 and Rhodium-Peptide Library 1.** The material released from PL1 and Rh-PL1 resin by irradiation at 375 nm was analyzed by HPLC. HPLC was carried out with an HP1100 equipped with a PDA detector and a Vyadac C<sub>18</sub> column. A flow rate of 4 mL/min, a column temperature of 30 °C, and a gradient of water (0.1% TFA) and acetonitrile (0.1% TFA) were used in the analysis (Table 3.1).

**Table 3.1. HPLC Conditions for Analysis of PL1 and Rh-PL1.**

PL1		
time (min)	water (0.1 % TFA) (%)	acetonitrile (0.1 % TFA) (%)
0	97	3
5	97	3
10	90	10
20	70	30
25	70	30
Rh-PL1		
time (min)	water (0.1 % TFA) (%)	acetonitrile (0.1 % TFA) (%)
0	95	5
5	95	5
30	75	25
33	60	40
38	60	40

### 3.2.6. Library Screening.

***A Fluorogenic DNA Substrate.*** Initially we considered using a fluorogenic DNA substrate in screening assays. We prepared a 15-mer DNA duplex with a fluorescein donor attached to the 5' end of one strand and a rhodamine acceptor attached to the 5' end of the complement. The 15-mer DNA strands were synthesized using an ABI 392 DNA Synthesizer (A: 5'-GGC ACG GAT CCC AGC-3' and B: 5'-GCT GGG ATC CGT GCC-3'). 5'-Fluorescein phosphoramidite and tetramethylrhodamine-dT were purchased from Glen Research, and these phosphoramidites were incorporated on the DNA synthesizer with an extended coupling time. The strands were purified by HPLC. Fluorescence spectra were obtained using an ISS Fluorometer.

***Multiple-Round Plasmid Cleavage Assay.*** To facilitate rapid screening, we attempted to include two rounds in each screening experiment. In the first round many beads (50 to 100) were distributed to each well of a 96-well filtration plate (MILLIPORE, R5 Solvent Resistant Plate, Hydrophilic PTFE, 5  $\mu$ m pore size, pre-wet with 100  $\mu$ L of HEPES buffer). A polypropylene tube containing deprotected resin in HEPES buffer (15 mM, pH 6 to 7) was gently agitated to evenly suspend the beads, and a 40  $\mu$ L aliquot was transferred to a well.

The plate of beads was irradiated under an inverted Spectroline TR-302 transilluminator (302 nm) for 5 minutes. To block wavelengths below 350 nm, the plate was shielded with a lucite lid. After irradiation the buffer, presumably carrying the released Rh-conjugates, was drained into a collection plate containing pUC19 (2.5  $\mu$ L of 320  $\mu$ M stock) and  $\text{Zn}^{2+}$  (2  $\mu$ L, varying concentration). The buffer was drained using a MILLIPORE Multiwell Vacuum Filtration Manifold (Figure 3.5). The collection plate of

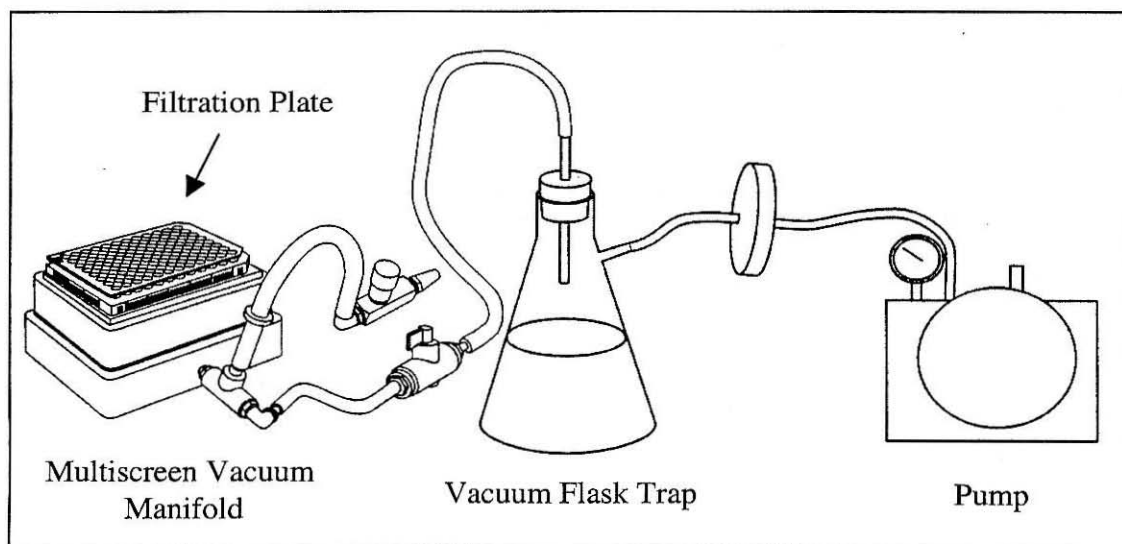


**Figure 3.5. Apparatus Used for Library Screening.** Library beads were distributed to a 96-well filtration plate. After irradiation of the beads, the buffer in the wells was drained into a collection plate with a MILLIPORE Multiscreen Vacuum Manifold

buffer, conjugate, plasmid, and  $\text{Zn}^{2+}$  was carefully sealed with tape and placed in a 37 °C incubator for 24 to 48 hours. The filtration plate was wrapped in foil and set aside.

A mixture of sodium dodecyl sulfate (5%, SDS), glycerol (10%), bromophenol blue, and xylene cyanol was added to each well, and the contents of the well were loaded on a 1% agarose gel. The gel was run for 2 to 4 h at 85 V, stained with ethidium bromide, and visualized using the transilluminator. The wells that produced the most nicked plasmid were noted. The beads were collected from the best wells by pipeting, and were redistributed to a new filtration plate. For the second round of screening, only 1 bead was placed in each well. The irradiation, incubation, and electrophoresis steps were repeated.

***Single-Bead Plasmid Cleavage Assay.*** The deprotected Rh-PL2 resin was suspended in buffer (15 mM HEPES, pH 6.5). One to two beads were distributed to the wells of a 96-well filtration plate (pre-wet with 100  $\mu\text{L}$  of HEPES buffer). The beads were captured and transferred with a P10 pipetman, and were delivered in 10  $\mu\text{L}$  of buffer. As a control, several wells of the plate were left empty. An additional 30  $\mu\text{L}$  of buffer (15 mM HEPES, pH 6) was added to each well.

The filtration plate was shielded with a lucite lid, and irradiated for 10 minutes under the inverted transilluminator. After irradiation, the buffer in each well was drained into a collection plate. The filtration plate containing the beads was wrapped in foil and set aside. The collection plate already contained plasmid (2.5  $\mu\text{L}$  of a 320  $\mu\text{M}$  stock of pUC19) and  $\text{Zn}^{2+}$  (2  $\mu\text{L}$  of a 1 mM or 2 mM stock solution). In the final reaction mixture, the concentration of plasmid was approximately 20  $\mu\text{M}$ , and the concentration of  $\text{Zn}^{2+}$  was 50  $\mu\text{M}$  or 100  $\mu\text{M}$ . As a control, several wells of the collection plate did not

contain  $\text{Zn}^{2+}$ . The collection plate was carefully sealed with tape and was placed in the 37 °C incubator for 24 to 48 hours.

The reactions were quenched by the addition of a mixture containing SDS, glycerol, bromophenol blue, and xylene cyanol. Sample from each well was analyzed on a 1% agarose gel. Gels were run for 2 to 4 hours at 85 V. The gels were stained by soaking in a solution of ethidium, and were visualized using the transilluminator.

### **3.2.7. Identification of Selected Conjugates.**

The lanes of the agarose gel with the greatest amount of nicked plasmid were determined by visual inspection. The bead or beads were collected from the corresponding well of the filtration plate using a pipetman and 200  $\mu\text{L}$  of water. These “hit” beads were submitted for Edman sequencing at the PPMAL. If two beads were found in a well, they were sequenced together. For promising lanes the percentage of nicked plasmid was quantitated using an LKB Bromma Ultrascan XL Enhanced Densitometer and Pharmacia Gelscan XL software. Also, the average percentage of nicked plasmid was determined for the 7 wells in the same column as the “hit” well.

### **3.2.8. Resynthesis of Selected Conjugates.**

*Automated Synthesis of Peptides.* The three selected peptides were prepared by the Beckman Institute Biopolymer Synthesis Center at Caltech using an ABI433 peptide synthesizer and N-Fmoc-L- $\alpha$ -amino acids. The synthesis was analogous to the synthesis of the Bam peptide described in Chapter 2. The amino acid protecting groups employed

were as follows: Glu(OtBu), His(Trt), and Lys(tBoc). The peptide-resins were received and stored dry at 4 °C.

**Removal of the N-terminal Fmoc Protecting Group.** The peptide-resin (150 mg, 15  $\mu$ mol) was placed on a medium sintered glass funnel and soaked with DMF for 5 minutes. For 30 minutes a 2% solution of DBU in DMF (100 mL) was drained slowly through the funnel. The peptide-resin was rinsed with DMF, CH<sub>2</sub>Cl<sub>2</sub>, and 1:1 CH<sub>2</sub>Cl<sub>2</sub>:methanol. After thorough rinsing the peptide-resin was dried on a lyophilizer.

**Coupling of the Metallointercalator and Peptide.** The resin bound peptides were combined with racemic [Rh(phi)<sub>2</sub>bpy'']Cl<sub>3</sub> (1 eq.), PyBOP (1.5 eq.), and DIPEA (3 eq.) in DMF and stirred at ambient temperature overnight. The conjugates were cleaved from the resin and deprotected with a cocktail of TFA, water, and triisopropylsilane (95:5:5). The cleaved conjugates were precipitated in ice-cold t-butyl methyl ether, collected by centrifugation, dissolved in 5% acetic acid, and lyophilized.

**HPLC Purification.** The intercalator-peptide conjugates were HPLC purified on a semipreparative Vyadac C18 reversed phase column using a water (0.1% TFA)/acetonitrile (0.1% TFA) gradient and a flow rate of 4 mL/min. The percentage of acetonitrile was increased from 15 to 40% over 20 minutes. Chromatograms were monitored at 220 and 360 nm, and the desired product was eluted between 15 and 20 minutes. After lyophilization, the intercalator-peptide conjugates were obtained as fluffy orange solids in 2 to 10% yield.

**Mass Spectrometry.** Electrospray ionization mass spectrometry (ESI MS) was carried out with a Finnigan LCQ Ion Trap Mass Spectrometer.



**Rhodium-Selected Peptide 1, (Rh-SP1):** *[Rh(phi)bpy]''-EPAAAEHAEAKAHA KG-CONH<sub>2</sub>].* ESI MS *m/z* observed (calculated): (Rh-SP1 + 2H)<sup>5+</sup> 471.3 (471.3); (Rh-SP1 + H)<sup>4+</sup> 588.7 (588.9); (Rh-SP1)<sup>3+</sup> 784.7 (784.8); (Rh-SP1 - H)<sup>2+</sup> 1176.7 (1176.5).

**Rhodium-Selected Peptide 2, (Rh-SP2):** *[Rh(phi)bpy]''-EPHAAHHAEEHAAAA KG-CONH<sub>2</sub>].* ESI MS *m/z* observed (calculated): (Rh-SP2 + 3H)<sup>6+</sup> 395.7 (395.4); (Rh-SP2 + 2H)<sup>5+</sup> 474.6 (474.3); (Rh-SP2 + H)<sup>4+</sup> 593.0 (592.6); (Rh-SP2)<sup>3+</sup> 790.3 (790.5); (Rh-SP2 - H)<sup>2+</sup> 1185.0 (1185.2).

**Rhodium-Selected Peptide 3, (Rh-SP3):** *[Rh(phi)bpy]''-EPAAAEHAEAKAHA KG-CONH<sub>2</sub>].* ESI MS (i) *m/z* observed (calculated): (Rh-SP3 + 3H)<sup>6+</sup> 413.3 (413.3); (Rh-SP3 + 2H)<sup>5+</sup> 495.7 (495.7); (Rh-SP3 + H)<sup>4+</sup> 619.3 (619.4); (Rh-SP3)<sup>3+</sup> 825.4 (825.5); (Rh-SP3 - H)<sup>2+</sup> 1237.5 (1237.8).

### 3.2.9. Plasmid Cleavage Assays with Selected Conjugates.

**Plasmid DNA.** Plasmid DNA (pBR322 or pUC19) was obtained from NEBiolabs and dialyzed on centricon filters to remove EDTA. Alternatively, pUC19 was amplified using DH5α cells, isolated using a QIAGEN kit, treated with a metal-chelating resin (Chelex 100, Biorad), and dialyzed on centricon filters.

**Metal Solutions.** Aqueous solutions of ZnCl<sub>2</sub> were prepared by two methods. In the first method, ZnCl<sub>2</sub>, a very hygroscopic salt, was weighed and dissolved in water. Alternatively, zinc metal was massed and dissolved in concentrated hydrochloric acid, and then diluted with water. Though more accurate, this second method resulted in more acidic solutions. Aqueous solutions of Zn(NO<sub>3</sub>)<sub>2</sub> were prepared by weighing the salt and dissolving it in water.

**Buffers.** Sodium borate (20 mM, pH 6), HEPES (15 mM, pH 6), citrate (15 mM, pH 6), and a two-metal ion buffer (See Chapter 2 for details) were used in plasmid cleavage experiments.

**Plasmid Cleavage Experiments.** In a typical plasmid cleavage experiment intercalator-peptide (5  $\mu$ M), divalent metal cation (5 or 50  $\mu$ M), and plasmid (40  $\mu$ M base pairs) were combined in buffer and incubated at 37 °C for 24 to 48 hours. The reactions were quenched by the addition of a mixture of SDS, glycerol, bromophenol blue, and xylene cyanol. The cleavage products were analyzed by electrophoresis on 1% agarose gels. The gels were stained with ethidium bromide, and visualized with UV light.

### 3.3. Results

#### 3.3.1. Preparation of the Rhodium-Peptide Library.

To optimize the peptide composition of our artificial nuclease, Rh-P1, we created two libraries of conjugates. First, the peptide libraries were generated on solid support using a manual split-pool method (Figure 3.6). To facilitate library screening, we selected a Tentagel resin and a photocleavable nitrobenzyl linker (Figure 3.6). Once the peptide libraries were completed, the  $[\text{Rh}(\text{phi})_2\text{bpy}]^{3+}$  complex was coupled to the N-terminus of the resin-bound peptide (Figure 3.7). For off-bead screening assays, the entire conjugate could be released by irradiation at 375 nm (Figure 3.7).

**Synthesis of the Peptide Libraries.** The first peptide library we created, Peptide Library 1 (PL1), consisted of 27 different 13-mer peptides. The peptides contained

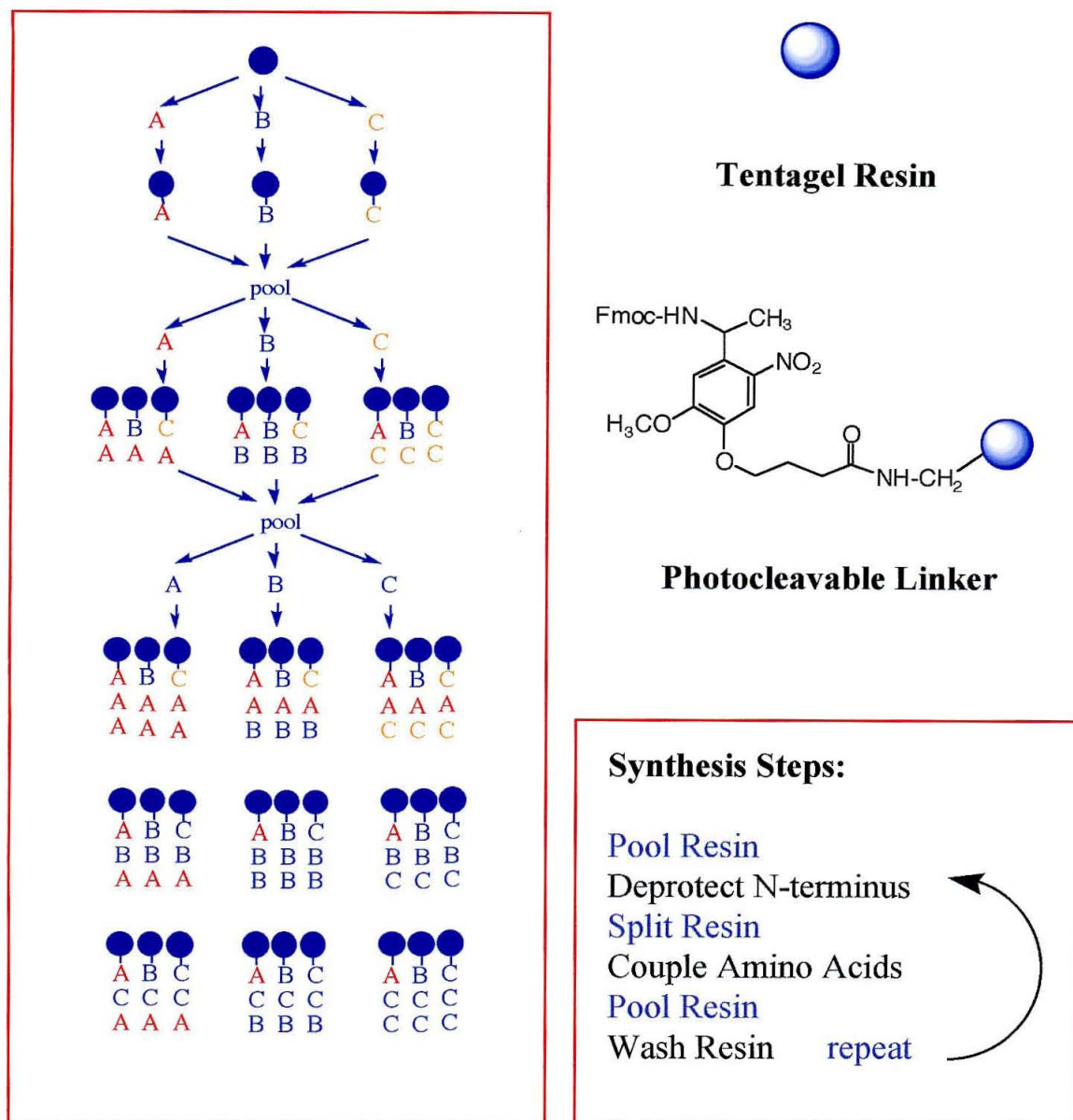


**Figure 3.6. Preparation of the Peptide Library.** A split pool synthesis strategy (left) was used in the preparation of a one-bead-one-peptide library. The library was synthesized on a Tentagel resin with a photocleavable linker.

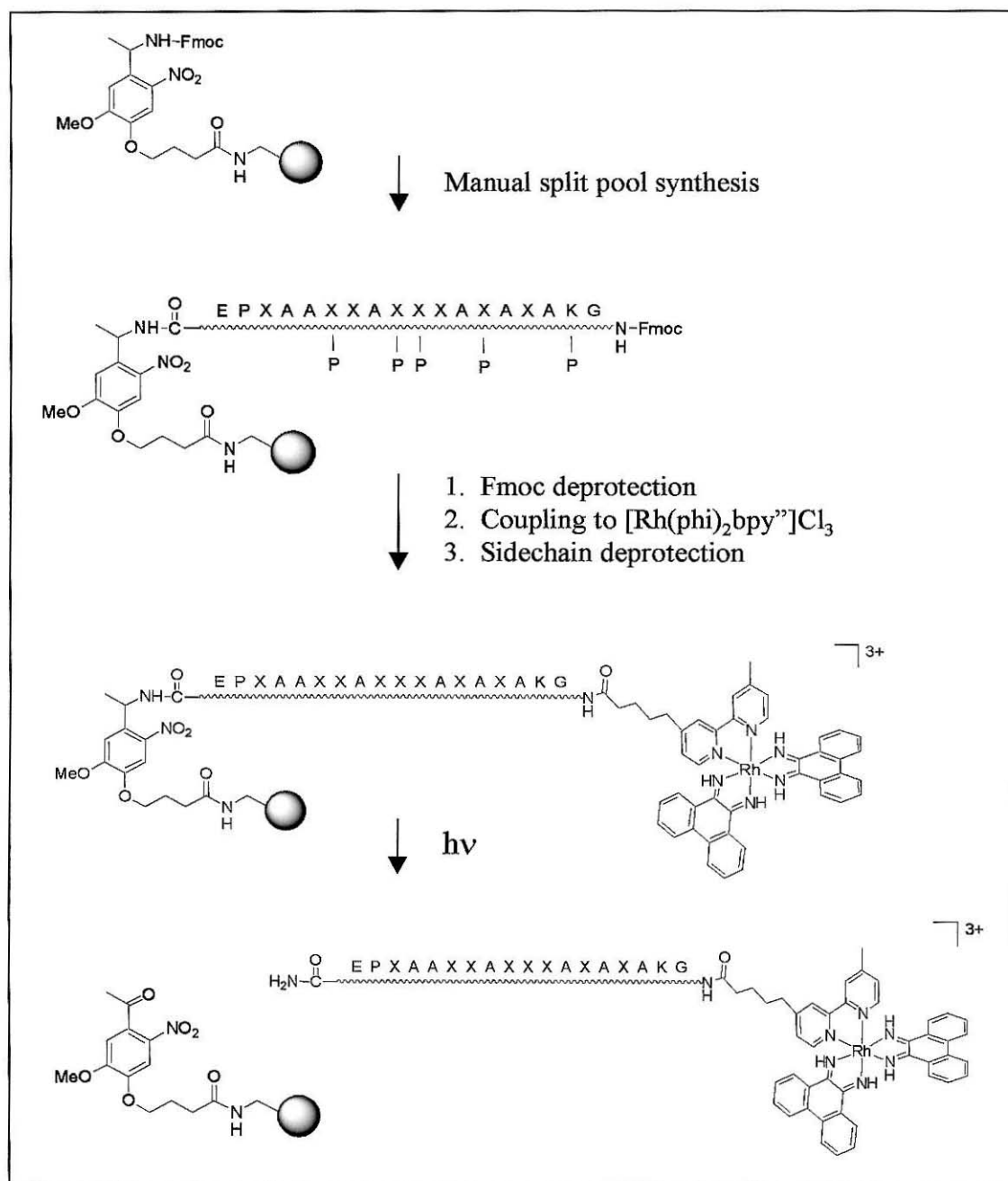


**Figure 3.7. Synthesis and Release of a Rhodium-Peptide Library.** Peptide libraries were prepared on a Tentagel resin with a photocleavable linker.  $[\text{Rh}(\text{phi})_2\text{bpy}']^{3+}$  was coupled to the N-terminus of the peptide library. For screening assays the library of conjugates was released by irradiation. P = sidechain protecting groups.

alanine, glycine, glutamic acid, histidine, and lysine residues. Three positions in the peptide were randomized with Glu, His, and Lys (Ala-X-His-Ala-Ala-Glu-His-Ala-Ala-X-X-Ala-Gly, where X = variable position,  $3^3 = 27$ ). The Tentagel resin beads used for PL1 synthesis had a diameter of 130  $\mu\text{m}$  and an average loading of 130 pmol/bead. The synthesis results for PL1 are presented in Table 3.2.

There was considerable variation in the coupling times required for different residues and for different positions in the peptide. Lysine gave the lowest coupling yields, and histidine gave the highest. Even with 9 h coupling times, the yield for Ala coupling reactions at positions 3, 5, 9 and 11 could not be increased to 98%, but with very short coupling time Ala was incorporated at position 13 with 98.1% yield.

The second peptide library we created, Peptide Library 2 (PL2), consisted of over 16,000 different peptides. Seven positions in a 16-mer peptide were randomized with Ala, Glu, His, and Lys (Glu-Pro-X-Ala-Ala-X-X-Ala-X-X-X-Ala-X-Ala-Lys-Gly, X = variable residue,  $4^7 = 16,384$ ). For PL2 we switched to a Tentagel resin with a larger bead diameter (140 to 170  $\mu\text{m}$ ) and an average loading of 120 pmol. These larger beads showed greater mechanical stability during synthesis and screening. The synthesis results for PL2 are presented in Table 3.3.

Again, variation in coupling yield was observed for different residues and at different peptide positions. The average coupling yields decreased as follows: histidine (98.2%) > glutamic acid (97.2%) > alanine (96.9%) > lysine (96.7%). The coupling yield also seemed to decrease as the peptide grew longer and longer. The average coupling yield was 98.4% for residues 1 to 5, 97.6% for residues 6 to 10, and 95.9% for residues 11 to 16. This effect may be due to aggregation or secondary structure of the growing

**Table 3.2. Synthesis Conditions and Yield for PL1 (AXHAAEHAAXXAG).**

<i>position</i>	<i>residue</i>	<i>reagent</i> <sup>a</sup>	<i>Coupling time (h)</i>			<i>Yield (%)</i>	
			<i>Coupling step:</i>			<i>Coupling step:</i>	
			<b>A</b>	<b>B</b>	<b>C</b>	<b>B</b>	<b>C</b>
1	G	HOAt	1	1		98.6	
2	A	HOAt	1	1		96.9	
3	E	HOAt	1	9	3	97.6	98.3
	H	HOAt	1	9	3	98.6	99.2
	K	HOAt	1	9	3	97.3	97.0
4	E	HOAt	2	2	6		98.4
	H	HOAt	2	2	6		98.8
	K	HOAt	2	2	6		97.6
5	A	HOBt	2	9		97.4	
6	A	HOBt	2	3		97.6	
7	H	HOBt	3	15		99.1	
8	E	HOBt	2	3		98.6	
9	A	HOAt	2	9		97.8	
10	A	HOAt	2	3		97.5	
11	H	HOBt	1	9		97.3	
12	E	HOBt	1	2		97.6	
	H	HOBt	1	2		99.2	
	K	HOBt	1	2		96.8	
13	A	HOBt	1	2		98.1	

<sup>a</sup> The reagent used in combination with PyBOP to activate the amino acid for coupling.

**Table 3.3. Synthesis Conditions and Yield for PL2 (EPXAAXXAXXXAXAKG).**

<i>position</i>	<i>residue</i>	<i>Coupling Time (h)</i>		<i>Yield (%)</i>
		Coupling step:		Coupling step:
		<b>A</b>	<b>B</b>	<b>B</b>
1	G	1	9	96.5
2	K	1	2	98.9
3	A	1	9	98.9
4	A	1	2	98.0
	E	1	2	98.7
	H	1	2	99.5
	K	1	2	97.9
5	A	1	9	98.4
6	A	1	2	96.0
	E	1	2	97.2
	H	1	2	97.8
	K	1	2	96.5
7	A	1	9	96.2
	E	1	9	97.4
	H	1	9	98.0
	K	1	9	97.2
8	A	1	2	98.0
	E	1	2	98.2
	H	1	2	98.8
	K	1	2	97.6
9	A	1	9	97.6
10	A	1	2	97.7
	E	1	2	98.1
	H	1	2	98.9
	K	1	2	97.8

11	A	1	2	94.6
	E	1	2	95.2
	H	1	2	96.9
	K	1	2	92.5
12	A	1	2	95.9
13	A	1	2	95.9
14	A	1	12	95.3
	E	1	12	95.9
	H	1	12	97.3
	K	1	12	95
15	P	1	22	99.3
16	E	1	9	96.6



peptide chain.<sup>20</sup> Residues with high alanine content have a greater propensity for aggregation, and certainly PL2 does contain a large number of alanine residues.

***Characterization of the Peptide Libraries.*** Although it is difficult to rigorously characterize a library of peptides, Edman sequencing was completed for PL1, and amino acid analysis was applied to PL1 and PL2. With these two methods, the results were basically as expected. Amino acid analysis gave values that were very close to a statistical distribution of residues at the randomized positions. For PL1 we analyzed over 7 equivalents of the library (7 x 27 beads), and we observed that the amount of Glu was a little bit higher than expected for statistical distribution, and His was a bit lower. This is opposite of what we would have predicted based on coupling yields. With PL2 we only analyzed 2% of the library (0.02 x 16,384), and as expected, there was greater variation from statistical incorporation at randomized positions. The levels of Glu and His were low, and the levels of Ala and Lys were high.

PL1 was also analyzed by HPLC. Resin bearing peptide library 1 was suspended in a sodium borate buffer and was irradiated at 365 nm. After 60 minutes of irradiation the buffer was injected into the HPLC. At 30 °C and with a water:acetonitrile gradient, the different peptides are fairly well separated (Figure 3.8). The peptide material elutes between 12 and 18 minutes, and it is almost possible to discern 27 peaks and shoulders in the chromatogram. The peaks are of varying intensity, but this is in part explained by overlap of the different products and varying extinction coefficients at 210 nm.

***Coupling Rhodium Complex to the Peptide Libraries.*** The carboxylate linker of  $[\text{Rh}(\text{phi})_2\text{bpy}]^{3+}$  was linked to the N-terminus of a resin-bound peptide library using standard peptide coupling strategies. PyBOP, HOBT, and DIPEA were used in the

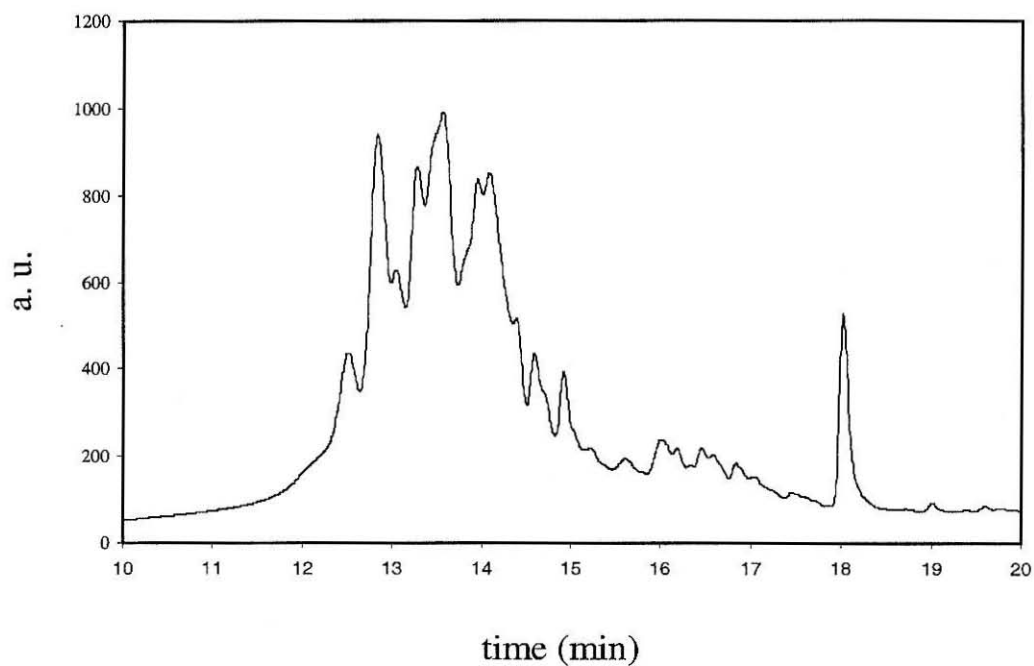


**Figure 3.8. HPLC Analysis of Peptide Library 1.** The library of peptides was released from the solid support by irradiation at 365 nm for 60 min, and injected into the HPLC. The chromatogram was monitored at 210 nm.

activation of the metal complex. The coupling yield for Rh-PL1 was estimated at 90% by Edman sequencing. This yield was determined by comparing the average pmole of peptide detected for an aliquot of beads before and after the coupling reaction. Because the Edman reaction requires a free N-terminus, the intercalator-peptide conjugates should be invisible during sequencing. To obtain an average value, 113 coupled beads (counted with 5x magnification) were submitted, and sequencing revealed that 90% of the N-termini were blocked; only 10% of the expected peptide was detected. The sequencer detected approximately 1300 pmol of peptide, or only 12 pmol per bead.

### **3.3.2. The Release of Rh-Peptide Conjugates from Solid Support by Irradiation.**

Although on-bead screening is very convenient and has been applied in a number of combinatorial experiments,<sup>1</sup> it did not seem suitable for our library. With one end of the peptide tethered to a DNA intercalator and the other end tied to the Tentagel support, our peptide is highly constrained and unlikely to deliver  $\text{Zn}^{2+}$  to DNA. We were interested in performing off-bead screening, and we used a model intercalator-peptide conjugate and Rh-LP1 to investigate photocleavage of the nitrobenzyl linker and the release of conjugate from the resin.

***Experiments with a Model Conjugate.*** A model conjugate (Rh-EHAAKHS-CONH<sub>2</sub>) was prepared by automated peptide synthesis on Tentagel resin with a photocleavable nitrobenzyl linker. The resin bearing the conjugate was irradiated at several different wavelengths, and the release of Rh-peptide conjugate was monitored at 349 nm (Figure 3.9). Irradiation of the conjugate resin at 365 nm in a sodium borate buffer (25 mM, pH 6.5) produced a rapid initial release of Rh-EHAAKHS-CONH<sub>2</sub> into

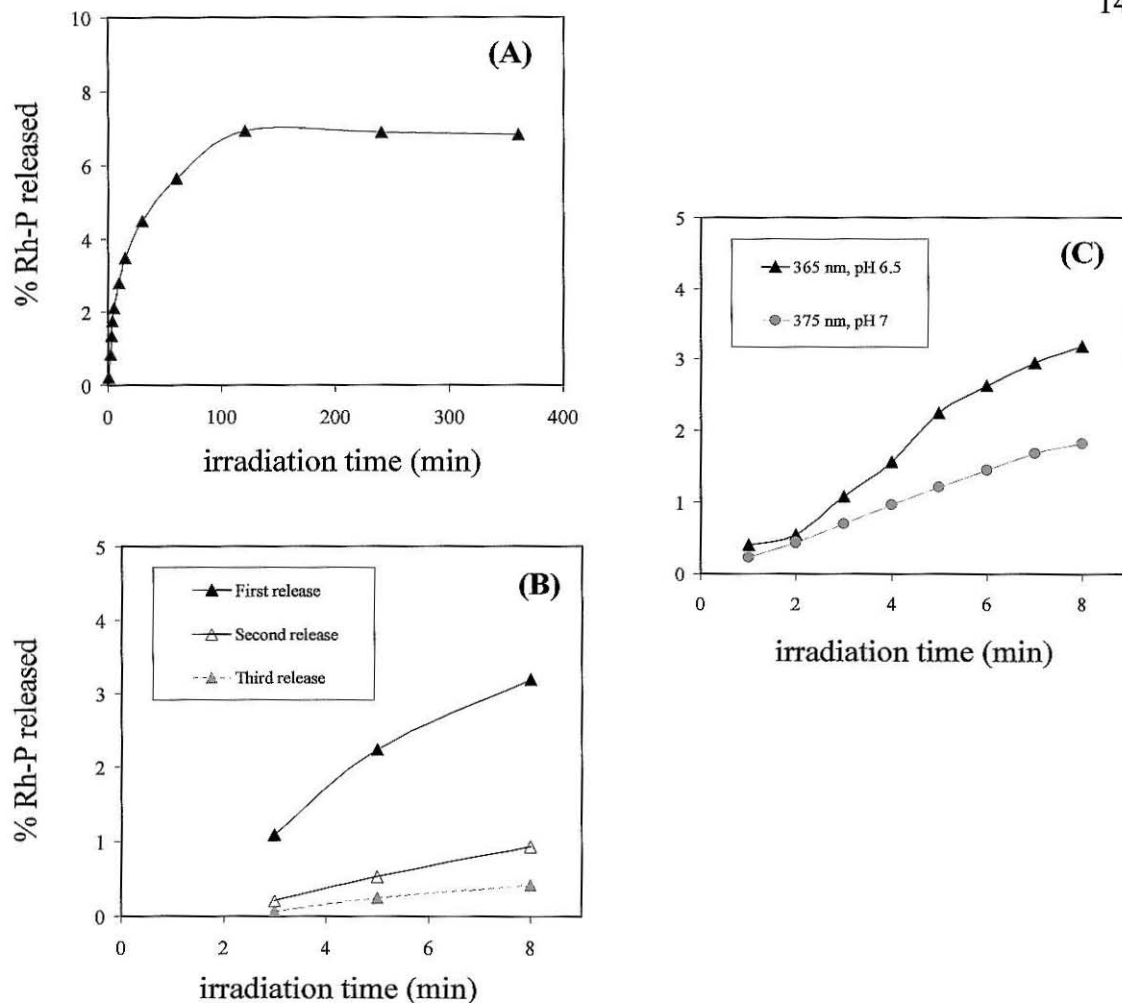


**Figure 3.9. The Release of Rh-Peptide from Solid Support with Irradiation.** A

Rh-EHAAKHS conjugate was prepared on a Tentagel resin with a photocleavable linker, and was released by irradiation. The percentage of released Rh-peptide was estimated from absorbance measurements at 349 nm and is plotted versus time.

**(A)** Irradiation at 365 nm in sodium borate buffer (pH 6.5). **(B)** Irradiation at 365 nm in sodium borate buffer (pH 6.5). After 8 min of irradiation the buffer was replaced. A second and third release were attempted. **(C)** Irradiation at 365 nm (triangles) and 375 nm (circles) in sodium borate buffer (pH 6.5 and 7).

solution (Figure 3.9 A). A spectrum obtained for the buffer solution showed the typical absorbance bands of the Rh-peptide conjugate. After 30 minutes of irradiation the rate of release began to level off, and after 2 hours the spectrum suggested decomposition of the complex. ESI analysis of the decomposed material indicated the loss of the phi ligands. The resin beads also showed a change in color during the irradiation; within 30 minutes they changed from orange to brown. The amount of conjugate released into solution was approximately 6% of the total conjugate attached to the resin.

The rhodium complex absorbs strongly at 365 nm. To explore whether a light filter effect was interfering with the cleavage of the nitrobenzyl linker, the borate buffer was replaced with new buffer at 8 minute intervals during the irradiation (Figure 3.9 B). The removal of released Rh-peptide from the cuvette did not significantly improve the overall release of conjugate from the resin. After 24 minutes of irradiation approximately 5% of the conjugate had been released. Although multiple releases of conjugate from the resin are possible, they are not homogeneous. The second and third release gave 40% and 20% of the material released during the first 8 minutes of irradiation.

Increasing the irradiation wavelength to 375 nm or 380 nm and narrowing the slit width of the lamp (thus focusing and reducing the intensity of the beam) did not improve the yield of released conjugate. Approximately 3% of the conjugate was released after 24 minutes, and 6% was released after 4 hours. The release was slower at higher wavelength (Figure 3.9 C), but the decomposition of the rhodium complex was also slower; therefore, longer irradiations were possible. When 8 minute irradiation intervals were attempted at 375 nm, the second and third intervals gave 60% and 40% of the material of the first release.

**Experiments with Rh-LP1.** Resin bearing Rh-LP2 was also used in release experiments. The resin was irradiated at 375 nm in sodium borate buffer (pH 7.4), and again, the release of Rh-LP2 was monitored at 349 nm (Figure 3.10). With 60 minutes of irradiation less than 3% of the conjugate was released from the resin. To explore whether released conjugate was actually still associated with the resin bead, an aliquot of beads was removed and rinsed with a 0.01% solution of TFA in acetonitrile. A significant amount of noncovalent conjugate does appear to be sticking to the beads, and with the rinsing step, the recovery of conjugate from the resin is increased to 6%.

**HPLC Analysis of Released Rh-LP1.** Resin bearing Rh-LP2 was irradiated at 375 nm and an aliquot of the released library was taken at 3, 8, 24, and 60 minutes. The aliquots were analyzed by reverse phase HPLC (Figure 3.11). By monitoring at 210 nm both free peptide and coupled peptide can be detected, but at 360 nm only the coupled peptide absorbs. The chromatogram at 210 nm shows small amounts of free peptide eluting at 20 and 30 minutes, but most of the released material absorbs at 360 nm. The conjugates elute between 32 and 40 minutes.

The distribution of peaks in the chromatogram changes during the course of the irradiation. The nonpolar peptides (longer retention time) dominate the chromatogram for the shorter irradiation times, but decrease relative to the more polar peptides with longer irradiations. It is possible that the surface properties of the resin change during the irradiation, and that the nonpolar peptides begin to aggregate on the bead with extended irradiation. The nonuniform release of conjugates with different peptide compositions was a concern, and a potential obstacle in screening assays.

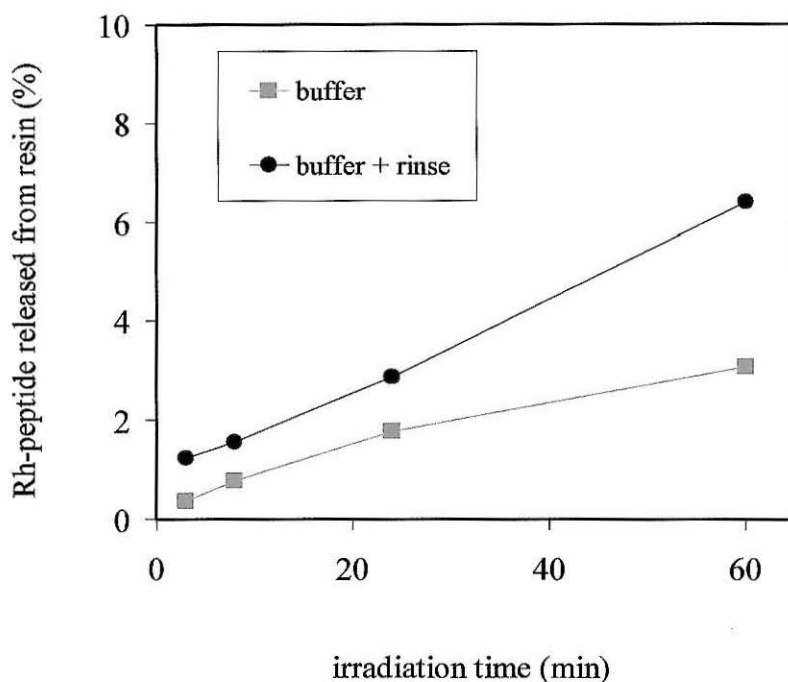


**Figure 3.10. The Release of Rh-PL1 from Solid Support with Irradiation.** Rh-LP1 resin (49 mg) was suspended in sodium borate buffer (25 mM, pH 7.4, 357  $\mu$ L), and was irradiated at 375 nm (slit width 4 mm). The absorbance at 360 nm was measured at 3, 8, 24, and 60 min and the percentage of released Rh-peptide was estimated. A plot of Rh-peptide released from resin vs. irradiation time is presented. The % of released Rh-peptide was determined for the buffer solution containing the resin beads (squares) and for the buffer solution plus material released from the beads with a 0.1% solution of TFA in acetonitrile (circles).

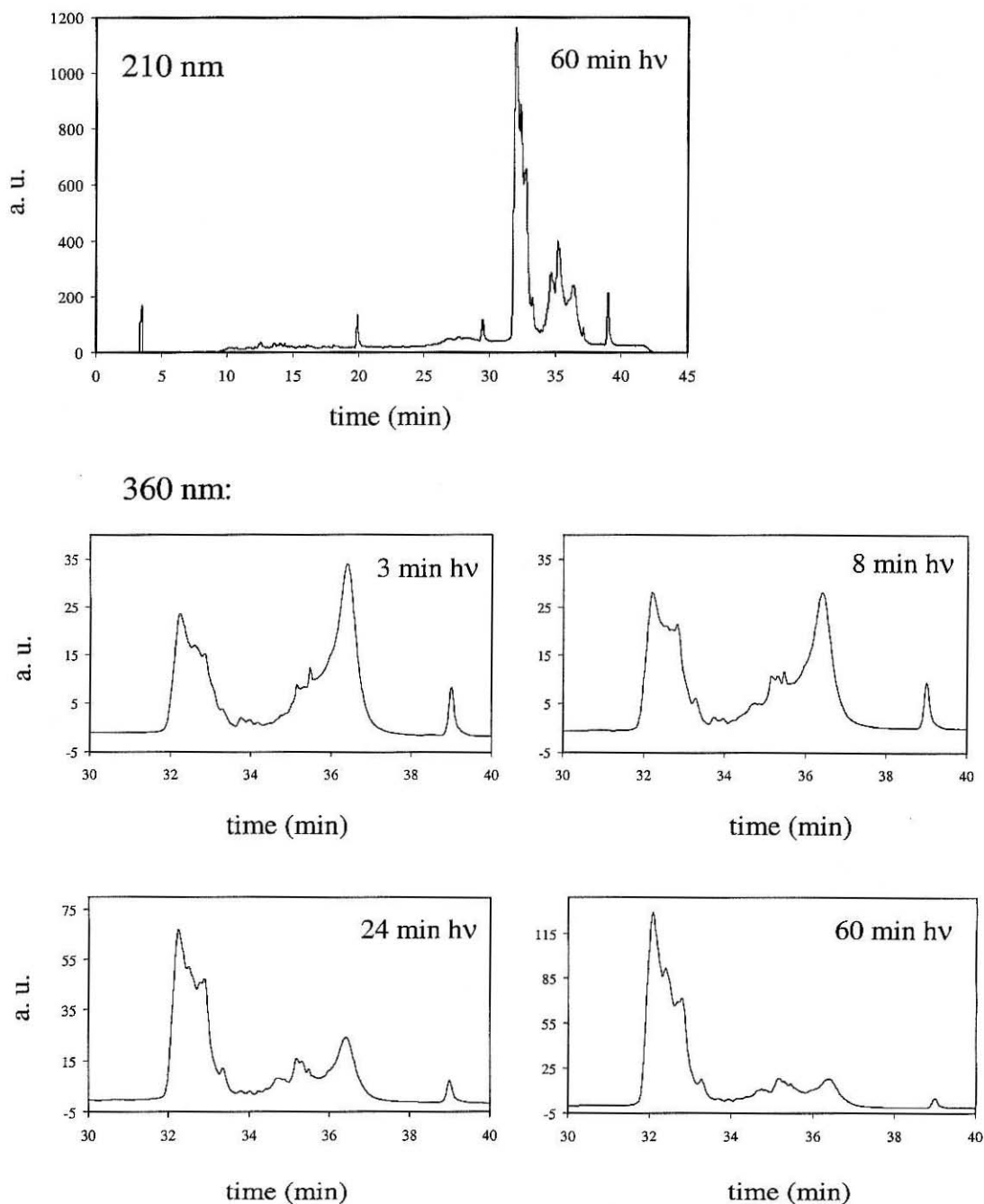


**Figure 3.11. HPLC Analysis of Rhodium-Peptide Library 1.** The library of Rh-peptide conjugates was released from the solid support by irradiation at 375 nm for 3, 8, 24, or 60 min, and injected into the HPLC. The chromatograms were monitored at 210 nm and 360 nm.



### 3.3.3. The Development of a Screening Strategy to Select Artificial Nucleases.

The development of an efficient screening assay is a vital step in a combinatorial experiment; indeed, the screening strategy can severely limit the size of the library. We ran into a number of roadblocks as we tested various screening approaches. Ultimately we were forced to screen our library bead-by-bead using a plasmid cleavage assay. Before we were reduced to this inefficient screening method, we explored the use of a fluorogenic DNA substrate, or a multiple-round plasmid cleavage screen.

*A Fluorogenic Substrate for Library Screening.* Initially we considered using a fluorogenic DNA substrate in our hydrolysis screen. A fluorogenic DNA substrate would boast both a donor and acceptor fluorophore. The emission of the donor fluorophore is quenched through fluorescence resonance energy transfer to the acceptor.<sup>21</sup> Cleavage of the DNA substrate separates the donor and acceptor, and thus restores the emission of the donor. Fluorogenic DNA substrate have been applied in cleavage studies with natural nucleases and small molecules.<sup>22,23</sup>

5'-Fluorescein phosphoramidite and TAMRA-dT phosphoramidite were incorporated at the 5' ends of complementary 15-mer oligonucleotides. The purified DNA strands were studied using fluorescence spectroscopy. Fluorescein was excited with 480 nm light, and gave an intense emission band centered around 520 nm. As expected the fluorescence of the fluorescein donor was quenched by the addition of the strand bearing the TAMRA acceptor (Figure 3.12). The fluorescence at 520 nm was significantly reduced, and a new fluorescence signal at 545 nm was observed for the excited TAMRA fluorophore. The intensity at 520 nm could be partially restored by

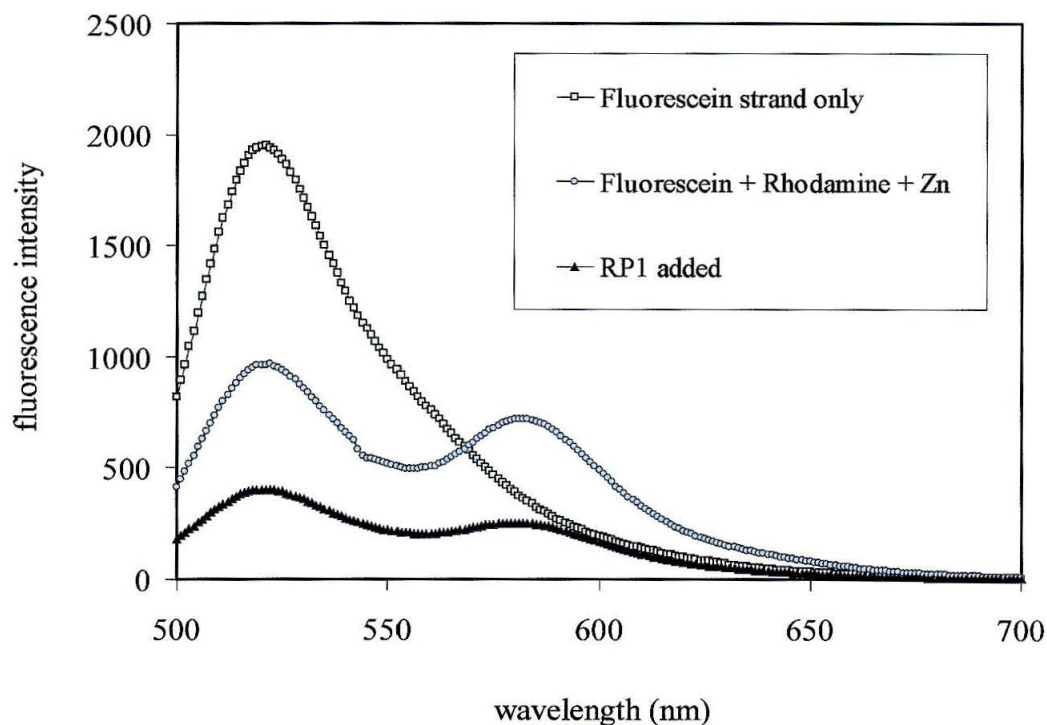


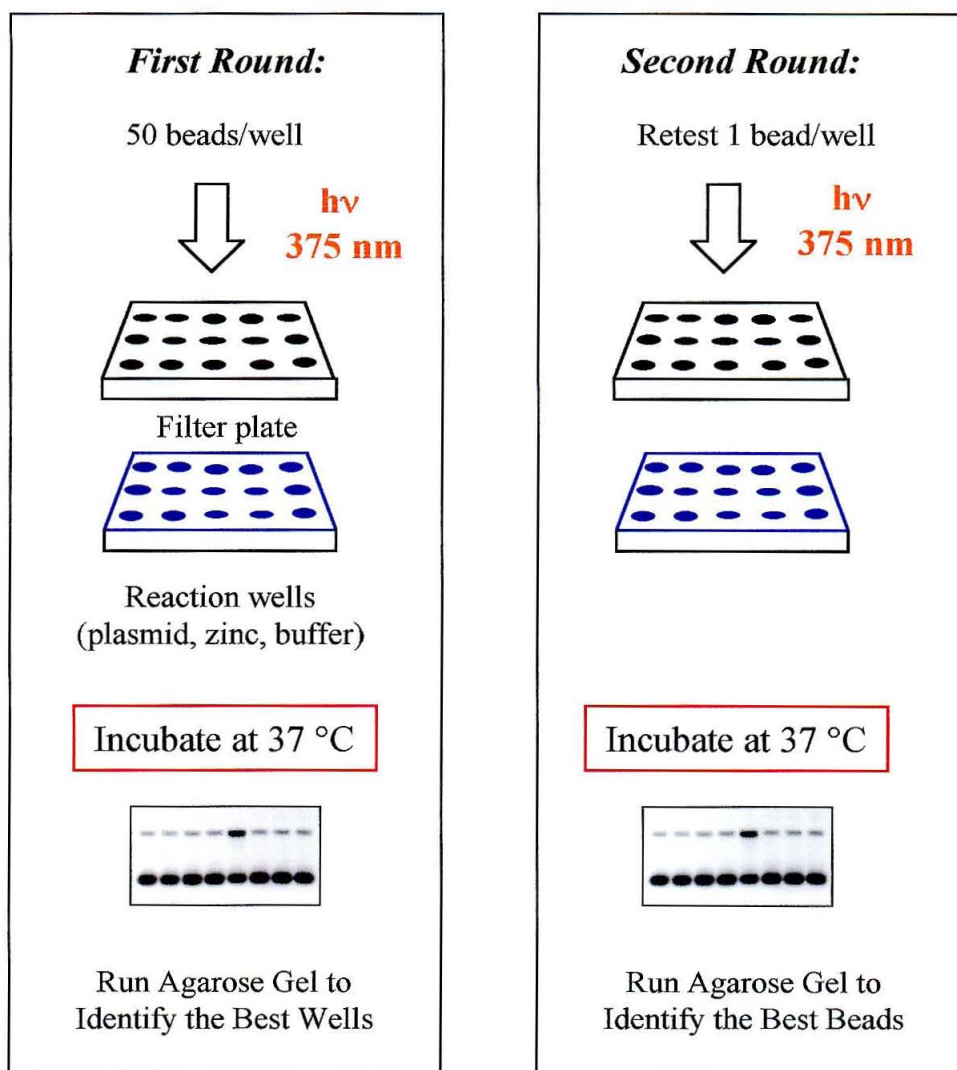
**Figure 3.12. The Spectra of a Fluorogenic Substrate with Rh-P1.** A 15-mer duplex with a fluorescein donor attached to the 5' end of one strand and a rhodamine acceptor attached to the 5' end of the complement strand was prepared. The fluorescein donor emits at 520 nm when excited with 480 nm light. Addition of the rhodamine strand quenches emission at 520 nm, and gives rise to a new signal at 545 nm. Addition of rhodium complex reduces the intensity at both 520 and 545 nm.

incubation of the DNA substrate with a restriction enzyme or by  $[\text{Rh}(\text{phi})_2\text{bpy}']^{3+}$  photocleavage.

In these preliminary studies we also discovered that the donor fluorescence was dramatically quenched by the addition of rhodium complex. The quenching was observed both with the duplex bearing the two fluorophores (Figure 3.12), and for the single-strand of DNA bearing fluorescein. The sensitivity of the fluorogenic substrate to rhodium complex precluded its use in a screening assay.

***A Multiple-Round Plasmid Cleavage Assay.*** As was described in Chapter 2, the plasmid cleavage assay is a very convenient method for detecting DNA cleavage events. A nick in a supercoiled plasmid produces an open circular product that migrates more slowly through an agarose gel. Double-stranded cleavage or two nicks within 12 to 16 base pairs results in a linear DNA product with intermediate mobility. We decided to apply a plasmid cleavage assay to our library.

To facilitate rapid screening of our 16,000 member library, we included two rounds in each screening experiment (Figure 3.13). In the first round, 20 to 100 beads were distributed to each well of a 96-well filtration plate. The beads were irradiated for 5 minutes to release a portion of the conjugate from the resin. The released conjugate was drained into a 96-well collection plate, and was incubated with plasmid and divalent cation. The plasmid products of the 96 reactions were analyzed by agarose gel electrophoresis, and the beads in the most promising wells were redistributed to a new filtration plate for a second round of screening. In the second round, only 1 bead was tested per well.

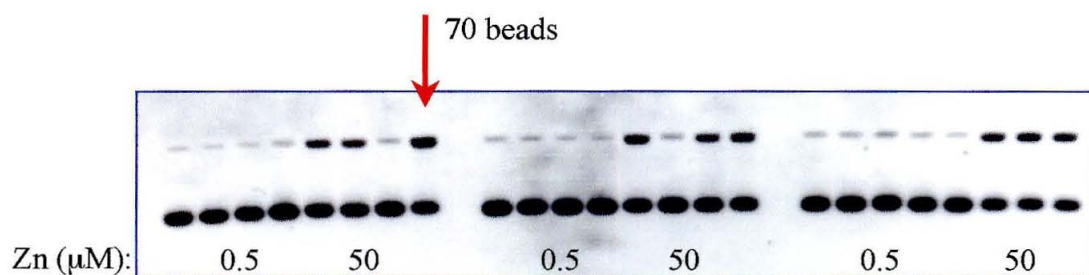
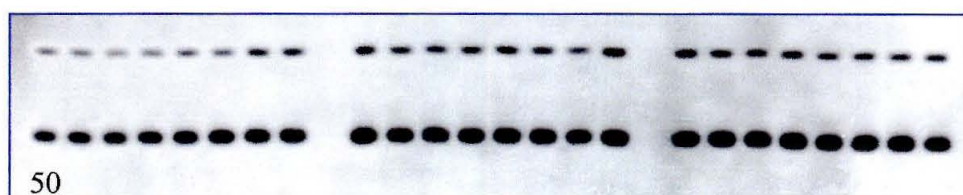


**Figure 3.13. A Plasmid Cleavage Assay for Library Screening.** To screen Rh-PL2 for hydrolysis activity, a plasmid cleavage assay was developed. Beads were distributed to the wells of a filtration plate and irradiated to release the Rh-peptide conjugates. The released material was drained into reaction wells and incubated with plasmid and zinc. The levels of plasmid cleavage in each well were assessed by agarose gel electrophoresis. We originally intended to distribute many beads to each well for a first round of screening, and to examine individual beads in a second round.

A typical screening result is presented in Figure 3.14. Significant levels of nicked plasmid were observed when the material released from a collection of beads was incubated with plasmid and  $\text{Zn}^{2+}$  (50  $\mu\text{M}$  or greater). Very low Zn concentrations (Figure 3.14, 0.5  $\mu\text{M}$ ) or  $\text{Mg}^{2+}$  (data not shown) did not result in nicked plasmid. Also, little cleavage was observed at pH 7. As was consistently observed for Rh-P1, the best cleavage was obtained at pH 6. Peaks in cleavage were observed for individual wells, and importantly, these peaks did not correlate with a high bead count in the well. This suggested that we were discriminating between conjugates with different peptide composition. The number of “hit” wells was actually quite high in the first round, at least 50% for 50  $\mu\text{M}$   $\text{Zn}^{2+}$  concentrations. A second round of screening was attempted with the 70 beads found in a promising well (Figure 3.14). In this experiment, and in every experiment, no significant plasmid cleavage was observed in a second round of screening. As our studies with a model conjugate and Rh-PL1 clearly demonstrated, multiple releases of conjugate from the resin are not homogeneous. This may explain the failure of our second round.

***On-Bead Screening.*** We briefly considered using an on-bead plasmid cleavage assay. When plasmid was directly incubated with many beads (20 to 50 per well), it was extensively degraded in every well; there was little variation among the wells. When plasmid was directly incubated with a single bead, no cleavage of the plasmid was observed. This approach was also abandoned.

***A Single-Bead Plasmid Cleavage Assay.*** Finally we resorted to bead-by-bead screening of our rhodium-peptide library. Individual beads were distributed to the wells of a filtration plate and irradiated for 10 min. The released material was collected and

**Round 1 (20 to 100 beads/well)****Round 2 (1 bead/well)**

**Figure 3.14. Two rounds of screening with Rh-Peptide Library 2.** The library was screened using the plasmid cleavage assay. In the first round of the screen, 20 to 100 beads were distributed to a filtration plate and irradiated. The released conjugates were drained into a 96-well plate containing pUC19 (40  $\mu\text{M}$  bp), Zn (0.5 or 50  $\mu\text{M}$ ), and HEPES buffer (15 mM, pH 7). The plate was incubated at 37 °C for 24 h, and then the contents of the wells were analyzed by agarose gel electrophoresis. A selection from the gel is shown above. The lane indicated by an arrow showed fairly high levels of nicked plasmid, and the 70 beads from the corresponding well were redistributed to a filtration plate for a second round of screening.



incubated with plasmid and  $\text{Zn}^{2+}$  (50 or 100  $\mu\text{M}$ ). Plasmid cleavage was analyzed by agarose gel electrophoresis.

Bead-by-bead screening is slow and fairly tedious, and only a small portion of Rh-PL2 was screened. In 12 screening assays I tested approximately 1000 beads, or 0.06 equivalents of the 16,000 member library. Nonetheless, we did identify “hit” wells, wells that showed above average levels of nicked plasmid. The results of the 12 screening experiments are summarized in Table 3.4, and sections of the agarose gels that contain hit wells are presented in Figure 3.15. The percentage of nicked plasmid was determined for control reactions, for a set of 7 or 8 average wells, and for the hit wells. The average cleavage level varied significantly from screen to screen, and hits were observed in half of the screening assays. The percentage of hit wells was approximately 1%.

As described in Table 3.5, four different control reactions were included in most of the screening assays. The level of nicked plasmid observed with many beads was often very comparable to the level achieved with a hit bead. When a bead was not added to the well, the resulting percentage of nicked plasmid was generally lower, at least a little bit lower, than the average percentage for wells containing beads. There were some unexpected peaks in cleavage when  $\text{Zn}^{2+}$  was omitted from an incubation reaction (Table 3.4, Screen 6, 7, 8, 9, and 11). This may be due to the presence of small amounts of  $\text{Fe}^{2+}$  in a plasmid stock solution. We have previously observed with Rh-P1, that the addition of  $\text{Zn}^{2+}$  can cause a decrease in cleavage for a particular stock of plasmid, and we attributed this to iron contamination. As we have previously observed Rh-P1, essentially no cleavage was observed at pH 7 or with  $\text{Mg}^{2+}$  (data not shown).

**Table 3.4. Summary of Single-Bead Screening of Rhodium-Peptide Library 2.**

Screen	Conditions <sup>a</sup>	Cleavage Levels (% nicked plasmid)			Comments
		Controls <sup>b</sup>	Average <sup>c</sup>	Hits <sup>d</sup>	
1	50 $\mu\text{M}$ $\text{Zn}^{2+}$	36/22/6/--	60	88 96	
2	50 $\mu\text{M}$ $\text{Zn}^{2+}$	51/12/13/--	30	none	peaks in cleavage clustered
3	50 $\mu\text{M}$ $\text{Zn}^{2+}$	--	20	57	
4	50 $\mu\text{M}$ $\text{Zn}^{2+}$	--	40	none	no peaks in cleavage
5	100 $\mu\text{M}$ $\text{Zn}^{2+}$	44/18/14/20	26	43 44	
6	100 $\mu\text{M}$ $\text{Zn}^{2+}$	58/22/21/68	29	55	
7	100 $\mu\text{M}$ $\text{Zn}^{2+}$	56/34/56/67	49	none	peaks in cleavage at the edge of the plate
8	100 $\mu\text{M}$ $\text{Zn}^{2+}$	74/34/46/63	64	none	no peaks in cleavage
9	100 $\mu\text{M}$ $\text{Zn}^{2+}$	76/36/44/51	34	66	
10	100 $\mu\text{M}$ $\text{Zn}^{2+}$	46/26/28/30	30	58 54	
11	100 $\mu\text{M}$ $\text{Zn}^{2+}$	79/36/72/52	39	none	no peaks in cleavage
12	100 $\mu\text{M}$ $\text{Zn}^{2+}$	49/26/25/32	29	44	

<sup>a</sup> One to two beads were tested per well. Material was released through a 10 min irradiation with a transilluminator. The plasmid cleavage assay was completed with pUC19 (20  $\mu\text{M}$  bp),  $\text{Zn}^{2+}$  (concentration listed in table), and HEPES buffer (15 mM, pH 6). Reactions were incubated for 48 h incubation at 37 °C.

<sup>b</sup> The control reactions are listed as follows: many beads / no beads / no beads, no zinc / no zinc.



<sup>c</sup> The average % of nicked plasmid was determined through quantitation of the 7 wells in the same column as the hit, or a randomly selected column of 8 wells.

<sup>d</sup> The screening hits were determined by visually inspecting the agarose gel for large amounts of nicked plasmid. The most promising lanes of the gel were quantitated.

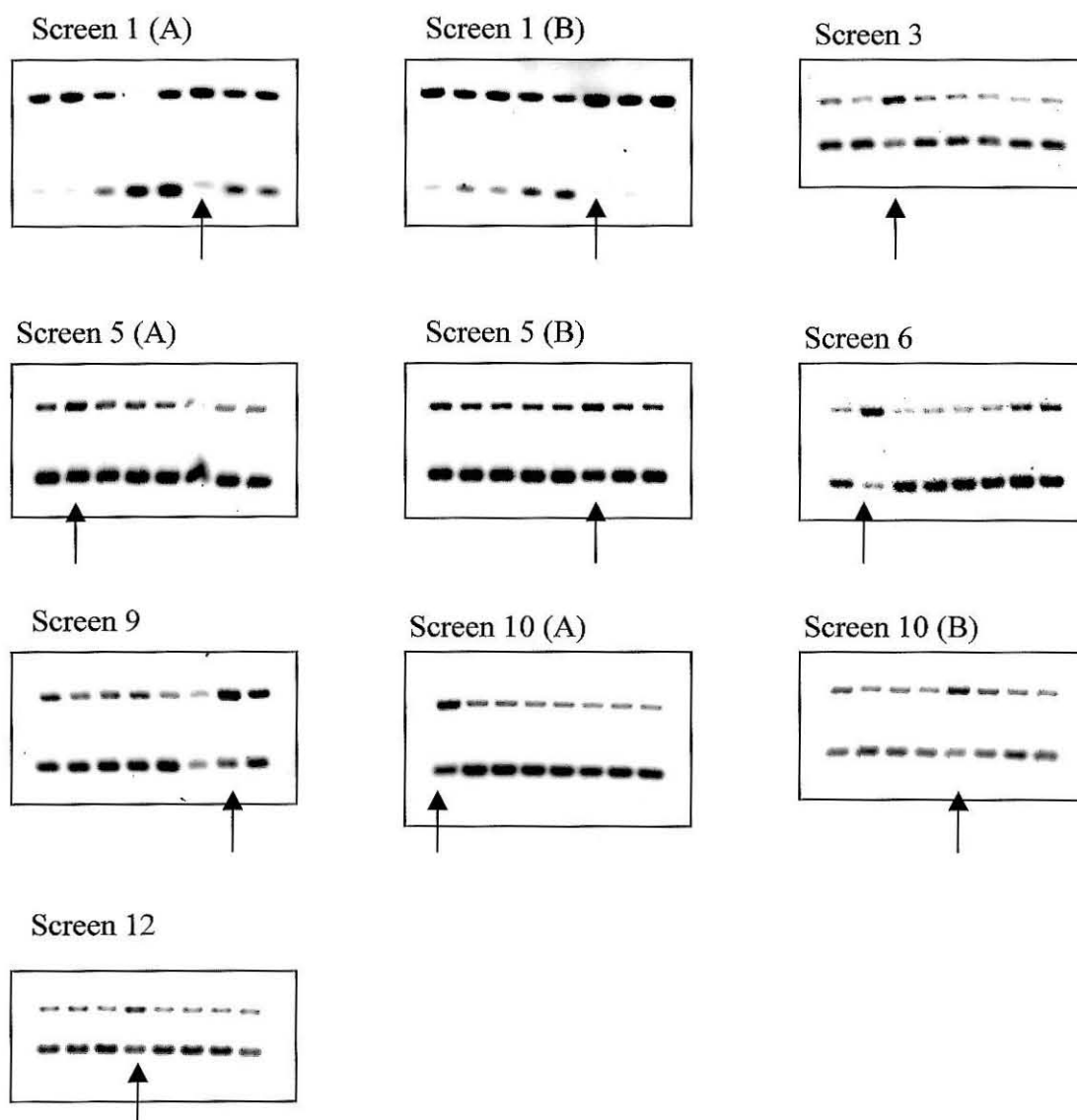


**Figure 3.15. Single-Bead Screening with Rh-Peptide Library 2.** Agarose gels from single-bead screening of Rh-LP2 are presented. These gel sections contain “hit” lanes, lanes that show higher levels of nicked plasmid. The hits are indicated with arrows.

**Table 3.5. Control Reactions for Single-Bead Plasmid Cleavage Screening.**

	<b>Number of Beads</b>	<b>Zinc Concentration (<math>\mu\text{M}</math>)</b>
<i>1</i>	20 to 50	50 or 100
<i>2</i>	0	50 or 100
<i>3</i>	0	0
<i>4</i>	1 or 2	0

The difference in nicked plasmid percentage between hit and average wells ranged from 45 to 15%. The beads from the 11 best wells were submitted for Edman sequencing. In two cases (Screen 1 and 3), the hit well contained two beads, and these beads were sequenced together. In some experiments the wells that showed high levels of nicked plasmid were suspiciously clustered, and these wells were disregarded. This was most often observed for wells at the very edge of the collection plate, and was caused by inadequate sealing of the wells and partial evaporation of the reaction buffer.

#### **3.3.4. Identification of the Conjugates Selected from Rh-LP2.**

The peptides attached to the hit beads were identified through Edman sequencing (Figure 3.16). Sequencing results are reported in Table 3.6. Importantly, there was plenty of peptide available on the selected beads to allow for decoding; indeed, an average of 20 pmol of peptide was detected for each bead submitted for analysis. We were concerned that blocking of the N-terminus with rhodium complex, and the release of peptide during screening would prevent reliable sequencing, but this was not the case.

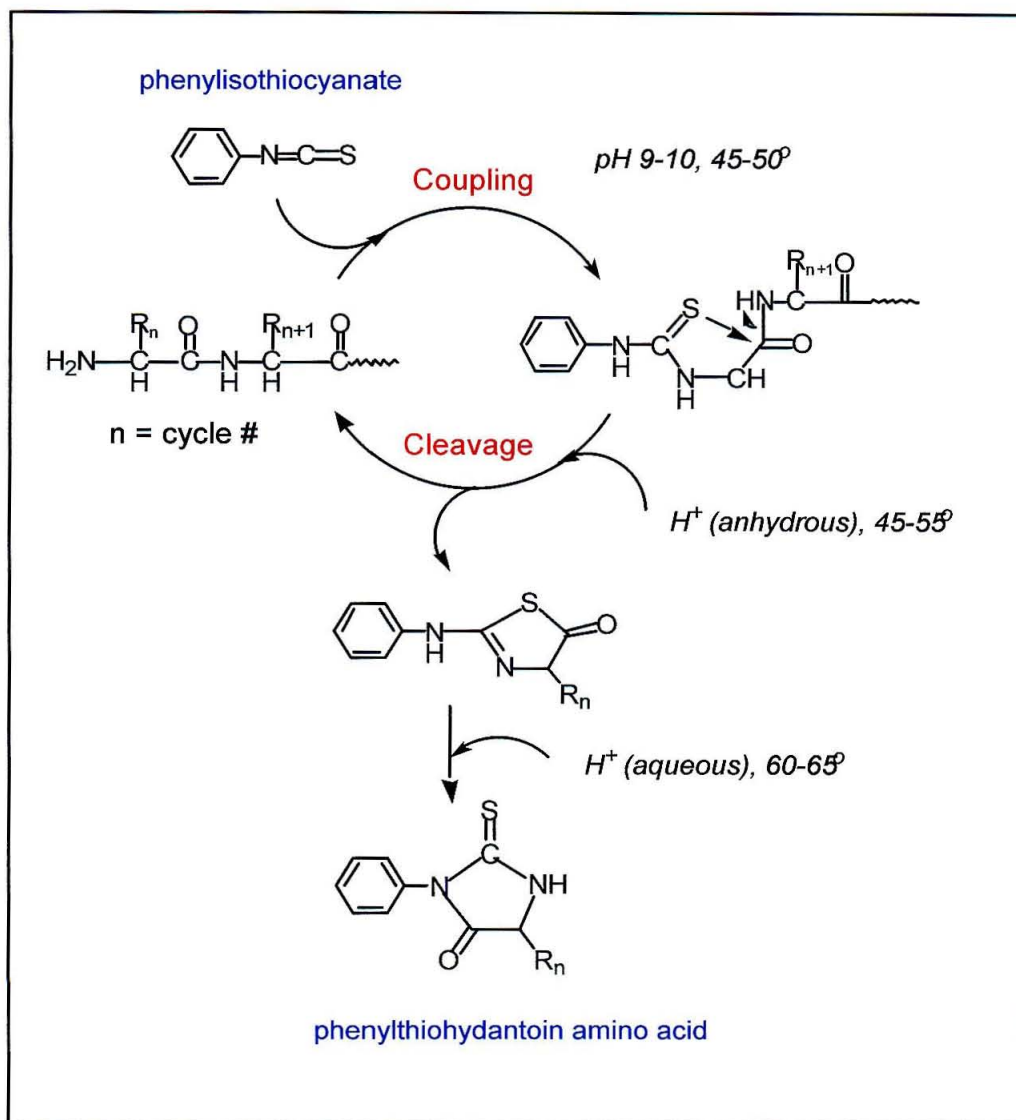


**Figure 3.16. The Edman Sequencing Reaction.** The identity of the peptide attached to a selected bead can be determined by Edman sequencing. Through reaction with phenylisothiocyanate and treatment with acid the N-terminal residue is cleaved from the peptide. The cleaved amino acids are identified by HPLC retention. Through repeated cycles the entire peptide is decoded.

**Table 3.6. Summary of Sequencing Results for Selected Beads from Rh-PL2.**

Hit <sup>a</sup>	Cleavage Levels <sup>b</sup>			Peptide Composition <sup>c</sup>
	(% nicked plasmid)			
	Avg.	Hit	Diff.	
1A <sup>d</sup>	60	88	28	E-P- <b>K</b> -A-A- <b>E</b> - <b>H</b> -A- <b>K</b> - <b>A</b> - <b>E</b> -A- <b>H/K</b> -A-K-G
2B	60	96	36	E-P- <b>H</b> -A-A- <b>H</b> - <b>H</b> -A- <b>E/X</b> - <b>H</b> -A-A- <b>A</b> -A-K-G
3 <sup>d</sup>	20	57	37	E-P- <b>A/K</b> -A-A- <b>K/A</b> - <b>E*</b> -A- <b>K/H</b> -A/ <b>K</b> - <b>E*/X</b> -A- <b>*</b> / <b>H</b> -A-K-G
5A	26	43	17	E-P- <b>K</b> -A-A- <b>E</b> - <b>E</b> -A- <b>H</b> - <b>H</b> - <b>H</b> -A- <b>E/X1/X2</b> -A-K-G
5B	26	44	18	E-P- <b>E</b> -A-A- <b>K</b> - <b>E/X</b> -A- <b>E/X</b> - <b>H</b> -A-A- <b>A</b> -A-K-G
6A	25	60	45	E-P- <b>A</b> -A-A- <b>E</b> - <b>H</b> -A- <b>E</b> - <b>A</b> - <b>K</b> -A- <b>H</b> -A-K-G
6B	29	55	26	E-P- <b>K</b> -A-A- <b>H</b> - <b>E</b> -A- <b>K</b> - <b>E</b> - <b>K</b> -A- <b>A</b> -A-K-G
9	34	66	32	E-P- <b>H</b> -A-A- <b>E</b> - <b>A</b> -A- <b>K</b> - <b>E/X</b> - <b>H</b> -A- <b>A</b> -A-K-G
10A	25	58	29	E-P- <b>A</b> -A-A- <b>H</b> - <b>H</b> -A- <b>H</b> - <b>H</b> - <b>K</b> -A- <b>K</b> -A-K-G
10B	36	54	18	E-P- <b>E</b> -A-A- <b>A</b> - <b>K</b> -A- <b>H</b> - <b>H</b> - <b>K</b> -A- <b>H</b> -A-K-G
12	29	44	15	E-P- <b>K</b> -A-A- <b>E</b> - <b>E</b> -A- <b>H</b> -A- <b>H</b> -A- <b>A</b> -A-K-G

<sup>a</sup> The wells selected in the plasmid cleavage assay are labeled with the number of the screen (See Table 3.4). If more than one hit well was selected in a single screening assay, the two wells are labeled A and B.

<sup>b</sup> The % of nicked plasmid was quantitated for the 7 wells in the same column as the hit well (Avg.), and for the hit well. The difference in average cleavage and hit cleavage is also presented.

<sup>c</sup> The peptide composition was determined by Edman sequencing. The variable positions are shown in red. The asterisk indicates a decomposition product commonly observed with Glu. X indicates an unidentified residue. This also may be a decomposition product from Glu.

<sup>d</sup> The hit well contained two beads.

Fairly high levels of histidine were observed in our 11 selected peptides, particularly at the center of the peptide (Figure 3.17). Two peptides contained two His residues, two contained three His, four contained two His, and no selected peptides were without His (Figure 3.18). There was at least one peptide without Lys, Glu, or Ala. Ala was incorporated to the greatest extent near the termini of the peptide.

There were a few glitches in the sequencing. Particularly for Glu positions, a large amount of a second product, perhaps a decomposition product resulting from Glu, was observed. Towards the C-terminus of the peptide there were a few residues that could not be clearly identified. Again, the unidentified residues may actually be related to decomposition of Glu. It is important to note that when the two beads from hit 1A were sequenced together, a mixture of residues was only indicated at position 13. This is a peculiar result, and it suggests that one bead was lost in route to the sequencer. This is one of the risks of a split-pool library of peptides. If a bead, and they are small, is accidentally misplaced, it is impossible to determine the composition of a selected peptide.

A ranking of the selected peptides is presented in Table 3.7. To assess our screening approach, and to explore the activity of the selected peptides, we decided to individually prepare two of the best conjugates. The three selected conjugates are pictured in Figure 3.19. The peptides for hit 6A and 2B were synthesized by automated peptide synthesis, and were coupled to  $[\text{Rh}(\text{phi})_2\text{bpy}]^{3+}$ . They were dubbed Rh-SP1 (Selected Peptide 1) and Rh-SP2 (Selected Peptide 2). In addition we prepared a peptide based on the levels of incorporation at each peptide position (Figure 3.17). The sequence

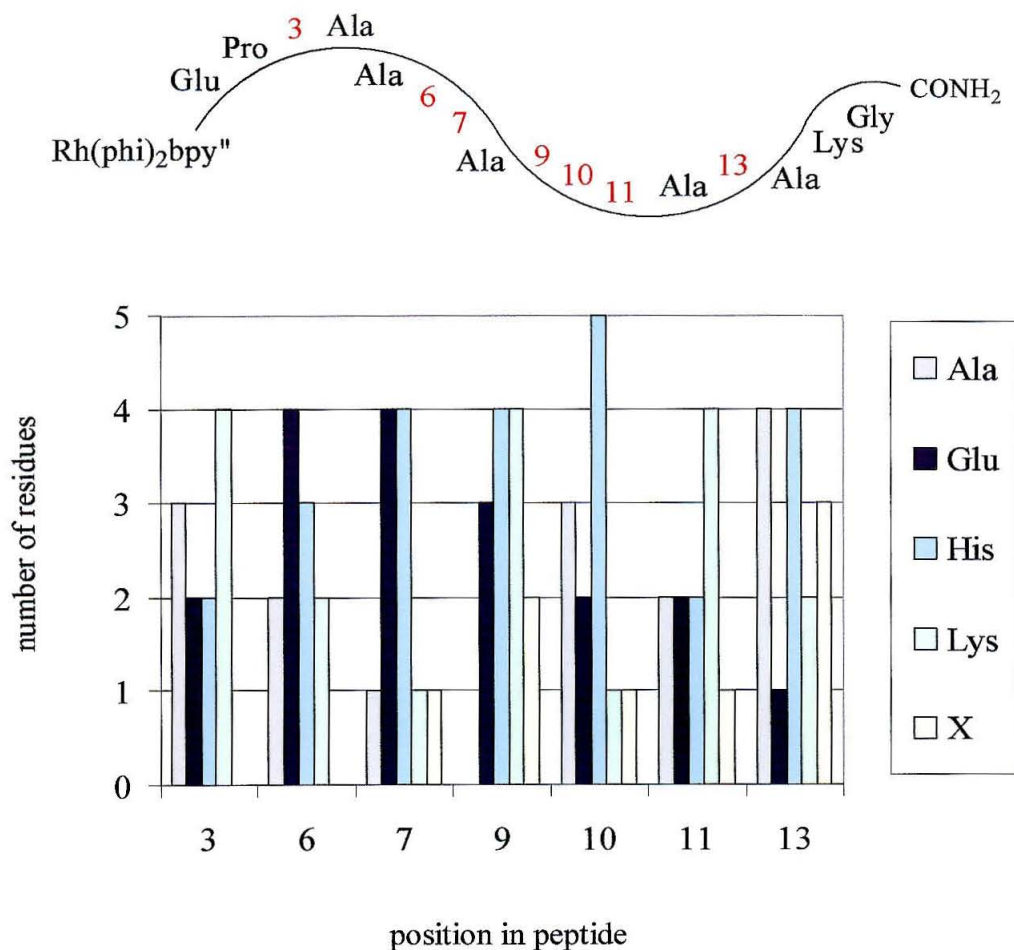


**Figure 3.17. Residue Incorporation at Variable Positions in Rh-LP2.** The number of Ala, Glu, His, Lys, and X (unidentified) residues incorporated at the variable positions of Rh-LP2 are shown. These results are based on 12 screening experiments and 11 selected and sequenced beads.

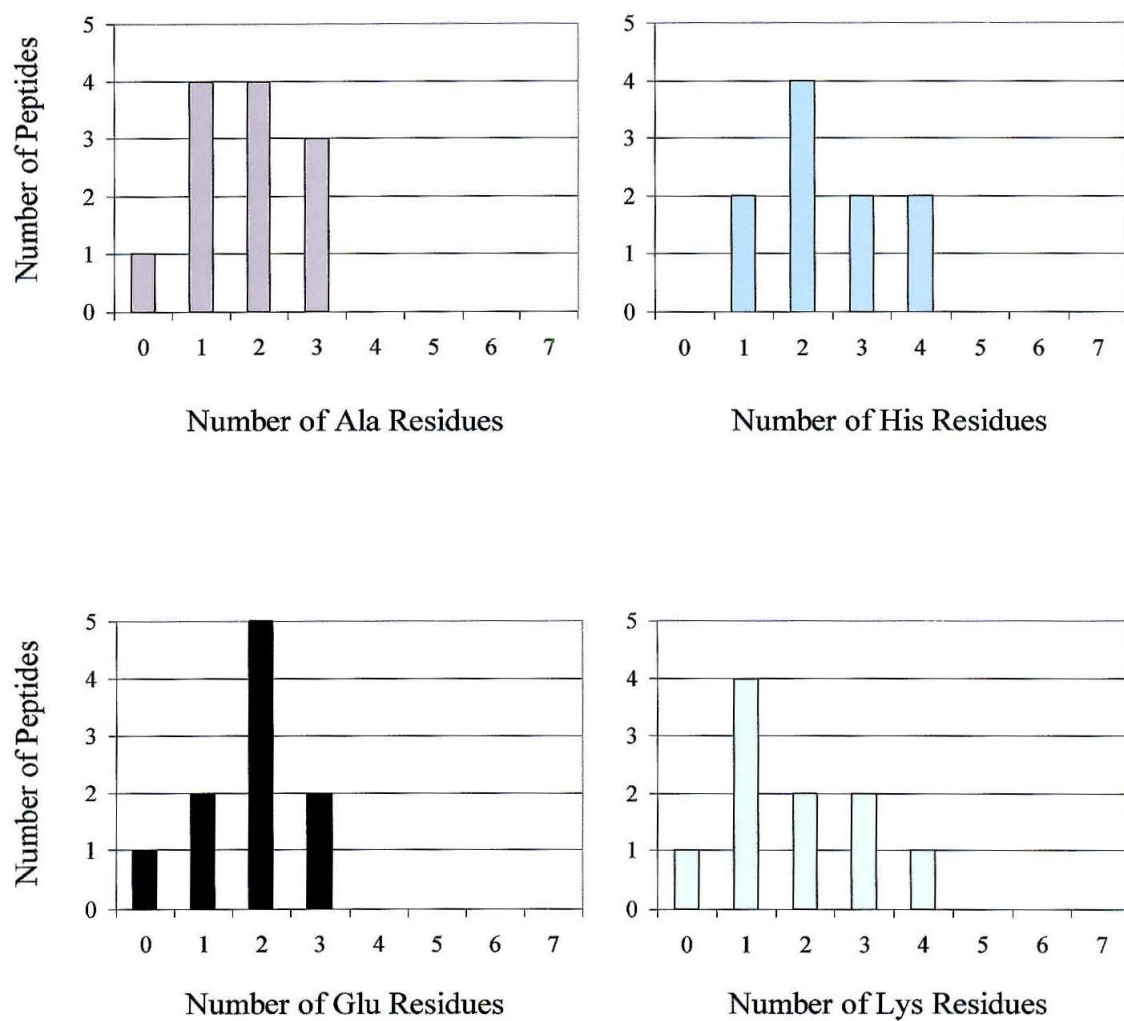


**Figure 3.18. Number of Ala, Glu, His, and Lys Residues in Selected Peptides.**

These results are based on eleven selected peptides.



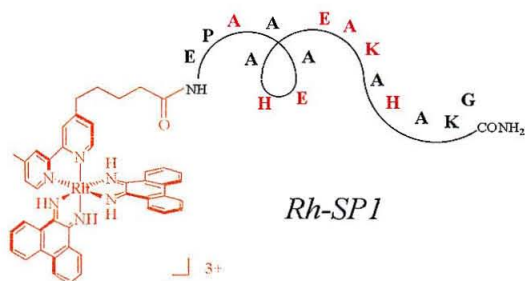
**Table 3.7. A Ranking of the Selected Peptides.**

Hit	Diff. <sup>a</sup>	Variable Position in Peptide:						
		3	6	7	9	10	11	13
<b>6A<sup>b</sup></b>	45	A	E	H	E	A	K	H
<b>3<sup>c</sup></b>	37	A/K	A/K	E*	H/K	A/K	E*/X	*/H
<b>2B<sup>b</sup></b>	36	H	H	H	E/X	H	A	A
<b>9</b>	32	H	E	A	K	E/X	H	A
<b>10A</b>	29	A	H	H	H	H	K	K
<b>1A<sup>c</sup></b>	28	K	E	H	K	A	E	H/K
<b>6B</b>	26	K	H	E	K	E	K	A
<b>5B</b>	18	E	K	E/X	E/X	H	A	A
<b>10B</b>	18	E	A	K	H	H	K	H
<b>5A</b>	17	K	E	E	H	H	H	E/X1,2
<b>12</b>	15	K	E	E	H	A	H	A

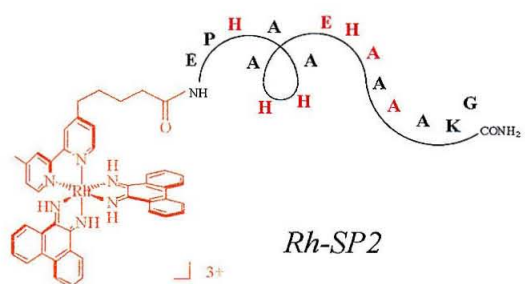
<sup>a</sup> Difference = (% Nicked Plasmid for Hit Well) – (% Nicked Plasmid for Average Well).

<sup>b</sup> Two of the best selected conjugates were synthesized for further study.

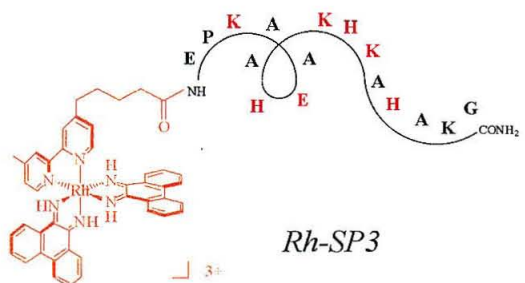
<sup>c</sup> The hit well contained two beads.



$\text{Rh}(\text{phi})_2\text{bpy}^+$ -Glu-Pro-Ala-Ala-Ala-Glu-His-Ala-Glu-Ala-Lys-Ala-His-Ala-Lys-Gly-CONH<sub>2</sub>



$\text{Rh}(\text{phi})_2\text{bpy}^+$ -Glu-Pro-His-Ala-Ala-His-His-Ala-Glu-His-Ala-Ala-Ala-Ala-Lys-Gly-CONH<sub>2</sub>



$\text{Rh}(\text{phi})_2\text{bpy}^+$ -Glu-Pro-Lys-Ala-Ala-Glu-His-Ala-Lys-His-Lys-Ala-His-Ala-Lys-Gly-CONH<sub>2</sub>

**Figure 3.19. Schematic of the Three Rhodium-Peptide Conjugates Selected by Library Screening.** Three conjugates were selected from Rh-PL2 by the plasmid screening assay. The conjugates were named Rh-SP1, Rh-SP2, and Rh-SP3 (SP = selected peptide).

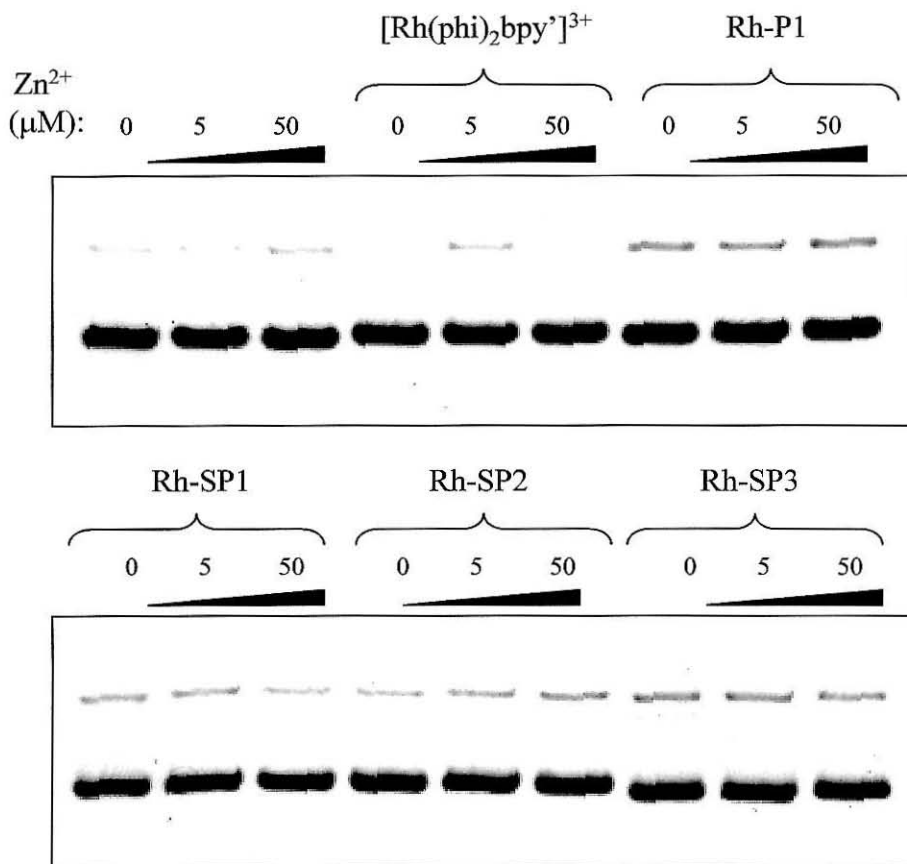


**Figure 3.20. Plasmid Cleavage Assays with Rh-P1, Rh-SP1, Rh-SP2 and Rh-SP3.**

The selected intercalator-peptide conjugates were tested against Rh-P1 in plasmid cleavage assays. Agarose gels are shown for a typical experiment. Very little plasmid cleavage was observed with any of the conjugates. In this experiment the conjugate (5 μM) was combined with ZnCl<sub>2</sub> (5 or 50 μM) and pUC19 (40 μM bp) in sodium borate buffer (20 mM, pH 6). The reactions were incubated for 24 h at 37 °C.

of this peptide was Glu-Pro-Lys-Ala-Ala-Glu-His-Ala-Lys-His-Lys-Ala-His-Ala-Lys-Gly-CONH<sub>2</sub>, and the corresponding conjugate was named Rh-SP3 (Selected Peptide 3).

### 3.3.5. Testing Selected Conjugates Against Rh-P1 in Plasmid Cleavage Assays.

The three selected conjugates, Rh-SP1, Rh-SP2 and Rh-SP3, were pitted against Rh-P1 in plasmid cleavage experiments. A variety of buffers (HEPES, sodium borate, citrate, and Zn<sup>2+</sup>-ion buffer), and different stocks of plasmid (both pUC19 and pBR322, purchased and harvested from bacteria) were used in these experiments. Despite a great deal of tinkering with assay conditions, very little plasmid cleavage has been observed for any of the conjugates, including Rh-P1. Occasional peaks in cleavage were observed with Rh-P1, Rh-SP1, and Rh-SP3, but these were not reproducible. A typical result is presented in Figure 3.20. A useful comparison of the activity of Rh-P1 and the selected conjugates has not been possible, but it is clear that our investment in a library method has not resolved the finicky hydrolysis chemistry of Rh-P1. We have not generated conjugates with robust hydrolysis activity against plasmid substrates.

## 3.4. Discussion

We have demonstrated that intercalator-peptide conjugates can be successfully applied to DNA hydrolysis.<sup>10,11</sup> The intercalating rhodium complex contributes DNA-binding affinity, and the peptide provides zinc-promoted reactivity. Our most active artificial nuclease to date is the Rh-P1 conjugate ( $\text{Rh} = [\text{Rh}(\text{phi})_2\text{bpy}]^{3+}$ , P1 = Asp-Pro-

Asp-Glu-Leu-Glu-His-Ala-Ala-Lys-His-Glu-Ala-Ala-Ala-Lys-CONH<sub>2</sub>). Although we have tethered a variety of peptides to the rhodium intercalator, peptides with subtle mutations in the P1 sequence, peptides inspired by natural endonucleases, and P1 peptides with helix-inducing covalent bridges,<sup>24</sup> we have seen no gains in activity.<sup>11</sup>

Coming to the end of our rational design strategies, we turned to a combinatorial strategy for the optimization of the Rh-P1 peptide. Here we describe the three steps in our combinatorial experiment: (i) the development of a library of intercalator-peptide conjugates, (ii) the screening of the library with a plasmid cleavage assay, and (iii) the identification of active conjugates by Edman sequencing.

### 3.4.1. The Rhodium-Peptide Library.

*The Design of Intercalator-Peptide Libraries.* To pursue an active artificial nuclease we designed two intercalator-peptide libraries. Rhodium-Peptide Library 1 (Rh-PL1) was primarily designed as a test library (Figure 3.2). The most important feature of this library was its small size. Rh-PL1 consisted of only 27 different intercalator-peptide conjugates; three positions in the tethered peptide were randomized with glutamic acid, histidine, and lysine. The sequence of the 13-mer peptide was as follows: Ala-X-His-Ala-Ala-Glu-His-Ala-Ala-X-X-Ala-Gly-CONH<sub>2</sub>, where X is a variable position. The entire peptide contained only five different types of residues (Ala, Glu, Gly, His, Lys). This intercalator-peptide library was used in the optimization of synthesis and screening conditions. Due to its small size it was more easily prepared and more susceptible to characterization, for example, by HPLC. Though primarily a test library, Rh-PL1 did retain some of the important features of the Rh-P1 conjugate. Like Rh-P1 it possessed

two histidine residues with i, i+4 spacing, and a large number of alanine residues. In addition, with lysine incorporated at a variable position, a salt bridge with glutamate would be possible.

Our hope for an artificial nuclease was mostly pinned on Rhodium-Peptide Library 2 (Figure 3.3). This library was of an intermediate size, consisting of over 16,000 different intercalator-peptide conjugates. Seven positions in a 16-mer peptide were randomized with alanine, glutamic acid, histidine, and lysine. The sequence of the peptide was as follows: Glu-Pro-X-Ala-Ala-X-X-Ala-X-X-X-Ala-X-Ala-Lys-Gly-CONH<sub>2</sub>, where X is a variable position. With 20 natural building blocks, and uncounted unnatural residues, a peptide library can become enormous very quickly. If we were to vary 16 positions with 20 different residues, we would create a library with greater than  $10^{20}$  different peptides. Varying seven positions with 20 residues would provide a library with greater than  $10^9$  peptides.

We decided to use Rh-P1 as a starting point, and to use an intermediate sized library to optimize the P1 composition (P1 = Asp-Pro-Asp-Glu-Leu-Glu-His-Ala-Ala-Lys-His-Glu-Ala-Ala-Ala-Lys-CONH<sub>2</sub>). Like Rh-P1, the peptides in Rh-PL2 are 16-mer peptides. To mimic Rh-P1 and to favor a helical conformation, Rh-LP2 was designed with a negative residue and a proline residue near the N-terminus, and a positive residue near the C-terminus. With the exception of a glycine at the C-terminus, the remaining fixed positions were alanine.

***The Preparation of Intercalator-Peptide Libraries.*** A split-pool approach was used for the preparation of the intercalator-peptide libraries (Figure 3.6). In the split-pool method,<sup>1</sup> a batch of synthesis resin is divided into several reactors and different amino

acids are incorporated in each of the reactors. To ensure an equimolar library, all coupling reactions must be forced to completion.<sup>25</sup> After the amino acid coupling reaction is completed, the resin from the different reactors is pooled, mixed, and again distributed. This process of splitting and pooling the resin is repeated until a full-length peptide has been assembled. Each position in the peptide is randomized, but there is only one type of compound attached to each synthesis bead. The different library members can be physically separated through the manipulation of resin beads.

The peptides were synthesized on a Tentagel support (polystyrene linked with polyethyleneglycol). The Tentagel resin swells in both organic and aqueous solutions; therefore, it is both practical for synthesis and compatible with aqueous screening assays. The size of the Tentagel bead is fairly homogeneous, but the loading of each bead does vary.<sup>25</sup> To ensure that all possible peptides were represented in the library, an excess of 100 beads per desired peptide were used for synthesis. To allow for off-bead screening, the peptides were linked to the solid support via a photocleavable nitobenzyl linker.<sup>26</sup>

The manual synthesis of the two peptide libraries, PL1 and PL2, proceeded smoothly. Limited characterization was carried out for our libraries; amino acid analysis, sequencing, and HPLC confirmed that we had successfully prepared 13-mer and 16-mer peptides with randomized positions. The synthesis yields for some of the individual coupling steps, particularly for positions close to the N-terminus, were lower than 98%. To ensure an equimolar library, every coupling reaction must be driven to completion, and it is possible that we have a percentage of peptides with deletions on our resin beads. With a library there is typically no opportunity for purification, and we proceeded directly to the rhodium coupling reaction.

To create libraries of intercalator-peptide conjugates, we activated and coupled  $[\text{Rh}(\text{phi})_2\text{bpy}'']^{3+}$  to the N-terminus of our resin-bound libraries. We used the  $\text{bpy}''$  ligand rather than  $\text{bpy}'$  for synthetic reasons, but the extra methylene group in  $\text{bpy}''$  may give added flexibility to the interactions of the DNA and the tethered peptide. The pendant carboxylate of the  $\text{bpy}''$  ligand and the terminal amine of the peptide library were linked with an amide bond.

Our sequencing results suggested a 90% yield for the rhodium coupling reaction. The average loading of peptide on the Tentagel resin was approximately 120 pmol per bead for PL1. After the coupling reaction, only 12 pmol per bead were detected by Edman sequencing. The coupled rhodium complex prevented sequencing by blocking the reaction of phenylisothiocyanate with the N-terminal amine. A 90% yield was ideal. A great deal of conjugate was available for screening assays, but 10% of the peptide was uncoupled and available for Edman sequencing.

***The Photocleavable Linker.*** The linker group that ties our library to solid support plays a very important role in our experiment. We required a linker that would be stable during synthesis and manipulation of the library, but that could be readily cleaved for off-bead assays. To facilitate multiple rounds of screening, we wanted a linker that would allow multiple releases of material from a single bead. In addition, to make decoding possible, we needed a linker and cleavage strategy that would reserve at least 1 pmol of peptide on each bead for Edman sequencing.

Photolabile linkers provided the best fit for our combinatorial experiment. Although not as commonly used as either the acid labile or base labile linkers, photolabile linkers have some very useful properties.<sup>27</sup> Importantly, these linkers can be



cleaved in situ. Since the cleavage reaction requires only light, the library can be released directly into the assay without intermediate steps. With other linkers the cleavage reagent, acid or base, must be removed prior to screening. In theory, the photocleavable linker is suited for multiple releases of the library. Simply by changing the irradiation time, the amount of released material can be modulated.

The most common photolabile linker, and the type we selected for our library, is the nitrobenzyl linker.<sup>27</sup> The spectrum and cleavage mechanism for this linker are presented in Figure 3.21. Upon irradiation, typically at 365 nm, a 1,5-hydrogen abstraction occurs.<sup>27</sup> Further rearrangement produces an acetal, and an elimination reaction ultimately releases the product. The alpha-methyl group and electron donating alkoxy substitutions on the aryl group both improve cleavage yield. The alpha-methyl group leads to formation of a ketone rather than an aldehyde; this ketone is less chromogenic, and reduces a trapping reaction between the nitroso group and the liberated product.<sup>26,27</sup> The alkoxy substituent produces a significant bathochromic shift in the principle absorbance bands, and thus increases the absorbance at 365 nm.<sup>26</sup> It is important to note that photolysis of support-bound linker is considerably slower than photolysis of a solution of linker due to light scattering, shielding, or shadowing effects.<sup>26</sup>

We obtained an amide-generating *o*-nitrobenzyl linker with an alpha-methyl group and a methoxy substituent on the aryl ring. Conveniently, the linker was commercially available on a Tentagel resin. Although this type of linker is reported to give > 95% yield with 3 h of irradiation in aqueous solution at 365 nm,<sup>28</sup> we observed dramatically lower yields under a variety of cleavage conditions (Figures 3.9 and 3.10). We changed the irradiation wavelength, adjusted the pH of the buffer, and included a

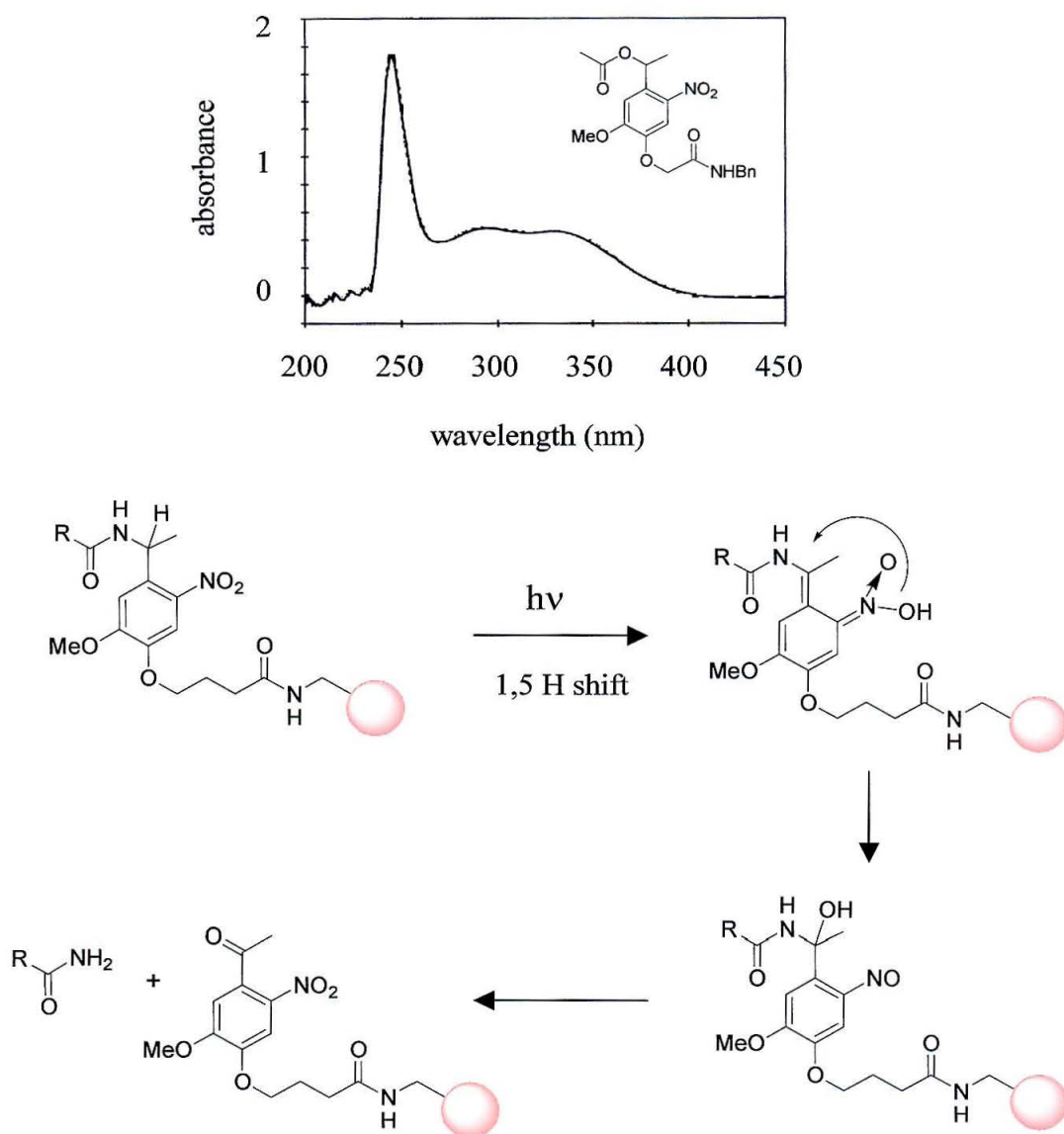


**Figure 3.21. Cleavage Mechanism of the Nitrobenzyl Linker.** The absorbance spectrum of a model nitrobenzyl linker (top) and the cleavage mechanism of the linker (bottom) are presented. Irradiation of the nitrobenzyl linker leads to a 1,5-hydrogen abstraction. Rearrangement gives the acetal. The acetal undergoes an elimination reaction to release peptide from the resin. Spectrum adapted from Holmes, 1997.<sup>26</sup>

dipeptide to compete with product trapping (data not shown), but we never obtained greater than a 7% release of our intercalator-peptide conjugates. In addition, we observed that the release occurred very rapidly, primarily within the first 8 minutes, and multiple releases from a batch of resin were not homogeneous.

In part we were constrained by the presence of the rhodium complex. The complex also absorbs at 365 nm and begins to lose ligands with prolonged irradiation. In addition, the tethered rhodium complex may aggravate the association of the released product with the solid support. It was observed that rinsing with 0.1% TFA in acetonitrile doubled the recovery of conjugate from the support, and this suggests that there is significant interaction between the resin and the liberated library. We have long suspected that the low yield for our intercalator-peptide conjugates is primarily due to poor release from solid support rather than poor coupling efficiency. We were not able to include a bead-rinsing step prior to the screening assay, and were forced to work with a low yield of released conjugate. Although the cleavage yields were disappointing, we did find the linker to be stable during library synthesis and acid deprotection. Resin that was left in ambient room light for several days did give product release, but the linker was stable when briefly handled in the light and stored in the dark.

The performance of our linker severely limited our screening assay. The low cleavage yield and the nonuniform release of conjugate frustrated a multiple round screening approach. With a 150 pmol loading of the resin, a 90% yield for the rhodium coupling reaction, and a 5% release of conjugate, we would obtain only 7 pmol of conjugate from a single bead. This corresponds to a 0.2  $\mu\text{M}$  concentration in a 40  $\mu\text{L}$  screening reaction. Typically we have used 5  $\mu\text{M}$  concentrations of Rh-P1 in plasmid

cleavage assays. To stand out in a screening assay, our library conjugates must be at least an order of magnitude more active than Rh-P1.

### 3.4.2. The Screening Strategy.

Particularly for a library of peptides, where methods for synthesis and decoding are fairly established, the screening step is the critical one. A poorly designed screen will produce artifacts, false leads, or no leads, or will severely limit the size of the library. The development of an appropriate screening assay for our intercalator-peptide libraries has proved very challenging.

If we were working with a purely peptide library, we could use a screening strategy that included an amplification step.<sup>29-31</sup> Our appended rhodium complex precludes this. If we were interested in binding behavior we could use spectroscopic tags on the binding partner. If we were interested in the hydrolysis of a colorimetric substrate such as bis(*p*-nitrophenyl)phosphate we could very conveniently explore a large library. But we are interested in DNA hydrolysis activity. Previous combinatorial experiments with metal complex nucleases have all involved very small libraries, and have relied on standard plasmid cleavage assays. With our 16,000 member library, we needed a high-throughput method for screening.

***A Fluorogenic DNA Substrate (False Start # 1).*** Initially we considered using a fluorogenic DNA substrate and a FRET based assay for DNA cleavage. Fluorescence assays can be very efficient, and are compatible with 96-well microtiter plates.<sup>32</sup> With this in mind, we designed a fluorogenic DNA substrate, a duplex with pendant fluorophores. A donor fluorophore is attached to one end of the short duplex, and an

acceptor fluorophore is attached to the opposite end. The acceptor quenches the fluorescence of the donor by a fluorescence resonance energy transfer (FRET) mechanism until a cleavage event physically separates the donor and acceptor.<sup>21</sup> The DNA strand breaks are marked by a recovery of donor fluorescence. The fluorogenic substrate allows the continuous monitoring of DNA cleavage, and has been used to study the kinetics of nucleases.<sup>22</sup> We planned to screen the rhodium-peptide libraries by distributing beads on a plate, introducing a fluorogenic DNA substrate, and then using irradiation to trigger a local release of conjugate. Active beads would be identified by the increased fluorescence of the cleaved DNA substrate. Schreiber et al. have used a similar strategy for library screening.<sup>33</sup>

We prepared a 15-mer DNA duplex with fluorescein incorporated at the 5' end of one strand and tetramethylrhodamine incorporated at the 5' end of the complement. This fluorogenic substrate was well behaved, at least until we added rhodium complex. We discovered that the addition of rhodium, either the free complex or a conjugate, significantly quenched the fluorescence emission of the fluorescein and rhodamine pair (Figure 3.12). This quenching effect did require DNA, but not necessarily duplex DNA. The emission of free fluorescein was not quenched by rhodium complex, but the emission of fluorescein at the end of the 15-mer single strand was quenched. The fact that duplex is not required suggests that the DNA base stack is not serving as a pathway for quenching. These fluorophores are very sensitive to deprotonation, and it is possible that the rhodium complex or conjugate, both of which contain carboxylate groups, are affecting the local pH of the fluorophore. Regardless of the mechanism, we decided that the fluorogenic substrate was not compatible with our library of rhodium conjugates. In a

screening assay it would not be possible to distinguish cleavage events from changes in rhodium concentration.

***A Multiple Round Plasmid Cleavage Assay (False Start # 2).*** We next turned to a high-throughput plasmid cleavage assay (Figure 3.13). In the first round of this assay, 20 to 100 beads were distributed to each well of a 96-well plate and irradiated. The released material was incubated with plasmid, and the most active aliquot of beads was identified by agarose gel electrophoresis of the plasmid products. In the second round of the assay, the best beads were redistributed to a new filtration plate, and to narrow in on the active conjugate, only one bead was tested in each well. This multiple-round plasmid cleavage assay allowed us to screen approximately 5000 beads per plate, and three equivalents of the library could be screened with only ten plates.

Although we saw significant levels of nicked plasmid and some variation from well-to-well in the first round of screening, we never observed significant cleavage in the second round. In large part this may be due to the poor performance of our photocleavable linker; the yield of released conjugate is simply too low to support two rounds of screening. Side reactions of the linker may be trapping our conjugates, or contaminating our reactions. Finally we turned to a bead-by-bead plasmid cleavage assay.

***A Bead-by-Bead Plasmid Cleavage Assay.*** Individual beads were distributed to a filtration plate and irradiated. The material released from a single bead was drained into a collection plate for incubation with plasmid and zinc. This bead-by-bead approach is miserably slow. To ensure that every individual member has been tested, it is necessary to screen several equivalents of a library, but I only screened 0.06 equivalents.

Although this was certainly not a high-throughput assay, although I only screened a small fraction of RPL2, we did observe encouraging results (Table 3.4). There was variation in nicked plasmid from well to well (Figure 3.15), and the cleavage was found to be dependant on bead, reaction pH, and metal. Occasionally there were unexpected peaks in cleavage without added  $\text{Zn}^{2+}$ , and these may be due to iron contamination of a plasmid stock. In 12 screening experiments we selected the beads in 11 wells for closer examination. To decode the peptide on these beads we used Edman sequencing.

### 3.4.3. The Selection and Identification of Conjugates.

Edman sequencing was a useful strategy for identifying the conjugates selected during the screening assay (Figure 3.16). Even though our library consists of Rh-peptide conjugates, which do not possess a free N-terminus for the initiation of the Edman reaction, we were able to reliably decode our “hit” peptides. In fact, we detected an average of 20 pmol of uncoupled peptide on our submitted beads. This is at least 10 times higher than the amount we expected after rhodium coupling and library release. It is possible that the yield of the rhodium coupling step was lower for RPL2 than for RPL1, or perhaps the rhodium intercalator does not complete preclude sequencing.

The sequencing results for the selected beads are presented in Table 3.6. Although we only sequenced the beads from 11 wells, and this is not a large sample size, the patterns of incorporation generally matched our expectations (Figure 3.17). For example, histidine, the residue that is most likely to coordinate  $\text{Zn}^{2+}$ , was a component in every selected conjugate (Figure 3.18). This gives the impression that our “hit” wells were not simply fluke events.

To further probe the effectiveness of our screening strategy, and to test the activity of our selected conjugates, we individually synthesized three conjugates. Rh-SP1 and Rh-SP2 were inspired by hit 6A and 2B. These were hits that showed the largest difference between nicked plasmid in the hit well and in the average well. They also had straightforward sequencing results, with only 1 amino acid clearly indicated for each position. In contrast Rh-SP3 was designed after analysis of the entire collection of selected and sequenced beads. The sequence of Rh-SP3 was based on the levels of residue incorporation observed at each variable position (Figure 3.17). Notably, Rh-SP1, Rh-SP2, and Rh-SP3 contain two, four, and three histidine residues.

Although we tested Rh-SP1, Rh-SP2, and Rh-SP3 in a number of plasmid cleavage experiments, we have not yet observed significant cleavage with any of these selected conjugates. Importantly, in the same experiments we did not observe plasmid cleavage with Rh-P1. Due to a systematic problem with the plasmid cleavage assay, a meaningful comparison of Rh-P1 and the selected conjugates has not been possible. However, it is clear that we have not created robust intercalator-peptide conjugates for DNA hydrolysis. We have not overcome many of the limitations of the Rh-P1 conjugate. It appears that our selected conjugates also require pH 6 for cleavage, and are very sensitive to metal concentration and the method of plasmid preparation.

#### **3.4.4. The Promise and Problems of our Combinatorial Approach.**

Our library approach was not very successful. We did not identify an active intercalator-peptide conjugate for DNA hydrolysis; we did not optimize the P1 composition. Nonetheless, our investment in a library project was not without reward.



We did learn some interesting lessons about the solid-phase synthesis of intercalator-peptide conjugates, the limitations of photocleavable linkers, the general plasmid cleavage properties of our library, and the compatibility of Rh-peptide libraries with Edman sequencing. In addition, we now have a very large number of Rh-peptide conjugates stored in our freezer.

We created over 16,000 different intercalator-peptide conjugates, and preparation of this large number of conjugates only took a few weeks. We have demonstrated that our rhodium intercalator is compatible with library synthesis; indeed, the coupling the  $[\text{Rh}(\phi)_2\text{bpy}]^{3+}$  to the library of peptides proceeded with high yield. We have focused our attention on DNA hydrolysis activity, but this library of conjugates might find other applications. It might be interesting to screen this library for DNA binding, or for oxidative DNA cleavage activity.

Our largest library was still rather modest in size. The variable positions were randomized with only four residues: Ala, Glu, His, and Lys. In fact the entire peptide only contained six types of residues. Perhaps we cannot expect dramatic changes in our conjugate properties with such a limited set of amino acids. To impact the solubility, the pH preference, the metal preference, and the cleavage activity of Rh-P1, we may need a much more diverse library, perhaps even artificial amino acids. Importantly, even when we screened large portions of Rh-PL2, 20 to 50 beads per well, we did not see significant plasmid cleavage at pH 7 or with  $\text{Mg}^{2+}$  or  $\text{Mn}^{2+}$ .

We ran into a number of obstacles during our design of a screening strategy. The photocleavable linker performed very poorly, particularly in combination with a rhodium complex, and we were only able to release a few pmole ( $< 10$ ) from each bead. The low

yield of our released conjugate forced us to use a bead-by-bead strategy. Our chances for success were significantly reduced with this low throughput screening strategy; we were only able to screen a small fraction of the conjugates in our 16,000 member library.

In addition, as our experiments with Rh-SP1, Rh-SP2, and Rh-SP3 emphasize, the plasmid cleavage assay is not completely straightforward. We have recently observed that the method of plasmid preparation can have a significant impact on cleavage results. For example, a small amount of iron contamination can eliminate the need for zinc, or incomplete removal of EDTA from a plasmid stock can interfere with metal-promoted cleavage. It is possible that some of these factors were complicating our screening efforts.

Our combinatorial experiment illustrates the critical importance of an effective screening strategy. It would have been wise to develop and thoroughly test the screening strategy prior to the preparation of the Rh-peptide library. We committed to a photocleavable linker early in our experiment, and this greatly narrowed our options for library screening.

### **3.5. Conclusions**

Combinatorial methods were applied to the development of intercalator-peptide conjugates for DNA hydrolysis. We prepared a 16,000-member library of rhodium-peptide conjugates by manual split pool synthesis. A small fraction of this library was screened using a plasmid cleavage assay, and the beads from the most active wells were

decoded with Edman sequencing. Based on the sequencing results, three intercalator-peptide conjugates were resynthesized and tested in plasmid cleavage assays. A meaningful comparison was not possible with Rh-P1, but it is clear that we have not created robust artificial nucleases. Like Rh-P1, our selected conjugates are very sensitive to the conditions of the plasmid cleavage assay. Our combinatorial experiment did demonstrate that rhodium-peptide conjugates are compatible with a highly parallel synthesis strategy, and with Edman sequencing. In addition, we observed that photocleavable linkers give very low yields under our selected conditions. Combinatorial chemistry is a powerful tool, but only if it includes an efficient screening strategy.

### 3.6. References

1. Lam, K. S.; Lebl, M.; Krcnak, V. *Chem. Rev.* **1997**, *97*, 411.
2. Barnes, C.; Balasubramanian *Curr. Op. Chem. Biol.* **2000**, *4*, 346-350.
3. Janda, K. D. *Proc. Natl. Acad. Sci. USA* **1994**, *91*, 10779-10785.
4. Carmi, N.; Balkhi, S. R.; Breaker, R. R. *Proc. Natl. Acad. Sci., USA* **1998**, *95*, 2233-2237.
5. Wilson, D. S.; Szostak, J. W. *Annu. Rev. Biochem.* **1999**, *68*, 611-647.
6. Santoro, S. W.; Joyce, G. F.; Sakthirel, K.; Gramatikova, S.; Barbas, C. F. *J. Am. Chem. Soc.* **2000**, *122*, 2433-2439.
7. Berg, R.; Simeonov, A.; Janda, K. D. *J. Comb. Chem.* **1999**, *1*, 96-100.
8. Berkessel, A.; Herault, D. A. *Angew. Chem. Int. Ed.* **1999**, *38*, 102-105.

9. Roigk, A.; Schneider, H.-J. *Eur. J. Org. Chem.* **2001**, 205-209.
10. Fitzsimons, M. P.; Barton, J. K. *J. Am. Chem. Soc.* **1997**, *119*, 3379-3380.
11. Copeland, K. D.; Fitzsimons, M. P.; Houser, R. P.; Barton, J. K. *Biochemistry* **2002**, *41*, 343-356.
12. Grant, G. A.; Crankshaw, M. W.; Gorka, J. *Methods in Enzymol.* **1997**, *289*, 395-419.
13. Biederman, K. J.; Lee, H.; Haney, C. A.; Kaczmarek, M.; Buettner, J. A. *J. Peptide Res.* **1999**, *53*, 234-243.
14. Jones, R. C. F.; Schofield, J. *J. Chem. Soc. Perkin Trans.* **1990**, *1*, 375-383.
15. Schmidt, J.; Soell *Chem. Ber.* **1908**, *41*, 3683.
16. Pschorr., *Chem. Ber.* **1902**, *35*, 2738.
17. Pyle, A. M.; Chiang, M. Y.; Barton, J. K. *Inorg. Chem.* **1990**, *29*, 4487-4495.
18. Stewart, J. M.; Young, J. D. *Solid Phase Peptide Synthesis*; 2<sup>nd</sup> ed.; Pierce Chemical Company: Rockford, Illinois, 1984.
19. Sarin, V. K.; Kent, S. B. H.; Tam, J. P.; Merrifield, R. B. *Anal. Biochem.* **1981**, *117*, 147-157.
20. Bedford, J.; Hyde, C.; Johnson, T.; Jun, W.; Owen, D.; Quibell, M.; Shepphard, R. *C. Int. J. Peptide Protein Res.* **1992**, *40*, 300-307.
21. Selvin, P. R. *Methods Enzymol.* **1995**, *246*, 300-337.
22. Ghosh, S. S.; Eis, P. S.; Blumeyer, K.; Fearon, K.; Millar, D. P. *Nucl. Acids Res.* **1994**, *22*, 3155-3159.
23. Biggins, J. B.; Prudent, J. R.; Marshall, D. J.; Ruppen, M.; and Thorson, J. S. *PNAS* **2000**, *97*, 13537-13542.

24. Phelan, J. C.; Skelton, N. J.; Braisted, A. C.; McDowell, R. S. *J. Am. Chem. Soc.* **1997**, *119*, 455-460.
25. Lebl, M.; Krchnak, V. *Methods in Enz.* **1997**, *289*, 337.
26. Holmes, C. P. *J. Org. Chem.* **1997**, *62*, 2370-2380.
27. James, I. W. *Tetrahedron* **1999**, *55*, 4855-4946.
28. Holmes, C. P.; Jones, D. G. **1995**, *60*, 2318-2319.
29. Smith, G. P.; Petrenko, V. A. *Chem. Rev.* **1997**, *97*, 391-410.
30. Roberts, R. W.; Szostak, J. W. *Proc. Natl. Acad. Sci.* **1997**, *94*, 12297-12302.
31. Schatz, P. J.; Cull, M. G.; Martin, E. L.; Gates, C. M. *Methods Enzymol.* **1996**, *267*, 171-191.
32. Bubaum, J. J.; Sigal, N. H. *Curr. Op. Chem. Biol.* **1997**, *1*, 72-28.
33. Borchardt, A.; Liberles, S. D.; Biggar, S. R.; Crabtree, G. R.; Schreiber, S. L. *Chem. Biol.* **1997**, *4*, 961-968.

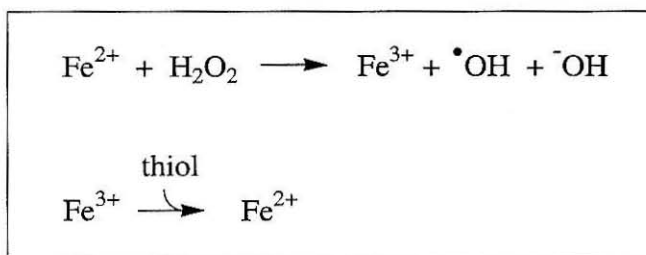
## **Chapter 4**

### **Oxidative Cleavage of DNA with Copper-Binding Peptides Tethered to Rhodium Intercalators**

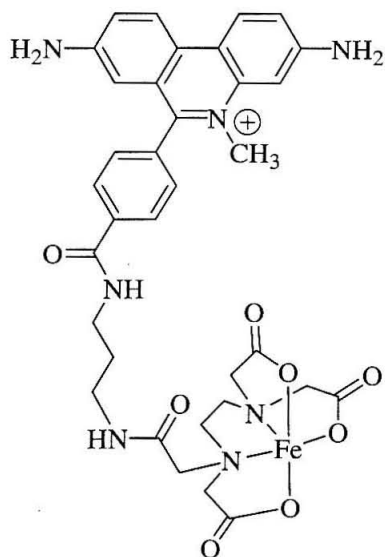
## 4.1. Introduction

The development of an artificial nuclease, a small molecule that promotes DNA hydrolysis, is an ambitious goal. To date artificial nucleases are poor mimics of their natural counterparts, and none of them have found practical application in the laboratory. In contrast, efficient oxidative scission of the DNA backbone has been demonstrated with a variety of chemical agents (Figure 4.1).<sup>1</sup> These agents typically are redox-active metal complexes, and promote indirect strand scission through oxidative or free-radical mechanisms. The deoxyribose ring is oxidized through metal-mediated redox reactions and collapses to give DNA fragments.

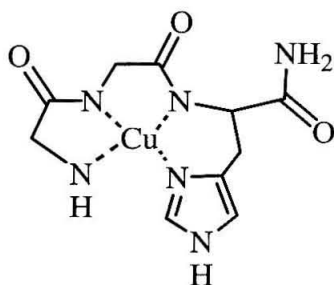
One of the most common agents for oxidative DNA cleavage is  $\text{Fe(EDTA)}^{2-}$ . This agent cleaves both single- and double-stranded DNA in the presence of  $\text{H}_2\text{O}_2$  or  $\text{O}_2$  and a reducing agent.<sup>2,3</sup> In the Fenton reaction,  $\text{Fe(II)}$  is oxidized to  $\text{Fe(III)}$  and a hydroxyl radical is produced:



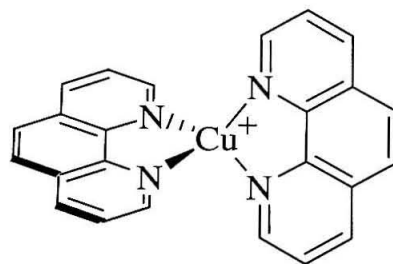
The diffusible hydroxyl radical abstracts a hydrogen atom from the sugar ring, and ultimately promotes DNA cleavage and the release of a DNA base.  $\text{Fe(EDTA)}^{2-}$  is particularly effective for footprinting because the diffusible hydroxyl radical is sequence neutral and quite small; it does not show any sequence selectivity. To increase the local



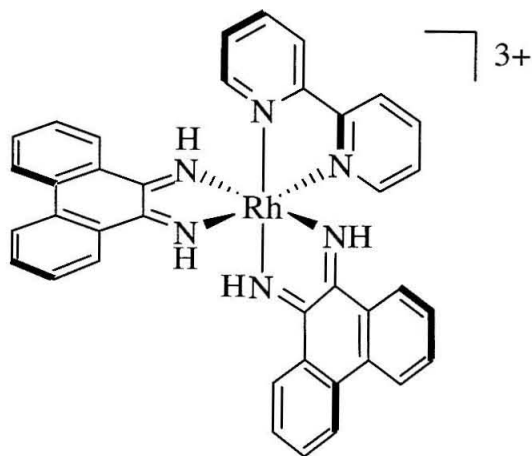
*Methidiumpropyl-EDTA-Fe(II)*



*Cu(II) or Ni(II)-Gly-Gly-His*



*Cu(phen)<sub>2</sub><sup>+</sup>*



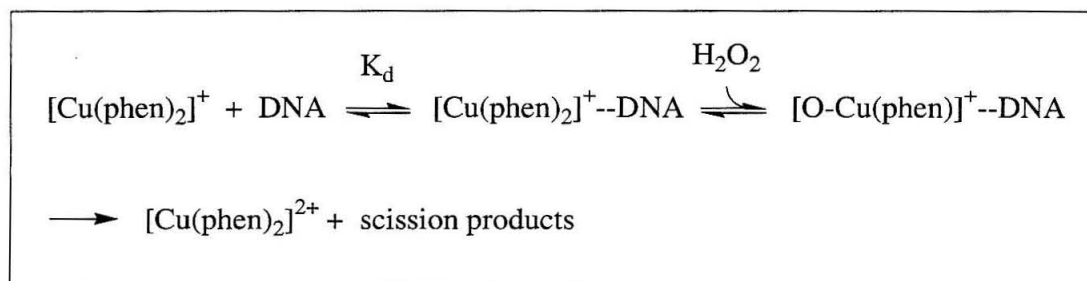
*[Rh(phi)<sub>2</sub>bpy]<sup>3+</sup>*

**Figure 4.1. Metal Complexes for Oxidative Cleavage of DNA.** In the presence of dioxygen and a reducing agent, or with photoactivation (rhodium complex), these agents abstract hydrogen from the deoxyribose ring and ultimately produce DNA strand breaks.



concentration of  $\text{Fe(EDTA)}^{2-}$  at the DNA backbone, this reagent has been tethered to methidium, a DNA intercalator that binds in the minor groove (Figure 4.1).

Phenanthroline complexes of copper also promote the cleavage of nucleic acids in the presence of hydrogen peroxide or dioxygen and a reductant (Figure 4.1).<sup>1,4</sup> The  $[\text{Cu(phen)}_2]^+$  complex is tetrahedral, and this geometry is particularly suited to binding in the minor groove. The proposed mechanism for DNA oxidation is as follows:



The tetrahedral Cu(I) complex binds to DNA and reacts with hydrogen peroxide, possibly losing a phenanthroline ligand, to generate a nondiffusible copper-oxo species which attacks the DNA. The copper-oxo species has not yet been characterized, but it may be a copper oxene or a copper-coordinated hydroxyl radical. Finally, the resulting Cu(II) species is released and reduced in solution to complete the redox cycle. The products are all consistent with hydrogen abstraction from the minor groove. In contrast with  $[\text{Fe(EDTA)}]^{2-}$ ,  $[\text{Cu(phen)}_2]^+$  does display structure preferences. This limits the utility of  $[\text{Cu(phen)}_2]^+$  in DNA footprinting experiments, but makes the complex a useful probe of the structural microheterogeneity of DNA.

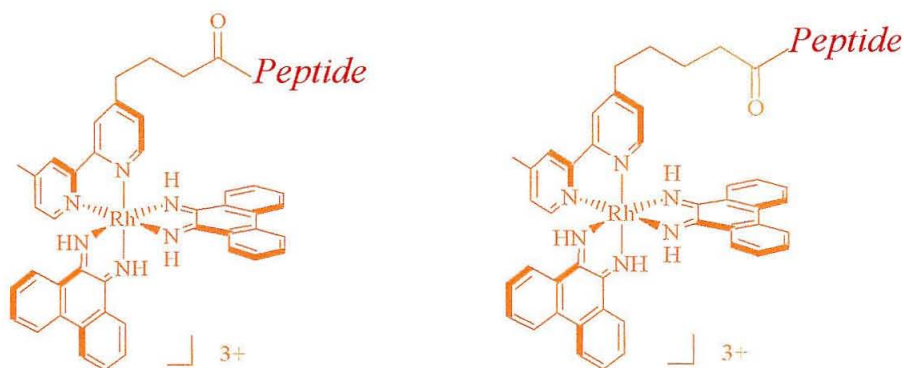
Simple tripeptides that bind copper or nickel have been demonstrated to cleave DNA substrates (Figure 4.1).<sup>5,6</sup> The tripeptide Gly-Gly-His is found at the N-terminus of the Cu(II) or Ni(II) chelating domain of serum albumin, and has been demonstrated to

bind metal with a  $K_d$  of  $10^{-16}$  to  $10^{-17}$  M.<sup>5</sup> In the presence of a oxygen and a reductant, Cu(II) or Ni(II)-Gly-Gly-His-CONH<sub>2</sub> produces deoxyribose damage and strand scission. It appears that the peptide complex resides in the minor groove and produces a nondiffusible oxidant. The complex is largely sequence neutral and shows only a slight preference for A/T-containing sites. The first two positions of the tripeptide can be varied, and were optimized using a combinatorial approach.<sup>6</sup> Increased DNA cleavage was observed with Pro, Met, Arg, or Lys in the amino-terminal position, and with Lys, Arg, Met, Ser, or Thr in the second position.

The list of metal complexes that oxidatively cleave DNA is long, and also includes Fe(II)-bleomycin,<sup>7</sup> 2,2'-bipyridine complexes of copper,<sup>8</sup> hydroxamic acids,<sup>9,10</sup> desferal,<sup>11</sup> and of course, our own phenanthrenequinone diimine complexes of Rh(III).<sup>12,13</sup> Inspired by all of these examples, and frustrated by the low activity and finicky behavior of our Zn<sup>2+</sup>-binding peptides,<sup>14</sup> we turned to a redox-active metal center. We began using our intercalator-peptide conjugates to deliver copper to DNA.

We have performed copper cleavage experiments with Rh-P1, but also with shorter histidine-containing tethered peptides (Figure 4.2). In the presence of intercalator-peptide conjugate and a reducing agent, typically mercaptopropionic acid (MPA), we produced copper damage in oligonucleotide or restriction fragment substrates. Copper cleavage experiments complement the photocleavage and hydrolysis studies and provide detailed information about the interactions of the tethered metallopeptides with DNA.

In addition, we have used intercalator-peptide conjugates to direct copper damage to mismatch sites. The pairing of the eight possible base mismatches is presented in

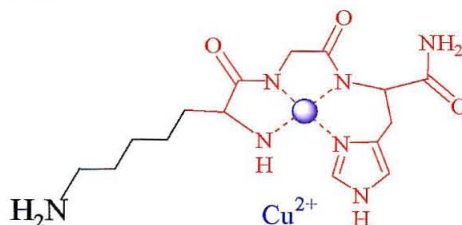
*Intercalators:**Tethered Peptides:*

*P1:*       $\text{H}_2\text{N}-\text{Asp}-\text{Pro}-\text{Asp}-\text{Glu}-\text{Leu}-\text{Glu}-\text{His}-\text{Ala}-\text{Ala}-\text{Lys}-\text{His}-\text{Glu}-\text{Ala}-\text{Ala}-\text{Ala}-\text{Lys}-\text{CONH}_2$

*AH:*       $\text{H}_2\text{N}-\text{Ala}-\text{His}-\text{Ala}-\text{Ala}-\text{His}-\text{Ala}-\text{CONH}_2$

$\text{H}_2\text{N}-\text{Ala}-\text{His}-\text{Ala}-\text{Ala}-\text{His}-\text{Ala}-\text{COOH}$

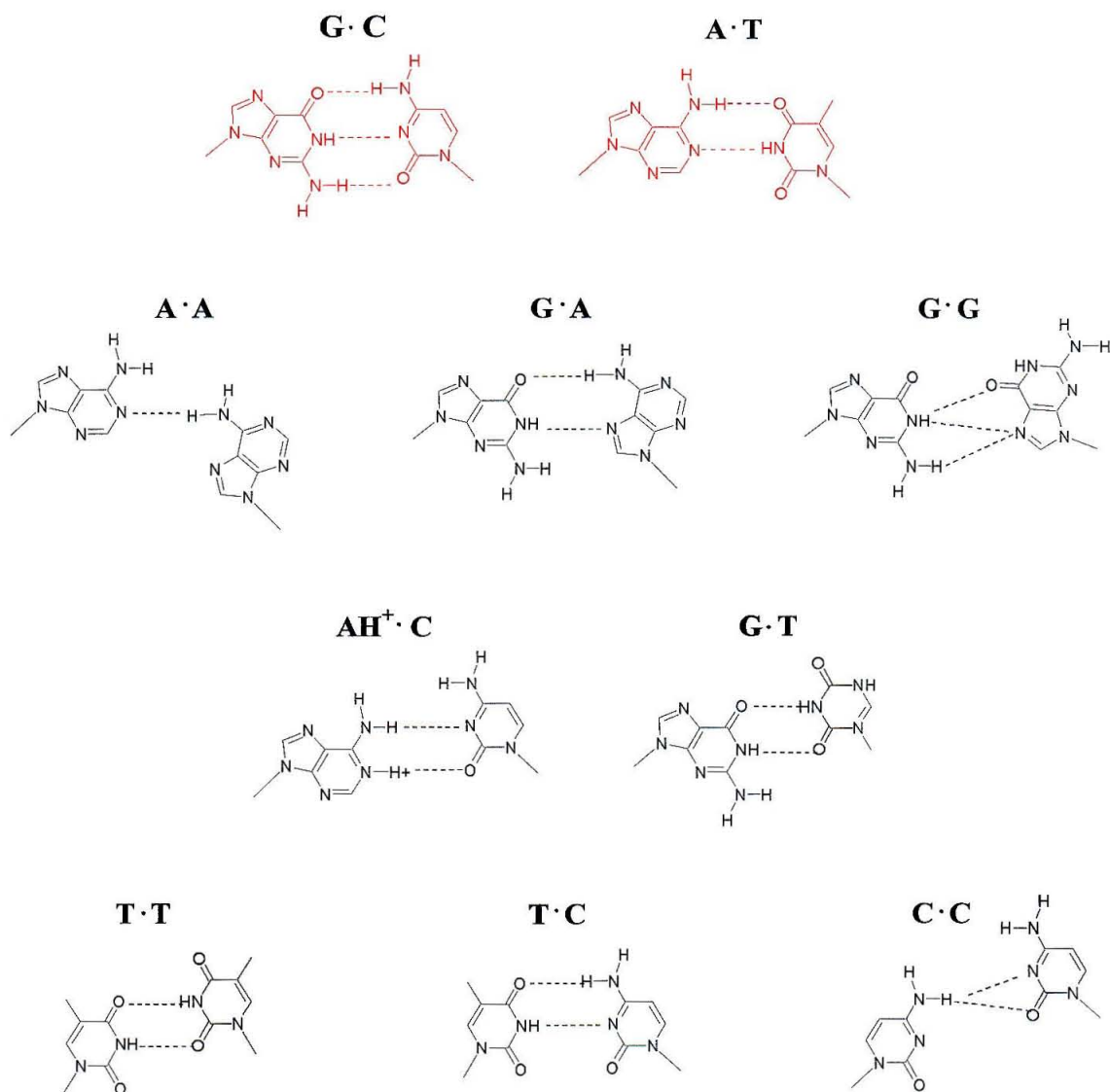
*KGH:*       $\text{H}_2\text{N}-\text{Lys}-\text{Gly}-\text{His}-\text{CONH}_2$



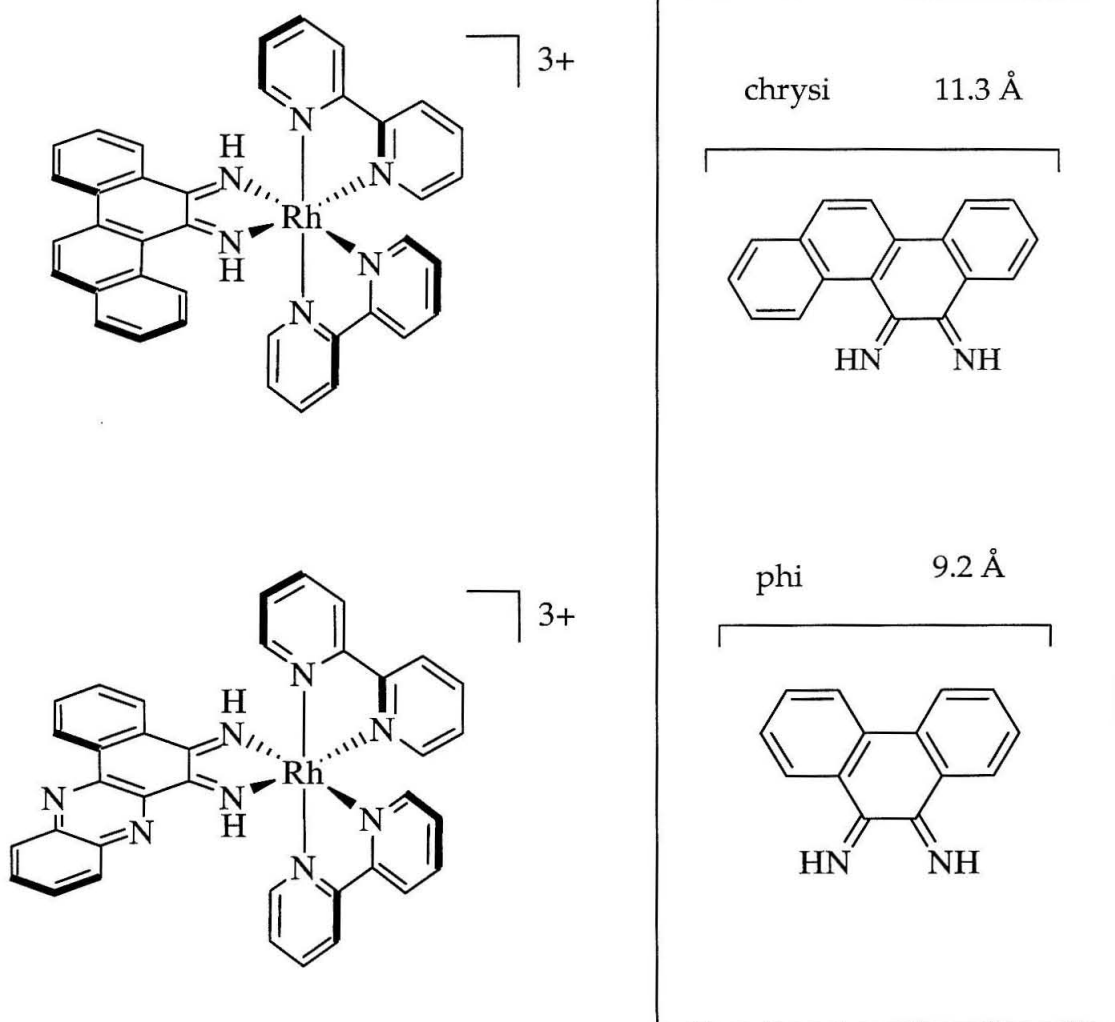
**Figure 4.2. Intercalator-Peptide Conjugates for Oxidative Cleavage of DNA.** The  $[\text{Rh}(\text{phi})_2\text{bpy}']^{3+}$  and  $[\text{Rh}(\text{phi})_2\text{bpy}'']^{3+}$  complexes were coupled to four different peptides: P1, AHAAHA-CONH<sub>2</sub>, AHAAHA-COOH, and KGH. The intercalator binds with high affinity to DNA and the peptide delivers copper to the backbone to promote oxidative strand scission.

Figure 4.3. The detection and the repair of DNA mismatches is a critical cellular mechanism, and is also an important laboratory goal.

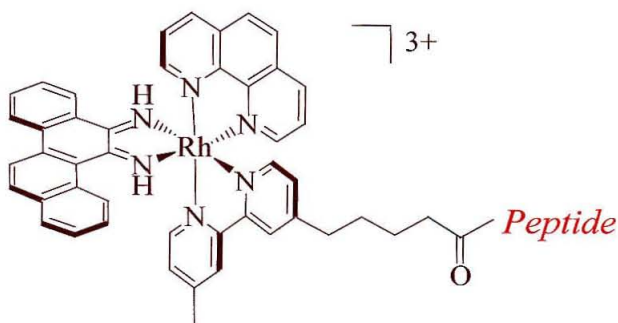
In the Barton group, we have demonstrated that rhodium complexes with bulky intercalating ligands, such as 5,6-chrysenequinone diimine (chrysi) or benzophenazine-5,6-dione diimine (phzi), selectively bind, and upon photoactivation, cleave near mismatch sites in DNA (Figure 4.4).<sup>15-17</sup> Steric interactions prevent binding of the chrysi or phzi ligands at standard intercalation sites; however, at mispairs, where the energetic cost of DNA distortion has already been paid, the complexes bind with high affinity. The binding constant of  $[\text{Rh}(\text{bpy})_2\text{chrysi}]^{3+}$  (bpy = bipyridine) at a CC mismatch was found to be 50 times larger than the non-specific binding constant, and this selectivity allowed the discrimination of a single mismatch within a 2725 bp DNA plasmid heteroduplex.<sup>16</sup> This complex was tested against the eight possible base mismatches in sixteen sequence contexts, and cleavage was observed at 82% of the mismatch sites.<sup>17</sup> We have tethered two histidine-containing peptides to a chrysenequinone diimine complex of Rh(III) (Figure 4.5).



**Figure 4.3. DNA Mismatches.** The standard Watson-Crick base pairs are shown in red, and the eight possible mismatch base pairs are shown in black.



**Figure 4.4. Rhodium Intercalators for DNA Mismatch Recognition.** The  $[\text{Rh}(\text{bpy})_2\text{chrysi}]^{3+}$  and  $[\text{Rh}(\text{bpy})_2\text{phzi}]^{3+}$  complexes bind selectively at mismatch sites in a DNA duplex. The chrysi and phzi ligands are wider than the standard phi intercalating ligand, and are excluded from matched sites.

*Intercalator:**Tethered Peptides:*

*PI:*     $\text{H}_2\text{N}$ -Asp-Pro-Asp-Glu-Leu-Glu-His-Ala-Ala-Lys-His-Glu-Ala-Ala-Ala-Lys- $\text{CONH}_2$

*AH:*     $\text{H}_2\text{N}$ -Ala-His-Ala-Ala-His-Ala- $\text{COOH}$

**Figure 4.5. Mismatch-Specific Intercalator-Peptide Conjugates for Oxidative Cleavage of DNA.** The  $[\text{Rh}(\text{phen})(\text{bpy})(\text{chrysi})]^{3+}$  complex was coupled to two different histidine-containing peptides: P1 and AHAAHA. The intercalator binds with high affinity at mismatch sites and the peptide delivers copper to the backbone to promote oxidative strand scission.

## 4.2. Materials and Methods

### 4.2.1. Preparation of Metal Complexes.

*Bis(phenanthrenequinone diimine)(4-butyric acid-4'-methyl-2,2'-bipyridine)-Rhodium(III) Trichloride,  $[Rh(phi)_2bpy']^{3+}$  (Rh).* The bpy' ligand and  $[Rh(phi)_2bpy']^{3+}$  complex were prepared according to literature methods.<sup>18-20</sup>

*Bis(phenanthrenequinone diimine)(4-valeric acid-4'-methyl-2,2'-bipyridine) - Rhodium(III) Trichloride,  $[Rh(phi)_2bpy'']^{3+}$  (Rh'').* The bpy'' ligand and the  $[Rh(phi)_2bpy'']^{3+}$  complex were prepared as described in Chapter 3.

*(1,10-Phenanthroline)(chrysenequinone diimine)(4-valeric acid-4'-methyl-2,2'-bipyridine)-Rhodium(III) Trichloride,  $([Rh(phen)(bpy'')(chrysi)]^{3+}$  (RhC'').* The bpy'' ligand was prepared as described in Chapter 3, and the rhodium complex was prepared as described in the literature.<sup>21,22</sup> Briefly, rhodium(III) trichloride (1 g, 1 eq.) was heated in concentrated HCl (30 mL) for 3 h, and then phenanthroline monohydrate (1.7 g, 2 eq.) was added to the refluxing solution. Approximately 10 min after the addition of phenanthroline, boiling water (300 mL) was added to the reaction and the flask was allowed to cool to room temperature. Crystals of  $[Rh(phen)Cl_4]phen^+$  were collected and refluxed in 70 mL of concentrated HCl to produce orange needles of  $[Rh(phen)Cl_4]H_3O^+$ . The chloride ligands were displaced by treatment with trifluoromethanesulfonic acid (25 g). After 24 h the triflic acid reaction was poured into anhydrous diethyl ether, and a yellow solid was collected by filtration. To produce  $[Rh(phen)(NH_3)_4]^{3+}$ , the solid was transferred to a flask and refluxed in concentrated ammonium hydroxide. After 30 min this reaction was rotavapped to dryness. The



chrysenequinone ligand (0.2 g, 0.9 eq.) was condensed with the amine complex (1.5 g, 1 eq.) in a basic (0.1 N NaOH) solution of 1:3 water:acetonitrile. Finally, the bpy" ligand was condensed with the amine complex by refluxing in 50:50 ethanol:water overnight. The three-ligand complex was purified by cation exchange chromatography (Sephadex SP C25, 0.05 M MgCl<sub>2</sub> to 0.5 M MgCl<sub>2</sub>), desalted, and lyophilized to give a brown solid. ESI MS *m/z* obsd. (calc.): (RhC" - H)<sup>2+</sup> 404.1 (404.3); (RhC" - 2H)<sup>+</sup> 807.3 (807.7). UV/vis (water): λ<sub>max</sub>: 268 nm, 301 nm (shoulder), 313 nm (shoulder), 390 nm, 464 nm (shoulder).

#### 4.2.2. Synthesis of Metallointercalator-Peptide Conjugates.

**Automated Synthesis of Peptides.** The P1 and NH<sub>2</sub>-AHAAHA-COOH peptides were prepared by the Beckman Institute Biopolymer Synthesis Center at Caltech using automated peptide synthesis as previously described for the Bam peptide (Chapter 2). The amino acid protecting groups employed were as follows: Asp(OtBu), Glu(OtBu), His(tBoc or Trt), and Lys(tBoc). The KGH-CONH<sub>2</sub> peptide was prepared using an Fmoc strategy, but the final lysine residue was protected with Fmoc on the side chain amine and with tBoc on the N-terminus (N-α-tBoc-N-ε-Fmoc-L-Lysine, Nova Biochem). The peptide-resins were received and stored dry at 4 °C.

**Manual Synthesis of Peptides.** The NH<sub>2</sub>-AHAAHA-CONH<sub>2</sub> peptide was prepared by manual solid-phase synthesis with an Fmoc protection strategy.<sup>23</sup> The peptide was assembled on a Rink AM resin (4-[2',4'-Dimethoxyphenyl-Fmoc-aminomethyl)-phenoxy acetamido-norleucyl aminomethyl resin, 0.66 mmol/g, Nova Biochem). Deprotection of the N-terminus was accomplished with 20% piperidine in

DMF. The Fmoc amino acids (Fmoc-Ala-OH and Fmoc-His(Trt), 2 eq.) were activated for coupling with benzotriazole-1-yl-oxy-tris-pyrrolidino-phosphonium hexafluorophosphate (PyBOP, 2 eq.), 1-hydroxy-benzotriazole (HOBt, 2 eq.), and diisopropylethylamine (DIPEA, 4 eq.). The coupling reaction was carried out in DMF in a polypropylene tube. The resin was agitated with gentle rocking. The efficiency of coupling was monitored using the ninhydrin assay, and the coupling steps were repeated two or three times to achieve > 98% coupling yield.<sup>24</sup> The peptide resin was stored dry at 4 °C.

***Removal of the N-terminal Fmoc Protecting Group.*** The peptide-resin (100 mg, 12  $\mu$ mol) was placed on a medium sintered glass funnel and soaked with DMF for 5 minutes. A 2% (v/v) solution of DBU in DMF was drained slowly through the funnel over a 30 minute period. The peptide-resin was rinsed with DMF, CH<sub>2</sub>Cl<sub>2</sub>, and 1:1 CH<sub>2</sub>Cl<sub>2</sub>:methanol. After thorough rinsing the peptide-resin was dried on a lyophilizer.

***Coupling of the Metallointercalator and Peptide.*** The resin bound peptides were combined with racemic rhodium complex (1-2 eq.), PyBOP (3 eq.), and DIPEA (6 eq.) in DMF and stirred at ambient temperature overnight. The conjugates were cleaved from the resin and deprotected with a cocktail of trifluoroacetic acid (TFA), water, and triisopropylsilane. The cleaved conjugates were precipitated in ice-cold t-butyl methyl ether, collected by centrifugation, dissolved in 5% acetic acid, and lyophilized.

***HPLC Purification.*** The intercalator-peptide conjugates were HPLC purified on a semipreparative Vyadac C18 reversed phase column using a water (0.1% TFA)/acetonitrile (0.1% TFA) gradient and a flow rate of 4 mL/min. The percentage of acetonitrile was increased from 10 to 40% over 25 minutes for RhC''-AH, and from 15 to 40% over 20 min for all other conjugates. Chromatograms were monitored at 220 and

360 nm. After lyophilization, the intercalator peptide conjugates were obtained as fluffy brown or orange solids in 2 to 20% yield.

#### 4.2.3. Characterization of Metallointercalator-Peptide Conjugates by UV-

##### Visible Spectroscopy and Mass Spectrometry.

**UV-Visible Spectroscopy.** Absorbance spectra were obtained with a Beckman DU 7400 Spectrophotometer. Again, each spectrum is found to be the sum of the individual spectra of the free peptide and the metallointercalator. The conjugates containing  $[\text{Rh}(\text{phi})_2\text{bpy}']^{3+}$  or  $[\text{Rh}(\text{phi})_2\text{bpy}'']^{3+}$  were quantitated using the molar absorptivity constant,  $\epsilon_{349} = 23,600 \text{ M}^{-1}\text{cm}^{-1}$ . The spectrum for the  $[\text{Rh}(\text{phen})(\text{bpy}'')(\text{chrysi})]^{3+}$  complex is presented in Figure 4.6. The conjugates containing  $[\text{Rh}(\text{phen})(\text{bpy}'')(\text{chrysi})]^{3+}$  were quantitated using  $\epsilon_{271} = 63,800 \text{ M}^{-1}\text{cm}^{-1}$ .

**Mass Spectrometry.** ESI mass spectrometry was carried out with two different instruments: (i) a Finnigan LCQ Ion Trap Mass Spectrometer, and (ii) a mass spectrometer at Colorado State University. MALDI mass spectrometry was carried out by the PPMAL at Caltech using a Voyager-Rp Mass Spectrometer.

$[\text{Rh}(\text{phi})_2(\text{bpy}'\text{-P1-COOH})]^{3+}$  (**Rh-P1**). ESI (i)  $m/z$  calc. (obsd.):  $(\text{Rh-P1} + 2\text{H})^{5+}$  497.7 (497.3);  $(\text{Rh-P1} + \text{H})^{4+}$  621.7 (621.4);  $(\text{Rh-P1})^{3+}$  828.4 (828.2);  $(\text{Rh-P1} - \text{H})^{2+}$  1241.6 (1241.8).

$[\text{Rh}(\text{phi})_2(\text{bpy}''\text{-AHAAHA-CONH}_2)]^{3+}$  (**Rh''-AH-NH<sub>2</sub>**). ESI (i)  $m/z$  calc. (obsd.):  $(\text{Rh}''\text{-AH})^{3+}$  447.5 (447.8);  $(\text{Rh}''\text{-AH} - \text{H})^{2+}$  670.8 (671.1);  $(\text{Rh}''\text{-AH} - 2\text{H})^{+}$  1341.3 (1343.3).

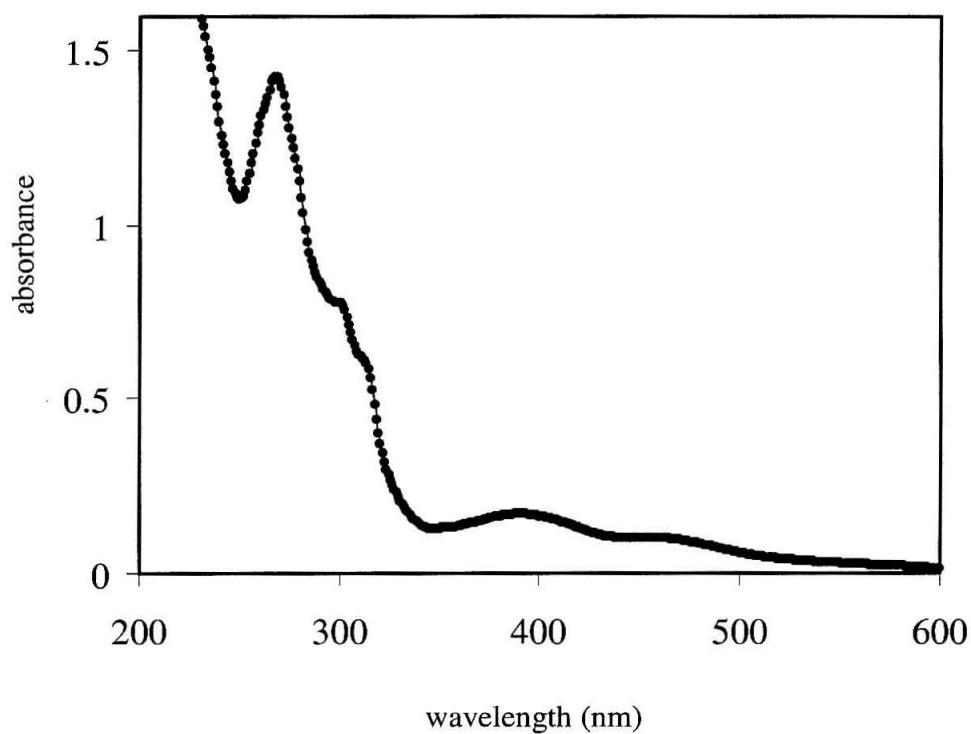


**Figure 4.6. UV-Visible Spectrum of [Rh(phen)(bpy'')(chrysi)]<sup>3+</sup>.** The spectrum was collected for a 20  $\mu$ M sample of the rhodium complex in water.

$[Rh(phi)_2(bpy'-KGH-CONH_2)]^{3+}$  (*Rh-KGH*). ESI (i)  $m/z$  calc. (obsd.): (*Rh-KGH*)<sup>3+</sup> 364.6 (364.7); (*Rh-KGH* - H)<sup>2+</sup> 545.9 (546.5); (*Rh-KGH* - 2H)<sup>+</sup> 1090.6 (1092.0).

$[Rh(phen)(bpy''-P1)(chrysi)]^{3+}$  (*RhC''-P1*). ESI (ii)  $m/z$  obsd. (calc.): (*RhC''-P1*)<sup>3+</sup> 841.1 (841.2); 965.3 (?); 1147.6 (?); 1422.3 (?); 2002.8 (?); (*RhC''-P1* - *chrysi* - *phen*)<sup>+</sup> 2083.3 (2085.1); (*RhC''-P1* - 2H)<sup>+</sup> 2524.2 (2521.6). MALDI  $m/z$  obsd. (calc.): (*RhC''-P1* - *bpy''P1*)<sup>+</sup> 538.3 (537.4); (*bpy''P1* + H)<sup>+</sup> 1983.9 (1985.2); (*RhC''-P1* - *chrysi* - *phen*)<sup>+</sup> 2084.9 (2085.1); (*RhC''-P1* - *chrysi* - 2H)<sup>+</sup> 2266.1 (2265.3); (*RhC''-P1* - *phen* - 2H)<sup>+</sup> 2342.1 (2341.2); (*RhC''-P1* - 2H)<sup>+</sup> 2521.3 (2521.6).

$[Rh(phen)(bpy''-AHAHA-COOH)(chrysi)]^{3+}$  (*RhC''-AH-OH*). ESI (ii)  $m/z$  calc. (obsd.): Isomer 1 (*RhC''-AH*)<sup>3+</sup> 456.2 (456.1); 505.5 (?); (*RhC''-AH* - H)<sup>2+</sup> 683.6 (683.6); 797.7 (?); 875.4 (?); (*RhC''-AH* - *chrysi* - 2H)<sup>+</sup> 1105.3 (1110); (*RhC''-AH* - *phen* - 2H)<sup>+</sup> 1187.0 (1186.1). Isomer 2 (*RhC''-AH*)<sup>3+</sup> 455.9 (456.1); 563.6 (?); (*RhC''-AH* - H)<sup>3+</sup> 683.6 (683.6); (*RhC''-AH* - *chrysi* - 2H)<sup>+</sup> 1105.3 (1110); 1133.8 (?); (*RhC''-AH* - *phen* - 2H)<sup>+</sup> 1187.0 (1186.1); (*RhC''-AH* - H<sub>2</sub>O)<sup>+</sup> 1348.5 (1348.3). MALDI (i)  $m/z$  obsd. (calc.): Isomer 1 829.5 (?); (*RhC''-AH* - *phen* - *chrysi*)<sup>+</sup> 930.4 (929.8), (*RhC''-AH* - *phen* - *chrysi*)<sup>+</sup> 1111.5 (1110.0), (*RhC''-AH* - *phen* - *chrysi*)<sup>+</sup> 1187.5 (1186.1), (*RhC''-AH*)<sup>+</sup> 1365.6 (1366.3), 1488.6 (?). Isomer 2 (*RhC''-AH* - *bpy''-AH*)<sup>+</sup> 538.1 (537.4); (*RhC''-AH* - *phen* - *chrysi*)<sup>+</sup> 930.4 (929.8); (*RhC''-AH* - *phen* - *chrysi*)<sup>+</sup> 1111.5 (1110.0); (*RhC''-AH* - *phen* - *chrysi*)<sup>+</sup> 1187.6 (1186.1); (*RhC''-AH*)<sup>+</sup> 1365.6 (1366.3).

#### 4.2.4. Photocleavage and Copper Cleavage of DNA Restriction Fragments.

**Preparation of the Restriction Fragments.** A 3'-radiolabeled restriction fragment was prepared by first digesting pUC19 with *Bam*HI. The linearized plasmid

was labeled using the Klenow fragment of *E. coli* Pol I and [ $\alpha$ - $^{32}$ P]dGTP. A second digestion was completed with *Bgl*II. A 5'-radiolabeled restriction fragment was prepared by first digesting pUC19 with *Bam*HI. The 5'-phosphate was removed from the linearized plasmid with shrimp alkaline phosphatase, and a radiolabeled phosphate was incorporated using polynucleotide kinase and [ $\gamma$ - $^{32}$ P]dATP. The labeled fragments were isolated from a 6% nondenaturing PAGE gel and were desalted using Biospin columns (Biorad). The radiolabeled fragments were counted with a scintillation counter, and combined with cold calf thymus DNA (100  $\mu$ M) and buffer to create a DNA stock solution.

**Photocleavage.** For photocleavage experiments, the labeled restriction fragment (100  $\mu$ M base pairs with calf thymus carrier) was combined with rhodium conjugate (2, 5, or 10  $\mu$ M), and  $\text{Cu}^{2+}$  (20  $\mu$ M) in buffer (20 mM Tris-HCl, 15 mM NaCl pH 7.5 to 8, 25 mM). The 40  $\mu$ L samples were equilibrated for 15 minutes, and then irradiated for 5 minutes at 313 nm using a Hg/Xe lamp equipped with a monochromator. A light control sample containing buffer and DNA was irradiated for 15 minutes. A dark control sample containing DNA,  $\text{Cu}^{2+}$ , and 10  $\mu$ M rhodium conjugate was not irradiated. After the irradiations the samples were dried under vacuum.

**Copper Cleavage.** To explore copper cleavage, the labeled fragment (100  $\mu$ M base pairs) was combined with rhodium conjugate,  $\text{Cu}^{2+}$  (20  $\mu$ M), and mercaptopropionic acid (MPA, 200  $\mu$ M) in buffer (Tris-HCl, pH 7.85, 25 mM). The 40  $\mu$ L reactions were incubated at ambient temperature for 4 hours, and then dried under vacuum. The experiment included several control samples: (1) DNA in buffer was incubated at ambient temperature for 4 hours, (2) DNA in buffer was incubated with 20  $\mu$ M  $\text{Cu}^{2+}$  and

200  $\mu\text{M}$  MPA at ambient temperature for 4 hours, (3) DNA in buffer was incubated with 20  $\mu\text{M}$   $\text{Cu}^{2+}$  and 10  $\mu\text{M}$  rhodium conjugate at ambient temperature for 4 hours, (4) DNA in buffer was incubated with 20  $\mu\text{M}$   $\text{Cu}^{2+}$  and 10  $\mu\text{M}$  rhodium conjugate at 37  $^{\circ}\text{C}$  for 24 hours, and (5) DNA in buffer was incubated with 10  $\mu\text{M}$  rhodium conjugate at ambient temperature for 4 hours.

***Distamycin Experiments.*** Photocleavage and copper cleavage samples were prepared as described above, but 5  $\mu\text{M}$  distamycin, a small molecule that binds in the minor groove, was included in the reactions.

***Gel Analysis of Cleavage Products.*** Photocleavage and copper cleavage reaction samples were suspended in formamide loading dye (formamide, bromophenol blue, and xylene cyanol), denatured on a 90  $^{\circ}\text{C}$  heat block, and analyzed by 8% PAGE. The gels were heated for 1 hour at 2000 V (90 W) prior to loading of the samples, and the samples were electrophoresed for approximately 2 hours at 2000 V. The gels were dried under vacuum at 80  $^{\circ}\text{C}$  in a Biorad gel dryer. The gels were visualized using Phosphor screens and a Phosphoimager, and quantitated using ImageQuant software.

#### **4.2.5. Photocleavage and Copper Cleavage of Oligonucleotides.**

***Preparation of Radiolabeled Duplex.*** Four different oligonucleotide substrates were used in these experiments. A 42-mer duplex and 40-mer duplex were prepared and tested with the  $[\text{Rh}(\text{phi})_2\text{bpy}]^{3+}$  conjugates. A 35-mer hairpin and a 25-mer duplex, each containing a CC mismatch site, were tested with the  $[\text{Rh}(\text{phen})(\text{bpy})(\text{chrysi})]^{3+}$  conjugates. The sequences of the four DNA substrates were as follows:

42-mer:

5'-CTG CCA TAG TTC GCA TAT GCC GCA TAT ACC GCG TAC GCA TCG-3'  
 3'-GAC GGT ATC AAG CGT ATA CGG CGT ATA TGG CGC ATG CGT AGC-5'

40-mer:

5'-CGT GTA TTA CGG ACT ACG TAG GCT AGC CAG CGT GGA ACG C-3'  
 3'-GCA CAT AAT GCC TGA TGC ATC CGA TCG GTC GCA CCT TGC G-5'

35-mer hairpin (mismatch in bold):

5'-CAT CAT GTC **CTG** CCC TTT TT G GGC **ACG** ACA TGA TG-3'

25-mer (mismatch in bold):

5'-GGT CAG CCA AAT **CGA** CCG CAA TCA C-3'  
 3'-CCA GTC GGT TTA **CCT** GGC GTT AGT G-5'

The individual oligonucleotide strands were synthesized on an ABI 392 DNA Synthesizer, and purified by HPLC. The strands were quantitated using the absorbance at 260 nm. Radiolabel was incorporated at the 5' end of one strand by incubation with T4 polynucleotide kinase and [ $\gamma$ - $^{32}$ P]-ATP. The labeled strand was purified on a 10% polyacrylamide gel, and isolated from the gel using the crush and soak method. The labeled material was desalted with Biospin columns (Biorad), dried under vacuum, and quantitated using a scintillation counter. The labeled strand was annealed with cold strand and complement in buffer to give a DNA stock solution.

**Photocleavage Experiments.** The labeled duplex or hairpin was combined with rhodium complex (2, 5, or 10  $\mu$ M) in buffer (20 to 25 mM Tris-HCl, pH 7.5). The 20 to



40  $\mu\text{L}$  samples were equilibrated for 15 minutes, and then irradiated for 15 minutes at 313 nm using the Hg/Xe lamp. The chrysi complex can also promote photocleavage when irradiated with lower energy light, and in one experiment with RhC''-P1 the samples were irradiated at 365 nm. Light control and dark control samples were included in all experiments. After irradiation the samples were dried under vacuum.

***Copper Cleavage Experiments.*** To achieve copper cleavage, the labeled duplex or hairpin was combined with rhodium complex (2, 5, or 10  $\mu\text{M}$ ),  $\text{Cu}^{2+}$  (20 or 50  $\mu\text{M}$ ), and MPA (200 or 500  $\mu\text{M}$ ) in buffer (20 to 25 mM Tris-HCl, pH 7.5). The experiments included several control samples: (1) DNA in buffer, (2) DNA in buffer with  $\text{Cu}^{2+}$  and MPA, (3) DNA in buffer with  $\text{Cu}^{2+}$  and rhodium conjugate, (4) DNA in buffer with rhodium conjugate. A control reaction (K) with untethered KGH, copper, and MPA was also prepared since this tripeptide is known to bind copper tightly and to promote oxidative strand scission. All the samples were incubated for 4 to 24 hours at ambient temperature or at 37  $^{\circ}\text{C}$ , and after incubation they were dried under vacuum.

***Gel Analysis of Cleavage Products.*** Photocleavage and copper cleavage reaction samples were suspended in formamide loading dye (formamide, bromophenol blue, and xylene cyanol), denatured on a 90  $^{\circ}\text{C}$  heat block, and analyzed by 20% PAGE. The gels were heated for 1 hour at 1800 V (85 W) prior to loading of the samples, and the samples were electrophoresed for approximately 2 hours at 1800 V. The gels were visualized using Phosphor screens and a Phosphoimager, and quantitated using ImageQuant software.

### 4.3. Results

#### 4.3.1. Preparation of Metallointercalator-Peptide Conjugates.

*Conjugates of  $[Rh(phi)_2bpy]^{3+}$ .* Four different peptides were successfully coupled to the  $[Rh(phi)_2bpy']^{3+}$  or the  $[Rh(phi)_2bpy'']^{3+}$  complex (Table 4.1). HPLC analysis of the crude coupling mixtures suggested predominantly one product, and ESI mass spectrometry confirmed that we had created the desired chimeras. For Rh-P1, peaks corresponding to the  $5^+$ ,  $4^+$ ,  $3^+$ , and  $2^+$  ions were detected, and the observed  $m/z$  values very closely matched calculated values. For the smaller conjugates, Rh''-AH and Rh-KGH, the  $3^+$ ,  $2^+$ , and  $1^+$  ions were detected, and again, the observed  $m/z$  values were very close to calculated values.

**Table 4.1. Conjugates of  $[Rh(phi)_2bpy]^{3+}$ .**

Abbreviation	Intercalator	Peptide
Rh-P1	$[Rh(phi)_2bpy']^{3+}$	D-P-D-E-L-E-H-A-A-K-H-E-A-A-A-K-CONH <sub>2</sub>
Rh''-AH-NH <sub>2</sub>	$[Rh(phi)_2bpy'']^{3+}$	A-H-A-A-H-A-CONH <sub>2</sub>
Rh''-AH-OH	$[Rh(phi)_2bpy'']^{3+}$	A-H-A-A-H-A-COOH
Rh-KGH	$[Rh(phi)_2bpy']^{3+}$	K-G-H-CONH <sub>2</sub>

The KGH peptide was attached to the rhodium complex by a slightly different strategy. Since the N-terminus of the tripeptide assists in the coordination of metal ions, we formed an amide bond with the lysine side chain and left the *terminal amine free* for

copper coordination. This modified approach gave typical yields; a 15% yield of the Rh-KGH product was isolated.

**Mismatch-Specific Conjugates.** To create conjugates that would selectively bind at mismatch sites in DNA, we coupled the P1 and the AHAAHA-COOH peptides to a rhodium complex with a large chrysi intercalator (Table 4.2). We attached our peptides to the three-ligand complex,  $[\text{Rh}(\text{phen})(\text{bpy}'')(\text{chrysi})]^{3+}$ .

**Table 4.2. Conjugates of  $[\text{Rh}(\text{phen})(\text{bpy}'')(\text{chrysi})]^{3+}$ .**

Abbreviation	Intercalator	Peptide
Rh''C-P1	$[\text{Rh}(\text{phen})(\text{bpy}'')(\text{chrysi})]^{3+}$	D-P-D-E-L-E-H-A-A-K-H-E-A-A-A-K-CONH <sub>2</sub>
Rh''C-AH-OH	$[\text{Rh}(\text{phen})(\text{bpy}'')(\text{chrysi})]^{3+}$	A-H-A-A-H-A-COOH

The  $[\text{Rh}(\text{phen})(\text{bpy}'')(\text{chrysi})]^{3+}$  complex has many isomers; the arrangement of ligands around the metal center can be  $\Delta$  or  $\Lambda$ , the carboxylate arm on the bpy ligand can be axial or equatorial to chrysi, and the unsymmetrical chrysi ligand can have two different orientations. Some of these isomers could be separated by HPLC. Under standard HPLC conditions, the Rh''C-AH-OH conjugate gave four peaks, and two were sufficiently resolved to allow for separate collection (Figure 4.7). In some of our experiments we studied these two isomers separately. The arrangement of the carboxylate arm is expected to have the greatest impact on HPLC mobility, and it is

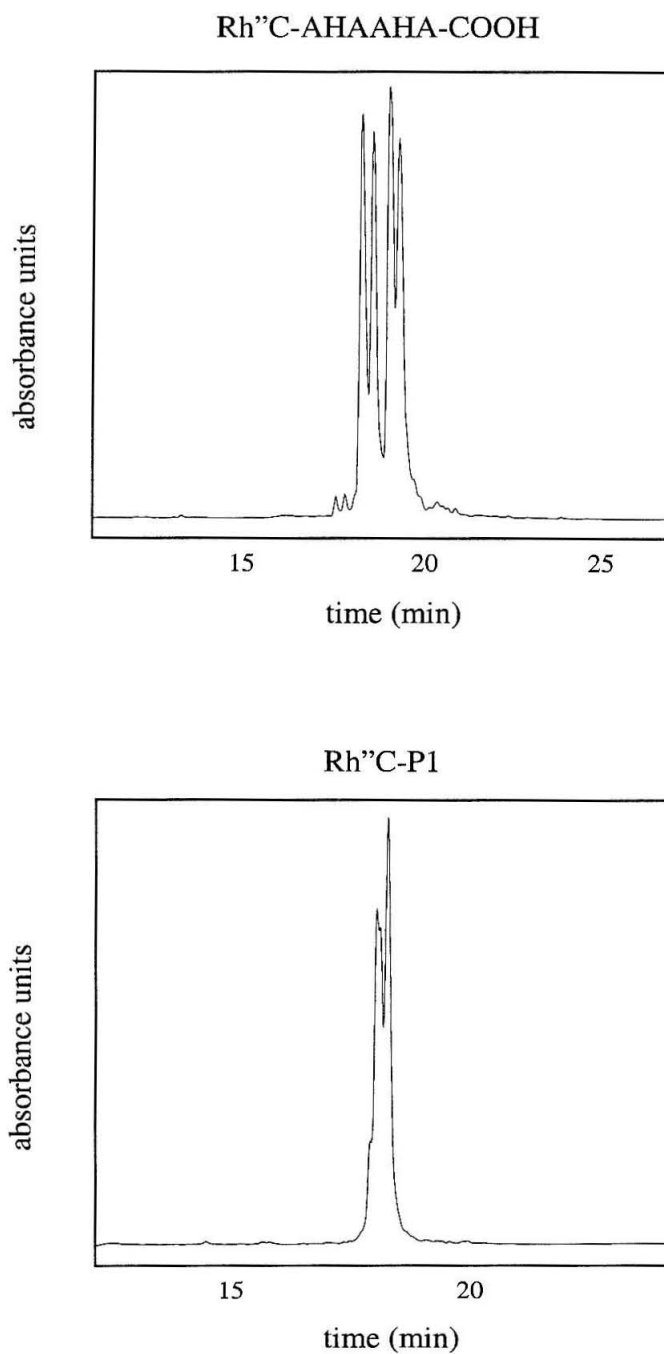


**Figure 4.7. The HPLC Chromatograms for  $[\text{Rh}(\text{phen})(\text{bpy}'')(\text{chrysi})]^{3+}$  conjugates.**

The chromatograms at 220 nm are presented for the Rh''C-AHAAHA-COOH and the Rh''C-P1 conjugates.

likely that our two collected products have different orientations of the carboxylate and pendant peptide. With Rh<sup>III</sup>C-P1 the isomers were not well separated by HPLC; therefore, all of the Rh<sup>III</sup>C-P1 products were collected in a single fraction. This mixture of isomers was used in cleavage experiments.

Although the HPLC chromatograms suggested clean reaction and gave predominantly one cluster of peaks, the mass spectrometry results for these conjugates were not straightforward. In contrast to the [Rh(phi)<sub>2</sub>bpy']<sup>3+</sup> complex, the [Rh(phen)(bpy'')(chrysi)]<sup>3+</sup> complex decomposes and fragments during ESI mass spectrometry. Peaks corresponding to the 3<sup>+</sup> and 2<sup>+</sup> parent ions were observed, but a large number of other peaks were detected. Some of the peaks corresponded to the loss of the chrysi or phen ligand, and some are likely due to peptide fragmentation. As described in Chapter 2, laser desorption promotes ligand loss, and MALDI analysis also gave a large number of peaks. Although we did not identify all of the fragments observed in the mass spectrum, HPLC analysis and UV-visible spectroscopy suggest the successful preparation of desired conjugates.

#### **4.3.2. Photocleavage and Copper Cleavage of a Restriction Fragment by**

##### **Rhodium-Peptide Conjugates.**

Because efficient and reproducible oxidative cleavage of linear DNA is easier to achieve than hydrolytic cleavage, we have used our Rh-peptide conjugates to deliver a redox-active metal, Cu<sup>2+</sup>, to a plasmid restriction fragment. In these experiments, the pattern of [Rh(phi)<sub>2</sub>bpy]<sup>3+</sup> photocleavage reveals the intercalation sites of the conjugate and the pattern of copper damage reveals the interactions of the peptide and the DNA.

**Rh-P1.** Upon irradiation, the photoactivated Rh-P1 conjugate produced strand breaks across the plasmid restriction fragment (Figure 4.8, left). The photocleavage pattern produced by the Rh-P1 conjugate suggested fairly sequence neutral binding with some preference for 5'-Pu-*Py*-Pu-3' sites (Figure 4.9, cleavage at the italicized *Py*). The five sites with most intense photocleavage were 5'-ACGC-3' sites.

In the presence of  $\text{Cu}^{2+}$  and mercaptopropionic acid (MPA), the Rh-P1 conjugate also promoted oxidative strand breaks at specific locations in a plasmid restriction fragment (Figure 4.8, right). Incubation of the fragment with  $\text{Cu}^{2+}$  and MPA gave a low level of background damage across the DNA substrate (Lane 2), but with the addition of Rh-P1, a few sites in the fragment were especially targeted for damage. The sites of copper damage are displaced slightly from the sites of intense photocleavage. Although there is some correlation between photocleavage and copper cleavage, not all sites with equally intense photocleavage had corresponding sites of intense copper damage. The sites that were most intensely damaged by copper were sites with high A/T content, for example, 5'-ATTAAG-3' and 5'-TAAAA-3'.

The cleavage reaction requires a reductant. Without MPA there is almost no damage to the fragment. Also, the Rh-P1 conjugate plays a critical role in delivering the copper to the DNA; the extent and pattern of damage changes with the addition of Rh-P1. The presence of histidine in the peptide was essential for the copper-mediated reaction; neither  $[\text{Rh}(\text{phi})_2\text{bpy}]^{3+}$ , Rh-Bam, nor Rh-P4 promoted damage to the restriction fragment under identical conditions (data not shown).

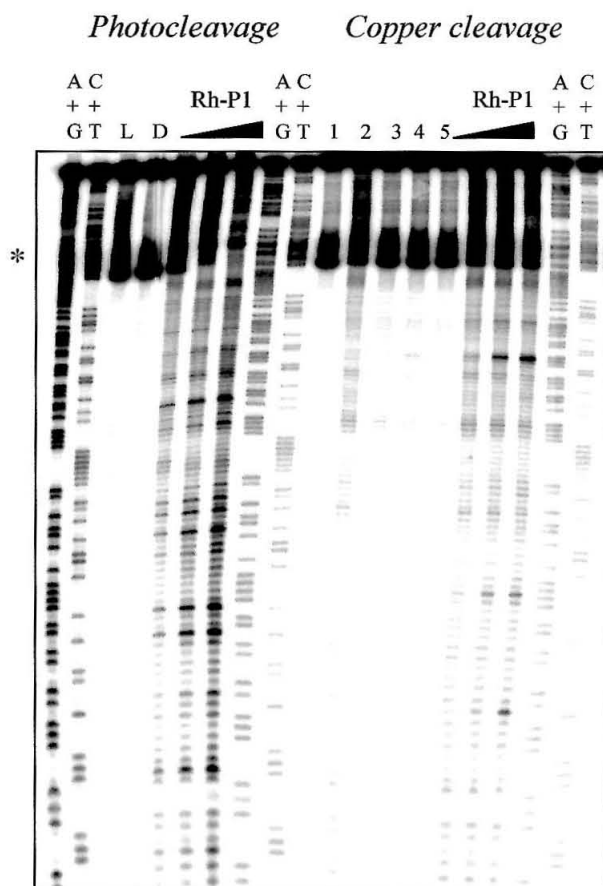


**Figure 4.8. Photocleavage and Copper Cleavage of a Restriction Fragment by Rh-P1.** Photocleavage and copper cleavage were carried out with a 175-mer restriction fragment (3'-labeled, 100  $\mu$ M), rhodium complex (2, 5, 10  $\mu$ M), and  $\text{Cu}^{2+}$  (20  $\mu$ M), in buffer (20 mM Tris-HCl, 15 mM NaCl, pH 7.6). Photocleavage samples were irradiated for 5 min at 313 nm. MPA (200  $\mu$ M) was added to copper cleavage samples, and the samples were incubated at ambient temperature for 4 h. Lanes are labeled as follows: A+G, C+T, Maxam-Gilbert sequencing reactions; L, irradiation without rhodium; D, no irradiation; 1, incubation of DNA without rhodium or copper; 2, Cu and MPA; 3, Cu and Rh; 4, Cu and Rh for 24 h; 5, Rh complex. The asterisk indicates a band due to renaturation.

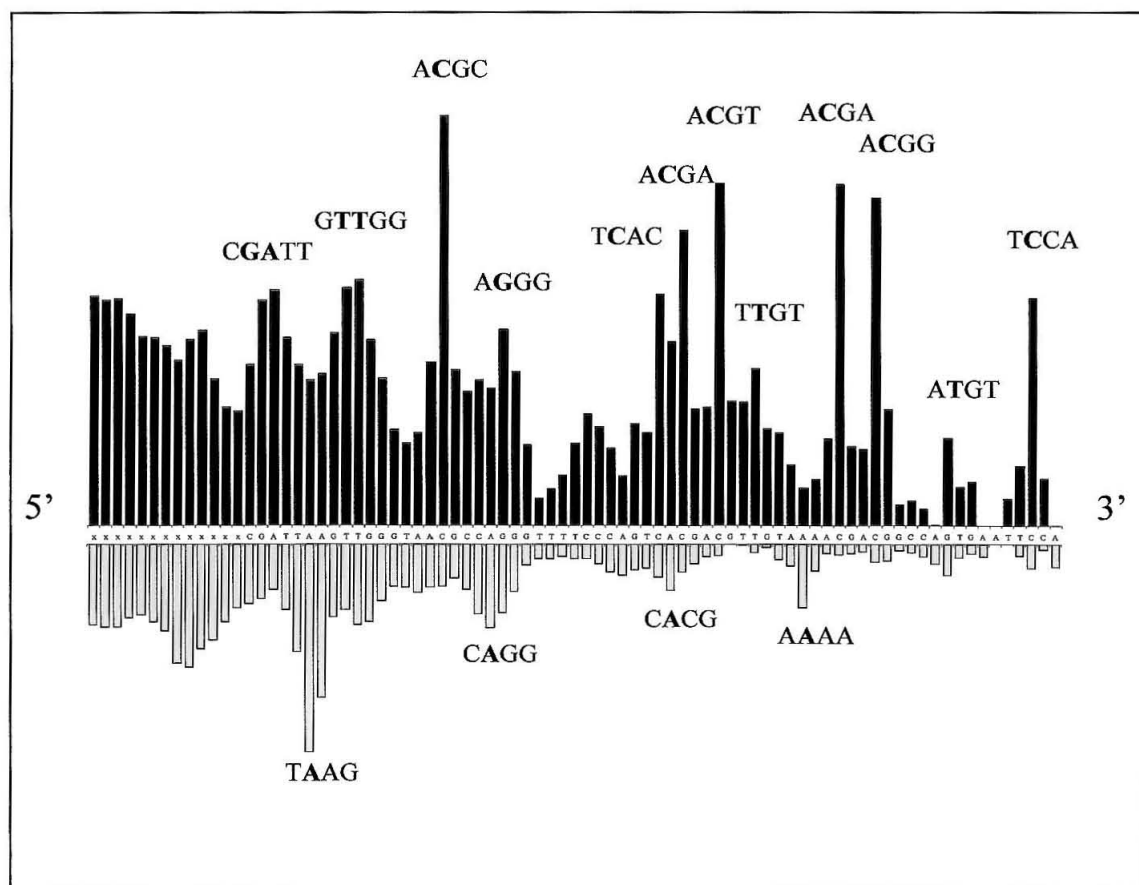


**Figure 4.9. A Bar Plot Comparing Photocleavage and Copper Cleavage with Rh-P1.** Cleavage experiments were completed with a 175-mer restriction fragment, and the resulting gel (Figure 4.7) was quantitated. The cleavage for 5  $\mu$ M intercalator-peptide conjugate is shown. The black bars indicate photocleavage, and the gray bars indicate copper cleavage. The length of the bars shows the relative amounts of a particular type of cleavage product, but no meaningful comparison can be made between photocleavage and copper cleavage efficiency. The sites of most intense cleavage are labeled with a four base sequence: 5'-N-N-N-N-3', where the cleavage site is shown in bold.



***Rh''-AH.*** The pattern of copper damage changed when P1 was replaced with a much shorter histidine-containing peptide. A hexamer peptide (AHAAHA) was tethered to  $[\text{Rh}(\text{phi})_2\text{bpy}'']^{3+}$  and was incubated with the restriction fragment,  $\text{Cu}^{2+}$ , and MPA (Figure 4.10 and Figure 4.11). To probe the involvement of the C-terminus in the coordination and delivery of copper, both amide and acid forms of this hexamer peptide were tethered and tested. The photocleavage patterns observed for these conjugates were very similar to the pattern observed for Rh-P1, and again the pattern suggested sequence-neutral binding to the DNA (Figure 4.12). Again, 5'-ACGA-3' sites were preferred sites for binding and photocleavage, but intense cleavage was also observed at a 5'-TTGGG-3' site.

The copper damage with Rh''-AH was not as dramatically localized to specific sites as with Rh-P1, and the peaks in damage produced by Rh''-AH were not observed at precisely the same positions as the peaks in damage produced by Rh-P1. This is not surprising for peptides with different lengths and different  $\text{Cu}^{2+}$ -coordination sites. The C-terminus does not appear to play a significant role in copper binding or damage, and both the acid and amide peptides gave very similar damage patterns. With both Rh-P1 and Rh''-AH, there seemed to be a slight preference for copper damage at flexible AT-rich sequences.

***The Impact of Distamycin.*** Distamycin is a small organic molecule that binds tightly in the minor groove of a DNA duplex.<sup>25</sup> This small molecule is selective for A/T-rich sites, for example, the binding constant of distamycin is  $2.5 \times 10^7 \text{ M}^{-1}$  for an ATTA site and  $5.0 \times 10^5 \text{ M}^{-1}$  for a TAGG site.<sup>26</sup> By including distamycin in our reactions we

*Photocleavage      Copper cleavage*

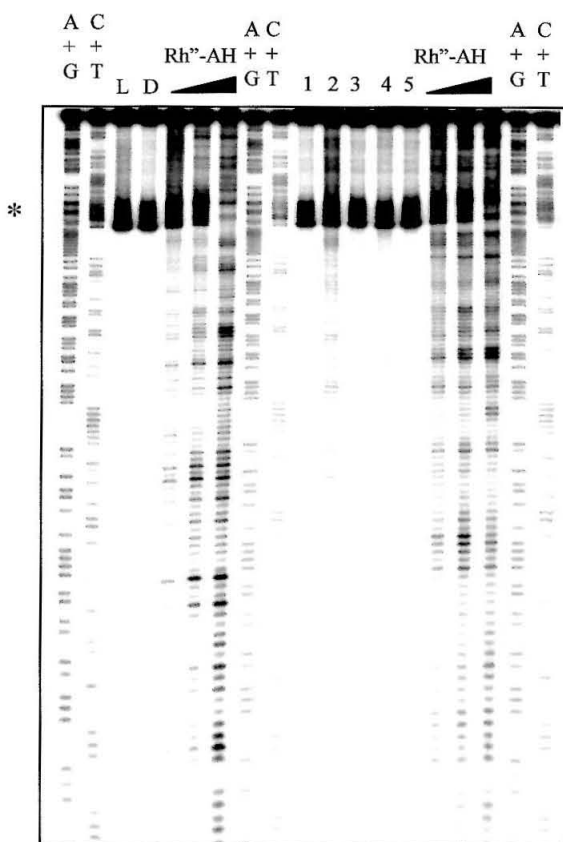


**Figure 4.10. Photocleavage and Copper Cleavage of a Restriction Fragment by Rh<sup>III</sup>-AHAAHA-CONH<sub>2</sub>.** Photocleavage and copper cleavage were carried out with a 175-mer restriction fragment (3'-labeled, 100 μM), rhodium complex (2, 5, 10 μM), and Cu<sup>2+</sup> (20 μM), in buffer (20 mM Tris-HCl, 15 mM NaCl, pH 7.6). Photocleavage samples were irradiated for 5 min at 313 nm. MPA (200 μM) was added to copper cleavage samples, and the samples were incubated at ambient temperature for 4 h. Lanes are labeled as follows: A+G, C+T, Maxam-Gilbert sequencing reactions; L, irradiation without rhodium; D, no irradiation; 1, incubation of DNA without rhodium or Cu; 2, Cu and MPA; 3, Cu and Rh; 4, Cu and Rh for 24 h; 5, rhodium complex. The asterisk indicates a band due to renaturation of the fragment.

*Photocleavage      Copper cleavage*

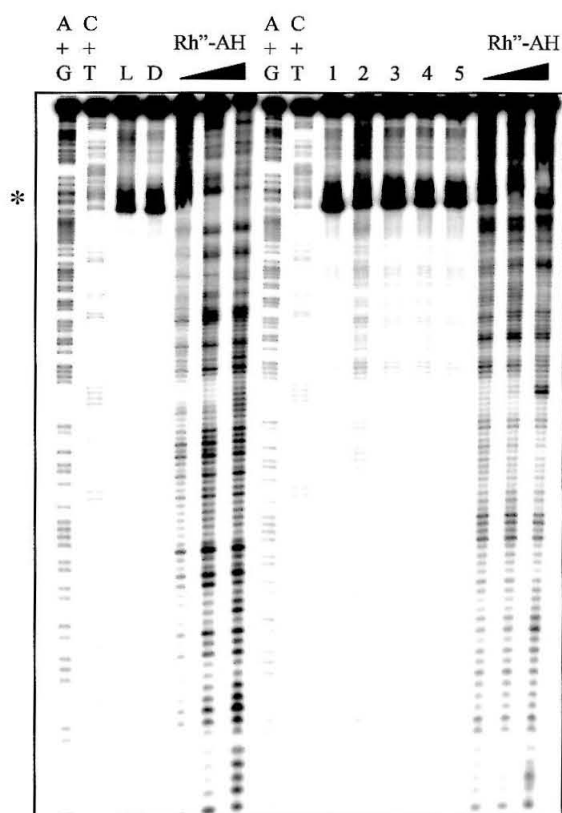


**Figure 4.11. Photocleavage and Copper Cleavage of a Restriction Fragment by Rh'''-AHAAHA-COOH.** Photocleavage and copper cleavage were carried out with a 175-mer restriction fragment (3'-labeled, 100  $\mu$ M), rhodium complex (2, 5, 10  $\mu$ M), and Cu<sup>2+</sup> (20  $\mu$ M), in buffer (20 mM Tris-HCl, 15 mM NaCl, pH 7.6). Photocleavage samples were irradiated for 5 min at 313 nm. MPA (200  $\mu$ M) was added to the copper cleavage samples, and the samples were incubated at ambient temperature for 4 h. Lanes are labeled as follows: A+G, C+T, Maxam-Gilbert sequencing reactions; L, irradiation without rhodium; D, no irradiation; 1, incubation of DNA without rhodium or Cu; 2, Cu and MPA; 3, Cu and Rh; 4, Cu and Rh for 24 h; 5, rhodium complex. The asterisk indicates a band due to renaturation of the fragment.

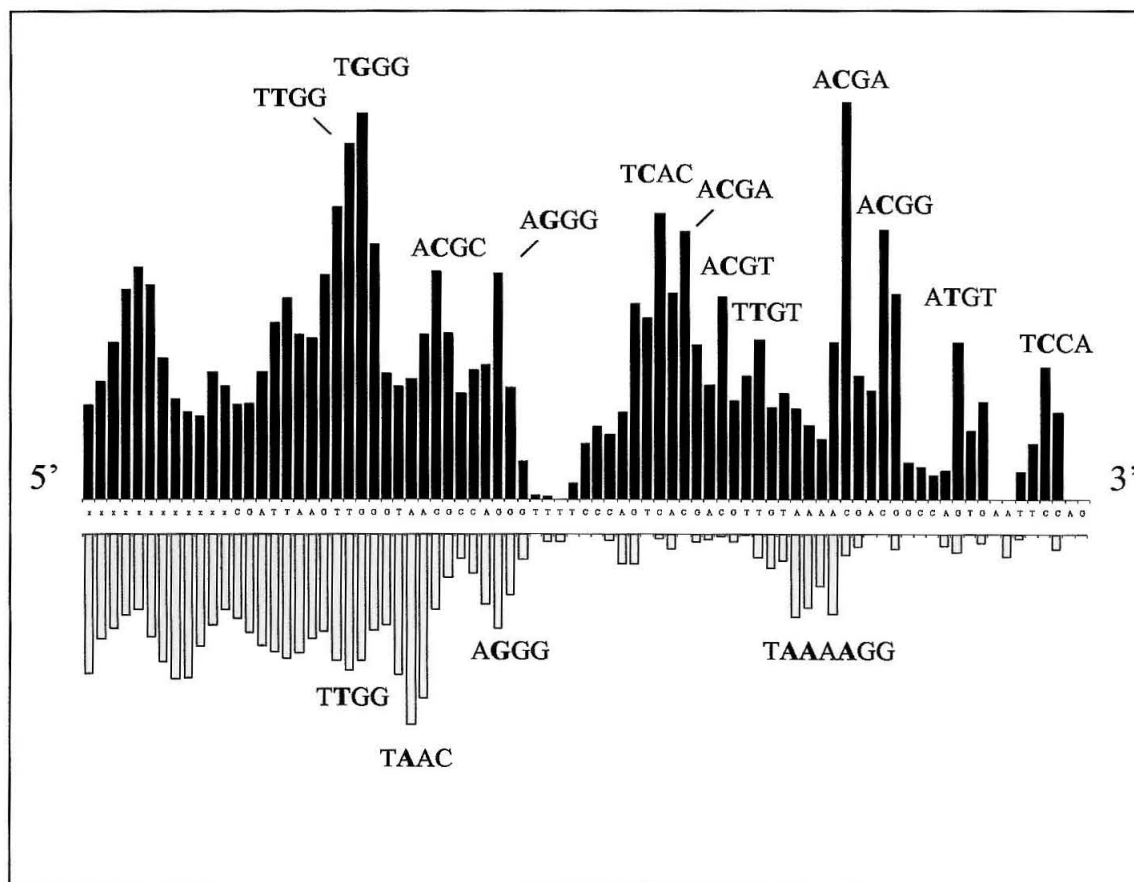


**Figure 4.12. A Bar Plot Comparing Photocleavage and Copper Cleavage with Rh"-AHAHA-COOH.** Cleavage experiments were completed with a 175-mer restriction fragment, and the resulting gel (Figure 4.11) was quantitated. The cleavage for 5  $\mu$ M intercalator-peptide conjugate is presented. The black bars indicate photocleavage, and the gray bars indicate copper cleavage. The length of the bars shows the relative amounts of a particular type of cleavage product, but no meaningful comparison can be made between photocleavage and copper cleavage efficiency. The sites of most intense cleavage are labeled with a four base sequence: 5'-N-N-N-N-3', where the cleavage site is shown in bold.

explored the groove preference of the copper-binding peptide. Does the peptide deliver the reactive moiety to the major or minor groove?

The addition of distamycin to the reactions was found to impact both the photocleavage and copper cleavage patterns of Rh-P1 and Rh''-AH (Figure 4.13 and Figure 4.14). The A/T rich regions of the restriction fragment, the preferred sites for distamycin, were largely protected from both photocleavage and copper cleavage. The rhodium complex binds from the major groove and abstracts a hydrogen atom from the major groove;<sup>12</sup> nonetheless, the minor groove binder left footprints in our ladder of photocleavage. Since our sites of intense copper cleavage are also localized at A/T rich regions, copper damage was almost eliminated by the addition of 5  $\mu$ M distamycin. This result does not rigorously establish that the copper reaction occurs from the minor groove. As our photocleavage results clearly demonstrate, distamycin can disrupt cleavage reactions that occur from the major groove.

#### **4.3.3. Photocleavage and Copper Cleavage of Oligonucleotide DNA by Rhodium-Peptide Conjugates.**

We have also tested our copper-binding conjugates with oligonucleotide substrates. A 42-mer DNA duplex was combined with Rh-P1 for photocleavage and copper cleavage reactions. Previously we demonstrated effective hydrolysis of this 42-mer duplex with Rh-P1 and  $\text{Zn}^{2+}$ .<sup>14</sup> As expected, Rh-P1 gave fairly uniform photocleavage across the oligonucleotide (Figure 4.15). The tethered P1 peptide reduced the intensity of photocleavage, but did not change the pattern of damage relative to  $[\text{Rh}(\text{phi})_2\text{bpy}]^{3+}$ . Although the duplex and Rh-P1 conjugate were incubated with  $\text{Cu}^{2+}$

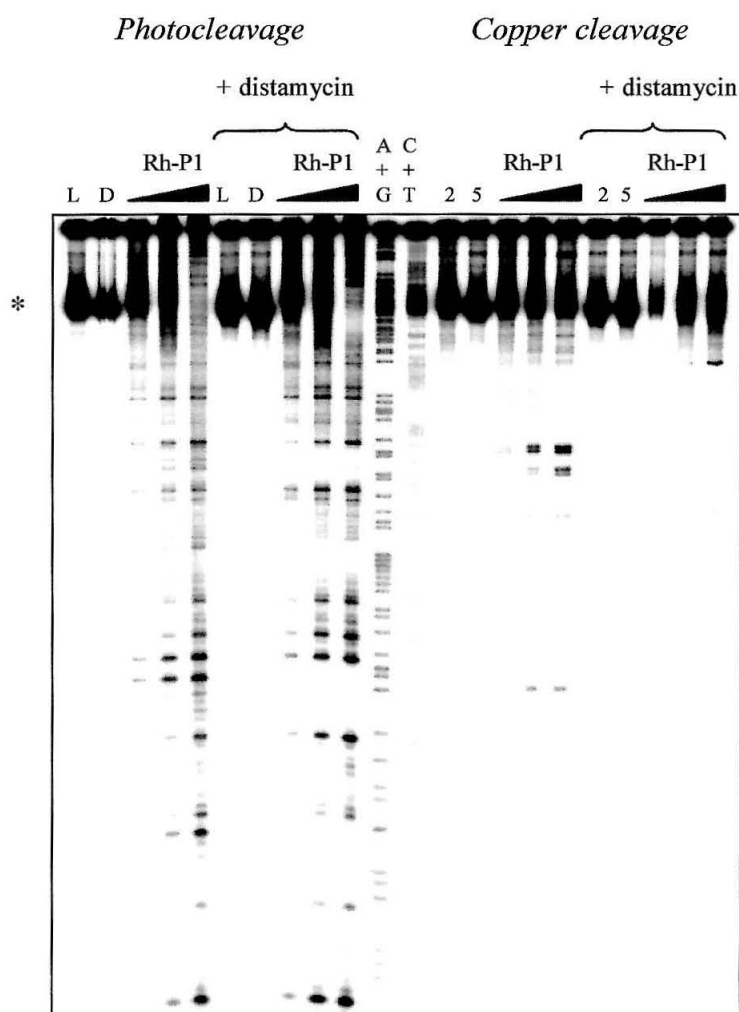


**Figure 4.13. The Impact of Distamycin on the Photocleavage and Copper Cleavage of a Restriction Fragment by Rh-P1.** Photocleavage and copper cleavage were carried out with a 175-mer restriction fragment (5'-labeled, 100  $\mu$ M), rhodium complex (2, 5, 10  $\mu$ M), and  $\text{Cu}^{2+}$  (20  $\mu$ M), in buffer (20 mM Tris-HCl, 15 mM NaCl, pH 7.6). Photocleavage samples were irradiated for 5 min at 313 nm. MPA (200  $\mu$ M) was added to copper cleavage samples, and the samples were incubated at ambient temperature for 4 h. Distamycin (5  $\mu$ M) was added to 1 set of reactions. Lanes are labeled as follows: L, light control; D, dark control; 2, Cu and MPA; 5, 10  $\mu$ M Rh-P1.

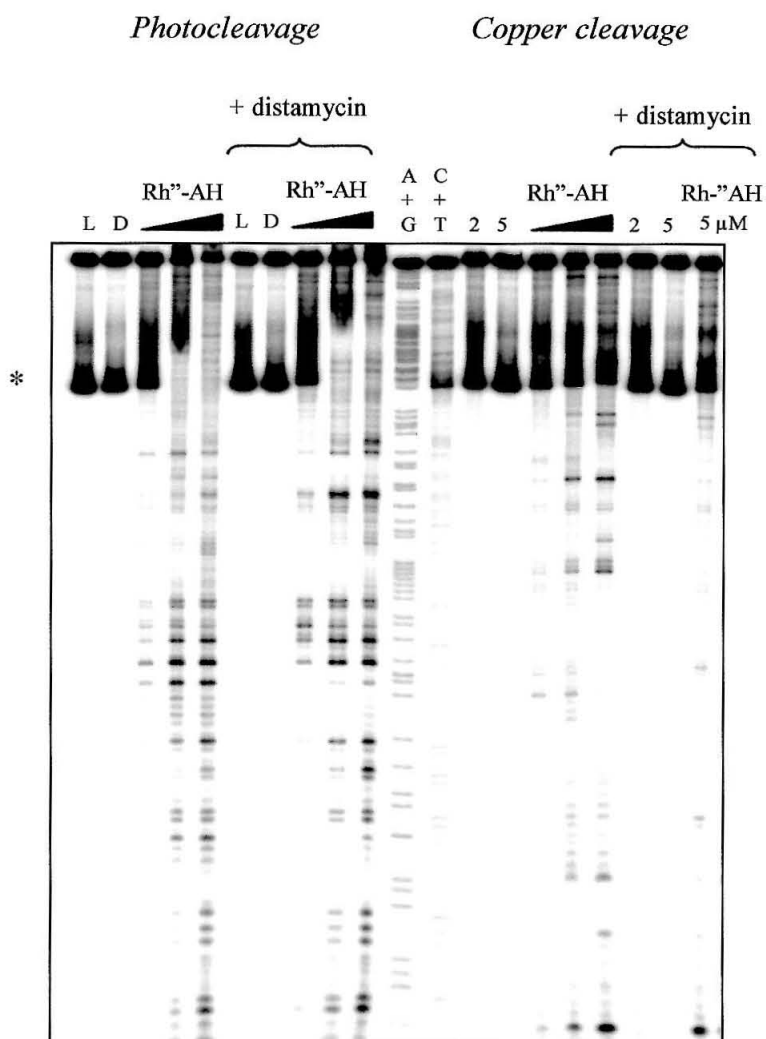


**Figure 4.14. The Impact of Distamycin on the Photocleavage and Copper Cleavage of a Restriction Fragment by Rh<sup>III</sup>-AHAAHA-COOH.** Photocleavage and copper cleavage were carried out with a 175-mer restriction fragment (5'-labeled, 100 μM), rhodium complex (2, 5, 10 μM), and Cu<sup>2+</sup> (20 μM), in buffer (20 mM Tris-HCl, 15 mM NaCl, pH 7.6). Photocleavage samples were irradiated for 5 min at 313 nm. MPA (200 μM) was added to Cu cleavage samples, and the samples were incubated at ambient temperature for 4 h. Distamycin (5 μM) was added to 1 set of reactions. Lanes are labeled as follows: L, light control; D, dark control; 2, Cu and MPA; 5, 10 μM Rh-P1.

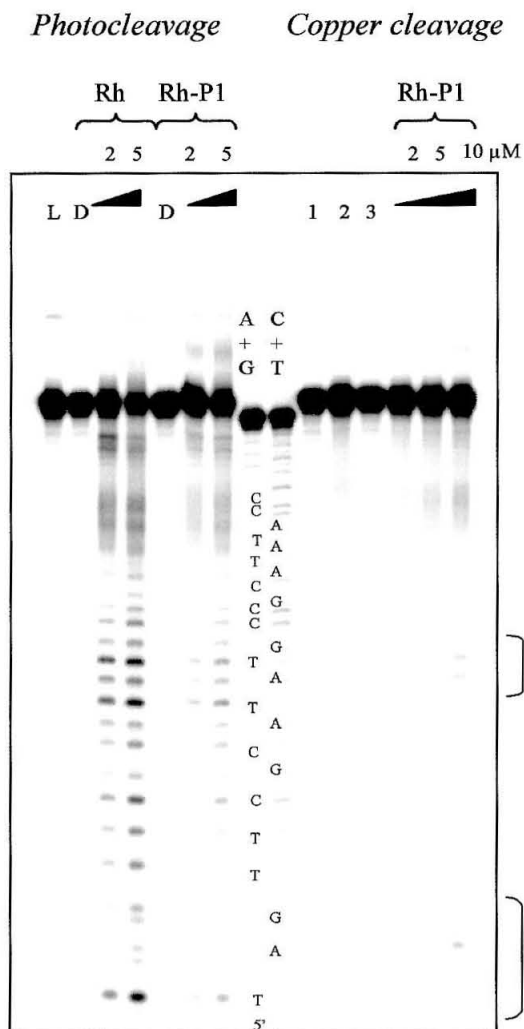


**Figure 4.15. Photocleavage and Copper Cleavage of an Oligonucleotide by Rh-P1.**

A 42-mer duplex (5'-labeled, 100  $\mu$ M bp) was combined with  $[\text{Rh}(\text{phi})_2\text{bpy}]^{3+}$  (Rh) or the Rh-P1 complex in Tris-HCl (25 mM, pH 7.5). To promote photocleavage the samples were irradiated at 313 nm for 15 min. For copper reactions, both  $\text{Cu}^{2+}$  (50  $\mu$ M) and MPA (500  $\mu$ M) were added, and the samples were incubated for 15 h at 37  $^{\circ}\text{C}$ . Lanes are labeled with the rhodium complex concentration ( $\mu$ M). L, light control; D, dark control; 1, DNA alone; 2, Cu and MPA; 3, Cu and 10  $\mu$ M Rh-P1.



and MPA for 15 h at 37 °C, very little copper damage was observed for this substrate (Figure 4.15). A very small amount of copper damage is observed at 5'-TAG-3' and 5'-TATG-3' sites in the oligonucleotide, but this damage is barely above the damage observed in a control reaction with  $\text{Cu}^{2+}$  and MPA.

A 40-mer DNA duplex was also combined with Rh-P1, Rh''-AH-OH, or Rh-KGH for photocleavage or copper cleavage reactions (Figure 4.16). The three conjugates gave nearly identical photocleavage patterns, and the damage was most intense at two 5'-ACGX-3' sites (cleavage at the italicized base). Again, the  $[\text{Rh}(\text{phi})_2\text{bpy}]^{3+}$  complex shows a slight preference for 5'-Pu-Py-Pu-Py-3' sites, so this photocleavage result is not surprising. The intensity of photocleavage is slightly greater for the Rh-KGH conjugate, and this conjugate also causes greater smearing of the parent band. The Rh-KGH conjugate, with its short tethered peptide, most likely has the greatest affinity for DNA. Bulkier peptides, such as P1 or AH, reduce the binding and photocleavage of the metallointercalator.

As was observed for the 42-mer, Rh-P1 did not promote any significant copper damage in the 40-mer duplex. The pattern and intensity of damage in Rh-P1 lanes was identical to the pattern and intensity of damage in a control lane for  $\text{Cu}^{2+}$  and MPA (Figure 4.16). The Rh-KGH peptide gave similar results. In contrast, the Rh''-AH-OH conjugate promoted small amounts of copper damage near the sites of intense photocleavage. We know that  $[\text{Rh}(\text{phi})_2\text{bpy}]^{3+}$  cleaves with 5' asymmetry, so we can assign the intercalation site based on the photocleavage pattern. Copper cleavage is observed on both the 5' and 3' side of the intercalation site. It is interesting to note that

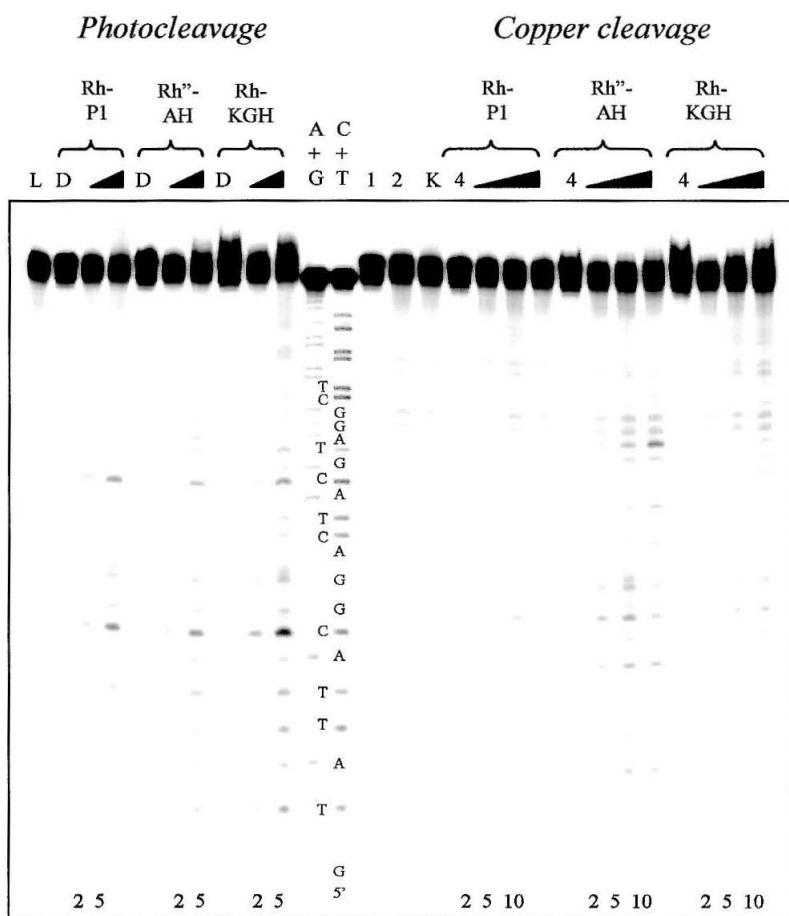


**Figure 4.16. Photocleavage and Copper Cleavage of an Oligonucleotide by Rh-P1, Rh''-AHAHA-COOH, and Rh-KGH.** Photocleavage and copper cleavage were carried out with a 40-mer duplex (5'-labeled, 2 μM), rhodium complex (2, 5, 10 μM), and Cu<sup>2+</sup> (20 μM), in buffer (25 mM Tris-HCl, pH 7.5). Photocleavage samples were irradiated for 15 min at 313 nm. MPA (500 μM) was added to copper cleavage samples, and the samples were incubated at 37 °C for 24 h. Lanes are labeled as follows: A+G, C+T, Maxam-Gilbert sequencing reactions; L, irradiation without rhodium; D, no irradiation; 1, incubation of DNA without rhodium or Cu; 2, Cu and MPA; K, Cu, MPA, and KGH peptide; 4, 10 μM conjugate, no Cu or MPA. The conjugate concentration is given at the bottom of the gel.

the copper damage primarily occurs at purine bases, and the separation between the site of intercalation and the site of copper damage varies from one to three bases.

#### 4.3.4. Photocleavage and Copper Cleavage of Oligonucleotides by Mismatch

##### Specific Rhodium-Peptide Conjugates.

To specifically target mismatch sites for copper cleavage, we attached the P1 peptide and the AHAAHA-COOH peptide to a rhodium complex bearing the bulky chrysi intercalator. These novel conjugates were tested with substrates containing CC mismatches. The CC mismatch is a particularly destabilizing mispair, and is well recognized by the  $[\text{Rh}(\text{bpy})_2\text{chrysi}]^{3+}$  complex.<sup>17</sup>

***Rh''C-P1.*** The Rh''C-P1 conjugate was combined with a 25-mer duplex for photocleavage, copper cleavage, and zinc cleavage reactions (Figure 4.17). Importantly, the conjugate is still mismatch specific. Like  $[\text{Rh}(\text{phen})(\text{bpy}'')(\text{chrysi})]^{3+}$ , the conjugate specifically binds at the CC mismatch, and with photoactivation, cleaves on the 3' side of the mismatch site. Very little copper damage, and absolutely no zinc damage were observed near the mismatch site. The metallointercalator is very selective for mismatches, but the metal-binding P1 peptide fails. It is not active for copper-promoted oxidation or zinc-promoted hydrolysis of DNA.

***Rh''C-AH-OH.*** The Rh''C-AH-OH conjugate was combined with a 35-mer hairpin for photocleavage and copper cleavage reactions (Figure 4.18). With the hairpin substrate it is possible to view the damage that occurs in each strand of the hairpin stem. Both isomers of the RhC''-AH-OH conjugate were found to bind and photocleave at the CC mismatch site in the 35-mer hairpin. Damage was observed at the base on the 3' side

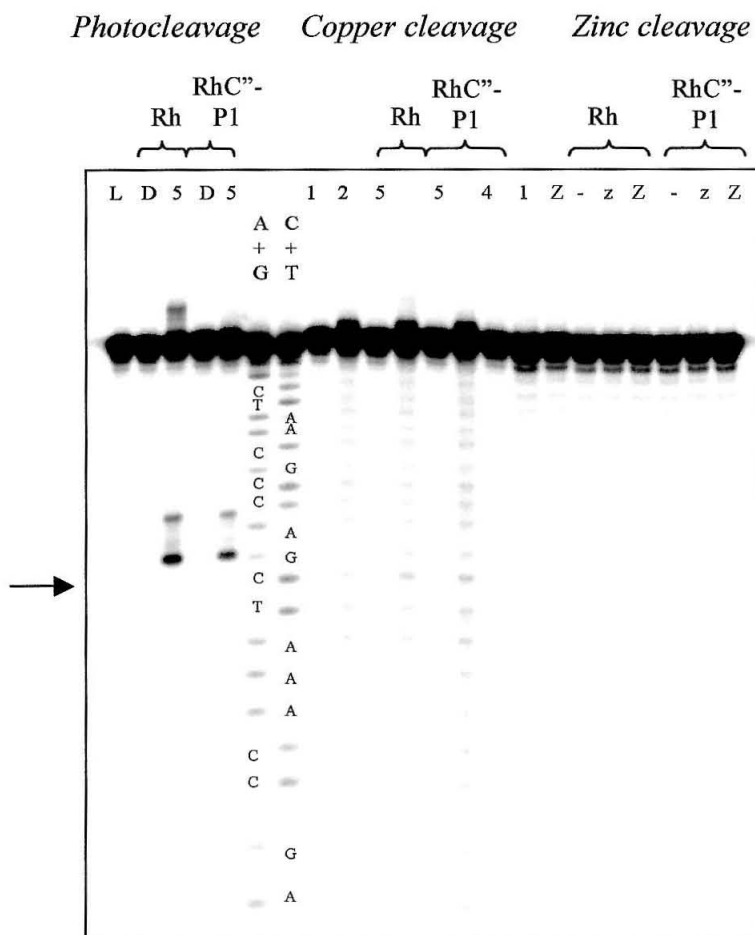


**Figure 4.17. Photocleavage, Copper and Zinc Cleavage of a Duplex with a Mismatch Site by [Rh(phen)(bpy<sup>3+</sup>)-P1](chrysi)]<sup>3+</sup>.** A 25-mer duplex with a CC mismatch was combined with [Rh(phen)(bpy<sup>3+</sup>)(chrysi)]<sup>3+</sup> (Rh, 5  $\mu$ M) or RhC<sup>3+</sup>-P1 (5  $\mu$ M) in Tris-HCl (25 mM, pH 7.5). To promote photocleavage the samples were irradiated at 365 nm for 15 min. For copper reactions, both Cu<sup>2+</sup> (50  $\mu$ M) and MPA (500  $\mu$ M) were added, and the samples were incubated for 22 h at 37 °C. Zn<sup>2+</sup> reactions were carried out in a sodium borate buffer with 5 or 50  $\mu$ M Zn<sup>2+</sup> (z or Z). These samples were incubated for 40 h at 37 °C. Lanes are as follows: L, light control; D, dark control; 1, DNA alone; 2, Cu and MPA; 4, Cu and Rh complex; 5, Rh complex.

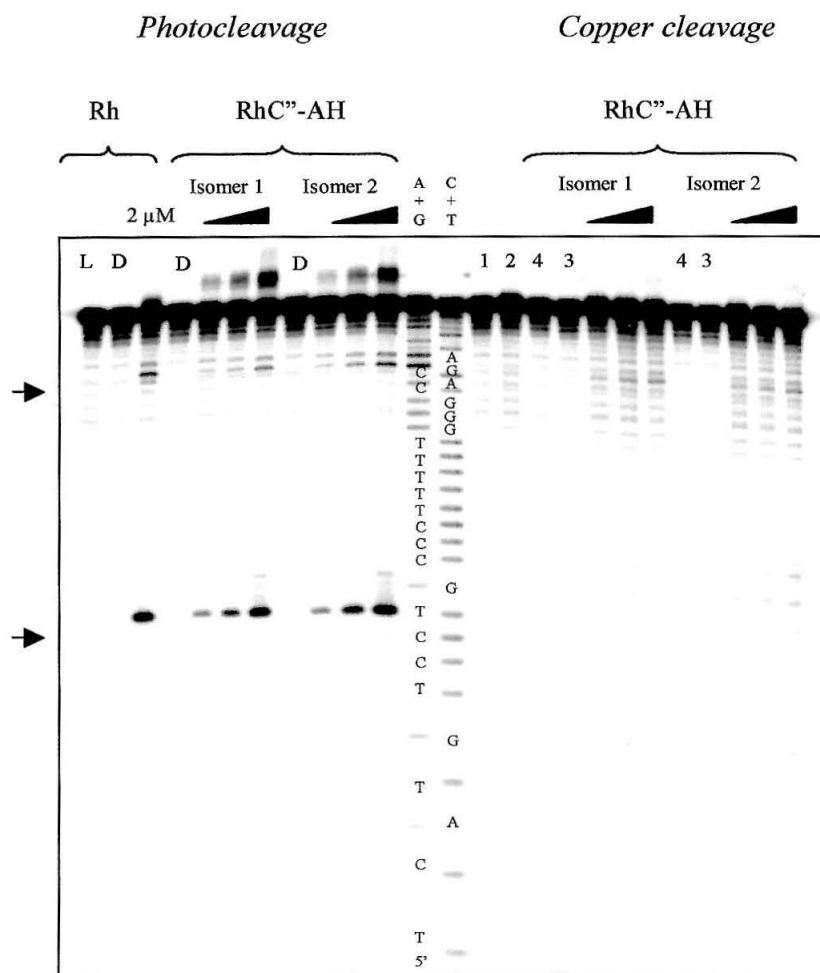


**Figure 4.18. Photocleavage and Copper Cleavage of a Hairpin with a Mismatch Site by  $[\text{Rh}(\text{phen})(\text{bpy}''\text{-AHAAHA-COOH})(\text{chrysi})]^{3+}$ .** A 35-mer hairpin with a CC mismatch was combined with  $\Delta\text{-}[\text{Rh}(\text{bpy})_2\text{chrysi}]$  (Rh) or RhC''-AH (2, 5, 10  $\mu\text{M}$ ) in Tris-HCl buffer (25 mM, pH 7.5). For photocleavage reactions, the samples were irradiated at 365 nm for 15 min. For copper cleavage reactions, both  $\text{Cu}^{2+}$  (20  $\mu\text{M}$ ) and MPA (200  $\mu\text{M}$ ) were added, and the samples were incubated at ambient temperature for 4 h. The lanes are labeled as follows: L, light control; D, dark control; 1, DNA alone; 2, Cu and MPA; 3, Cu and Rh; 4, Rh complex. The CC mispair is marked with arrows.

of the mismatch, and although the cleavage was not symmetrical, it was observed on both strands of the hairpin stem. With both isomers of RhC''-AH-OH, a modest amount of copper damage was also observed near the CC mismatch. This damage was only observed in one strand of the hairpin stem. Although a very small effect, this result prompted us to continue experiments with Rh''C-AH-OH.

The Rh''C-AH-OH conjugate was also tested with a 25-mer duplex containing a CC mismatch (Figure 4.19). With photoactivation, the two isomers cleaved the 25-mer on the 3' side of the CC mispair. Although less efficient than the  $\Delta$  isomer of the  $[\text{Rh}(\text{bpy})_2\text{chrysi}]^{3+}$  complex, the Rh''C-AH-OH complex did give very intense photocleavage damage near the mismatch site, and there was little difference in the intensity of damage for the two isomers. In addition, a significant band appeared above the parent band with irradiation of the conjugate and DNA, and this band might be due to crosslinking reactions between the peptide and DNA.

The Rh''C-AH-OH conjugate also promoted copper damage in the 25-mer substrate. In the presence of  $\text{Cu}^{2+}$ , MPA, and conjugate, damage was observed across the oligonucleotide, and the most intense damage was concentrated near the mismatch site. Importantly, the  $[\text{Rh}(\text{bpy})_2\text{chrysi}]^{3+}$  complex, without tethered peptide, also increased the amount of copper damage at the mismatch site. With the tethered peptide the amount of copper damage was greater, but was also less focused near the mismatch.

To increase the intensity and selectivity of copper damage at mismatch sites we tested our conjugates and complexes under a variety of conditions (Table 4.3). We varied the concentration of copper and reductant, the temperature, and the length of incubation. We used MPA, ascorbic acid, and hydrogen peroxide as activating agents, and we tested

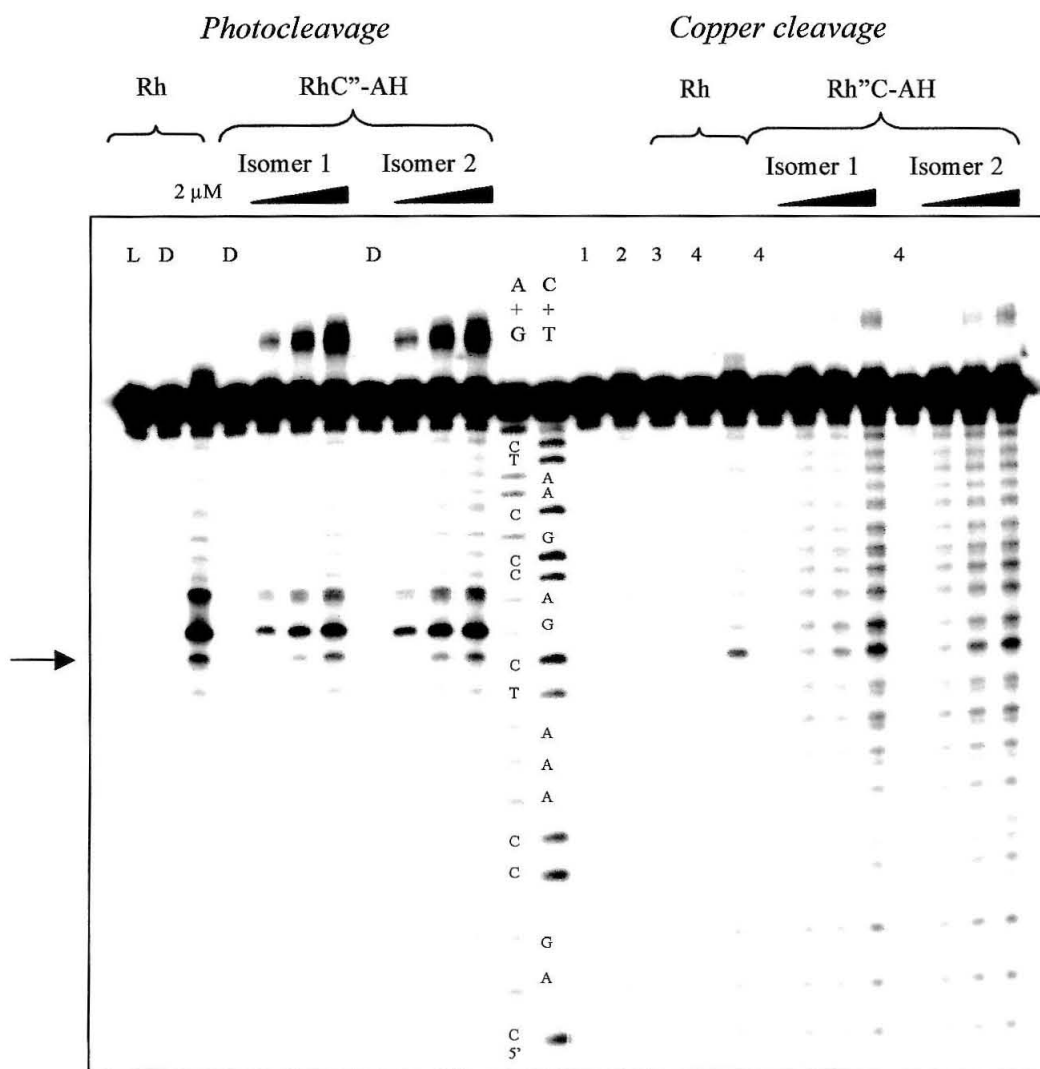


**Figure 4.19. Photocleavage and Copper Cleavage of a Duplex with a Mismatch Site by  $[\text{Rh}(\text{phen})(\text{bpy})''\text{-AHAAHA}(\text{chrysi})]^{3+}$ .** A 25-mer duplex with a CC mismatch (100  $\mu\text{M}$  base pairs) was combined with  $\Delta\text{-}[\text{Rh}(\text{bpy})_2\text{chrysi}]$  (Rh, 2  $\mu\text{M}$ ) or  $\text{RhC}''\text{-AH}$  (2, 5, 10  $\mu\text{M}$ ) in Tris-HCl buffer (25 mM, pH 7.5). For photocleavage reactions, the samples were irradiated at 313 nm for 15 min. For Cu cleavage reactions, both  $\text{Cu}^{2+}$  (50  $\mu\text{M}$ ) and MPA (500  $\mu\text{M}$ ) were added, and the samples were incubated for 17 h at 37  $^\circ\text{C}$ . The lanes are labeled as follows: L, light control; D, dark control; 1, DNA alone; 2, Cu and MPA; 3, Cu and Rh; 4, 10  $\mu\text{M}$  Rh.

a variety of DNA substrates. In all of our experiments, we never improved on the result presented in Figure 4.19.

**Table 4.3. Conditions for Copper Cleavage Experiments with Mismatch-Specific Complexes and Conjugates.**

	Conditions Tested
Copper/Reductant Concentration ( $\mu\text{M}$ )	20 / 200
	50 / 500
	100 / 1000
Activating Agents	MPA
	MPA + $\text{H}_2\text{O}_2$
	Ascorbic Acid
	Ascorbic Acid + $\text{H}_2\text{O}_2$
Incubation Time	4 to 24 hours
	0 to 20 min pre-incubation
Incubation Temperature	Ambient
	37 °C
Buffer	Tris-HCl, 25 mM, pH 7.5
	Tris-HCl, NaOAc, NaCl, pH 7.5
DNA Substrates	35 mer hairpin with CC mismatch
	25 mer duplex with CC mismatch
	26 mer duplex with CC mismatch



## 4.4. Discussion

We have applied our metallointercalator-peptide conjugates for the delivery of both  $\text{Zn}^{2+}$  and  $\text{Cu}^{2+}$  to DNA substrates. The ionic radii of  $\text{Cu}^{2+}$  (0.72 Å) and  $\text{Zn}^{2+}$  (0.74 Å) are actually quite similar.<sup>27</sup> Copper(II) is a borderline hard-soft metal, and prefers a square planar geometry.<sup>27</sup> Histidine has a larger stability constant for coordination of  $\text{Cu}^{2+}$  ( $K_1 = 10.6$ ) than for coordination of  $\text{Zn}^{2+}$  ( $K_1 = 6.7$ ).<sup>28-31</sup>

With  $\text{Zn}^{2+}$  we promote hydrolysis of the DNA backbone, but with redox-active  $\text{Cu}^{2+}$  we promote oxidative strand scission. Although DNA hydrolysis is more biologically relevant and is preferred for many applications, it is also more difficult to achieve than oxidative cleavage. The creation of artificial nuclease is an ambitious goal, and our most promising nuclease mimic, Rh-P1, has not provided reliable cleavage of DNA oligonucleotides.<sup>14,32</sup> In contrast, our metallointercalator-peptide conjugates provide predictable and reproducible copper cleavage of linear DNA substrates.

Copper cleavage reagents, such as  $[\text{Cu}(\text{phen})_2]^+$  or  $\text{Cu}(\text{II})\text{-KGH}$ , generate nondiffusible reactive species, either a copper-oxo species or a metallopeptide-bound radical.<sup>1,5</sup> These nondiffusible species must be positioned near the DNA backbone in order to achieve strand scission. This is an important consideration in the design of copper cleavage reagents. In contrast,  $\text{Fe}(\text{EDTA})^{2-}$ , produces a diffusible hydroxyl radical. It does not need to be carefully delivered to DNA, and it gives scattered damage across a DNA substrate.

Because copper reagents form nondiffusible reactive species, our copper cleavage studies allowed us to map the interactions of our metallointercalator-peptide conjugates

with DNA. Photocleavage indicated the site of intercalation, and copper cleavage revealed the interactions of the tethered peptide and DNA. In addition, since oxidative scission is easier to achieve than hydrolysis, we have designed a conjugate for mismatch-specific copper cleavage.

#### 4.4.1. The Copper-Binding Peptides.

**P1.** As described in Chapter 1, the P1 peptide is a 16-mer peptide with two histidine residues. The peptide was designed with helix-inducing features, but CD study suggests that the actual helical content is quite low, < 20%.<sup>33</sup> The two histidine residues are located at *i* and *i*+4 positions and would be presented on one face of the helix. The addition of  $\text{Zn}^{2+}$  actually causes a slight increase in helicity; it appears that metal coordination by the two histidine residues helps to nucleate helix formation.<sup>33</sup>

The histidine pair not only creates a binding site for  $\text{Zn}^{2+}$ , but also for  $\text{Cu}^{2+}$ . The binding of Rh-P1 with both  $\text{Zn}^{2+}$  and  $\text{Cu}^{2+}$  was studied by mass spectrometry.<sup>33</sup>

**AHAAHA.** The AHAAHA peptide is a simple 6-mer peptide. Like the P1 peptide, it contains two histidine residues, but in contrast to P1, it is too short to support any interesting peptide conformation. Must a peptide have defined conformation in order to effectively bind and deliver copper to DNA? The answer seems to be no. Indeed, the AHAAHA peptide gave the most promising copper cleavage results with two different metalointercalators. To explore whether the C-terminus of the AHAAHA peptide was involved in metal coordination and delivery, we prepared both the acid and the amide forms of the peptide. We have observed very similar cleavage results with both of these peptides.

**KGH.** As described previously, the Gly-Gly-His peptide binds nickel(II) or copper(II) at physiological pH through the histidine imidazole nitrogen, two deprotonated amide nitrogens, and the terminal  $\alpha$ -amine (Figure 4.2).<sup>5</sup> This tripeptide motif is found at the tail of serum albumin. With chemical activation, metal complexes of Xaa-Xaa-His promote oxidative cleavage of DNA.<sup>5,6</sup> We decided to tether this optimized copper-binding motif to our metallointercalator. Since the N-terminus of the tripeptide is involved in metal coordination, we incorporated a lysine residue at the N-terminus and coupled our metallointercalator through the lysine side chain. This strategy has been employed for the attachment of the tripeptide to proteins, and should not interfere with metal binding.<sup>5</sup>

#### 4.4.2. Oxidative Cleavage of DNA with Copper-Binding Peptides Tethered to Metallointercalators.

We attached our copper-binding peptides to the  $[\text{Rh}(\text{phi})_2\text{bpy}']^{3+}$  and  $[\text{Rh}(\text{phi})_2\text{bpy}'']^{3+}$  intercalators to create a set of conjugates. The use of both the bpy' and bpy'' ligand was not by design, but was a matter of convenience. Nevertheless, the bpy'' ligand does possess an extra methylene unit, and this may give added flexibility to peptide-DNA interactions. The most interesting copper cleavage results were actually obtained with the  $[\text{Rh}(\text{phi})_2\text{bpy}''\text{-AHAHA}]^{3+}$  conjugates.

We tested our copper-binding conjugates against three different DNA substrates: a 175-mer restriction fragment from pUC19, a 42-mer duplex, and a 40-mer duplex. The DNA substrates were incubated with  $\text{Cu}^{2+}$  (20 to 50  $\mu\text{M}$ ), MPA (200 to 500  $\mu\text{M}$ ), and varying amounts of conjugate. The  $\text{Cu}^{2+}$  and MPA alone produced some strand scission;

a weak ladder of damage was observed. Under the right conditions our conjugates greatly increased the amount of copper damage, and changed the pattern of copper damage.

***Rh-P1.*** The Rh-P1 conjugate was demonstrated to direct copper cleavage to a few sites in the restriction fragment (Figure 4.8), but promoted very little cleavage in two oligonucleotide substrates (Figures 4.15 and 4.16). There were only a few sites in the 175-mer fragment that were vulnerable to Rh-P1 promoted copper damage, so it is not entirely surprising that the 40-mer and 42-mer oligonucleotides were not cleaved by Rh-P1.

The histidine residues in the P1 peptide clearly play an important role in directing copper damage. The Rh-P4 conjugate, a mutant of Rh-P1 that contains glutamic acid residues instead of histidine residues, did not promote copper cleavage in the restriction fragment. Rh-Bam and  $[\text{Rh}(\text{phi})_2\text{bpy}]^{3+}$  also failed to promote or direct copper cleavage.

***Rh''-AH.*** The Rh''-AH conjugate was not as selective as Rh-P1; more sites in the 175-mer fragment were damaged (Figures 4.10 and 4.11). The Rh''-AH-OH conjugate also promoted modest copper cleavage in the 40-mer duplex (Figure 4.16). The sites of copper cleavage in the duplex were located only one to three bases from the intercalation site. A schematic model that shows the relationship between intercalation and cleavage for Rh''-AH is presented in Figure 4.20.

***Rh-KGH.*** The Rh-KGH conjugate was not tested with a restriction fragment, and did not promote copper damage in a 40-mer DNA substrate (Figure 4.16). The reactive species generated with the Rh-KGH conjugate is not diffusible, and may be a metallopeptide-bound radical.<sup>5</sup> Although the KGH peptide motif certainly binds copper

with greater affinity than the P1 or AHAAHA peptide, the tethered peptide may not be positioned for reaction with the DNA backbone on the timescale of the radical. Notably, we did not observe any cleavage with the free KGH peptide under the conditions of our experiment. It is possible that with some optimization, perhaps employing Ni(II) rather than Cu(II), or attaching the motif to the  $[\text{Rh}(\text{phi})_2\text{bpy}']^{3+}$  intercalator, our Rh-KGH conjugate might promote oxidative damage to DNA.

***The DNA Substrate.*** Our experiments with copper dramatically emphasize the difference between a plasmid DNA substrate and a linear DNA substrate. As described in Chapter 1 and 2, a 24 h incubation of 5  $\mu\text{M}$  copper with supercoiled plasmid DNA results in 100% conversion to a nicked product. The addition of Rh-P1 or Rh-Bam to a reaction containing copper and plasmid actually reduces the amount of nicking.

In contrast, incubation of a restriction fragment or oligonucleotide with 20  $\mu\text{M}$   $\text{Cu}^{2+}$  for 24 h causes no damage (Figure 4.8 and Figure 4.16, Lane 4). The parent band remains intact. To cleave the DNA backbone, a reductant, such as MPA, must be added to the reaction. With linear DNA substrates, the addition of Rh-P1 or Rh''-AH to the reaction increases the amount of copper damage and directs the damage to specific sites (Figure 4.8, 4.10, and 4.11).

#### **4.4.3. Insights into the Interactions of Tethered Peptides and DNA.**

The copper cleavage experiments with restriction fragments and Rh-P1 revealed some of the requirements for metallointercalator-peptide interactions with DNA. Comparisons of photocleavage and copper cleavage patterns demonstrated that binding of the metallointercalator in and of itself is not sufficient for promoting copper cleavage.

Photocleavage results revealed that the metallointercalator-peptide binds across the restriction fragment with only a weak preference for 5'-ACGX-3' sites. In contrast, Rh-P1 promoted copper cleavage occurred intensely at very few sites. In order to achieve oxidative strand scission, not only must the metallointercalator bind to the DNA, the flexible P1 peptide must also be correctly oriented to deliver copper to the backbone. With a short peptide like Rh-AHAHA, the correct orientation for copper delivery is more accessible. The preference for copper cleavage at A/T-rich sequences for both Rh''-AH and Rh-P1 suggests that the flexibility of the DNA may also be important for reaction.

It has not been possible to definitively establish the groove that is targeted by our copper-binding peptides. Distamycin, a minor groove binder, greatly reduced the copper cleavage observed with both Rh-P1 and Rh''-AH (Figures 4.13 and 4.14). Distamycin and our conjugates both prefer A/T rich regions.<sup>26</sup> Perhaps distamycin directly displaces the peptide from the minor groove. Alternatively, the effects of this minor groove binder might be transmitted across to the major groove. Although the rhodium complex binds and abstracts the C3' hydrogen from the major groove, it also is impacted by distamycin binding. A footprint appears in the photocleavage pattern at A/T rich sites.

Experiments with Rh''-AH-OH and a 40-mer duplex provided a more detailed picture of conjugate-DNA interactions (Figure 4.16). In the 40-mer substrate there are two sites with intense photocleavage, 5'-ACGG-3' and 5'-ACGT-3'. Since the rhodium complex is known to cleave with 5' asymmetry, we can assign the intercalation site. The intercalator binds at the 5'-CG-3' step. Copper cleavage is observed at purine bases on each side of the intercalation site. The identity of the base appears to be more *critical*

than the distance from the intercalation site. A schematic view of Rh<sup>III</sup>-AH-OH binding and cleavage is presented in Figure 4.20.

Our copper studies have provided some general lessons about metallointercalator-peptide conjugates, and some of these lessons apply to our DNA hydrolysis experiments. For example, the weak binding preferences of the rhodium intercalator should not be ignored. They determine the DNA sequences that are within the reach of a tethered peptide. Although we are interested in reactions at the deoxyribose ring, the sequence of DNA has an important impact on peptide-mediated reactions. It appears that the peptide has greater access to the DNA in A/T-rich regions. Also a long flexible peptide like P1 can be a liability. Although a longer peptide may fold into a useful conformation, it also can access nonproductive conformations. In our copper experiments, a short unstructured peptide was found to be more reactive than the P1 peptide.

Of course there is a significant difference between the copper and zinc chemistry. The copper center reacts with oxygen to produce a nondiffusible copper-oxo species or peptide radical, and this species is very reactive. If it is not properly positioned for attack of the deoxyribose ring, it will find something else with which to react. This is likely the reason that we have observed very little copper damage with our Rh-KGH conjugate. In contrast, the zinc center most likely serves as a Lewis acid to activate water or stabilize leaving groups; it is not a highly reactive center.



**Figure 4.20. A Schematic Model for Photocleavage and Copper Cleavage with the  $[\text{Rh}(\text{phi})_2(\text{bpy}''\text{-AHAAHA-COOH})]^{3+}$  Conjugate.** The  $\text{Rh}''\text{-AH}$  conjugate binds at two 5'-ACGX-3' sites in a 40-mer duplex. The conjugate intercalates between the CG step, and upon irradiation cleaves at the 5' C. The peptide promotes copper damage on both sides of the intercalation site. The sites of copper damage are indicated with blue dashed arrows.



#### 4.4.4. Development of a Mismatch-Specific Conjugate for DNA Cleavage.

The ability to recognize and achieve reaction at DNA mismatches is increasingly important in this day of sequenced genomes. Cheap and convenient strategies for locating the mutations that give rise to diseased states or for mapping the location of single nucleotide polymorphisms are in high demand. To create a new tool for DNA mismatch recognition, we have attached the P1 and AHAAHA-COOH peptides to a  $[\text{Rh}(\text{phen})(\text{bpy}')(\text{chrysi})]^{3+}$  complex.

**DNA Mismatches.** Our genetic material is under daily assault. Both chemical damage, and to a lesser extent, the mis-incorporation of bases during replication threatens to scramble some of the vital information contained in the genome. It is estimated that a human cell faces approximately 50,000 damage events and 1000 replication mistakes each day.<sup>34</sup> The eight possible DNA mismatches are presented in Figure 4.3. What are the characteristics of mismatch sites that set them apart from correctly paired and undamaged sites? Also, how can mismatches be detected in the laboratory?

The incorporation of a base mismatch does not bring significant changes in the placement of functional groups or the overall conformation of a B-form DNA helix;<sup>34</sup> however, these mismatches can have important thermodynamic and kinetic consequences. Mismatches commonly cause a destabilization of the helix, and duplexes with mispairs often denature at lower temperatures. The consequences of mismatch incorporation are strongly dependent on both the mismatch and the sequence context.<sup>34</sup> The free energy of duplexes containing mismatches range from strongly destabilized (2.72 kcal/mol) for a CC mismatch to strongly stabilized (-2.58 kcal/mol) for a GG mispair.<sup>35</sup> Kinetically, some mismatches produce an increase in the rate of base pair

opening events. For example, the GG mispair shows rapid interconversion between different conformations ( $10^4 \text{ s}^{-1}$  at 303 K).<sup>36</sup>

***Mismatch-Specific Metallointercalators.*** As described in Chapter 1, the Barton group has developed a method of mismatch recognition that exploits the kinetic and thermodynamic destabilization of mismatch sites. To specifically target DNA mismatches, rhodium complexes were prepared with bulky intercalating ligands.<sup>15</sup> This simple steric-exclusion strategy was successful, and the  $[\text{Rh}(\text{bpy})_2\text{chrysi}]^{3+}$  complex was demonstrated to selectively bind, and upon photoactivation, cleave in the vicinity of mismatch sites.

Although our photoactivated metallointercalators are a very useful tool for mismatch recognition, they are not suited to all applications. Specifically, the equipment required for photoactivation is not always available, particularly for medical applications. For this reason we sought to modify our metallointercalators with copper-binding peptides. This chimera would not require photoactivation; cleavage at a mismatch site could be chemically triggered with  $\text{Cu}^{2+}$  and a reductant. For some applications, this would be a critical advantage.

***Copper-Promoted Cleavage with Mismatch-Specific Conjugates.*** Although we were not able to match the efficiency of the photocleavage reaction, we did observe copper damage near a CC mismatch with the  $\text{Rh}''\text{C-AH-OH}$  conjugate. This was observed with two different DNA substrates, a 35-mer hairpin and a 25-mer duplex (Figures 4.18 and 4.19). With the 25-mer substrate, the selectivity for cleavage at the mismatch site was fairly modest; indeed, a ladder of damage products was observed. Importantly, the  $\Delta$  isomer of the  $[\text{Rh}(\text{bpy})_2\text{chrysi}]^{3+}$  complex also directed copper

cleavage to the mismatch site, and was more selective than the Rh<sup>III</sup>-C-AH-OH conjugate (Figure 4.19). We have not observed any copper-promoted cleavage with our other metallointercalators, [Rh(phi)<sub>2</sub>bpy']<sup>3+</sup> and [Rh(phi)<sub>2</sub>bpy'']<sup>3+</sup>. Photocleavage reactions confirmed that the Rh<sup>III</sup>-C-P1 conjugate was binding at mismatch sites, but this conjugate failed to give any significant copper damage near the CC mispair.

We have not created a practical tool for identifying DNA mismatches; nevertheless, the Rh<sup>III</sup>-C-AH conjugate is promising. In the development of artificial nucleases, very little attention has been given to DNA binding and DNA recognition. Of course, natural restriction enzymes show extremely selective DNA cleavage, and a true artificial nuclease would possess sequence selectivity. We have demonstrated that the metallointercalator can be tuned to provide this selectivity. The appended peptides did not change the selectivity of the [Rh(phen)(bpy'')(chrysi)]<sup>3+</sup> intercalator for mismatch sites. Although the P1 and AHAHA peptides are not particularly reactive, they were selectively delivered to mismatch sites. This represents a first step towards sequence selective artificial nucleases.

## 4.5. Conclusions

We have tethered copper-binding peptides to metallointercalators to create reagents for oxidative DNA cleavage. In the presence of Cu<sup>2+</sup> and MPA our conjugates promote strand scission. By comparing the photocleavage pattern produced by the metallointercalator with the copper cleavage pattern of the metallopeptide we have

dissected the interactions of our conjugates with DNA. Although our conjugates bind with little sequence selectivity, the copper reaction was primarily observed at A/T rich sites, and the pattern of copper damage was found to depend on the appended peptide. Finally, by attaching a short histidine-containing peptide to a chrysenequinone diimine complex of Rh(III), we have created a reagent that directs copper damage to mismatch sites. Together these experiments provide insight into the interactions of tethered peptides with DNA, and also move us one step closer to a sequence-selective artificial nuclease.

## 4.6. References

1. Sigman, D. S.; Mazumder, A.; Perrin, D. M. *Chem. Rev.* **1993**, 93, 2295-2316.
2. Dervan, P. B. *Science* **1986**, 232, 464-471.
3. Tullius, T. D. *Annu. Rev. Biophys. Chem.* **1989**, 18, 213-237.
4. Zelenko, O.; Gallagher, J.; Xu, Y.; Sigman, D. S. *Inorg. Chem.* **1998**, 37, 2198-2204.
5. Long, E. C. *Acc. Chem. Res.* **1999**, 32, 827-836.
6. Huang, X.; Pieczko, M. E.; and Long, E. C. **1999**, *Biochemistry*, 38, 2160-2166.
7. Stubbe, J.; Kozarich, J. W. *Chem Rev.* **1987**, 87, 1107-1136.
8. DeRosch, M. A.; Trogler, W. C. *Inorg. Chem.* **1990**, 29, 2409-2416.
9. Hashimoto, S.; Yamashita, R.; Nakamura, Y. *Chem Lett.* **1992**, 1639-1642.
10. Hashimoto, S.; Nakamura, Y. *J. Chem. Soc. Chem. Commun.* **1995**, 1413-1414.

11. Joshi, R. R.; Likhite, S. M.; Kumar, R. K.; Ganesh, K. N. *Biochim. Biophys. Acta* **1994**, *1199*, 285-292.
12. Sitlani, A.; Long, E. C.; Pyle, A. M.; Barton, J. K. *J. Am. Chem. Soc.* **1992**, *114*, 2303-2312.
13. Pyle, A. M.; Long, E. C.; Barton, J. K. *J. Am. Chem. Soc.* **1989**, *111*, 4520-4522.
14. Copeland, K. D.; Fitzsimons, M. P.; Houser, R. P.; Barton, J. K. *Biochemistry* **2002**, *41*, 343-356.
15. Jackson, B. A., Barton, J. K. *J. Am. Chem. Soc.* **1997**, *119*, 12986-12987.
16. Jackson, B. A., Alekseyev, V. Y., Barton, J. K. *Biochemistry* **1999**, *38*, 4655-4662.
17. Jackson, B. A., Barton, J. K. *Biochemistry* **2000**, *39*, 6176-6182.
18. Ciana, L. D.; Hamachi, I.; Meyer, T. J. *J. Org. Chem.* **1989**, *54*, 1731-1735.
19. Gillard, R. D.; Osborn, J. A.; Wilkinson, G. J. *J. Chem. Soc.* **1965**, 1951-1965.
20. Pyle, A. M.; Chiang, M. Y.; Barton, J. K. *Inorg. Chem.* **1990**, *29*, 4487-4495.
21. Murner, H. A.; Jackson, B. A.; Barton, J. K. *Inorg. Chem.* **1998**, *37*, 3007.
22. Jackson, B. A. *Ph.D Thesis* **2000**, California Institute of Technology.
23. Stewart, J. M.; Young, J. D. *Solid Phase Peptide Synthesis*; 2<sup>nd</sup> ed.; Pierce Chemical Company: Rockford, Illinois, 1984.
24. Sarin, V. K.; Kent, S. B. H.; Tam, J. P.; Merrifield, R. B. *Anal. Biochem.* **1981**, *117*, 147-157.
25. Pelton, J. G.; Wemmer, D. E. *Proc. Natl. Acad. Sci. U.S.A.* **1989**, *86*, 5723-5727.
26. Baliga, R.; Crothers, D. M. *J. Am. Chem. Soc.* **2000**, *122*, 11751-11752.
27. Christianson, D. W. *Adv. Prot. Chem.* **1991**, *42*, 281-355.
28.  $K_1 = [ML]/[M][L]$  where M is the metal ion and L is the free amino acid ligand.

29. Sillen, L. G.; Martell, A. E. in *Stability Constants of Metal-Ion Complexes* ed.; The Chemical Society, Burlington House, 1964, pp 504-507.
30. Martell, A. E.; Smith, R. M. in *Critical Stability Constants* ed.; Plenum Press: New York, 1974; Vol. 1, pp 61-62.
31. Perrin, D. D. in *Organic Ligands* ed.; Pergamon Press: Oxford, 1979, pp 412-416.
32. Fitzsimons, M. P.; Barton, J. K. *J. Am. Chem. Soc.* **1997**, *119*, 3379-3380.
33. Fitzsimons, M. P. *Ph.D. Thesis* **1998**, California Institute of Technology.
34. Rajski, S. R.; Jackson, B. A.; Barton, J. K. *Mutation Research* **2000**, *447*, 49-72.
35. SantaLucia, J. *Proc. Natl. Acad. Sci. USA* **1998**, *95*, 1460-1465.
36. Lane, A. N., Peck, B. *Eur. J. Biochem.* **1995**, *230*, 1073-1087.

## **Chapter 5**

### **DNA Crosslinking with Metallointercalator-Peptide Conjugates**

## 5.1. Introduction

Oxidative damage to DNA has been implicated as a factor in aging and in diseases, including cancers, neurodegenerative disorders, and chronic inflammatory diseases.<sup>1-4</sup> Oxidative damage can lead to a variety of DNA lesions, and one important but poorly characterized lesion, is the DNA-protein crosslink.<sup>5-7</sup> Many endogenous and environmental agents can produce covalent links between DNA and protein,<sup>5,6</sup> and these crosslinks are now recognized as a biomarker for aging and disease.<sup>8</sup> The cell likely employs a number of strategies for the removal of these structurally diverse and bulky lesions, and recent studies have suggested a role for nucleotide excision repair proteins and ubiquitin-dependent proteases.<sup>5,9</sup> Here we describe the development of a metallointercalator-peptide conjugate to model and explore DNA-protein crosslinking.

A family of octahedral metallointercalators that bind to and react with DNA have been designed in our laboratory.<sup>10</sup> The metallointercalators are substitutionally inert complexes of rhodium and ruthenium, and they boast planar aromatic ligands. The planar aromatic ligands insert deeply between the DNA base pairs, without causing significant disruptions in DNA conformation.<sup>11</sup> The intercalating and ancillary ligands of these complexes have been varied systematically to achieve site-specificity, and reactivity. As a result, these metallointercalators provide useful probes of DNA structure and DNA-mediated electron transfer.<sup>12,13</sup>

Short peptides can be tethered to metallointercalators to give conjugates with novel recognition or reactive properties. Through the attachment of a 13-mer recognition helix from a DNA binding protein, we transformed a sequence-neutral rhodium complex




into an intercalator that preferentially targets the sequence 5'-TCA-3'.<sup>14</sup> By attaching metal-binding peptides to a rhodium intercalator, we were able to promote hydrolysis or oxidative cleavage of the DNA backbone.<sup>15,16</sup> These studies, as well as studies from other laboratories,<sup>17,18</sup> demonstrate that DNA intercalators can be harnessed for the delivery of peptides to DNA, peptides that would not otherwise bind to DNA.

Dipyridophenazine complexes of ruthenium, such as  $[\text{Ru}(\text{bpy})_2\text{dppz}]^{2+}$  and  $[\text{Ru}(\text{phen})_2\text{dppz}]^{2+}$ , are particularly useful probes for DNA. These complexes have rich spectroscopic properties and show dramatic changes in luminescence on DNA binding. Indeed, they have been dubbed molecular "light switches" for DNA; in aqueous solutions the complexes show no detectable photoluminescence, but on the addition of DNA, intense emission centered around 630 nm is observed.<sup>19,20</sup> Intercalation of the dppz ligand into DNA prevents protonation of the phenazine nitrogen atoms by water, and thus blocks solvent quenching of the luminescence of the excited state.<sup>19</sup> Also, the redox properties of these dppz complexes of ruthenium have facilitated the study of charge transport through DNA.<sup>21,22</sup> In particular, the Ru(III) complex, generated in situ using the flash-quench technique, serves as a potent DNA oxidant, and yields long-range oxidizative damage to DNA.

The flash-quench technique, originally developed for the study of protein electron-transfer,<sup>23</sup> has been successfully adapted for studies with DNA.<sup>21,22,24,25</sup> In a flash-quench experiment (Figure 5.1), a photosensitive DNA intercalator, such as  $[\text{Ru}(\text{phen})_2\text{dppz}]^{2+}$  or  $[\text{Ru}(\text{phen})(\text{bpy}')(\text{dppz})]^{2+}$ , is excited by irradiation with visible light. The excited state species surrenders an electron to an oxidative quencher, and is converted into a strong oxidant (1.6 V). The oxidized intercalator can then undergo back-

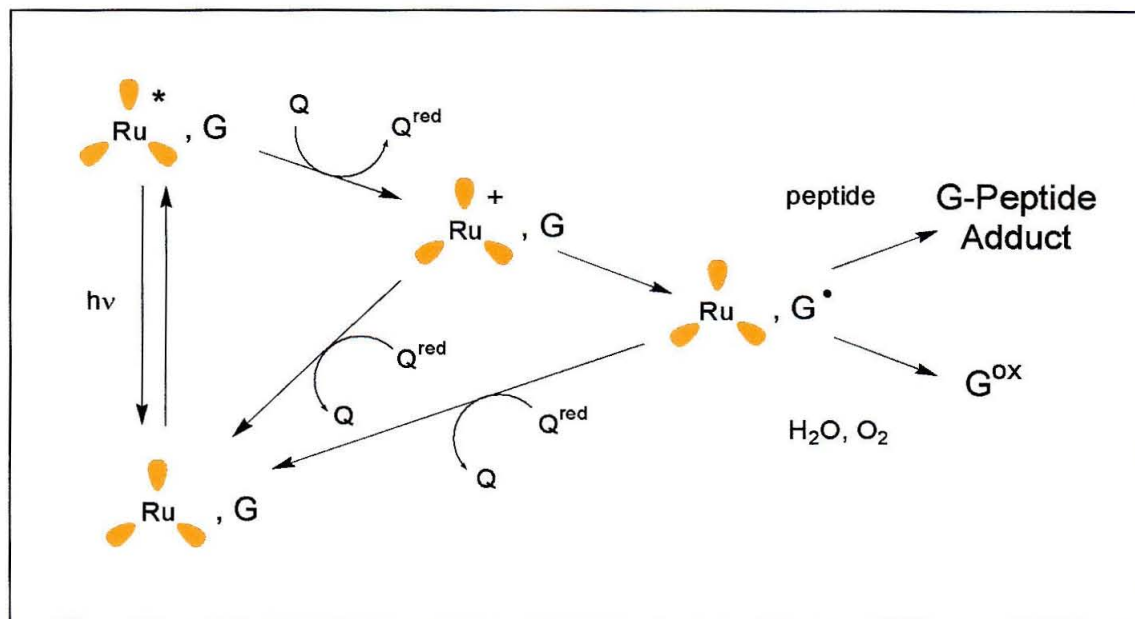


**Figure 5.1. The Flash-Quench Cycle.** The ruthenium intercalator is photoexcited by irradiation at 442 nm. The excited state ruthenium intercalator reacts with an oxidative quencher to produce a strong Ru(III) oxidant. The Ru(III) complex oxidizes guanine sites in DNA to generate guanine radical. Permanent DNA lesions result if the guanine radical reacts with water, oxygen, or peptide. G = guanine,  $\text{G}^\bullet$  = guanine radical,  $\text{G}^{\text{ox}}$  = permanent guanine lesion, Q = quencher, and  $\text{Q}^{\text{red}}$  = reduced quencher,  = ruthenium intercalator.

electron transfer with the reduced quencher, or can steal an electron from a guanine site in DNA.

Of all the DNA bases, guanine boasts the lowest oxidation potential (1.3 V),<sup>26</sup> and is the most vulnerable to oxidative damage, particularly when two or three guanines are clustered together on a DNA strand.<sup>27-29</sup> Using the  $[\text{Ru}(\text{phen})_2\text{dppz}]^{2+}$  intercalator and  $[\text{Ru}(\text{NH}_3)_6]^{3+}$  as quencher in a flash-quench experiment, the neutral guanine radical has been seen in poly(dG-dC) by transient absorption spectroscopy.<sup>25</sup> Because DNA is an effective medium for charge transport, the guanine radical is very mobile in DNA. Indeed, guanine damage has been observed over distances as great as 200 Å from a tethered oxidant.<sup>30-32</sup> Permanent guanine damage results when the guanine radical reacts with oxygen or with water to form products such as 8-oxo-G, Fapy-G, oxazolone, imidazolone, or spiroiminodihydantoin.<sup>33-35</sup>

The flash-quench chemistry of  $[\text{Ru}(\text{phen})_2\text{dppz}]^{2+}$  has also been applied in exploring electron transfer between DNA and proteins. Can proteins sense oxidative damage to DNA or participate in electron transfer reactions with DNA? To probe these questions, we used free  $[\text{Ru}(\text{phen})_2\text{dppz}]^{2+}$  or a DNA-tethered  $[\text{Ru}(\text{phen})(\text{bpy}')(\text{dppz})]^{2+}$  complex and the tripeptides, Lys-Tyr-Lys or Lys-Trp-Lys.<sup>36,37</sup> These peptides bind with modest affinity to DNA; the positively charged Lys residues associate with the polyanionic backbone and the aromatic residue intercalate. The Lys-Trp-Lys-Gly peptide has a dissociation constant of  $5.9 \times 10^{-4}$  M for *E. coli* DNA, and binds with slightly higher affinity to AT alternating sequences or at abasic sites.<sup>38,39</sup> Also, the aromatic residues are thermodynamically vulnerable to oxidation by the guanine radical. The oxidation potentials of Tyr, Trp, and guanine radical are 0.9, 1.0, and 1.3 V.<sup>26,37</sup> With

this system we demonstrated that electron transfer occurs from peptides to DNA. By transient absorption spectroscopy both the Trp and Tyr radical were detected.<sup>36,37</sup> The guanine radical was found to be a key intermediate in the peptide-to-DNA electron transfer; indeed, the rise of the Tyr radical signal and the disappearance of the guanine radical signal occurred with the same kinetics, and no Trp or Tyr radical was observed in studies with a poly(dA·dT) substrate. Importantly, we also discovered that peptide radicals generated by the flash-quench method could react to give DNA-peptide crosslinks. DNA-peptide crosslinking adducts were detected for the Lys-Tyr-Lys peptide but not for the Lys-Trp-Lys peptide.

If proteins are included in the flash-quench reaction, the guanine radical can react with the residues of the protein to form DNA-protein crosslinks. Recently, Stemp et al. introduced this strategy for forming crosslinks.<sup>6</sup> By exploiting the flash-quench chemistry of  $[\text{Ru}(\text{phen})_2\text{dppz}]^{2+}$ , they were able to produce covalent adducts between DNA and histone protein, presumably through the nucleophilic attack of amino acid residues at the guanine radical. Stemp et al. have shown that DNA-protein crosslinking depends on quencher, and in experiments with  $[\text{Co}(\text{NH}_3)_5\text{Cl}]^{2+}$ , methyl viologen, and  $[\text{Ru}(\text{NH}_3)_6]^{2+}$  they found that the cobalt quencher, a sacrificial quencher that decomposes upon reduction, produced the highest levels of crosslinking.<sup>6</sup> With the cobalt quencher, back-electron transfer is not possible, and the lifetime of the guanine radical increases.

Many agents can produce covalent links between DNA and protein. DNA-protein crosslinks have been demonstrated with transition metal complexes, for example, with complexes of Ni(II), Cr(VI), Fe(II), and with 1,10-phenanthroline Cu(II).<sup>40-43</sup> In a recent study, specific crosslinking between the MutY protein and a duplex containing 8-oxoG

was initiated by the one-electron oxidant  $\text{Na}_2\text{IrCl}_6$ .<sup>44</sup> A number of chemotherapeutic reagents, including cisplatin, neocarzinostatin, and Fe(III) bleomycin have also been shown to form DNA-protein crosslinks,<sup>7,43,45,46</sup> and the mutagenic effects of aldehydes have been attributed primarily to DNA-protein crosslinking.<sup>47-49</sup> Finally, crosslinking can be induced by exposure to UV light, visible light with  $^1\text{O}_2$  photosensitizers, or ionizing radiation.<sup>50-55</sup> Although there are many strategies for producing crosslinks, the flash-quench chemistry of  $[\text{Ru}(\text{phen})_2\text{dppz}]^{2+}$  generates a single class of crosslinking products and provides a useful foothold for detailed study of DNA-protein crosslinking.<sup>6</sup> Building on our work with tripeptides and the foundation laid by Stemp et al., we now are using the flash-quench technique to create DNA-peptide adducts.

By attaching very short peptides to a ruthenium intercalator, we have created a model system for DNA-protein crosslinking (Figure 5.2). The ruthenium intercalator,  $[\text{Ru}(\text{phen})(\text{bpy}')(\text{dppz})]^{2+}$ , serves three important roles: (i) through the flash-quench reaction it oxidizes DNA and initiates crosslinking, (ii) it provides binding affinity for peptides that would not otherwise bind to DNA, and (iii) it serves as a fluorescent tag. The peptide provides a variety of functional groups that can react with the oxidized DNA to produce crosslinks, and can be conveniently tuned to explore the potential of different peptide compositions for crosslinking.

We have pursued DNA crosslinking studies with Ru-peptide conjugates for a number of reasons. First, oxidative damage to DNA, including the generation of covalent adducts between DNA and protein, is an important factor in aging and disease. By using simple peptides in the crosslinking reaction we are able to explore the reactivity of individual amino acids, and we may gain valuable insights into the biology of DNA-

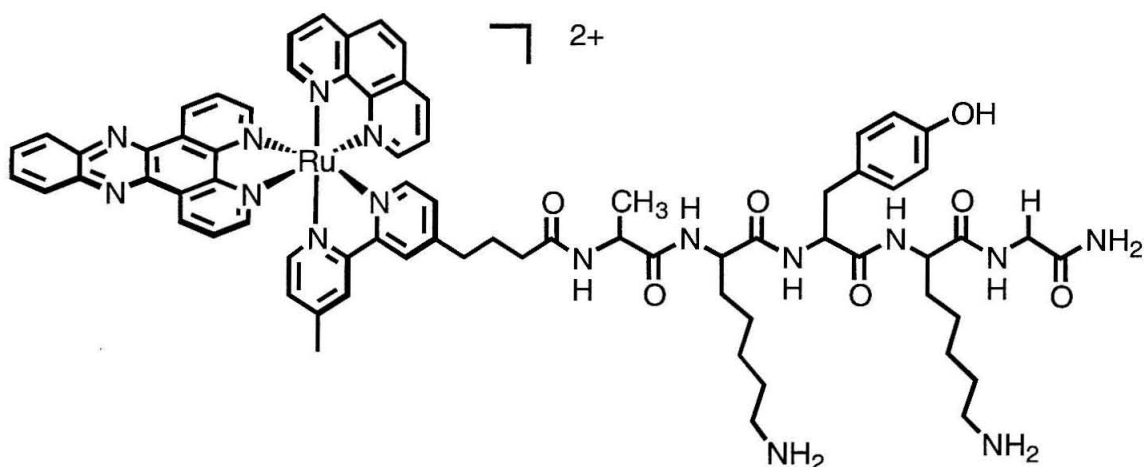


**Figure 5.2. A Ruthenium Metallointercalator-Peptide Conjugate for DNA Crosslinking,  $[\text{Ru}(\text{phen})(\text{bpy}')\text{-AKYKG}(\text{dppz})]^{2+}$ .** The ruthenium intercalator provides binding affinity and participates in a flash-quench reaction that oxidizes DNA. The tethered peptide forms covalent crosslinks at the oxidized site in DNA.

protein crosslinking. Second, the ruthenium-peptide conjugates provide information about the interactions of tethered peptides with DNA, and help us to better understand our Rh-peptide conjugates. The fluorescence of the ruthenium complex allows for convenient determination of the binding constants of conjugates, and the extent of crosslinking is an indicator for close interaction between the DNA and the peptide. Finally, these conjugates might be useful as fluorescent photocrosslinking probes. Once the peptide has forged covalent links with the DNA, the ruthenium complex is also covalently attached and serves as a fluorescent tag.

## 5.2. Materials and Methods

### 5.2.1. Synthesis of Ligands and Metal Complexes.

*Dipyridophenazine (dppz).* The dppz ligand was synthesized according to literature methods.<sup>56</sup>

*4-Butyric acid-4'-methyl-2,2'-bipyridine (bpy').* The bpy' ligand was synthesized according to literature methods.<sup>57,58</sup>

*Bis(1,10-phenanthroline)(dipyridophenazine)-Ruthenium(II) Dichloride, [Ru(phen)<sub>2</sub>dppz]Cl<sub>2</sub>.* The [Ru(phen)<sub>2</sub>dppz]Cl<sub>2</sub> complex was prepared according to literature methods.<sup>59</sup>

*(1,10-Phenanthroline)(4-butyric acid-4'-methyl-2,2'-bipyridine) (dipyridophenazine)-Ruthenium(II) Dichloride, [Ru(phen)(bpy')(dppz)]Cl<sub>2</sub> (Ru).* And the [Ru(phen)(bpy')(dppz)]Cl<sub>2</sub> complex was prepared according to literature methods.<sup>60,61</sup>

### 5.2.2. Preparation of Peptides and Metallointercalator-Peptide Conjugates.

**Automated Peptide Synthesis.** The Beckman Institute Biopolymer Synthesis Facility at Caltech synthesized the peptides on solid support. As described for the Bam peptide (Chapter 2), automated peptide synthesis was carried out with an ABI 433 peptide synthesizer and N-Fmoc-L-amino acids. All peptides were prepared with a carboxamide at the C-terminus. The protecting groups used in the synthesis are as follows: Arg(Pmc), Cys(Trt), Glu(OtBu), His(Trt), Lys(tBoc), Ser(tBu), and Tyr(tBu). The peptides were received on the resin and stored at - 4 °C.

**Deprotection of the N-terminus.** The N-terminal protecting group was manually removed with a 2% solution of 1,8-diazabicyclo[5.4.0]undec-7-ene (DBU) in DMF, and the peptides were cleaved from the resin and deprotected with a cocktail of trifluoroacetic acid (TFA), water, and triisopropylsilane (TIS).

**Preparation of Untethered Peptides.** The peptides were precipitated by filtration into ice-cold t-butyl methyl ether, redissolved in 5% acetic acid, and lyophilized. Next they were HPLC purified on a semipreparative Vyadac C18 reversed phase column using the following solvents: A: water (0.1% TFA) and B: 70:30 water:acetonitrile (0.1% TFA). The percentage of B was held at 10% for 5 minutes and was then increased to 100% over 35 minutes. Chromatograms were monitored at 220 and 260, and the peptides eluted between 8 to 20 minutes. Peptides were quantitated by absorbance measurements, using  $\epsilon_{280} = 1280 \text{ M}^{-1}\text{cm}^{-1}$  for tyrosine containing peptides, and  $\epsilon_{280} = 5690 \text{ M}^{-1}\text{cm}^{-1}$  for tryptophan-containing peptides.<sup>62</sup>

**Preparation of Ruthenium-Peptide Conjugates.** After removal of the N-terminal protecting group, the resin-bound peptides were combined with racemic



[Ru(phen)(bpy')(dppz)]<sup>2+</sup> (1 eq.), PyBOP (3 eq.), and diisopropylethylamine (6 eq.) in DMF and stirred at ambient temperature overnight. As with the free peptides, the conjugates were cleaved from the resin and deprotected with the TFA cocktail, precipitated by filtration into ice-cold t-butyl methyl ether, redissolved in 5% acetic acid, and lyophilized. The intercalator-peptide conjugates were HPLC purified on a semipreparative Vyadac C18 reversed phase column using a water (0.1% TFA)/acetonitrile (0.1% TFA) gradient and a flow rate of 4 mL/min. The percentage of acetonitrile was held at 15% for 5 minutes and then increased from 15 to 40% over 20 minutes. Chromatograms were monitored at 260 and 440 nm, and the desired material eluted between 20 to 25 minutes. After lyophilization, the intercalator-peptide conjugates were obtained as fluffy orange solids in 5 to 20% yield.

### 5.2.3. Characterization of Ruthenium-Peptide Conjugates by UV-Visible

#### Spectroscopy and Mass Spectrometry.

**UV-Visible Spectroscopy.** The spectral characteristics of intercalator-peptide conjugates by UV-visible spectroscopy have been found to be the sum of those of the intercalator and peptide separately. The absorption of [Ru(phen)(bpy')(dppz)]<sup>3+</sup> in the visible region ( $\epsilon = 19,000 \text{ M}^{-1} \text{ cm}^{-1}$  at 440 nm) provides a convenient handle for quantification.

**Mass Spectrometry.** MALDI mass spectrometry was used to verify the identity of the purified chimeras. MALDI MS was carried out by the PPMAL at Caltech using a Voyager-Rp Mass Spectrometer, and results are presented for isomer 1 of each of the conjugates.

**[Ru(phen)(bpy'-AKAKG-CONH<sub>2</sub>)(dppz)]<sup>3+</sup>, Ru-KAK.** MS *m/z* obsd. (calc.):

(Ru-KAK - bpy'KAK)<sup>+</sup> 566.1 (564.5), (Ru-KAK - H)<sup>+</sup> 1274.7 (1274.4), 1418.7 (?).

**[Ru(phen)(bpy'-AKEKG-CONH<sub>2</sub>)(dppz)]<sup>3+</sup>, Ru-KEK.** MS *m/z* obsd. (calc.):

1049.5 (?), (Ru-KEK - phen - H)<sup>+</sup> 1151.5 (1153.2), (Ru-KEK - H)<sup>+</sup> 1332.6 (1332.4), 1476.7 (?).

**[Ru(phen)(bpy'-AKHKG-CONH<sub>2</sub>)(dppz)]<sup>3+</sup>, Ru-KHK.** MS *m/z* obsd. (calc.):

(Ru-KHK)<sup>2+</sup> 671.2 (670.7), (Ru-KHK - H)<sup>+</sup> 1340.5 (1340.5).

**[Ru(phen)(bpy'-AKKKG-CONH<sub>2</sub>)(dppz)]<sup>3+</sup>, Ru-KKK.** MS *m/z* obsd. (calc.):

(Ru-KKK - H)<sup>+</sup> 1331.7 (1331.5).

**[Ru(phen)(bpy'-AKSKG-CONH<sub>2</sub>)(dppz)]<sup>3+</sup>, Ru-KSK.** MS *m/z* obsd. (calc.):

1260.5 (?), (Ru-KSK - H)<sup>+</sup> 1290.5 (1290.4), 1435.6.

**[Ru(phen)(bpy'-AKWKG-CONH<sub>2</sub>)(dppz)]<sup>3+</sup>, Ru-KWK.** MS *m/z* obsd. (calc.):

(Ru-KWK)<sup>2+</sup> 695.2 (695.3), (Ru-KWK - H)<sup>+</sup> 1391.5 (1389.5).

**[Ru(phen)(bpy'-AKYKG-CONH<sub>2</sub>)(dppz)]<sup>3+</sup>, Ru-KYK.** MS *m/z* obsd. (calc.):

(Ru-KYK - H)<sup>+</sup> 1367.7 (1366.5).

**[Ru(phen)(bpy'-ARYRG-CONH<sub>2</sub>)(dppz)]<sup>3+</sup>, Ru-RYR.** MS *m/z* obsd. (calc.):

(Ru-RYR - H)<sup>+</sup> 1422.6 (1422.5).

**[Ru(phen)(bpy'-GAKYKG-CONH<sub>2</sub>)(dppz)]<sup>3+</sup>, Ru-KYK-6.** MS *m/z* obsd. (calc.):

1408.6 (?), (Ru-KHK-6 - H)<sup>+</sup> 1424.6 (1423.5), 1567.6 (?).

**[Ru(phen)(bpy'-AGAAA-CONH<sub>2</sub>)(dppz)]<sup>3+</sup>, Ru-GAA.** MS *m/z* obsd. (calc.):

(Ru-GAA - H)<sup>+</sup> 1146.4 (1146.2).

**[Ru(phen)(bpy'-AGKAG-CONH<sub>2</sub>)(dppz)]<sup>3+</sup>, Ru-GKA.** MS *m/z* obsd. (calc.):

1011.4 (?), (Ru-GKA - H)<sup>+</sup> 1202.6 (1203.3).

$[Ru(phen)(bpy'-AGYAG-CONH_2)(dppz)]^{3+}$ , *Ru-GYA*. MS  $m/z$  obsd. (calc.):  
(*Ru-GYA* - H)<sup>+</sup> 1238.4 (1238.3).

#### 5.2.4. Characterization of Ruthenium-Peptide Conjugates by Circular Dichroism Spectroscopy.

Samples of Ru-peptide conjugate (5  $\mu$ M) were prepared in a sodium borate buffer (25 mM, pH 7), and circular dichroism spectra were obtained with an Aviv 62A DS Instrument.

#### 5.2.5. Determination of DNA Binding Constants of Metallointercalator-Peptide Conjugates.

The  $[Ru(phen)(bpy')(dppz)]^{2+}$  complex is fluorescent in the presence of DNA, and binding constants were determined for several ruthenium-peptide conjugates by fluorescence titration. A dilute solution of the ruthenium-peptide conjugate (0.5  $\mu$ M) was prepared and buffered with sodium phosphate (10 mM, pH 7). High sodium chloride concentrations (100 mM) were used to drop the affinity of the conjugates into a measurable range. The ruthenium-peptide solution was titrated with solutions of calf-thymus DNA (Pharmacia, dialyzed with buffer and quantitated by absorbance at 260 nm). To avoid dilution of the conjugate sample, the DNA solutions were prepared with a matching concentration of ruthenium-peptide. After each addition of DNA, the sample was excited at 442 nm and the emission spectrum was obtained using an ISS K2 Fluorometer. The area under the fluorescence peak was determined and plotted against the log of DNA base pair concentration. The final fluorescence value ( $F_f$ ), the

fluorescence observed for fully bound ruthenium complex, was determined from a sigmoidal fit of this plot, and an initial fluorescence value ( $F_i$ ) was established from the spectrum obtained before the first addition of DNA. The fraction of bound ruthenium complex for each fluorescence measurement ( $F$ ) was determined using the following expression:

$$\text{Bound Ru} / \text{Total Ru} = (F - F_i) / (F_f - F_i)$$

Using this fraction, the concentrations of bound and free ruthenium complex were determined for each DNA concentration, and a Scatchard plot was prepared by plotting  $R/C_{\text{free}}$  vs.  $R$  (where  $R$  = concentration of bound ruthenium / concentration of DNA base pairs, and  $C_{\text{free}}$  = concentration of free ruthenium)<sup>63,64</sup> The binding constant for an average binding site in the DNA substrate was obtained from the y-intercept of this plot, and the number of ruthenium complexes bound per base pair was obtained from the x-intercept.

#### 5.2.6. Flash-Quench Crosslinking with Ruthenium-Peptide Conjugates and DNA.

**Preparation of Oligonucleotides.** The strands of a 20-mer DNA duplex with 1 GG site (5'-TCA GAG TCT GGC TCG CAC TC-3' and complement) and a 40-mer DNA duplex with 4 GG sites (5'-CGT GTA TTA CGG ACT ACG TAG GCT AGC CAG CGT GGA ACG C-3' and complement) were prepared using an ABI 392 DNA synthesizer, purified by HPLC, and annealed by slow cooling from 90 °C.

**Crosslinking Reaction.** In a typical flash-quench crosslinking reaction, the duplex (5  $\mu$ M) was combined with conjugate (20  $\mu$ M) and  $[\text{Co}(\text{NH}_3)_5\text{Cl}]\text{Cl}_2$  quencher (200  $\mu$ M) in a buffer containing sodium phosphate (10 mM, pH 7) and sodium chloride (20 mM). The total volume of each reaction was 20  $\mu$ L. The quencher and ruthenium complex were added in the dark, and the sample was allowed to equilibrate for 10 to 20 minutes. The samples were irradiated at 442 nm for 1 to 30 minutes using a 1000 W Hg/Xe lamp equipped with a monochromator or a He/Cd laser. A light control sample containing only duplex, and a quencher control sample containing duplex and quencher were also irradiated. A dark control sample containing duplex, quencher, and ruthenium conjugate was not irradiated. After irradiations were completed, the samples were extracted with phenol/chloroform to remove noncovalent ruthenium-peptide from the samples.

**Analysis of Crosslinking by Gel Electrophoresis.** For gel experiments, one strand of the DNA duplex was radiolabeled by incubation with  $\gamma$ - $^{32}\text{P}$  ATP and polynucleotide kinase. The labeled strand was purified on a 10% polyacrylamide gel, excised and recovered from the gel by the crush and soak method,<sup>65</sup> and desalted with BioSpin columns (Biorad). The labeled strand was included in an annealing reaction with unlabeled strands. After the flash-quench reaction and extraction procedure, some samples were treated with 10% aqueous piperidine for 30 minutes at 90 °C to promote strand scission. All samples were dried and redissolved in denaturing (formamide, bromophenol blue, and xylene cyanol) or nondenaturing (glycerol and marker dyes) loading buffer. The samples were analyzed on 15 or 20% denaturing gels (2000 V, 2 hours), or on 10 or 15% native gels (150 V, 3 hours). The native gels were dried under

vacuum in a gel drier for 90 minutes at 80 °C. The gels were exposed to phosphor screens and visualized using a Phosphoimager. Using the ImageQuant program, the extent of crosslinking for a sample was estimated by integrating the counts above the parent band (corrected for background) and dividing by the counts in the entire lane (corrected for background).

***Analysis of Crosslinking by Absorbance Measurements.*** For absorbance experiments, ruthenium-peptide (20  $\mu\text{M}$ ), duplex (5  $\mu\text{M}$ ), quencher (200  $\mu\text{M}$ ), and buffer were combined to give a total reaction volume of 200  $\mu\text{L}$ . Prior to the addition of the  $[\text{Co}(\text{NH}_3)_5\text{Cl}]\text{Cl}_2$  quencher, a UV-vis spectrum was obtained for each sample using a Beckman DU 7400 Spectrophotometer, and the absorbance at 440 nm was noted. After adding the quencher, the samples were irradiated for 3 minutes at 442 nm with a He/Cd laser. The samples were mixed once during the irradiation by pipetting. After irradiation the samples were phenol-chloroform extracted, precipitated by the addition of ethanol, dried on the benchtop, and then redissolved in 1:1 water:acetonitrile. A second spectrum was obtained, and the absorbance at 440 nm recorded. The fraction of crosslinked ruthenium-peptide complex was estimated from the ratio of the absorbance at 440 nm after and prior to irradiation and extraction.

#### **5.2.7. Characterization of Crosslinked Material by Spectroscopy and Mass**

##### **Spectrometry.**

To further characterize the crosslinking adducts, two identical samples containing ruthenium conjugate, quencher, and 20-mer duplex were prepared. One was irradiated at 442 nm and one was kept in the dark. Both samples were extracted to remove

noncovalent ruthenium complex, and then were precipitated by the addition of ethanol. The material was redissolved in 1:1 water:acetonitrile and absorption and fluorescence spectra were obtained for each sample using a Beckman DU 7400 Spectrophotometer and an ISS Fluorometer. In addition, several crosslinking samples were analyzed with an Applied Biosystems Voyager DE Pro MALDI TOF Mass Spectrometer. A saturated solution of 2,4,6-trihydroxyacetophenone was used for the laser desorption/ionization matrix.<sup>66</sup>

## 5.3. Results

### 5.3.1. The Creation of Ruthenium-Peptide Conjugates.

Using standard solid-phase peptide coupling strategies, short peptides have been coupled to the  $[\text{Ru}(\text{phen})(\text{bpy}')(\text{dppz})]^{2+}$  complex to create a family of intercalator-peptide chimeras (Figure 5.2, Table 5.1). Although the dppz ligand can decompose in acid, it was found to be stable during peptide deprotection and cleavage, despite a 3 hour treatment with TFA. The conjugates were synthesized cleanly, and with modest overall yields (5 to 20%). The identity of the chimeras was confirmed by mass spectrometry. As was observed for the  $[\text{Rh}(\text{phen})(\text{bpy}'')(\text{chrysi})]^{3+}$  complex (Chapter 4), significant fragmentation occurred during ESI mass spectrometry, and MALDI was a more useful method for study of our ruthenium-peptide conjugates. Preparation of the Ru-AKCKG conjugate was also attempted, but HPLC analysis of the crude material showed a bewildering number of side products. Studies with this conjugate were abandoned.

**Table 5.1. Ruthenium-Peptide Conjugates.**

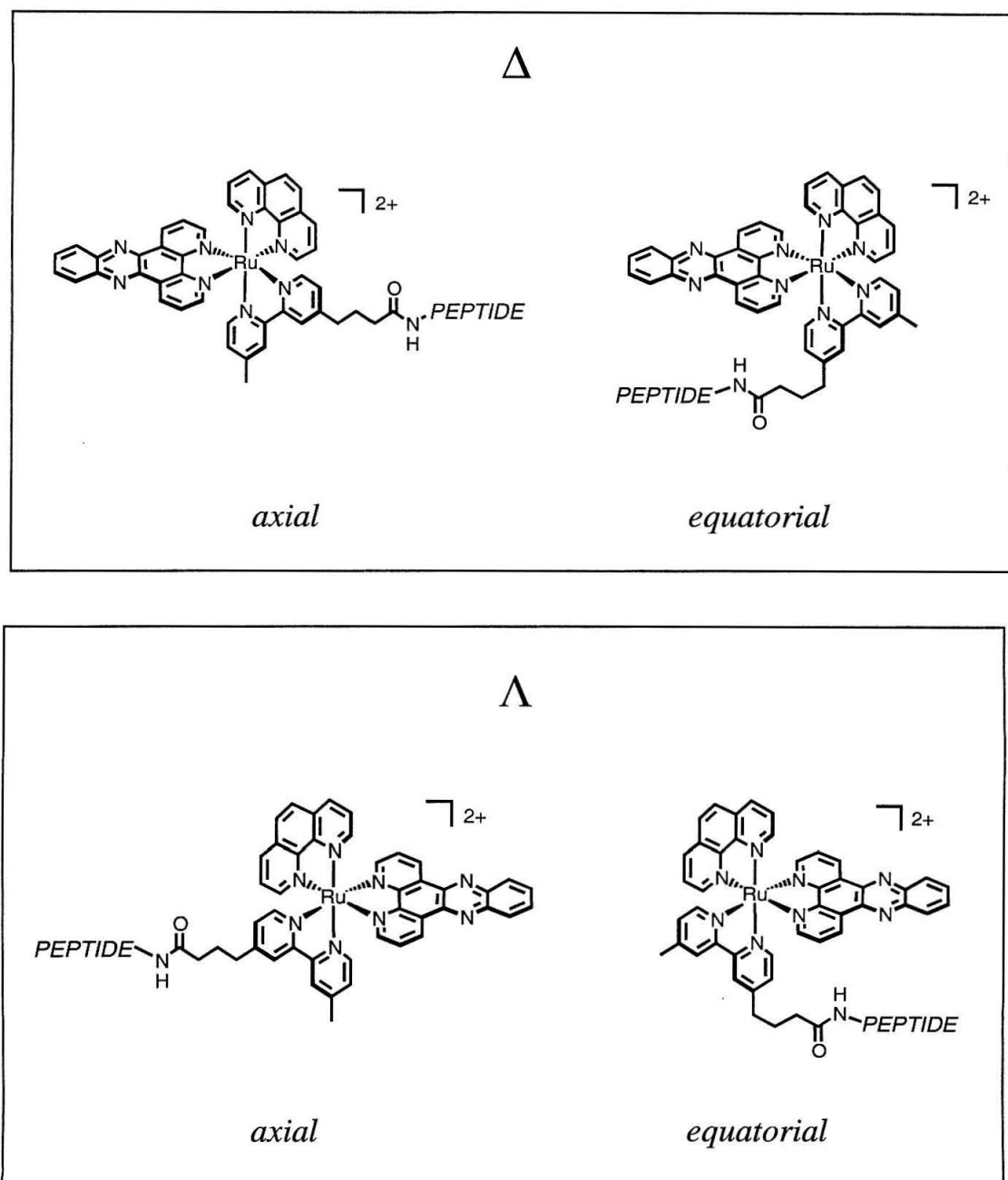
abbreviation	conjugate <sup>a</sup>
<i>Lys-Lys Framework</i>	
Ru-KAK	Ru – Ala-Lys-Ala-Lys-Gly – CONH <sub>2</sub>
Ru-KEK	Ru – Ala-Lys-Ala-Lys-Gly – CONH <sub>2</sub>
Ru-KHK	Ru – Ala-Lys-His-Lys-Gly – CONH <sub>2</sub>
Ru-KKK	Ru – Ala-Lys-Lys-Lys-Gly – CONH <sub>2</sub>
Ru-KSK	Ru – Ala-Lys-Ser-Lys-Gly – CONH <sub>2</sub>
Ru-KWK	Ru – Ala-Lys-Trp-Lys-Gly – CONH <sub>2</sub>
Ru-KYK	Ru – Ala-Lys-Tyr-Lys-Gly – CONH <sub>2</sub>
<i>Arg-Arg Framework</i>	
Ru-RYR	Ru – Ala-Arg-Tyr-Arg-Gly – CONH <sub>2</sub>
<i>6-mer Peptide</i>	
Ru-KYK-6	Ru – Gly-Ala-Lys-Tyr-Lys-Gly – CONH <sub>2</sub>
<i>Gly-Ala Framework</i>	
Ru-GAA	Ru – Ala-Gly-Ala-Ala-Gly – CONH <sub>2</sub>
Ru-GKA	Ru – Ala-Gly-Lys-Ala-Gly – CONH <sub>2</sub>
Ru-GYA	Ru – Ala-Gly-Tyr-Ala-Gly – CONH <sub>2</sub>

<sup>a</sup> Ru = [Ru(phen)(bpy')(dppz)]<sup>2+</sup>

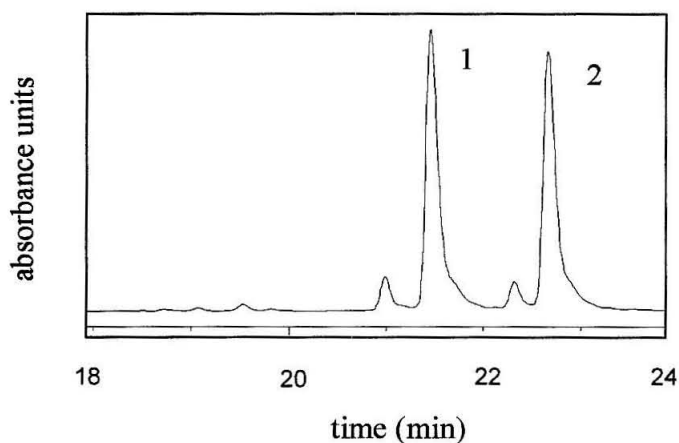
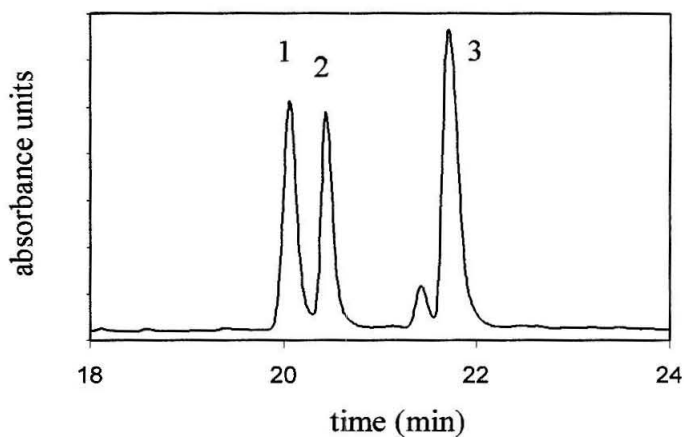


***The Isomers of the Ruthenium Complex.*** The  $[\text{Ru}(\text{phen})(\text{bpy}')(\text{dppz})]^{2+}$  complex has four different isomers (Figure 5.3). The arrangement of ligands around the metal center can be  $\Delta$  or  $\Lambda$ , and the position of the carboxylate linker and peptide arm can be “axial or equatorial” to the dppz ligand. Two of these isomers were easily separated by standard HPLC, and occasionally, depending on peptide composition, the first well-resolved peak was split into two peaks. Two representative HPLC chromatograms are presented in Figure 5.4. Only the Ru-KYK, Ru-KWK, and Ru-RYR conjugates showed significant splitting of the first peak. For the Ru-KYK conjugate the three HPLC peaks were separately collected. All three products were found by MALDI mass spectrometry to be identical, and to have the expected mass of the Ru-KYK conjugate.

To further probe the identity of the separated Ru-KYK products, the material from peaks 1, 2, and 3 was analyzed by circular dichroism spectroscopy (Figure 5.5). Peaks 1 and 2 give intense CD bands with opposite sign; they are clearly enantiomers. The circular dichroism spectrum confirms that peaks 1 and 2 are  $\Delta$  and  $\Lambda$  isomers of the ruthenium complex. Peak 3 is a racemic mixture of the  $\Delta$  and  $\Lambda$  isomers, and gives a flat CD spectrum. As expected, the position of the peptide arm appears to have a greater influence on conjugate mobility than the stereochemistry of the ruthenium metal center. Peaks 1 and 2, eluting near 20 minutes, appear to be one arm arrangement, and peak 3, eluting near 22 minutes, appears to be a different arm arrangement. The small peak that elutes before peak 3 was not collected or analyzed; it may be an impurity or perhaps it is a small amount of separated isomer.



**Figure 5.3. The Four Isomers of the Ruthenium Complex.** The  $[\text{Ru}(\text{phen})(\text{bpy})''(\text{dppz})]^{2+}$  complex has four isomers. The arrangement of ligands about the Ru center can be  $\Delta$  or  $\Lambda$ , and the carboxylate arm can be axial or equatorial to the dppz ligand.

**Ru-AKHKG-CONH<sub>2</sub>****Ru-AKYKG-CONH<sub>2</sub>**

**Figure 5.4. HPLC Purification of Ruthenium-Peptide Conjugates.** The chromatograms at 440 nm are presented for the Ru-KHK and Ru-KYK conjugates. The Ru-KYK, Ru-RYR, and Ru-KWK conjugates showed separation of the faster products (20 to 21 min) into two peaks, but the remaining conjugates did not.

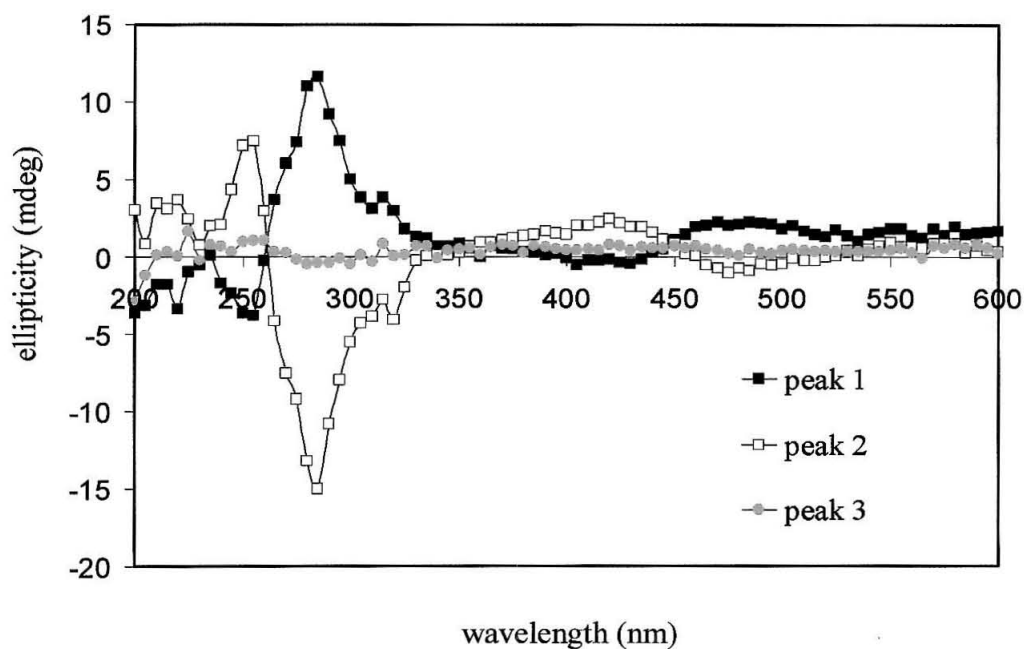


**Figure 5.5. Circular Dichroism Spectra for the Ru-KYK Conjugate.** CD spectra were obtained for the three peaks of the Ru-KYK conjugate isolated by HPLC (See Figure 5.4). The spectra were obtained for 5  $\mu$ M samples of the ruthenium conjugate in sodium borate buffer (25 mM, pH 7).

The ability to separate  $\Delta$  and  $\Lambda$  by HPLC depends on the interactions of the peptide with the ruthenium complex, and the extent of communication between the peptide and ruthenium center varies with peptide composition and with axial or equatorial positioning of the peptide arm. Since many of the conjugates did not show any separation of the peak near 20 minutes, for all of the conjugates only two HPLC fractions were collected and used in experiments. For example, for Ru-KYK, the material from peaks 1 and 2 was combined and is referred to as isomer 1. The material from peak 3 is referred to as isomer 2.

### 5.3.2. DNA Binding Constants of Ru-Peptide Conjugates.

The  $[\text{Ru}(\text{phen})(\text{bpy}')(\text{dppz})]^{2+}$  complex is a DNA “light switch,” it is fluorescent only when bound to DNA.<sup>19</sup> Taking advantage of this property, DNA binding constants were estimated by fluorescence titration for several ruthenium-peptide conjugates (Table 5.2, Figure 5.6). The  $[\text{Ru}(\text{phen})_2\text{dppz}]^{2+}$  complex and our ruthenium-peptide conjugates bind to DNA with high affinity; the binding constant for  $[\text{Ru}(\text{phen})_2\text{dppz}]^{2+}$  has been estimated at  $10^6$  to  $10^7 \text{ M}^{-1}$ .<sup>19,67,68</sup>

For dilute solutions of conjugate (0.5  $\mu\text{M}$ ) in 10 mM sodium phosphate and 100 mM NaCl, the binding constants ranged from  $1 \times 10^6$  to  $9 \times 10^6 \text{ M}^{-1}$ . Like the untethered metallointercalator, all of our conjugates bind tightly to DNA. The attachment of the short peptide does modulate the binding affinity, but not dramatically. As expected, the Ru-GYA conjugate generally gave the smallest binding constants; the presence of Lys residues in the tethered peptide increased the DNA binding affinity. There were modest changes in binding affinity as the central position in the lysine peptide was varied, and

**Table 5.2. Binding Constants of Ruthenium-Peptide Conjugates<sup>a</sup>**

<i>Conjugate</i>	<i>Isomer<sup>b</sup></i>	<i>K (x 10<sup>-6</sup>) M<sup>-1</sup></i>	<i>Ru/base pair</i>
Ru-GYA	1	2	0.3
	2	3	0.7
Ru-KAK	1	5 (0.6)	0.4 (0.1)
	2	5	0.6
Ru-KWK	1	1	0.5
	2	5	0.7
Ru-KYK	1	5 (2)	0.3 (0.1)
	2	9	0.7

<sup>a</sup> Binding constants were determined by fluorescence titration. A 0.5  $\mu\text{M}$  solution of Ru-peptide conjugate in 10 mM sodium phosphate (pH 7) and 100 mM NaCl was titrated with CT DNA, and the change in fluorescence intensity was monitored. Binding constants and Ru/base pair values were determined from Scatchard plots. The values were determined in one or two trials. If two trials were performed, the standard deviation is indicated. The binding constant for  $[\text{Ru}(\text{phen})_2\text{dppz}]^{2+}$  was found to be  $3 \times 10^6 \text{ M}^{-1}$  for a 0.25  $\mu\text{M}$  solution in 10 mM sodium phosphate (pH 7) and 100 mM NaCl.

<sup>b</sup> Two isomers of the Ru-peptide conjugate can be separated by HPLC, and are numbered according to the order of elution.

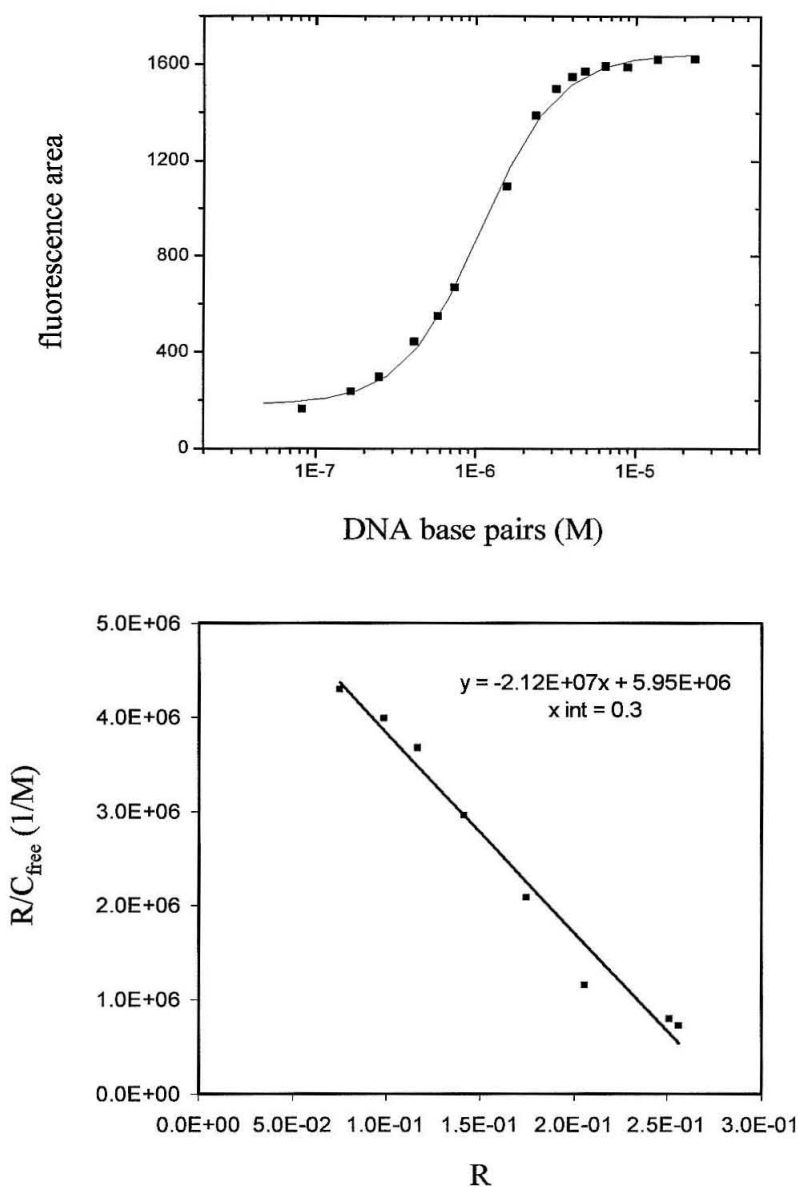


**Figure 5.6. The Determination of Binding Constants by Fluorescence Titration.**

A plot of fluorescence area vs. DNA concentration is presented for isomer 1 of the Ru-AKAKG conjugate (top). The binding constant and the number of conjugates per DNA base pair was determined from a Scatchard plot (bottom).  $C_{\text{free}}$  = concentration of free Ru complex,  $R = [\text{concentration of bound Ru}]/[\text{DNA base pair concentration}]$ .

the binding constants were greatest for the Ru-KYK conjugate. For the Ru-KWK and Ru-KYK conjugates, isomer 2 showed tighter binding than isomer 1. This suggests that the arrangement of the carboxylate arm for isomer 2 produces more favorable interactions of the peptide and DNA.

The number of ruthenium complexes per base pair was also determined from Scatchard plots (Figure 5.6), and ranged from 0.3 to 0.7. These numbers are surprisingly high. Particularly with the pendant 5-mer peptide, we expected no more than one ruthenium complex for every 4 to 5 base pairs (0.2 Ru/bp). It is possible that the ruthenium-peptide conjugates are clustered on the DNA, or perhaps we have not fully optimized the conditions of our titration.

### 5.3.3. Flash-Quench Crosslinking of Ru-Peptide Conjugates and DNA.

We have demonstrated that crosslinks can be generated between Ru-peptide conjugates and DNA using flash-quench chemistry. Ru-peptide conjugates were combined with DNA duplex and  $[\text{Co}(\text{NH}_3)_5\text{Cl}]^{2+}$  quencher, and the samples were irradiated for several minutes at 442 nm. After phenol-chloroform extraction to remove noncovalent conjugate from the sample, crosslinking adducts were detected by gel electrophoresis or by absorbance measurements.

***Gel Analysis of Crosslinking.*** A typical gel experiment with a 20-mer duplex containing a single GG site and two different Ru-peptide conjugates is presented in Figure 5.7. As indicated in Figure 5.1, guanine radical can react with the ruthenium-peptide conjugate, but it also can react with oxygen or water to give a variety of permanent guanine lesions. In our experiments we observe a competition between these



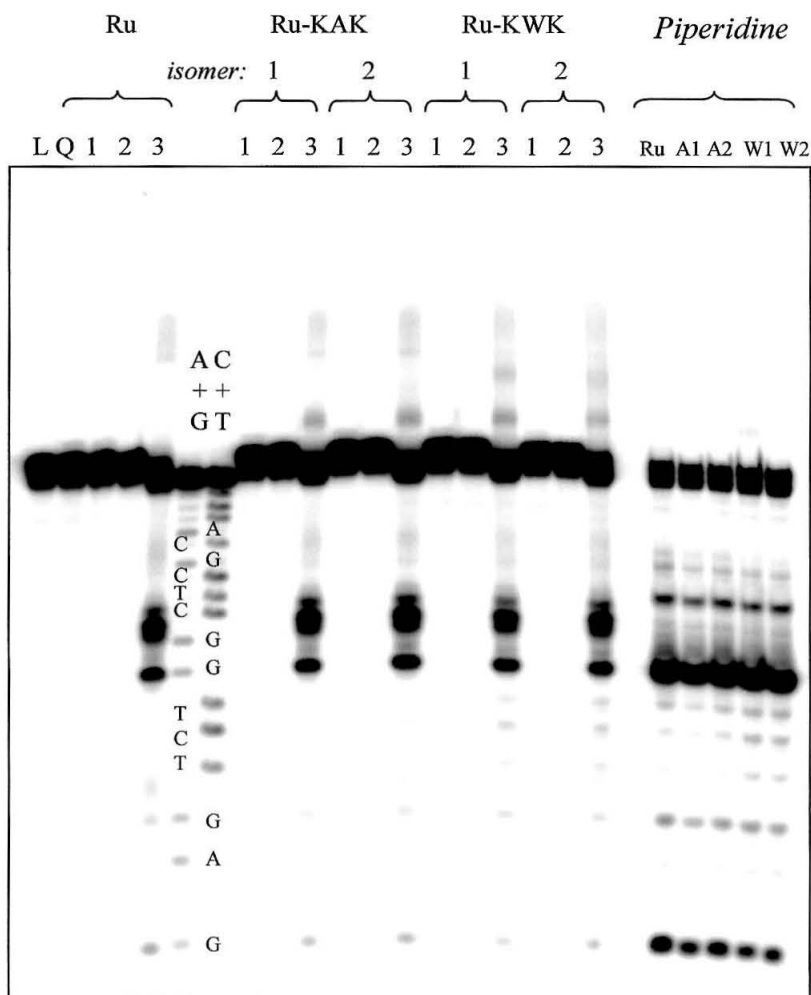


**Figure 5.7. Gel Analysis of Flash-Quench Crosslinking Reactions.** 20-mer duplex (5'-labeled, 5  $\mu$ M) and  $[\text{Co}(\text{NH}_3)_5\text{Cl}]^{2+}$  quencher (200  $\mu$ M) were combined with  $[\text{Ru}(\text{phen})_2\text{dppz}]^{2+}$  (Ru), Ru-KAK, or Ru-KWK (10  $\mu$ M) in a volume of 40  $\mu$ L. The samples were irradiated for 2 min with the lamp. After extraction, crosslinking reactions and control samples were analyzed on a 20% denaturing gel. Lanes are labeled as follows: A+G, C+T, Maxam-Gilbert reactions; L, light control; Q, quencher control; 1, dark control; 2, duplex and Ru irradiated; 3, duplex, quencher, and Ru irradiated. Also, crosslinking reactions were treated with piperidine to promote strand scission.

two pathways. In gel experiments, material above the parent band suggests crosslinking adducts, and material below the parent band indicates reaction with water or oxygen.

With two different peptide conjugates, Ru-KAK and Ru-KWK, a significant amount of material was observed above the parent band on a denaturing polyacrylamide gel (Figure 5.7, Lane 3). Light and quencher are both essential ingredients in the crosslinking reaction, and control samples that were kept in the dark (Lane 1) or that did not contain quencher (Lane 2) showed no signs of crosslinking. The fact that no slow moving material is observed above the parent band in the dark control samples also rules out a gel shift from noncovalent ruthenium complex. It appears that the phenol-chloroform extraction effectively removes noncovalent ruthenium-peptide conjugate from the samples. The ruthenium complex mediates the flash-quench chemistry, and as expected, irradiation of the duplex with light (L), or irradiation of duplex and quencher (Q) produced essentially no damage to the DNA. Interestingly, a small amount of material was also observed above the parent band for  $[\text{Ru}(\text{phen})_2\text{dppz}]^{2+}$  flash-quench reactions, but clearly the peptide greatly enhances crosslinking and produces a different pattern of bands above the parent strand.

Although oxidative damage or crosslinking to a DNA base does not generally produce DNA strand scission, treatment with hot piperidine can promote cleavage at the damaged site.<sup>33</sup> Significant damage occurs at the 5' G of the GG site for both  $[\text{Ru}(\text{phen})_2\text{dppz}]^{2+}$  and Ru-peptide reactions (Lane 3, below parent band). Without piperidine treatment, a variety of oxidative products with different gel mobilities are produced; though they arise from damage at the 5'-G, not all of them migrate at the 5' G.

Upon piperidine treatment, clean strand scission occurs; the material above the parent band disappears, and the fragments observed below the parent band are largely converted into a new product that migrates with the 5' G. Since our crosslinking adducts are piperidine labile, we can conveniently determine the site of crosslinking. Piperidine treatment reveals that the 5' G of the GG site is the primary site of oxidative damage. It is the preferred site for reaction with water and oxygen, but also for reaction with conjugate. The only significant bands to arise upon treatment with piperidine are the bands at the 5' G of the GG site and the bands at the 5' G of a GAG site.

There are some interesting differences between the crosslinking reactions of the Ru-KAK and Ru-KWK conjugates. For Ru-KWK reactions, but not the for Ru-KAK reactions, the smear of slow moving material extends from the parent band to the wells of the denaturing gel. This difference is more easily visualized on a native gel (Figure 5.8), where only the Ru-KWK lanes show material caught in the wells. However, upon piperidine treatment, the Ru-KAK and Ru-KWK lanes on the denaturing gel are essentially the same (Figure 5.7).

The fraction of DNA that has formed crosslinking adducts can be estimated by integrating the counts above the parent band and dividing by the counts in the entire lane. For this experiment, isomer 1 and 2 of Ru-KAK show 4 and 5% crosslinked DNA, and isomer 1 and 2 of Ru-KWK show 6 and 5% crosslinked DNA. Though they produce a different pattern of slow moving material on denaturing gels, the two different conjugates give very similar quantities of crosslinked material. It is important to note that we have not carried out our experiment under single-hit conditions; it is possible that more than one damage event has occurred for each labeled strand. If multiple damage events occur

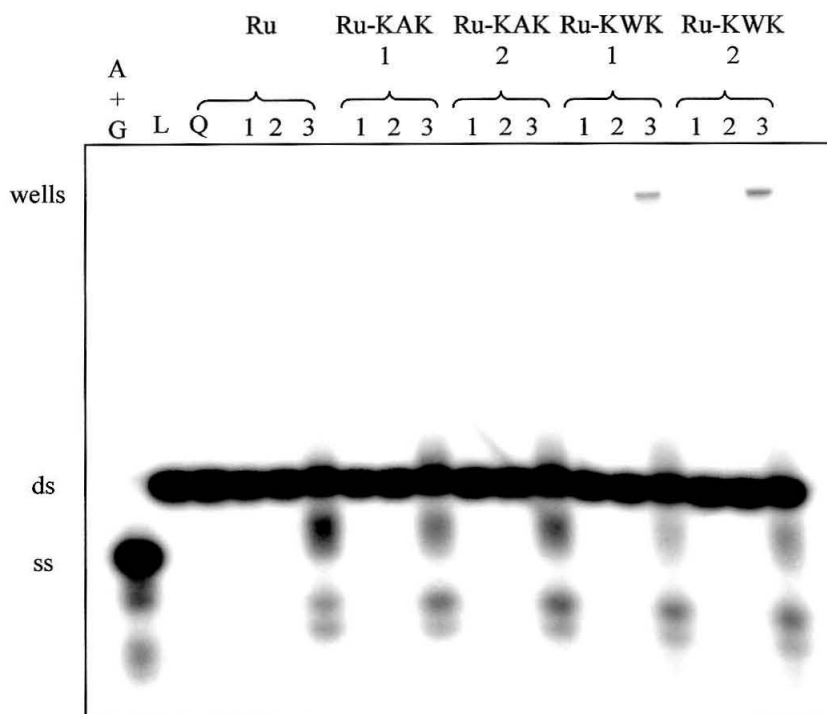


**Figure 5.8. Native Gel Analysis of Flash-Quench Crosslinking Reactions.** 20-mer duplex (5'-labeled, 5  $\mu$ M) and  $[\text{Co}(\text{NH}_3)_5\text{Cl}]^{2+}$  quencher (200  $\mu$ M) were combined with  $[\text{Ru}(\text{phen})_2\text{dppz}]^{2+}$  (Ru), Ru-KAK, or Ru-KWK (10  $\mu$ M) in a volume of 40  $\mu$ L. The samples were irradiated for 2 min with the lamp. After extraction, crosslinking reactions and control samples were analyzed on a 15% native gel. Lanes are labeled as follows: A+G, C+T, Maxam-Gilbert reactions; L, light control; Q, quencher control, duplex irradiated with quencher; 1, dark control; 2, duplex and Ru irradiated; 3, duplex, quencher, and Ru irradiated.

per strand, the percentages we determine from the gel will underestimate the extent of crosslinking.

***Analysis of Crosslinking by Absorbance Measurements.*** We can also detect crosslinking adducts by absorbance measurements. Although this method provides less information about all the flash-quench chemistry that is occurring in our reaction, it does allow us to estimate the percentage of crosslinked ruthenium conjugate. For this experiment, two identical samples of Ru-KYK-6 with quencher and 20-mer duplex were prepared. One was irradiated at 442 nm and one was kept in the dark. Both samples were extracted to remove noncovalent ruthenium complex from the sample, and then were precipitated by the addition of ethanol. The irradiated sample gave an orange pellet that suggested crosslinking, and the dark control sample gave only a white pellet of DNA. The material was redissolved in 1:1 water:acetonitrile and absorption spectra were obtained for each sample. The irradiated sample, but not the dark control sample, showed the expected absorbances for ruthenium complex. By measuring the absorbance at 440 nm of the Ru-KYK-6 sample after the irradiation, extraction, and precipitation procedure, the amount of ruthenium conjugate remaining in the sample was found to be 30% of the original amount of ruthenium conjugate. Again, this number underestimates the extent of crosslinking. We typically use a 20 to 50  $\mu\text{L}$  sample in irradiation experiments, but this experiment required a 200  $\mu\text{L}$  sample. This large volume will not be as effectively irradiated as a small volume. In addition, after precipitation the orange pellet was not always completely resuspended.

#### 5.3.4. The Impact of Peptide Composition on Crosslinking.

To further explore the impact of peptide composition on crosslinking, we prepared a family of ruthenium-peptide conjugates (Table 5.1). Most of our conjugates contained lysine or arginine residues to promote electrostatic interactions with the negatively charged DNA, but we also prepared a few conjugates with the uncharged Ala-Gly-X-Ala-Gly peptide. Although these peptides have lower affinity for DNA, we expected that our ruthenium intercalator would effectively deliver them for crosslinking reaction.

A gel experiment that pits the Ru-KYK conjugate against the Ru-GYA conjugate is pictured in Figure 5.9. In this experiment a 40-mer DNA duplex (5  $\mu\text{M}$ ) with three GG sites was combined with  $\text{Co}(\text{NH}_3)_5\text{Cl}^{2+}$  quencher (200  $\mu\text{M}$ ), and either  $[\text{Ru}(\text{phen})_2\text{dppz}]^{2+}$ , Ru-KYK, or Ru-GYA (20  $\mu\text{M}$ ) in a buffer containing sodium phosphate (10 mM, pH 7) and sodium chloride (20 mM). The samples were irradiated at 442 nm for 0, 2, 5, or 15 minutes (Figure 5.9, Lanes 1-4). Again, material above the parent band suggests crosslinking, and material below the parent suggests reaction of guanine radical with oxygen or water. There is clearly more crosslinking with Ru-KYK than with Ru-GYA. Indeed, in this experiment, the formation of DNA-peptide adducts appears to be the major damage pathway in the presence of Ru-KYK. Prior to piperidine treatment, the levels of damage observed below the parent band are significantly reduced for Ru-KYK samples relative to Ru samples. Nonetheless, the Ru-GYA conjugate does give a significant level of crosslinking, and certainly crosslinks at higher levels than ruthenium complex without tethered peptide.

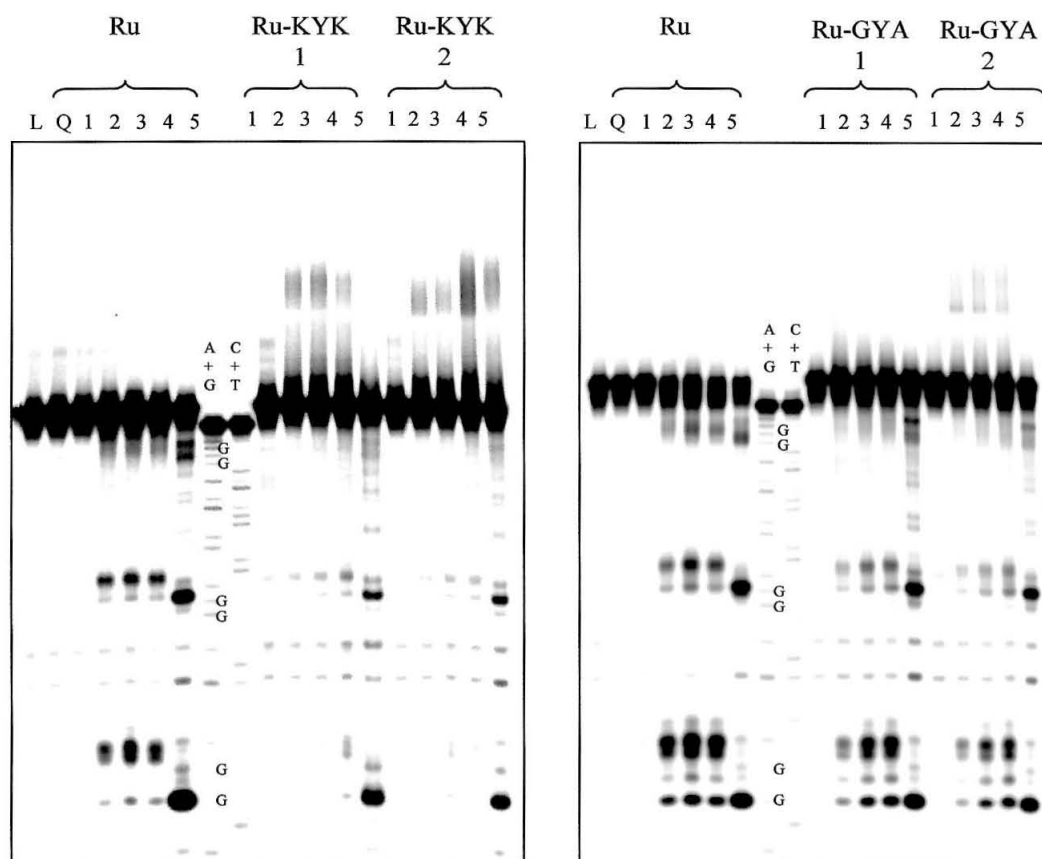


**Figure 5.9. Gel Analysis of Crosslinking with Ru-KYK and Ru-GYA.** 40-mer duplex (5'-labeled, 3 GG sites, 5  $\mu$ M) and  $[\text{Co}(\text{NH}_3)_5\text{Cl}]^{2+}$  quencher (200  $\mu$ M) were combined with  $[\text{Ru}(\text{phen})_2\text{dppz}]^{2+}$  (Ru), Ru-KYK, or Ru-GYA (20  $\mu$ M) in a 20  $\mu$ L volume. The samples were irradiated for varying amounts of time with the Hg/Xe lamp. After extraction, crosslinking reactions and control samples were analyzed on 15% denaturing gels. Lanes are labeled as follows: A+G, C+T, Maxam-Gilbert sequencing reactions; L, light control; Q, quencher control; 1, dark control; 2-4, duplex, ruthenium, and quencher irradiated for 2, 5, and 15 min; 5, duplex, quencher and ruthenium irradiated for 15 min and then treated with piperidine.

Quantitations of the two gels (Table 5.3) give a background level of 4% for the material above the parent band. The lanes for light control, quencher control,  $[\text{Ru}(\text{phen})_2\text{dppz}]^{2+}$ , and dark controls all show approximately 4 to 5% of the lane counts above the parent. The percentage of material above the parent band ranged from 11 to 18% for Ru-KYK and 7 to 10% for Ru-GYA, and did not increase steadily with irradiation time. The data suggest that the reaction is quite efficient, and multiple damage events in one strand may explain the drop in the percentage of material above the parent band with longer irradiation times.

On piperidine treatment (Figure 5.9, Lane 5), the material above the parent band is reduced, and the damage below the parent band is converted into products that migrate with the 5' G of the three GG sites. Because the pattern of damage in ruthenium and ruthenium-peptide conjugate lanes are very similar after piperidine treatment, it appears that we are generating crosslinking adducts primarily at the GG sites. The 5' G is the major damage product revealed by piperidine treatment.

The presence of Lys residues in the peptide clearly has a dramatic impact on crosslinking, and changing the central residue in the peptide can also produce subtle changes in crosslinking patterns (Ru-KYK vs. Ru-KAK). To more systematically explore the impact of peptide composition on crosslinking, a large number of conjugates were compared in a gel experiment and through absorbance measurements. The percentage of crosslinked DNA or crosslinked ruthenium complex was determined for each conjugate and is reported in Table 5.4. As described previously, both the gel and absorbance methods tend to underestimate the extent of crosslinking, but they do allow for rough comparisons between conjugates.



**Table 5.3. Percentage of Crosslinked DNA with Ru-KYK and Ru-AYG Conjugates<sup>a</sup>**

Control Reaction <sup>b</sup>	Length of Irradiation (min)	% Crosslinked DNA by Gel <sup>c</sup>
L	15	4
Q	15	4
Ru	15	4
Conjugate	isomer 1, isomer 2 <sup>d</sup>	
Ru-KYK	0	4, 5
	2	15, 11
	5	15, 11
	15	8, 18
Ru-GYA	0	5, 5
	2	8, 9
	5	7, 10
	15	7, 8

<sup>a</sup> Quantitation of the gel presented in Figure 5.9.

<sup>b</sup> L = light control, duplex irradiated. Q = quencher control, duplex and quencher irradiated. Ru = duplex, quencher, and  $[\text{Ru}(\text{phen})_2\text{dppz}]^{2+}$  irradiated.

<sup>c</sup> The percentage of crosslinked DNA was estimated by integrating the counts above the parent band and dividing by the counts in the entire lane.

<sup>d</sup> Two isomers of the Ru-peptide conjugate can be easily separated by HPLC, and are numbered according to the order of elution.

**Table 5.4. Percentage of Crosslinking Product for Ru-Peptide Conjugates.**

<i>Control Reaction</i>	<i>% Crosslinked Ru by Absorbance<sup>a</sup></i>	<i>% Crosslinked DNA by Gel<sup>b</sup></i>
L	--	1
Ru	6	9
Q Ru-KWK 1	--	2
D Ru-KYK 1	< 1	--
Q Ru-KYK 1	< 1	--

<i>Conjugate</i>	<i>% Crosslinked Ru by Absorbance<sup>a</sup> isomer 1, isomer 2<sup>c</sup></i>	<i>% Crosslinked DNA by Gel<sup>b</sup> isomer 1, isomer 2</i>
Ru-GAA	6, 5	--
Ru-GKA	15, 14	--
Ru-GYA	14, 10	--
Ru-KAK	26, 19	33, 32
Ru-KEK	23, 20	31, 25
Ru-KHK	31, 29	40, 38
Ru-KKK	36, 34	37, 37
Ru-KSK	29, 22	30, 31
Ru-KWK	34, 34	37, 39
Ru-KYK	36, 32	30, 41

Ru-KYK6	39, 31	--
Ru-RYR	21, 22	--

---

<sup>a</sup> The percentage of crosslinked Ruthenium complex was determined by measuring the absorbance at 440 nm of a sample before and after irradiation, extraction, and precipitation.

<sup>b</sup> The percentage of crosslinked DNA was estimated by quantitating the counts above the parent band and dividing by the counts in the entire lane.

<sup>c</sup> Two isomers of the Ru-peptide conjugate can be easily separated by HPLC, and are numbered according to the order of elution.

In absorbance experiments, the 20-mer duplex was combined with ruthenium complex and the intensity of absorbance at 440 nm, a wavelength corresponding to a ruthenium absorbance band, was recorded. After adding quencher, irradiating, extracting, precipitating, and resuspending, the absorbance at 440 nm was again recorded. The spectra for several samples before and after the irradiation and extraction procedure are presented in Figure 5.10. The data from these experiments suggest higher levels of crosslinking with positively charged peptides containing Lys or Arg, and show small changes in the overall levels of crosslinking as the central residue in the peptide is varied (Table 5.4). All the Lys-X-Lys peptides gave 20 to 36% crosslinked ruthenium complex, and the Gly-X-Ala peptides gave 5 to 15%. The Ru-GAA conjugate showed essentially no crosslinking; only 5% of the 440 nm signal was retained after irradiation and extraction. Introducing a single Lys or Tyr increased the extent of crosslinking to 15%. Among the Lys-X-Lys conjugates, the order of increasing crosslinking for this experiment was Ru-KEK < Ru-KAK ~ Ru-KSK < Ru-KHK < Ru-KWK ~ Ru-KYK ~ Ru-KKK. Changing the length of the peptide from a 5-mer to a 6-mer had little impact on the level of crosslinking. The Ru-KYK and Ru-KYK-6 conjugates gave very similar percentages in this absorbance experiment, and also in gel experiments. Though previous gel experiments suggested that conjugates with Arg and Lys were comparable, this absorbance experiment showed reduced crosslinking with Ru-RYR relative to Ru-KYK. The differences in crosslinking between the two isomers were small, and for all the conjugates except Ru-KWK and Ru-RYR, the percentage of crosslinking was slightly higher for isomer 1.

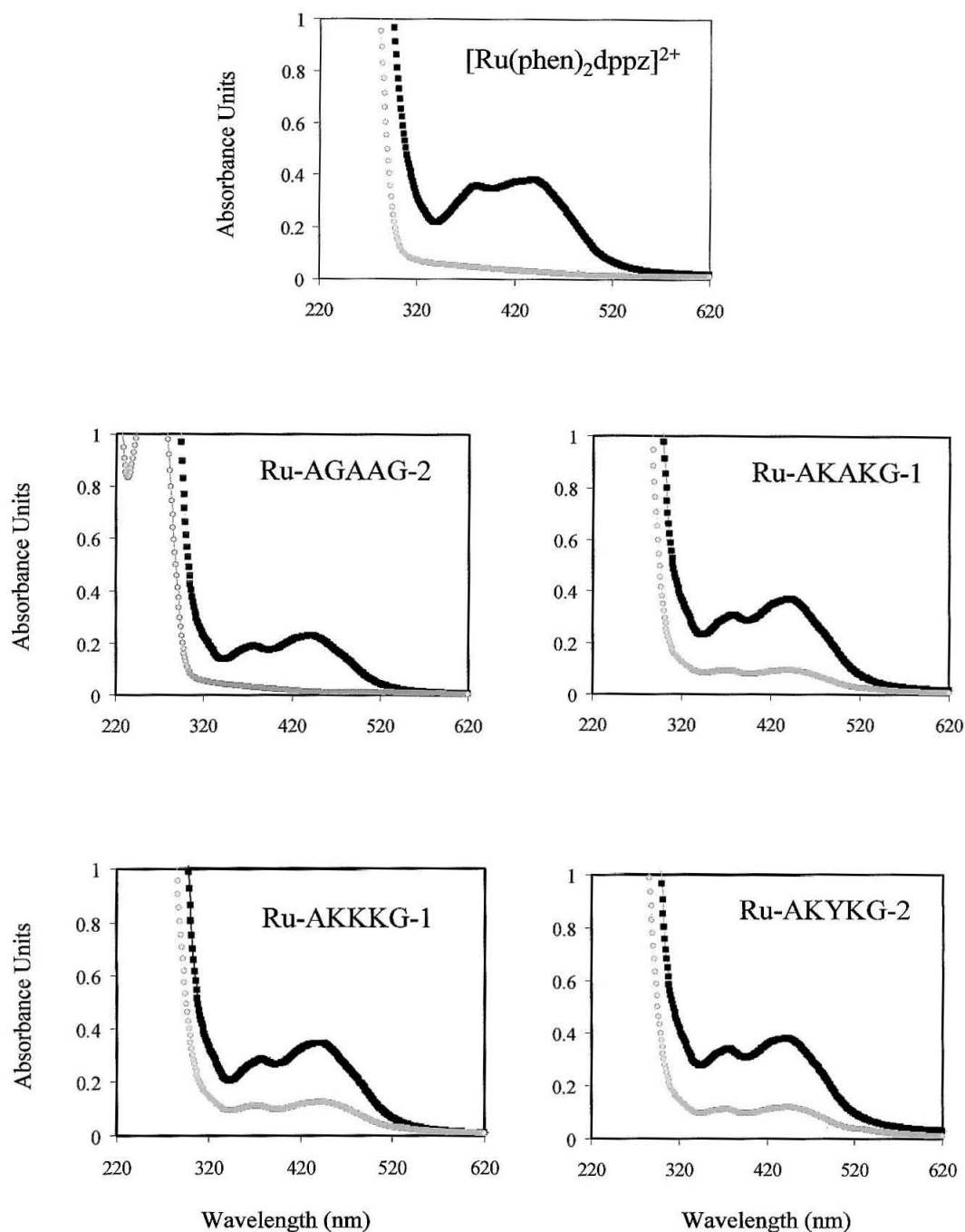


**Figure 5.10. UV-Visible Spectra for Crosslinking Reactions.** The spectra for samples containing  $[\text{Ru}(\text{phen})_2\text{dppz}]^{2+}$  and four different conjugates are presented. The spectra were collected before irradiation (black) and after irradiation and extraction (gray).

A gel experiment with a 40-mer DNA substrate gave very similar data (Table 5.4). The percentage of crosslinked DNA ranged from 25 to 40%. Varying the central residue had a modest impact of crosslinking, and for this one experiment, the order of increasing crosslinking was Ru-KEK < Ru-KSK ~ Ru-KAK < Ru-KKK < Ru-KYK < Ru-KWK < Ru-KHK. Again, the differences in crosslinking between the two isomers were fairly small.

### 5.3.5. The Role of the Ruthenium Metallointercalator in Flash-Quench Crosslinking Reactions.

In our crosslinking system the ruthenium intercalator was expected to play two important roles: (i) to initiate crosslinking through oxidation of DNA or peptide, and (ii) to provide DNA binding affinity for small peptides. Clearly the ruthenium intercalator does initiate crosslinking through the flash-quench cycle. Control samples without ruthenium complex or without quencher showed no crosslinking. To examine whether the ruthenium complex also was required for the delivery of peptides to DNA, we completed experiments with untethered peptide. A typical experiment is presented in Figure 5.11.

We prepared two sets of crosslinking reactions with the 20-mer duplex and cobalt quencher. One set contained a ruthenium-peptide conjugate, and one set contained equal concentrations of untethered peptide and  $[\text{Ru}(\text{phen})_2\text{dppz}]^{2+}$ . The samples were irradiated, extracted, and analyzed by gel electrophoresis. We actually observed greater levels of crosslinking with the free peptides than with the tethered peptides at both 2 and 20  $\mu\text{M}$  concentrations (Figure 5.11, Lanes 2 and 3). Clearly the metallointercalator is not

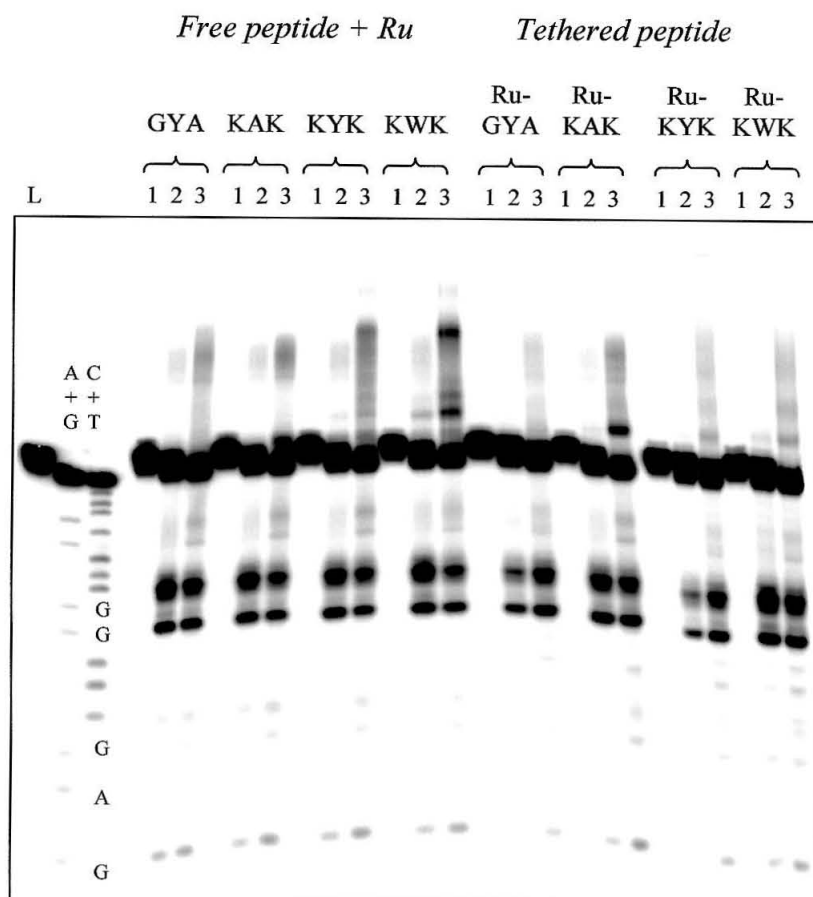


**Figure 5.11. Gel Analysis of Crosslinking with Untethered and Tethered Peptides.**

20-mer duplex (5'-labeled, 5  $\mu$ M) and  $[\text{Co}(\text{NH}_3)_5\text{Cl}]^{2+}$  quencher (200  $\mu$ M) were combined with  $[\text{Ru}(\text{phen})_2\text{dppz}]^{2+}$  (Ru) and free peptide, or with isomer 2 of a Ru-peptide conjugate. The samples were irradiated for 1 min with the He/Cd laser. After extraction, the crosslinking and control samples were analyzed on a 20% denaturing gel. Lanes are labeled as follows: A+G, C+T, Maxam-Gilbert sequencing reactions; L, light control; 1, dark control; 2, duplex, quencher, and either Ru (2  $\mu$ M) and free peptide (2  $\mu$ M), or Ru-peptide conjugate (2  $\mu$ M); 3, duplex, quencher, and either Ru (20  $\mu$ M) and free peptide (20  $\mu$ M), or Ru-peptide conjugate (20  $\mu$ M).

required for peptide delivery. Even for the uncharged GYA peptide, the peptide that is expected to have the lowest affinity for DNA, the crosslinking is greater with free peptide. As has been observed in all gel experiments, the peptides containing Trp and Tyr give a distinctive pattern of bands above the parent band, and create a slow mobility smear that extends right to the wells. This is true both with tethered and free peptides.

### 5.3.6. Characterization of Crosslinked Material by Spectroscopy and Mass

#### **Spectrometry.**

To further characterize the crosslinking adducts, two identical samples of the Ru-KYK-6 conjugate with quencher and 20-mer duplex were prepared. One was irradiated at 442 nm and one was kept in the dark. Both samples were extracted to remove noncovalent ruthenium complex from the sample, and then were precipitated by the addition of ethanol.

**Spectroscopy.** The material was redissolved in 1:1 water:acetonitrile and absorption and fluorescence spectra were obtained for each sample. The irradiated sample, but not the dark control sample, showed the expected absorbances for ruthenium complex in the visible region, and with excitation at 442 nm, gave a fluorescence peak centered around 630 nm (Figure 5.12).

**Mass Spectrometry.** Both samples were submitted for MALDI mass spec. The masses expected for the two intact DNA strands ( $m/z = 6069$  and  $6167$ ) were observed in the dark control sample, but in the irradiated sample the peak corresponding to the strand with the GG site was greatly reduced. Though clearly this strand is being converted into other products, presumably crosslinking products and other oxidative lesions, only one



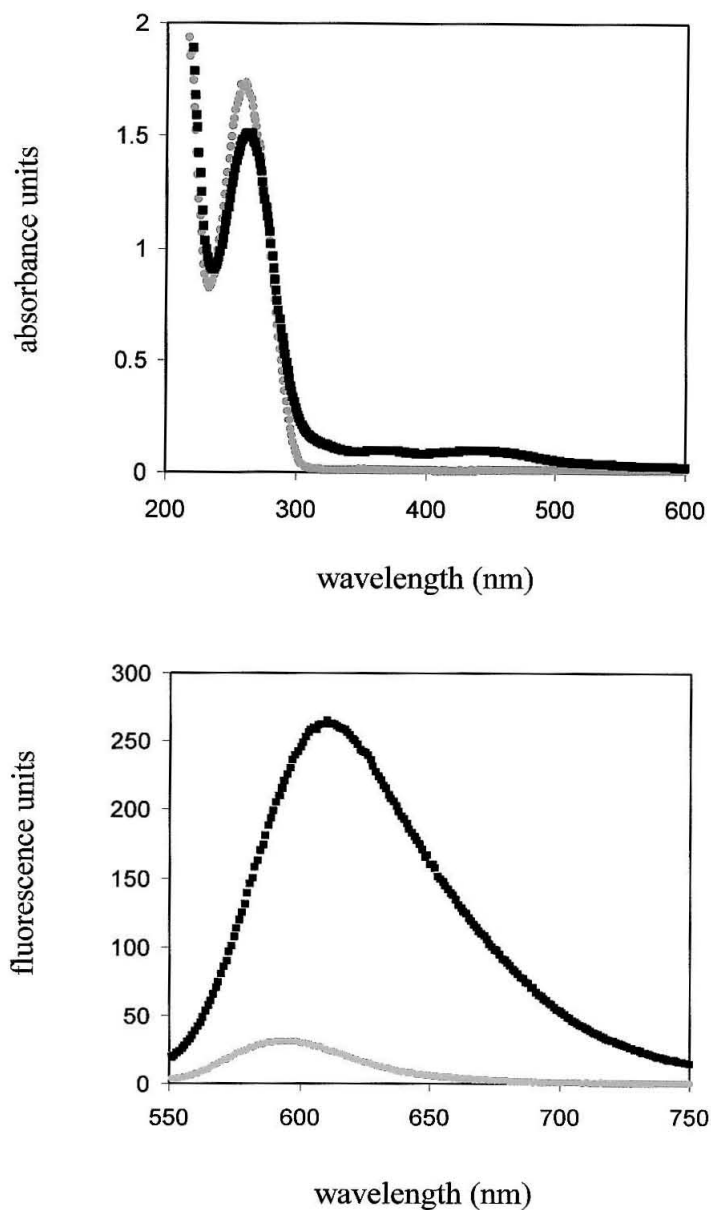


**Figure 5.12. Absorbance and Fluorescence Spectra for Crosslinked Material.**

Two samples of 20-mer duplex, Ru-KYK6, and quencher were prepared, and one sample was irradiated. The absorbance (top) and fluorescence (bottom) spectra for the irradiated (black squares) and dark control (gray circles) samples are shown. To obtain a fluorescence spectrum, the samples were excited at 442 nm.

new peak of lower mass was observed by mass spectrometry ( $m/z = 5977$ ). It appears that the Ru-KYK-6 crosslinking adducts detected on gels and through spectroscopic methods have poor desorption properties.

Although our crosslinking products are not easily analyzed by mass spectrometry, we did identify a crosslinking adduct between Ru-KAK and the 20-mer DNA duplex using MALDI MS. A sample containing Ru-KAK, quencher, and duplex was irradiated, extracted, precipitated, and resuspended. The mass spectrum of this sample showed peaks for the intact DNA strands, but also showed new peaks ( $m/z = 7346$  and  $8626$ ) that match the expected mass for one and two Ru-KAK conjugates crosslinked to strand A of the 20-mer.

## 5.4. Discussion

### 5.4.1. Metallointercalator-Peptide Conjugates as a Model System for Studying DNA-Protein Crosslinking.

To study DNA-protein crosslinking we have tethered short peptides to a ruthenium intercalator. The ruthenium intercalator,  $[\text{Ru}(\text{phen})(\text{bpy}')(\text{dppz})]^{2+}$ , binds with high affinity to DNA, and initiates crosslinking through a flash-quench reaction (Figure 5.1). The peptide provides a variety of functional groups that can react with oxidized DNA to forge crosslinks. In the flash-quench reaction, the Ru(III) complex, a powerful oxidant, is generated in situ by irradiating a sample of Ru-peptide conjugate, oxidative quencher, and DNA with visible light. The Ru(III) complex oxidizes guanine, the base

with the lowest oxidation potential. In turn the guanine radical reacts with water, oxygen, or the tethered peptide to generate permanent DNA damage, either oxidized guanine products or DNA-peptide crosslinks.

Evidence for the formation of DNA-peptide crosslinks was provided by gel analysis and by absorbance measurements. A sample containing Ru-peptide conjugate, DNA duplex, and  $[\text{Co}(\text{NH}_3)_5\text{Cl}]^{2+}$  quencher was irradiated at 442 nm, and then extracted to remove any unlinked Ru-peptide conjugate. For irradiated samples, but not for dark control samples, material that migrates more slowly than the full length DNA strand was detected on denaturing and native polyacrylamide gels (Figure 5.7 and 5.8), and the absorbance bands expected for the Ru-peptide conjugate were observed in the UV-vis spectrum (Figure 5.12). The crosslinking reaction is very efficient; indeed, 30 to 40% of the DNA substrate or ruthenium complex can be crosslinked during a one or two minute irradiation.

Our strategy for DNA-peptide crosslinking is fairly simple. We are able to control important variables and examine crosslinking levels. By systematically mutating our tethered peptide, we have determined the impact of peptide composition on binding and crosslinking. Through experiments with tethered and untethered peptide we have probed the importance of the metallointercalator for delivery of the peptides to DNA.

#### 5.4.2. The Tethered Peptide.

A family of 5-mer peptides was synthesized, and through standard solid-phase peptide coupling strategies, was tethered to the  $[\text{Ru}(\text{phen})(\text{bpy}')(\text{dppz})]^{2+}$  complex (Figure 5.2, Table 5.1). Our method for preparing ruthenium-peptide conjugates is a

general one, and is compatible with a variety of peptide compositions. Only peptides containing cysteine proved troublesome. Apart from studies of DNA-peptide crosslinking, there are a variety of reasons for incorporating a ruthenium metal center into a peptide,<sup>69</sup> and we have established a route to some very interesting chimeras.

For our binding and crosslinking studies we attached 5-mer peptides to our ruthenium complexes. These peptides should be long enough to allow interesting interactions between the peptide and DNA even when the dppz ligand is intercalated into the base stack, and short enough to remain unstructured. The N-terminal Ala was intended as a flexible spacer, the C-terminal Gly simplified synthesis and was intended to adsorb end effects, and the three central residues were varied in our studies. Though we did not thoroughly study the impact of peptide length on binding or crosslinking, we did compare the crosslinking levels of a 5-mer and 6-mer peptide and observed very little difference in gel experiments (data not shown) and absorbance studies (Table 5.4).

In our studies we have considered two types of peptides: peptides with positively charged residues (Lys or Arg) at positions 2 and 4, and peptides with aliphatic residues (Ala and Gly) at positions 2 and 4. Peptides containing lysine and arginine can have favorable electrostatic interactions with the polyanionic backbone of DNA. Also, lysine can serve as a nucleophile to attack oxidized guanine sites. Using a model system, Morin and Cadet have demonstrated that amino or hydroxy nucleophiles form crosslinks with one-electron oxidized 2'-deoxyguanine.<sup>70-72</sup> In contrast, Ala and Gly are simply bystanders; they are not expected to contribute to binding, and they are not expected to be as reactive as lysine or arginine. By creating peptides with Ala and Gly, we focused attention on the reactivity of position 3 of the peptide.

The peptide composition does have a significant impact on binding and crosslinking. Through fluorescence titration we determined that the conjugates bearing lysine residues generally showed greater affinity for DNA than the Ru-GYA conjugate; the additional positive charge of these conjugates increases DNA binding (Table 5.2). The binding constants for Lys-Lys conjugates ranged from  $1 \times 10^6$  to  $9 \times 10^6 \text{ M}^{-1}$ , and the binding constant for the Ru-GYA conjugate was  $2 \times 10^6 \text{ M}^{-1}$ . The Lys-Lys peptides also gave higher levels of crosslinking. In a gel experiment the percentage of crosslinked DNA was approximately two times greater for Ru-KYK than for Ru-GYA (Figure 5.9, Table 5.3).

The central residue in our peptide was tuned to explore the reactivity of individual amino acids. At position 3 we tested 7 different amino acids: Ala, Glu, His, Lys, Ser, Trp, and Tyr. These seven residues provide a variety of functional groups. We expected that incorporation of Ala at the central position would give the least reactive conjugate. With Glu and His we introduce a negatively charged acid group and an imidazole group. From the results of Morin and Cadet we expected Lys and Ser to act as nucleophiles and to attack at the guanine radical.<sup>70-72</sup> The Trp and Tyr peptides are particularly interesting because these aromatic residues can intercalate into DNA, and can be oxidized. Previously, in flash-quench experiments with ruthenium complex and tripeptides, we observed both the Trp and Tyr radical by transient absorption spectroscopy.<sup>36,37</sup> The guanine radical can oxidize Trp and Tyr if they are intercalated into the DNA  $\pi$  stack; therefore, a different crosslinking mechanism, a mechanism that involves a peptide radical, is possible with these two residues. In these previous experiments we did detect DNA-peptide adducts with the Lys-Tyr-Lys peptide, but not the Lys-Trp-Lys peptide. It

may be that we were simply not looking hard enough for crosslinks. In all of our gel experiments with the tripeptides we incubated our samples in hot piperidine, and this treatment releases crosslinked material.

Variation of the central residue did produce some change in binding affinity. The binding constants increased in the order Ru-KWK < Ru-KAK < Ru-KYK. This order is not the order expected for the free peptide. The Trp residue, through intercalation, is expected to contribute binding affinity. By tethering the peptides to an intercalating moiety we constrain them, and perhaps the tethered Trp peptide is not ideally positioned for intercalation into the base stack.

The differences that we observed in crosslinking as we varied the central position in our peptide were actually quite small. The overall levels of crosslinking were very similar for all of the Lys-Lys conjugates. Slightly lower percentages of crosslinked ruthenium were estimated for the Ala, Glu, and Ser conjugates (Table 5.4). Though the levels of crosslinking with Trp and Tyr were not higher than with His or Lys, we did consistently observe a different pattern of slow moving products with conjugates containing these residues (Figure 5.7 and 5.9). Perhaps this is due to different mobility properties of these peptide adducts, but it might also reflect a peptide radical mechanism and a different set of products. On piperidine treatment, the damage pattern observed for Trp and Tyr conjugates is very similar to the pattern observed with all the other conjugates. Even if a Trp or Tyr radical is generated in our flash-quench reactions, we still see permanent lesions primarily at the 5' G of the GG site.

### 5.4.3. The Ruthenium Metallointercalator.

The ruthenium metallointercalator was originally expected to perform three important functions: (i) to produce guanine radical and initiate crosslinking upon irradiation, (ii) to deliver low affinity peptides to DNA, and (iii) to provide a fluorescent tag for the conjugates and crosslinking adducts.

Clearly  $[\text{Ru}(\text{phen})(\text{bpy}')(\text{dppz})]^{2+}$  does perform the first function. Without ruthenium complex, quencher, or irradiation there is no crosslinking between DNA and peptide (Figure 5.7). But must the peptides be harnessed to the ruthenium intercalator in order to achieve efficient crosslinking? To explore the importance of the second function, we compared the crosslinking of untethered and tethered peptides (Figure 5.11). In these experiments,  $[\text{Ru}(\text{phen})_2\text{dppz}]^{2+}$  was included with the untethered peptide, for it is essential to initiation of the flash-quench chemistry.

Our results clearly demonstrate that the peptide does not need to be tethered; indeed, greater levels of crosslinking were actually achieved with free peptide than with the corresponding ruthenium-peptide conjugates (Figure 5.11). The Lys-Trp-Lys and Lys-Tyr-Lys peptides have modest affinity for DNA.<sup>38,39</sup> By attaching these peptides to the ruthenium intercalator we increase their affinity for DNA by at least two orders of magnitude, and increase their concentration near the DNA duplex (Table 5.2). For peptides that do not contain intercalating residues, and especially for the Ala Gly conjugates, the increase in affinity is expected to be even more dramatic. Yet it appears that even peptides that are transiently associated with DNA can be efficiently crosslinked.

In part, the increased crosslinking with the untethered peptide is due to the fact that  $[\text{Ru}(\text{phen})_2\text{dppz}]^{2+}$  has a longer excited state lifetime than the  $[\text{Ru}(\text{phen})(\text{bpy}')$

(dppz)]<sup>2+</sup> complex. It is also possible that by tethering the peptide we constrain important interactions between the peptide and DNA, and reduce the efficiency of crosslinking. The [Ru(phen)(bpy')(dppz)]<sup>2+</sup> complex has four isomers; the arrangement of ligands around the ruthenium center can be  $\Delta$  or  $\Lambda$ , and the carboxylate linker can be axial or equatorial to the dppz ligand. After attachment of our peptides via the carboxylate linker, the two isomers with different arm positions can be easily separated by HPLC. Isomer 2 generally gave higher binding constants (Table 5.2), but did not always give higher levels of crosslinking (Table 5.4). Although we have generated two different isomers that presumably orient the peptide differently relative to the DNA, neither isomer is perfectly suited for peptide delivery.

Although it reduces the extent of crosslinking, there are still compelling reasons for attaching peptides to the ruthenium intercalator. The rich spectroscopic properties of the ruthenium complex provide a convenient absorbance assay that allows for quantitation of crosslinking. Through fluorescence titration the binding constants of ruthenium-peptide conjugates can be directly determined. More importantly, we have demonstrated that the crosslinking adducts generated by the flash-quench technique are photoluminescent. We have created a photoactivated luminescent probe for DNA-peptide crosslinking. Each crosslinking event attaches a fluorescent tag to the DNA.

#### 5.4.4. The Characterization of Crosslinking Adducts.

Though our model system for DNA-peptide crosslinking is fairly simple, though we primarily see crosslinking at GG sites, we still seem to generate a large number of products. In gels, we see a smear of bands above the parent strand rather than a *distinct*



product. It is possible that we are observing multiple crosslinking events on a single DNA duplex, or that we are both fragmenting and crosslinking a single DNA strand. Perhaps the mobility of the crosslinking adduct varies with the interaction of the ruthenium complex with DNA. As was already described, we certainly see a different pattern of products with peptides that contain Trp or Tyr.

We have isolated crosslinking products by extraction and precipitation. Our adducts give the expected absorbances of the ruthenium complex, and are fluorescent (Figure 5.12). Although our products show poor desorption properties, DNA-conjugate adducts were detected by MALDI mass spectrometry. Mass spectrometry clearly shows that the strand containing GG is converted into products of different mass, and with the Ru-KAK conjugate we observed new peaks with masses that matched the expected mass of the DNA strand with one or two covalently linked conjugates.

#### **5.4.5. Insights and Applications for DNA-Protein Crosslinking.**

Our studies with Ru-peptide conjugates have provided some valuable insights into crosslinking chemistry. We have demonstrated that the reaction between oxidized DNA and peptides is very efficient and requires only transient interaction between the DNA and peptide. Although positively charged residues certainly facilitate crosslinking, we have shown that peptides of diverse composition can form crosslinks with DNA.

We have demonstrated a new strategy for generating DNA-peptide adducts at a single GG site in a DNA duplex, and this may provide a useful tool for the study of DNA-protein repair mechanisms.<sup>5</sup> In addition, we are particularly interested in probing the biological relevance of DNA charge-transport, and this study suggests a strategy for

identifying proteins that participate in electron transfer with DNA. By exploiting the flash-quench crosslinking chemistry and the luminescence of a DNA-tethered ruthenium complex, it may actually be possible to “go fishing” in cellular extracts for such proteins.

## 5.5. Conclusions

Short peptides have been tethered to a DNA-intercalating ruthenium complex to create a photoactivated crosslinking reagent. The ruthenium complex,  $[\text{Ru}(\text{phen})(\text{bpy}')(\text{dppz})]^{2+}$ , delivers the peptide to DNA, and initiates the crosslinking reaction by oxidizing DNA upon irradiation in the presence of a quencher. The tethered peptide, only 5 to 6 residues in length, forms crosslinks with the oxidized site in DNA. Crosslinking was detected and studied by gel electrophoresis and through spectroscopic measurements. The ruthenium-peptide complex is fluorescent when bound to DNA, and the binding constants for several intercalator-peptide conjugates were determined by fluorescence titration. The composition of the peptide affects both binding affinity and the extent of crosslinking. The greatest amounts of crosslinking were observed with tethered peptides that contained positively charged residues, either lysine or arginine. To test the impact of individual residues on crosslinking, the central residue in a 5-mer peptide was substituted with seven different amino acids. Though mutation of this position had only a small effect on the extent of crosslinking, it was discovered that peptides containing Trp or Tyr gave a distinctive pattern of products in gels. In experiments using untethered peptide and ruthenium complex, it was determined that

delivery of the peptide by the ruthenium intercalator is not essential for crosslinking; in fact, higher levels of crosslinking were observed with the free peptide. However, the crosslinking adducts produced with ruthenium-peptide conjugates are fluorescent, and thus provide a fluorescent crosslinking probe for DNA.

## 5.6. References

1. Kelly, S. O.; Barton, J. K. *Metal Ions Biol.* **1999**, *36*, 211.
2. Wiseman, H.; Halliwell, B. *Biochem. J.* **1996**, *313*, 17-29.
3. Ames, B. N.; Shigenaga, M. K.; Hagen, T. M. *Proc. Natl. Acad. Sci. U.S.A.* **1993**, *90*, 7915-7922.
4. Marnett, L. J.; Burcham, P. C. *Chem. Res. Toxicol.* **1993**, *6*, 771-785.
5. Minko, I. G.; Zou, Y.; Lloyd, R. S. *Proc. Natl. Acad. Sci. USA* **2002**, *99*, 1905-1909.
6. Nguyen, K. L.; Steryo, M.; Kurbanyan, K.; Nowitzki, K. M.; Butterfield, S. M.; Ward, S. R.; Stemp, E. D. A. *J. Am. Chem. Soc.* **2000**, *122*, 3585-3594.
7. Costa, M. J. *Cell. Biochem.* **1990**, *44*, 127.
8. Izzotti, A.; Cartiglia, C.; Taningher, M.; De Flora, S.; Balansky, R. *Mutat. Res.* **1999**, *446*, 215-223.
9. Quievryn, G.; Zhitkovich, A. *Carcinogenesis* **2000**, *21*, 1573-1580.
10. Erkkila, K. E.; Odom, D. T.; Barton, J. K. *Chem. Rev.* **1999**, *99*, 2777.

11. Kielkopf, C. L.; Erkkila, K. E.; Hudson, B. P.; Barton, J. K.; Rees, D. C. *Nat. Struct. Biol.* **2000**, *7*, 117-121.
12. Johann, T. W.; Barton, J. K. *Phil. Trans. R. Soc. Lond. A* **1996**, *354*, 299-324.
13. Núñez, M. E.; Barton, J. K. *Curr. Op. Chem. Biol.* **2000**, *4*, 199-206.
14. Sardesai, N. Y.; Zimmermann, K.; Barton, J. K. *J. Am. Chem. Soc.* **1994**, *116*, 7502-7508.
15. Fitzsimons, M. P.; Barton, J. K. *J. Am. Chem. Soc.* **1997**, *119*, 3379-3380.
16. Copeland, K. D.; Fitzsimons, M. P.; Houser, R. P.; Barton, J. K. *Biochemistry* **2002**, *41*, 343-356.
17. Sissi, C.; Rossi, P.; Felluga, F.; Formaggio, F.; Palumbo, M.; Tecilla, P.; Toniolo, C.; Scrimin, P. *J. Am. Chem. Soc.* **2001**, *123*, 3169-3170.
18. Tabor, A. B. *Tetrahedron* **1996**, *52*, 2229-2234.
19. Friedman, A. E.; Chambron, J.-C.; Sauvage, J.,-P.; Turro, N. J.; Barton, J. K. *J. Am. Chem. Soc.* **1990**, *112*, 4960-4962.
20. Hartshorn, R. M.; Barton, J. K. *J. Am. Chem. Soc.* **1992**, *114*, 5919-5925.
21. Murphy, C. J.; Arkin, M. R.; Jenkins, Y.; Ghatlia, N. J.; Bossmann, S. H.; Turro, N. J.; Barton, J. K. *Science* **1993**, *262*, 1025-1029.
22. Arkin, M. R.; Stemp, E. D. A.; Pulver, S. C.; Barton, J. K. *Chem. Biol.* **1997**, *4*, 389-400.
23. Chang, I. J.; Gray, H. B.; Winkler, J. R. *J. Am. Chem. Soc.* **1991**, *113*, 7056.
24. Dunn, D. A.; Lin, V. H.; Kochevar, I. E. *Biochemistry* **1992**, *31*, 11620.
25. Stemp, E. D. A.; Arkin, M. R.; Barton, J. K. *J. Am. Chem. Soc.* **1997**, *119*, 2921.
26. Steenken, S.; Jovanovic, S. V. *J. Am. Chem. Soc.* **1997**, *119*, 617.

27. Sugiyama, H.; Saito, I. *J. Am. Chem. Soc.* **1996**, *118*, 7063-7068.
28. Prat, F.; Houk, K. N.; Foote, C. S. *J. Am. Chem. Soc.* **1998**, *120*, 845-846.
29. Nakatani, K.; Dohno, C.; Saito, I. *J. Am. Chem. Soc.* **1999**, *121*, 10854-10855.
30. Núñez, M. E.; Hall, D. B.; Barton, J. K. *Chem. Biol.* **1999**, *6*, 85.
31. Schuster, G. B. *Acc. Chem. Res.* **2000**, *33*, 253-260.
32. Giese, B. *Acc. Chem. Res.* **2000**, *33*, 631-636.
33. Burrows, C. J.; Muller, J. G. *Chem. Rev.* **1998**, *98*, 1109-1151.
34. Luo, W.; Muller, J.; Rachlin, E. M.; Burrows, C. J. *Org. Lett.* **2000**, *2*, 613-616.
35. Cadet, J.; Berger, M.; Buchko, G. W.; Joshi, P. C.; Raoul, S.; Ravanat, J.-L. *J. Am. Chem. Soc.* **1994**, *116*, 7403-7404.
36. Wagenknecht, H.-A.; Stemp, E. D. A.; Barton, J. K. *J. Am. Chem. Soc.* **2000**, *1*, 1-7.
37. Wagenknecht, H.-A.; Stemp, E. D. A.; Barton, J. K. *Biochemistry* **2000**, *39*, 5483-5491.
38. Rajeswari, M. R.; Montenay-Garestier, T.; Helene, C. *Biochemistry* **1987**, *78*, 926.
39. Rajeswari, M. R. *J. Biomol. Struct. Dyn.* **1996**, *14*, 25.
40. Chakrabarti, S. K.; Bai, C. J.; Subramanian, K. S. *Toxicol. Appl. Pharmacol.* **2001**, *170*, 153-165.
41. Izzoti, A.; Cartiglia, C.; Taningher, M.; De Flora, S.; Balansky, R. *Mutat. Res.* **1998**, *440*, 233-244.
42. Altman, S. A.; Zastawny, T. H.; Randers-Eichhorn, L.; Cacciuttolo, M. A.; Akman, S. A.; Dizdaroglu, M.; Rao, G. *Free Radical Biol. Med.* **1995**, *19*, 897.
43. Gavin, I. M.; Melnick, S. M.; Yurina, N. P.; Khabarova, M. I.; Bavykin, S. G. *Anal. Biochem.* **1998**, *263*, 26.

44. Hickerson, R. P.; Chepanoske, C. L.; Williams, S. D.; David, S. S.; Burrows, C. J. *J. Am. Chem. Soc.* **1999**, *121*, 9901.
45. Pinto, A. J.; Lippard, S. J. *Biochim. Biophys. Acta* **1985**, *780*, 167-180.
46. Hashimoto, M.; Greenberg, M. M.; Kow, Y. W.; Hwang, J.-T.; Cunningham, R. P. *J. Am. Chem. Soc.* **2001**, *123*, 3161-3162.
47. Voitkun, V.; Zhitkovich, A. *Mutat. Res.* **1999**, *424*, 97-106.
48. Shaham, J.; Bomstein, Y.; Meltzer, A.; Kaufman, Z.; Palma, E.; Ribak, J. *Carcinogenesis* **1996**, *17*, 121.
49. Conaway, C. C.; Whysner, J.; Verna, L. K.; Williams, G. M. *Pharmacol. Ther.* **1996**, *71*, 29-55.
50. Saito, I.; Matsura, T. *Acc. Chem. Res.* **1995**, *18*, 134-141.
51. Shetlar, M. D. *Photochem. Photobiol. Rev.* **1980**, *5*, 105-197.
52. Strniste, G. F.; Rall, S. C. *Biochemistry* **1976**, *15*, 1712.
53. Blazek, E. R.; Hariharan, P. V. *Photochem. Photobiol.* **1984**, *40*, 5.
54. Ramakrishnan, N.; Clay, M. E.; Xue, L.; Evans, H. H.; Rodriguez-Antunez, A.; Oleinick, N. L. *Photochem. Photobiol.* **1988**, *48*, 297.
55. Villanueva, A.; Canete, M.; Trigueros, C.; Rodriguez-Borlado, L.; Juarranz, A. *Biopolymers* **1993**, *33*, 239.
56. Dickeson, J. E.; Summers, L. A. *Austr. J. Chem.* **1970**, *23*, 1023.
57. Ciana, L. D.; Hamachi, I.; Meyer, T. J. *J. Org. Chem.* **1989**, *54*, 1731-1735.
58. Gillard, R. D.; Osborn, J. A.; Wilkinson, G. J. *J. Chem. Soc.* **1965**, 1951-1965.
59. Amouyal, E.; Hornsi, A.; Chambron, J. C.; Sauvage, J. P. *J. Chem. Soc., Dalton Trans.* **1990**, *6*, 1841.

60. Strouse, G. F.; Anderson, P. A.; Schoonover, J. R.; Meyer, T. J.; Keene, F. R. *Inorg. Chem.* **1992**, *31*, 3004-3006.
61. Anderson, P. A.; Deacon, G. B.; Haarmann, K. H.; Keene, R.; Meyer, T. J.; Reitsma, D. A.; Skelton, B. W.; Strouse, G. F.; Thomas, N. C.; Treadway, J. A.; White, A. H. *Inorg. Chem.* **1995**, *34*, 6145-6157.
62. Gill, S. C.; von Hippel, P. H. *Anal. Biochem.* **1989**, *182*, 319-326.
63. Scatchard, G. *Ann. N. Y. Acad. Sci.* **1949**, *51*, 660-672.
64. Klotz, I. M. *Ligand-Receptor Energetics*; John Wiley & Sons, Inc.: New York, 1997.
65. Maniatis, T.; Fritsch, E. F. *Molecular Cloning*; Cold Spring Harbor Laboratory: Plainview, New York, 1982.
66. Jensen, O. N.; Kulkarni, S.; Aldrich, J. V.; Barofsky, D. F. *Nucl. Acids Res.* **1996**, *24*, 3866-3872.
67. Haq, I.; Lincoln, P.; Suh, D.; Nordén, B.; Chowdry, B. Z.; Chaires, J. B. *J. Am. Chem. Soc.* **1995**, *117*, 4788-4796.
68. Lincoln, P.; Broo, A.; Nordén, B. *J. Am. Chem. Soc.* **1996**, *118*, 2644-2653.
69. Kise, K. J.; Bowler, B. E. *Inorg. Chem.* **2002**, *41*, 379-386.
70. Cadet, J.; Morin, B. *Photochem. Photobiol.* **1994**, *60*, 102-109.
71. Cadet, J.; Morin, B. *Chem. Res. Toxicol.* **1995**, *8*, 792-799.
72. Cadet, J.; Morin, B. *J. Am. Chem. Soc.* **1995**, *117*, 12408-12415.

## **Chapter 6**

### Conclusions



## 6.1. Conclusions

DNA metallointercalators are useful tools for probing the structure and electronic properties of DNA.<sup>1,2</sup> We have extended the reach and expanded the functional diversity of our metallointercalators by tethering peptides through an ancillary ligand. We have now demonstrated that metallointercalator-peptide chimeras can participate in a variety of reactions with DNA. Tethered metal-binding peptides can promote hydrolysis or oxidative scission of the DNA backbone, and ruthenium-peptide conjugates can form crosslinks with DNA.

Our chimeras combine the rich spectroscopic and chemical properties of the metallointercalator with peptide chemistry. The metallointercalator contributes affinity for DNA, and can be tuned for sequence-selective binding. In addition, the  $[\text{Rh}(\phi)_2\text{bpy}]^{3+}$  intercalator serves as a photoreactive probe,<sup>3</sup> and the  $[\text{Ru}(\text{phen})(\text{bpy})(\text{dppz})]^{2+}$  intercalator oxidizes the DNA through a flash-quench reaction.<sup>4</sup> The peptide portion of our chimera provides a collection of functional groups that can deliver metals to the DNA backbone, or serve as nucleophiles. Peptides are conveniently prepared from readily available building blocks, and are easily coupled to metallointercalators through standard solid-phase techniques.<sup>5</sup>

To achieve DNA hydrolysis and create an artificial nuclease, we have tethered  $\text{Zn}^{2+}$ -binding peptides to the  $[\text{Rh}(\phi)_2\text{bpy}]^{3+}$  complex. Marilena Fitzsimons first demonstrated that a metallointercalator-peptide conjugate, Rh-P1, could cleave both plasmid and linear DNA substrates.<sup>6</sup> The P1 peptide is a designed  $\alpha$ -helix with two histidine residues for  $\text{Zn}^{2+}$  coordination. Importantly, we have now achieved plasmid

cleavage with a widely different tethered peptide. The Rh-Bam conjugate contains a 22-mer peptide that is modeled after a hairpin in the *Bam*HI endonuclease. The peptide includes several acidic residues, and in *Bam*HI, these residues position water and metal ions for catalysis. In the presence of  $\text{Zn}^{2+}$  and at pH 6, the Rh-Bam conjugate converts supercoiled plasmid to a nicked product. With both Rh-P1 and Rh-Bam, DNA cleavage is achieved under mild conditions and with low conjugate concentrations.

There are some important differences between the Rh-P1 and Rh-Bam conjugate. Rh-P1 is very sensitive to  $\text{Zn}^{2+}$  concentration, and shows maximum cleavage activity with stoichiometric metal. In contrast, Rh-Bam tolerates a range of metal concentrations and a wide variety of metal ions. Also, we have not observed the cleavage of linear DNA substrates by Rh-Bam, and thus we have not been able to directly establish a hydrolytic mechanism. Of course, the requirement for  $\text{Zn}^{2+}$  and other similarities with Rh-P1, make a hydrolytic mechanism very probable.

Although we have not created a more active conjugate with Rh-Bam, we have demonstrated that our strategy for DNA hydrolysis is a general one. This general strategy has a number of important features. The composition of an appended peptide can be conveniently mutated to test or tune reactivity. In contrast to many of the artificial nucleases described in the literature, our conjugates bind tightly to DNA. The intercalator provides binding affinity and allows us to cleave DNA using only micromolar concentrations. The intercalator also provides a photoreactive probe for conjugate binding. In addition, as we have demonstrated with the mismatch-specific Rh''C-AH conjugate, the metallointercalator can be modified to achieve sequence-selective binding and reaction.

Again, our artificial nucleases can be tuned through mutation of the peptide, and we sought to optimize the composition of the P1 peptide using combinatorial chemistry. A library containing over 16,000 metallointercalator-peptide conjugates was prepared by split-pool synthesis. Our conjugates were compatible with highly parallel synthesis strategies, and with Edman decoding, but we were unable to develop a high throughput screening strategy. We were only able to screen a small fraction of our library, and not surprisingly, we did not identify conjugates with robust hydrolysis activity.

To achieve oxidative scission of the backbone we have used our metallointercalator-peptide conjugates to deliver  $\text{Cu}^{2+}$  to DNA. The Rh-P1 conjugate and conjugates with shorter histidine-containing peptides promote DNA cleavage in the presence of copper and a reducing agent, such as MPA. This copper reaction is easier to achieve than hydrolysis, and has provided some interesting information about the interactions of tethered peptides with DNA.

Although in the past we have used peptides to confer sequence selectivity on a metallointercalator,<sup>8,9</sup> the tethered peptides used in our recent studies do not significantly change the binding preferences of the rhodium complex. The photocleavage intensity of the rhodium intercalator is reduced slightly, particularly by bulky peptides, but the pattern of damage is not perturbed. With  $[\text{Rh}(\text{phi})_2\text{bpy}]^{3+}$  we observed sequence neutral binding, with a slight preference for 5'-ACGX-3' sites.

Although our conjugates bind throughout a restriction fragment or oligonucleotide, the copper reaction is actually quite selective, and primarily occurs at A/T-rich regions. The greatest amount of copper damage was actually observed with a short, unstructured peptide (AHAAHA) that was not optimized for copper binding. The

size of the P1 peptide may actually be a liability as it is able to sample many non-reactive conformations.

Peptides have many attractive features, but there are also clearly some disadvantages to employing peptides for reaction with DNA. Whether borrowed from nature or thoughtfully designed, our tethered peptides are largely unstructured. The helical content of the P1 peptide was less than 30%, and the Bam peptide showed no evidence of hairpin formation. In contrast with a protein, a metallointercalator has no power to direct the conformation of a peptide or the orientation of a peptide relative to DNA. The flexibility of the tethered peptide limited our ability to predictably design chimeras for DNA recognition,<sup>8,9</sup> and it has also limited our ability to create and deliver reactive moieties to DNA. A floppy peptide does not create an effective coordination environment for a metal, and we have had little control over the stoichiometry of metal binding or the solubility of our metal.

Recently we have used metallointercalator-peptide conjugates for a very different reaction with DNA. By attaching 5-mer peptides to the  $[\text{Ru}(\text{phen})(\text{bpy}')(\text{dppz})]^{2+}$  intercalator we have created DNA crosslinking reagents. Through a flash-quench reaction the ruthenium intercalator oxidizes DNA and generates guanine radicals.<sup>10</sup> Peptides, tethered or untethered, can react with the oxidized guanine to forge covalent links to DNA. The ruthenium intercalator is fluorescent, and thus we have developed a fluorescent DNA crosslinking probe.

The crosslinking reaction is extremely efficient, and the extent and pattern of crosslinking varies with peptide composition. To achieve high levels of crosslinking (30 to 40%), the peptide must contain lysine or arginine residues. Our system has allowed us

to study the individual reactivity of amino acids, and we have observed a distinct pattern of damage with peptides containing Tyr or Trp.

Thus, metallointercalator-peptide conjugates are versatile tools for targeting and manipulating DNA. We have created artificial nucleases, oxidative cleavage reagents, and now a ruthenium-peptide conjugate for DNA crosslinking. Our approach to DNA hydrolysis provides a foothold for the future design of artificial nucleases. While the metal-peptide structures and their orientations on the DNA helix require better definition and control, our conjugates do possess several attractive features. For example, we have demonstrated that intercalators can be a very effective component of an artificial nuclease. Our copper-binding conjugates provide reliable and predictable cleavage of linear DNA substrates, and with these conjugates we have demonstrated a new strategy for cleavage at mismatch sites. Tethered peptides may not be ideal for metal coordination, but they are very effective for DNA-crosslinking. This application for our metallointercalator-peptide conjugates is quite promising. This simple system may provide some valuable insights into oxidative DNA damage, and provides a new tool for the study of DNA-protein crosslinking.

## 6.2. References

1. Johann, T. W.; Barton, J. K. *Phil. Trans. R. Soc. Lond. A* **1996**, 354, 299-324.
2. Núñez, M. E.; Barton, J. K. *Curr. Op. Chem. Bio.* **2000**, 4, 199-206.

3. Sitlani, A.; Long, E. C.; Pyle, A. M.; Barton, J. K. *J. Am. Chem. Soc.* **1992**, *114*, 2303-2312.
4. Nguyen, K. L.; Steryo, M.; Kurbanyan, K.; Nowitzki, K. M.; Butterfield, S. M.; Ward, S. R.; Stemp, E. D. A. *J. Am. Chem. Soc.* **2000**, *122*, 3585-3594.
5. Sardesai, N. Y.; Lin, S. C.; Zimmermann, K.; Barton, J. K. *Bioconj. Chem.* **1995**, *6*, 302-312.
6. Fitzsimons, M. P.; Barton, J. K. *J. Am. Chem. Soc.* **1997**, *119*, 3379-3380.
7. Copeland, K. D.; Fitzsimons, M. P.; Houser, R. P.; Barton, J. K. *Biochemistry* **2002**, *41*, 343-356.
8. Sardesai, N. Y.; Zimmermann, K.; Barton, J. K. *J. Am. Chem. Soc.* **1994**, *116*, 7502-7508.
9. Sardesai, N. Y.; Barton, J. K. *J. Biol. Inorg. Chem.* **1997**, *2*, 762-771.
10. Hastings, C. A.; Barton, J. K. *Biochemistry* **1999**, *38*, 10042-10051.